Modelling Large Scale Inhomogeneous Multihop Wireless Networks

Dene Hedges

Wadham College
University of Oxford

A thesis submitted for the degree of
Doctor of Philosophy

Hillary 2024

Abstract

Society's burgeoning demand for ubiquitous wireless connectivity, the drive for greater efficiency and profitability in industry and agriculture sectors and the growth in e-Health, for example, have led to increased densification, cohabitation of disparate technologies and increased inhomogeneity in wireless networks.

Whereas this densification enables the deployment of multihop relaying, which yields a number of tangible benefits, the performance analysis of large-scale relay networks ($\gg 2$ hops) is non-trivial and the relay selection for optimal performance can introduce a high processing complexity, typically high order polynomial time; potentially unsuited to lower power and edge-processing technologies.

This thesis is concerned with the modelling and analysis of large-scale inhomogeneous multihop wireless networks in a number of contexts and 'real-world' application scenarios. We analyse 2-hop connectivity within geometrically bounded networks, deriving a closed form expression for connection probability, and apply it in a device-to-device (D2D) context within a cellular-type network. We show that appreciable reductions in the burden on the cellular-infrastructure can be realised with this D2D approach.

Progressing to larger-scale networks, we propose a novel approach to multihop route optimisation by considering the limit of infinite relay node density, yielding an optimised equivalent continuous relay path, or continuum. The model is carefully constructed to maintain a constant connection density even though the node density scales without bound. This provides a formulation for determining performance extrema using methods from the field of calculus of variations. With our model, we show that processing complexity scales linearly with the number of points that sample the continuous path, which can be lower than the number of relay nodes in a large scale network. We demonstrate the effectiveness of this new approach and its potential by considering a network subjected to point sources of interference and to the problem of optimal covert routing in the presence of an eavesdropper.

Modelling Large Scale Inhomogeneous Multihop Wireless Networks



Dene Hedges

Wadham College

University of Oxford

A thesis submitted for the degree of

Doctor of Philosophy

Hillary 2024

Abstract

Society's burgeoning demand for ubiquitous wireless connectivity, the drive for greater efficiency and profitability in industry and agriculture sectors and the growth in e-Health, for example, have led to increased densification, cohabitation of disparate technologies and increased inhomogeneity in wireless networks.

Whereas this densification enables the deployment of multihop relaying, which yields a number of tangible benefits, the performance analysis of large-scale relay networks ($\gg 2$ hops) is non-trivial and the relay selection for optimal performance can introduce a high processing complexity, typically high order polynomial time; potentially unsuited to lower power and edge-processing technologies.

This thesis is concerned with the modelling and analysis of large-scale inhomogeneous multihop wireless networks in a number of contexts and 'real-world' application scenarios. We analyse 2-hop connectivity within geometrically bounded networks, deriving a closed form expression for connection probability, and apply it in a device-to-device (D2D) context within a cellular-type network. We show that appreciable reductions in the burden on the cellular-infrastructure can be realised with this D2D approach.

Progressing to larger-scale networks, we propose a novel approach to multihop route optimisation by considering the limit of infinite relay node density, yielding an optimised equivalent continuous relay path, or continuum. The model is carefully constructed to maintain a constant connection density even though the node density scales without bound. This provides a formulation for determining performance extrema using methods from the field of calculus of variations. With our model, we show that processing complexity scales linearly with the number of points that sample the continuous path, which can be lower than the number of relay nodes in a large scale network. We demonstrate the effectiveness of this new approach and its potential by considering a network subjected to point sources of interference and to the problem of optimal covert routing in the presence of an eavesdropper.

Acknowledgements

Personal

First and foremost, I am extremely grateful to my supervisor, Prof. Justin Coon, for his invaluable advice, continuous support, guidance and patience throughout my tenure at the University of Oxford.

Special thanks go to Dr. Gaojie Chen, Dr. David Simmons, Dr. Shuping Dang, Dr. Hashem Yassine, Dr. Shahriah E. Tajbakhsh, Dr. Orestis Georgiou, Dr. Jinchuan Tang, Dr. Mihai-Alin Badiu and many other colleagues (too many to mention), within the department of Engineering Science and other academic institutes, who have provided unconditional help and guidance throughout; together we have enjoyed many a stimulating conversation that has been instrumental in broadening my horizons, increasing my knowledge and has provided new perspectives on many facets of life.

Many thanks also, to Grahame Faulkner for his support with all things departmental, IT and for the many engaging conversations as we try and put the world to rights.

I would also like to thank all of the reviewers, who provided invaluable feedback during the processes of publishing my research.

Finally, I would like to express gratitude to my wife Hazel and my children, Leah and Jake, who have provided unwavering support throughout, without their tremendous understanding and encouragement, it would be not have been possible for me to complete my study. To Hazel, thank you for listening attentively, with convincing engagement, when I discuss my research.

Institutional

I would also like to express my sincere gratitude to my employer, HMGCC, for giving me the opportunity to pursue a part-time DPhil. This is a large commitment for any organisation and I only hope I can repay this investment with the newly acquired skills that I bring back into the business, the increased knowledge network across UK academia and the stronger enduring relationships we build with academia and the co-creation opportunities to come.

List of Publications

Journal Publications

1 **D. A. Hedges** and J. P. Coon, "On the Relationship Between Relay and Infrastructure Densities in Geometrically Bounded Relay-Assisted Wireless Networks," in IEEE Transactions on Vehicular Technology, vol. 67, no. 11, pp. 10983-10994, Nov. 2018, doi: 10.1109/TVT.2018.2866173

2 **D. A. Hedges**, J. P. Coon and G. Chen, "A Continuum Model for Route Optimization in Large-Scale Inhomogeneous Multi-Hop Wireless Networks," in IEEE Transactions on Communications, vol. 68, no. 2, pp. 1058-1070, Feb. 2020, doi: 10.1109/TCOMM.2019.2955105.

3 **D. A. Hedges** and J. P. Coon, "A Framework for Covert Multihop Route Planning," in IEEE Transactions on Communications, (Being prepared for submission).

Conference Publications

1 **D. A. Hedges**, J. P. Coon and O. Georgiou, "On the Connectivity of Two-Hop Networks in Finite Domains," in SCC 2017; 11th International ITG Conference on Systems, Communications and Coding, Hamburg, Germany, 2017, pp. 1-6.

2 **D. A. Hedges**, J. P. Coon and G. Chen, "A Continuum Model for Route Optimization in Large-Scale Inhomogeneous Multi-Hop Wireless Networks," in 27th European Signal Processing Conference (EUSIPCO), A Coruna, Spain, 2019, pp. 1-5, doi: 10.23919/EUSIPCO.2019.8903086.

Co-authored Publications

1 M.Z. Bocus, O. Gourgiou, J.P.Coon and **D.A.Hedges**, "Location-based coverage probability for distributed antenna systems in finite-area networks," in IEEE International Conference on Communications (ICC), Paris, France, 2017, pp. 1-6, doi: 10.1109/ICC.2017.7997380.

2 M.Chafii, J.P.Coon and **D.A.Hedges**, "DCT-OFDM With Index Modulation," in IEEE Communications Letters, vol. 21, no. 7, pp. 1489-1492, July 2017, doi: 10.1109/LCOMM.2017.2682843.

Contents

List of Publications **vii**

List of Figures **xiii**

List of Tables **xix**

List of Abbreviations **xxi**

List of Mathematical Notations **xxv**

1 Introduction **1**
- 1.1 Evolution of Wireless Communications . . . 2
  - 1.1.1 Cellular Networks . . . 3
  - 1.1.2 Ad-Hoc Networks . . . 4
  - 1.1.3 Internet of Things . . . 6
- 1.2 Future Gazing . . . 7
- 1.3 Multihop Wireless Networks . . . 9
  - 1.3.1 Relaying Methodologies . . . 13
- 1.4 Summary and Motivation . . . 14
- 1.5 Thesis Contributions and Organization . . . 15

2 Modelling Fundamentals **21**
- 2.1 Pairwise Wireless Connectivity Modelling . . . 22
  - 2.1.1 Pathloss . . . 22
  - 2.1.2 Channel Fading . . . 23
  - 2.1.3 Pairwise Connectivity Model . . . 24
  - 2.1.4 Justification for modelling with square law pathloss and Rayleigh fading . . . 26
- 2.2 Network Inhomogeneities . . . 27
  - 2.2.1 Interference . . . 27
  - 2.2.2 Geometric Boundary Effects . . . 30
- 2.3 Stochastic Geometry for Network Modelling . . . 32
  - 2.3.1 Binomial Point Process . . . 33

2.3.2 Poisson Point Process 35
2.3.3 Expectation of Sum of Functions over PPP 35
2.3.4 Expectation of Product of Functions over PPP 36
2.4 Large Scale Networks and Modelling 36
2.4.1 Variational Calculus 39
2.5 Summary 42

3 Two-Hop Relaying in Finite Domains 45
3.1 Introduction 46
3.2 Network Definitions and System Model 47
3.3 Connectivity Analysis 48
3.3.1 Connectivity in a Finite Domain $\mathcal{V}$ 49
3.3.2 Connectivity in the $\mathbb{R}^2$ plane 53
3.4 Asymptotic Behaviour of $\langle P_{12}^{(1,2)} \rangle$ 55
3.4.1 $\hat{\mathcal{V}} \to \infty$ 56
3.4.2 Sparse Network 56
3.5 Averaging over the terminal node $\mathbf{p}_2$ 59
3.6 Conclusion and Discussions 60

4 Relationship Between Relay and Infrastructure Densities in Geometrically Bounded Relay-Assisted Wireless Networks 63
4.1 Introduction 64
4.2 Network Definitions and System Model 66
4.3 Connectivity Analysis 67
4.3.1 Homogeneous Infrastructure 69
4.3.2 Inhomogeneous Infrastructure 74
4.4 Numerical analysis of relative densities of relay and infrastructure networks 80
4.5 Conclusion and Discussions 85

5 Continuum Model for Route Optimisation in Large-Scale Inhomogeneous Multi-Hop Wireless Networks 89
5.1 Introduction 90
5.2 Discrete Optimisation of Relay Locations 92
5.3 Continuum Model for End-to-End Outage Probability 93
5.3.1 General Formulation 94
5.3.2 Homogeneous System 94
5.3.3 Inhomogeneous System 95
5.4 Multi-hop Route Optimisation in the Presence of a Single Interferer 96
5.4.1 Stationary Paths 99

5.4.2 Single Directional Interferer . . . 101
5.5 Multiple Interferers . . . 105
5.5.1 Two Interferers . . . 107
5.5.2 Three Interferers . . . 109
5.6 Sampling the Continuum for Practical Deployments . . . 112
5.7 Conclusion and Discussions . . . 115

6 Framework for Covert Multihop Route Planning 119
6.1 Introduction . . . 120
6.2 Network Model . . . 122
6.2.1 End-to-End Connection Probability . . . 124
6.2.2 Antenna Model . . . 127
6.2.3 Coherent and Joint Detection . . . 128
6.3 Multi-hop Route Optimisation in the Presence of a Single Eavesdropper 131
6.4 Numerical Results . . . 134
6.4.1 Single Eavesdropper with No Shadowing . . . 134
6.4.2 Single Eavesdropper with Shadowing . . . 137
6.5 Application to Ad-Hoc Network Scenario . . . 139
6.6 Conclusion and Discussions . . . 142

7 Conclusions 145
7.1 Thesis Summary . . . 146
7.1.1 Research Question 1 . . . 147
7.1.2 Research Question 2 . . . 148
7.1.3 Research Question 3 . . . 149
7.1.4 Research Question 4 . . . 151
7.1.5 Research Question 5 . . . 152
7.2 Future Work . . . 153

Appendices

A 159
A.1 Interference Reduction in Multihop Networks . . . 159
A.2 Lagrangian Optimisation . . . 160

B 163
B.1 Evaluation of $\bar{H}_{12}^{(2_{\mathrm{I}})}$ . . . 163
B.2 Quasi-Convexity in $\mathcal{O}$ . . . 165

C 169
C.1 Proof of Proposition 1 . . . 169
C.2 Proof of Proposition 2 . . . 170

References **173**

List of Figures

1.1 Illustration of successive relaying. 11

2.1 'Hard' and 'Soft' pairwise connection functions for varying pathloss exponents, $\eta \in \{2, 3, 4, 5\}$. 26
2.2 Illustration of N-hop relay network. 29
2.3 Ratio of expectations of interference level with increasing number of multipath hops. 30
2.4 Illustration of a uniform random distributed of relay nodes within a circular geometrically boundary. 31
2.5 Illustration of 100 points generated by uniform BPP. 34
2.6 Characterisation of Processing Complexity. 37
2.7 Illustration of the Brachistochrone problem. 41

3.1 Direct and 2-hop connectivity between two terminal nodes, $\mathbf{p}_1$ and $\mathbf{p}_2$, in a finite convex domain $\mathcal{V}$ containing N uniformly distributed intermediate relay nodes $\mathbf{p}_k \in \Phi_B$. 49
3.2 Illustration of terminal node locations within circle of unit radius. . 52
3.3 $\langle H_{12}^{(2)} \rangle$ as a function of $\mathbf{p}_1$ and $\mathbf{p}_2$ within a circular domain of unit radius. Upper-left panel shows effect of variable angular offset and variable radial offset with $r_i = r_j$ and remaining panels show effect of fixed angular offsets $(0, \pi/2, \pi)$ with variable radial offsets of nodes. 53
3.4 $\langle H_{12}^{(2)} \rangle$ as a function of $|\mathbf{p}_2|$ where $|\mathbf{p}_1| = 0.5$ and $\mathbf{p}_1$ and $\mathbf{p}_2$ lie on the same radial axis of a circle of radius $R = 1$. The red circles represent results obtained by Monte-Carlo simulation. 54
3.5 $\langle H_{12}^{(2)} \rangle$ as a function of $\mathbf{p}_1$ and $\mathbf{p}_2$ within a rectangular domain of dimension 2×1. Upper-left panel shows excursion of $\mathbf{p}_1$ and $\mathbf{p}_2$ about $y_1 = 0$ and $x_2 = 0$ axes respectively and upper-right panel shows excursion of $\mathbf{p}_1$ and $\mathbf{p}_2$ both located on the central horizontal axes $y_1 = y_2 = 0$. Lower panels shows $\langle H_{12}^{(2)} \rangle$ as a function of position of mid-point $\overline{\mathbf{p}}_{12}$, along central horizontal axis (lower left plot) and along central vertical axis (lower right plot) and separation $|\mathbf{p}_2 - \mathbf{p}_1|$. 55

3.6 Connectivity performance (analysis, approximation and Monte-Carlo simulation) at boundary and centre of circular domain of radius $R = 10$ and total number of nodes $N \in \{50, 200, 500\}$. The boundary and central performances are the left and right curves respectively for each node density. 58

3.7 Left Panel: Average connection probability, via direct link or 2-hop path, $\langle P_1^{(1,2)} \rangle$, in a circular domain of unity radius and varying the position of a fixed node, $\mathbf{p}_1$, along a fixed radial axis. Right Panel: Improvement in average connection probability. Total relay nodes in network $N \in \{3, 5, 10, 20\}$. Results are supported by Monte-Carlo simulation as shown by red circles. 60

4.1 Direct and 2-hop connectivity between two terminal nodes, $\mathbf{p}_1$ and $\mathbf{p}_2$, in a finite convex domain $\mathcal{V}$ containing uniformly distributed intermediate relay nodes $\mathbf{p}_k \in \Phi_{\mathrm{R}}$ and non-uniformly distributed infrastructure nodes $\mathbf{p}_m, \mathbf{p}_n \in \Phi_{\mathrm{I}}$. 68

4.2 Outage probability as a function of ρ_{R}, for $\rho_{\mathrm{I}} \in \{0.5, 1, 1.5, 2\}$ and $\eta \in \{2, 3\}$, averaged over locations of relay and infrastructure nodes in a circular domain $\mathcal{V}$ of radius 2.5, as given by (4.4). Terminal node located at polar coordinates $2\angle 0$ and $2\angle \pi/2$. Blue markers show results from Monte Carlo simulations. Dashed red lines indicate upper bound as given by (4.6). 71

4.3 Illustration of the accuracy of first order approximation (4.15). The red solid traces show ρ_I as a function of ρ_R as defined by (4.4) (determined through successive approximation) and the black dashed traces show the first order approximation as given by (4.15). We fix $R = 4$ and $\kappa = 0.01$ and consider terminal nodes located within the central bulk region at radial and angular offsets $r_i \in \{0.5, 1.0, 1.5\}$ and $\pi/2$ respectively. 74

4.4 Realisations of the spatial distribution of infrastructure nodes, with density $\rho_{\mathrm{I}} = 10$ within a circle of radius $R = 4$, for $\alpha \in \{0.1, 1, 10\}$ and $\beta = 2$. 76

4.5 Outage probability as a function of ρ_{R}, averaged over locations of relay and infrastructure nodes over a circular domain $\mathcal{V}$ of radius 2.5, as given by (4.4), with appropriate substitutions and $\eta = 2$. Terminal node locations are both fixed at a radial offset of 2 with angular separation of $\pi/2$ and mean infrastructure density is $\rho_{\mathrm{I}} = 2$. Plot illustrates outage probability over a range of infrastructure spatial weighting factors $\alpha \in \{0.1, 1, 10\}$, $\beta = 2$ and includes results from Monte Carlo simulations. Dashed red lines indicate upper bounds derived from the application of the union bound of outage probabilities between terminal nodes and infrastructure nodes. . . . 78

4.6 Outage probability, averaged over relay, infrastructure and terminal node locations, as a function of weighting factor α for a range of domain radii $R \in \{2, 3, 4, 5, 10\}$. In all cases, mean densities of relay and infrastructure networks are fixed at $\rho_{\mathrm{R}} = 50$ and $\rho_{\mathrm{I}} = 2.5$. Dashed red lines indicate upper bounds derived from the application of the union bound of outage probabilities between terminal nodes and infrastructure nodes averaged over terminal node locations. . . 79
4.7 Infrastructure density, ρ_{I}, versus relay density, ρ_{R}, achieving an outage probability of $\kappa = 0.01$ averaged over positions of the terminal nodes over circular domain of radii $R \in \{1, 1.4, 1.8, 2.5, 4, 5\}$ and infrastructure spatial distribution weighting $\alpha \in \{0.1, 0.5, 1, 2, 10\}$. . 81
4.8 For fixed infrastructure density of $\rho_{\mathrm{I}} = 3$ and no relay network, we show the optimum spatial bias α_{opt} (minimising averaged outage probability) as a function of domain radius R. 84
4.9 Minimum infrastructure density, employing variable (non uniform) and uniform thinning, and optimum infrastructure spatial bias α_{opt} as a function of relay density for radii $R \in \{2.5, 3, 4\}$. 86
4.10 Reduction in infrastructure density by employment variable (non uniform) spatial thinning relative to the uniform spatial thinning case. 87

5.1 Multihop wireless network subject to single interferer. 92
5.2 Optimal routes with single interferer located at $(0, 0)$ for $k \in \{1, 3, 5, 10, 25, 50\}$, Terminal nodes located at Cartesian coordinates $(1, 0)$ and $(-1, 0)$. 101
5.3 Optimal routes with single interferer located at $(0, 0)$ for $k \in \{3, 5, 10, 25, 50\}$ Terminal nodes located at Cartesian coordinates $(0.5, 0)$ and $(0, 1)$. 102
5.4 Optimised routes in the presence of a directional interferer. The directivity is a cardioid pattern with 3 dB peak gain at $\pi/4$; $k \in \{1, 3, 5\}$. 105
5.5 Illustration of successive route approximations (labelled by iteration number) and standard deviation of radial offset from optimal route for each iteration (inner figure). 106
5.6 Optimal routes for 2 interferer scenario. Interferers located at positions $(0, 0)$ and $(1, \pi/2)$, indicated by crosses, and $k = 3$. The stationary paths from uppermost to lowermost are labelled 1, 2, and 3 respectively. 108
5.7 Verification of path stationarity by route perturbation. 109
5.8 Stationary paths (solid lines) for 3 interferer scenario for $k \in \{1, 2, 3\}$. Interferers are located at positions $(0, 0)$, $(0.5, \pi/6)$, $(0.5, \pi/3)$ (red crosses). The dashed lines represent approximations for the stationary paths for a single equivalent interferer located at position $(0.322, \pi/4)$. 110

5.9 Stationary paths (solid lines) for 3 interferer scenario for $k \in \{1, 2, 3\}$. Interferers are located at positions $(0, 0)$, $(0.683, 0)$, $(0.683, \pi/2)$ (red crosses). The dashed lines represent approximations for the stationary paths for a single equivalent interferer located at position $(0.322, \pi/4)$. 111
5.10 Outage probability versus the number of relay nodes placed on the continuum according to equi-spacing, equi-angle, equi-Euclidean and optimum angle placement strategies for $k = 5$. The dashed line represents the outage probability for a relay placement according to the discrete optimization of both radial and angular ordinates of relay nodes where $k = 5$. 115
5.11 Outage probability and % deviation in outage probability from the continuous path versus SNR for five relay nodes placed on the continuous path according to equi-spacing, equi-angle, equi-Euclidean, and optimum angle placement strategies for $k = 5$. 116
5.12 An example of the placement of 10 relay nodes according to the optimum-angle placement strategy (circle marker representing relay node location) and optimizing both radial and angle ordinates of 10 and 50 relay nodes (relay node locations represented by square and diamond markers respectively). 117

6.1 Multihop wireless network subject to single eavesdropper 123
6.2 Comparison of parabolic dish antenna and the approximation for $g(\theta)$ at peak $g_p \in \{6, 10, 20\}$. The solid line represents the gain of a parabolic antenna and the dashed line represents our antenna model. 128
6.3 Polar Plot of $g(\theta)$, $g_p \in \{1, 2, 3, 4, 6\}$. 129
6.4 Illustration of the connectivity between two infinitesimally close neighbouring nodes on the continuum. 131
6.5 Stationary routes for varying antenna peak gains, $g_p \in \{1, 2, 2.5, 3, 3.5, 4, 6, 10, 20\}$. 136
6.6 Stationary routes, subject to building shadowing, for varying antenna peak gains, $g_p \in \{1, 2, 3, 4, 6, 10\}$. Obstacle-1 is centred at Cartesian coordinates (-100, 300) with length 200m and width 100m and obstacle-2 is centred at Cartesian coordinates (-300, 100) with length 100m and width 100m. 138
6.7 Application of the route planning framework to a 'real-world' covert IoT ad-hoc network. 139
6.8 Expectation of $\mathrm{SNR_e}$ as a function of relay node density in a homogenous PPP. 141
6.9 Expectation of $\mathrm{P_c}$ as a function of relay node density in a homogenous PPP. 142

B.1 Illustration of function $A_1 - B_1$ with respect to r_1/R for a range of domain radii $R \in \{6, 7, 8, 9, 10\}$. Showing a single zero crossing. . . 167

List of Tables

5.1 Constants C_1 and C_2 associated with Fig. 5.2 (Left most pair) & Fig. 5.3 (Right most pair). 101

6.1 Parameters associated with Fig. 6.5. 135

List of Abbreviations

AF . . . . . Amplify-and-Forward

AI . . . . . Artificial Intelligence

AMIE . . . . . Aggregate Multi-hop Information Efficiency

AP . . . . . Access Point

AR . . . . . Augmented Reality

AWGN . . . . Additive white Gaussian Noise

BPP . . . . . Binomial Point Process

BS . . . . . Base-Station

CAPEX . . . . Capital Expenditure

CCCD . . . . . Complementary Cumulative Distribution Function

CCI . . . . . Co-Channel Interference

CDF . . . . . Cumulative Distribution Function

CDMA . . . . Code-Division Multiple Access

CSI . . . . . Channel State Information

dB . . . . . Decibel

DF . . . . . Decode-and-Forward

DSSS . . . . . Direct Sequence Spread Spectrum

D2D . . . . . Device-to-device

e-Health . . . Electronic-Health

EIRP . . . . . Effective Isotropic Radiated Power

EM . . . . . Electromagnetic

eMBB . . . . . Enhance Mobile Broadband

FDMA . . . . Frequency-Division Multiple Access

FFT . . . . . Fast Fourier Transform

FM . . . . . Frequency Modulation

GPS . . . . . Global Positioning System

ICI . . . . . Inter-Channel Interference

IEEE . . . . . Institute of Electrical and Electronics Engineers

i.i.d. . . . . . Independent and Identically Distributed

IBFD . . . . . In-Band Full Duplex

INR . . . . . Interference to Noise Ratio

IoE . . . . . Internet of Everything

IoT . . . . . Internet of Things

IoV . . . . . Internet of Vehicles

IP . . . . . Internet Protocol

i.u.d. . . . . . Independent and Uniformly Distributed

LCP . . . . . Logarithmic Connection Probability

LEO . . . . . Low Earth Orbit

LoS . . . . . Line of Sight

LPD . . . . . Low Probability of Detection

LTE . . . . . Long-Term Evolution

MAC . . . . . Medium Access Control (layer)

MANET . . . Mobile Ad-hoc Network

MCN . . . . . Multihop Cellular Network

MIPS . . . . . Million Instructions Per Second

ML . . . . . Maximum-Likelihood

MMS . . . . . Multimedia Messaging Service

mMTC . . . . Massive Machine Type Communication

MR . . . . . Mixed Reality

M2M . . . . . Machine-to-Machine

NB-IoT . . . . Narrow Band Internet of Things

n**G** . . . . . nth Generation (network)

NLoS . . . . . Non-Line of Sight

NP . . . . . Non-Polynomial

OPEX . . . . . Operating Expenditure

PIC . . . . . Programmable Interface Controller

PDF . . . . . Probability Density Function
PGFL . . . . . Probability Generating Functional
PhY . . . . . Physical (layer)
PMF . . . . . Probability Mass Function
PP . . . . . Point Process
PPP . . . . . Poisson Point Process
QoS . . . . . Quality of Service
RF . . . . . Radio Frequency
RNPP . . . . . Relay Node Placement Problem
SCP . . . . . Secure Connection Probability
SDN . . . . . Software Defined Network
SIC . . . . . Successive Interference Cancellation
SINR . . . . . Signal-to-Interference-plus-Noise Ratio
SIR . . . . . Signal-to-Interference Ratio
SMS . . . . . Short Messaging Service
SNR . . . . . Signal-to-Noise Ratio
TDMA . . . . Time Division Multiple Access
TFLOPS . . . Tera FLoating-point Operations per Second
UAV . . . . . Unmanned Aerial Vehicle
UE . . . . . User Equipment
UHD . . . . . Ultra High Definition
UWB . . . . . Ultra-Wideband
VANET . . . . Vehicular Ad-hoc Network
V2X . . . . . Vehicle to Infrastructure
VoIP . . . . . Voice over Internet Protocol
VR . . . . . Virtual Reality
WiFi . . . . . Wireless Fidelity: IEEE 802.11x standard
WLAN . . . . Wireless Local Area Networks
WMN . . . . . Wireless Mesh Network
WSN . . . . . Wireless Sensor Networks
3D . . . . . Three Dimensional
3GPP . . . . . Third Generation Partnership Project

List of Mathematical Notations

X	(upper case) One dimensional scalar random variable
x	(lower case) realisation of a one dimensional scalar random variable
$\mathbf{X}$	Vector or Matrix
$\mathbf{p}$	Position vector in $\mathbb{R}^2$.
$\mathbb{E}(\cdot)$ **or** $\langle\cdot\rangle$ . . .	Expectation of event enclosed.
$\mathbb{P}(\cdot)$	Probability of event enclosed.
erf	Error Function
erfc	Complementary Error Function
$\lvert\cdot\rvert$	Cardinality of a set or Lebesgue measure of Euclidean space
$\lVert\cdot\rVert$	l^2-norm
$\lfloor\cdot\rfloor$	Floor function
$\lceil\cdot\rceil$	Ceiling function
$\lfloor\cdot\rceil$	Rounding to nearest integer
$\mathbb{R}$	Set of real numbers
$\mathbb{R}^n$	n-dimensional Euclidean space
$\mathbb{Z}$	Set of integers
$\mathbb{Z}^+$	Set of positive integers
$\mathbb{N}$	Set of natural numbers
Φ, Φ_B, Φ_P . . .	Point process, binomial point process and Poisson point process respectively
$\mapsto$	Mapping to
$\sim \mathcal{CN}(\mu, \sigma^2)$ . .	Complex normal distribution with mean $\mu \in \mathbb{R}$ and variance $\sigma^2 \in \mathbb{R}_{>0}$
$\sim \mathbf{exp}(\lambda)$	Exponential distribution with rate parameter $\lambda > 0$
$\mathrm{Q}_n(a, b)$	n-th order Marcum-Q function

$\mathrm{I}_n(a)$ . . . . . n-th order modified Bessel function of the first kind

$O(\cdot)$ . . . . . Bachmann–Landau Big-O function describing the limiting behaviour of the function enclosed

$\binom{N}{k}$ . . . . . Binomial coefficient

$\dot{r}(\cdot)$ . . . . . First derivative of function r with respect to the domain variable

$\ddot{r}(\cdot)$ . . . . . Second derivative of function r with respect to the domain variable

$\frac{\partial H}{\partial f}$ . . . . . First partial derivative

$\frac{\partial^2 H}{\partial f^2}$ . . . . . Second partial derivative

$\mathcal{L}(\cdot)$ . . . . . Lagrangian function

1 Introduction

1.1 Evolution of Wireless Communications

Wireless communications has its origins dating back to the late 19th century with Guglielmo Marconi, an Italian inventor, sending morse-coded signals over short distances using electromagnetic (EM) waves that were generated by a spark-gap transmitter [1]; one could consider this as an early form of impulse ultra-wideband communications UWB [2]. In 1901 Marconi went on to demonstrate wireless transatlantic communications which, unknowingly at the time, exploited refraction of the RF signal within the ionosphere [3] to overcome the problem of non-line-of-sight (NLOS) propagation conditions due to the Earth's curvature. This invention is widely considered to represent the birth of wireless broadcast.

Over the subsequent decades, we have witnessed the birth of information theory, with Shannon's seminal work [4], and the introduction of many breakthrough technologies, the most salient including: radar, radio and television broadcast in the early to mid 1900s, satellite communications in the 1950s, global positioning systems in the 1970s [5–8] and mobile telephony, more commonly referred to as 'cellular' communications [9].

In 1984, the futurologist Ray Hammond predicted that the linking of computers around the world would have far reaching effects, and the spread of knowledge, the interchange of ideas and the dissemination of information would produce a revolution in our society [10]. This prediction became a reality, invoked a network revolution and generated a more profound impact than he had imagined. This became what we know as 'the internet' [11] and, although not a wireless technology per se, it is inextricably linked to the development of many modern wireless systems. Over the last few decades we have witnessed an increased convergence towards internet-centricity in wireless networks, as evidenced by the Internet-of-Everything philosophy [12], where wireless technologies, of one form or another, provide the connectivity between much of everything [13].

In the following sections, we expand on some of the more salient wireless network technologies and distil the key trends in wireless technology evolution that we consider pertinent to our research and provide context in framing this research thesis.

1.1.1 Cellular Networks

Cellular networks have been one of the most impactful developments of recent decades, with particular regard to their pervasiveness, influence and impact on social behaviour and the global economy [14]. Further, of all of the aforementioned technologies, the cellular network provides a convenient benchmark for the general advancement of wireless technology, principally due to the vast intellectual resources associated with its development, its rapid rate of evolution and how it underpins, pervades and harmonises with many other technologies and applications, e.g. cellular network timing derived from GPS, and conversely, cellular networks supporting assisted-GPS [15] and the integration of cellular and satellite networks [16].

Cellular networks have evolved through five generations during the last four decades [17]. The first-generation (1G) introduced in the 1980s providing voice communication using analog mobile technology [18]. The low-complexity analogue frequency modulation (FM) employed offered no real security to eavesdropping with 'en clair' transmission of voice. The Second Generation (2G) networks marked the transition from analogue to digital, supporting basic data services such as short message services (SMS) in addition to voice communication, as well as secure data transfer with the application of cryptography [19]. The third-generation (3G) introduced improved mobile broadband services and enabled new applications such as multimedia message services (MMS), video calls, and mobile TV. Fourth generation (4G) provided improved mobile broadband services, packet-centric (internet protocol, IP) communication, Voice-Over-IP (VoIP), ultra-high-definition (UHD) video streaming, and online gaming. 5G mobile communication networks are currently being deployed worldwide [20] and offer enhanced-Mobile-Broadband (eMBB), ultra-Reliable-Low-Latency Communication and massive-Machine-Type-Communication (mMTC) [21]. Further, 5G embraces software defined networking (SDN) to provide dynamic network reconfigurability and network abstraction [22]. The capabilities of 5G have enabled novel applications such as Virtual Reality (VR),

Augmented Reality (AR), Mixed Reality (MR), autonomous vehicles, Internet-of-Things (IoT) [23] and Industry 4.0 [24]; IoT and Industry 4.0 being key ingredients enabling the 'smart factory' of the future [25, 26].

Over the various generation increments, we observe the following key trends that we consider pertinent to this research thesis:

- cellular networks have evolved from having sparse homogeneous macro-cellular type architectures to higher density heterogeneous network architectures [27];
- the demands for services, e.g. data rates, capacity, latency, quality-of-service have increased exponentially [28, 29];
- successive cellular networks are subject to an increasing spatial densification of users and basestations [30–33];
- with increasing concerns over information privacy and security, significant attention is being placed upon network security, vulnerability and resilience [34–36];
- with increased global pressure to reduce carbon footprints, wireless networks are subject to increasing scrutiny with respect to their energy consumption [37];
- with finite, and costly, spectrum resources available there is increasing focus on spectral efficiency and spectrum usage [38];
- increasing network densification has led to co-channel interference as the limiting source of noise within the network [39].

1.1.2 Ad-Hoc Networks

Ad-hoc network is the generic term for a self-organising network of wireless devices that can communicate with each other in the absence of a fixed infrastructure [40]. These networks typically consist of equal nodes that communicate over wireless links without centralised control. The communication links are not necessarily direct, they can be established in a multi-hop fashion whereby every wireless device in the

network can act as a relay. Routing through the network is achieved by an ad-hoc routing protocol, which automatically discovers the neighbors and sets up routes. Such networks also support mobility, as the information about routes and topology are constantly updated. Ad-hoc networks have evolved under a number of ad-hoc paradigms such as Mobile Ad-hoc Networks (MANETs) [41], Vehicular Ad-hoc Networks (VANETs) [42, 43], Wireless Sensor Networks (WSNs) [44, 45], Wireless Mesh Networks (WMNs) [46, 47], and so on. Typical application areas include:

- Tactical military communications requiring resilience in 'battle-field' scenarios where the environment is typically devoid of infrastructure [48].
- Communication in environments subject to high signal attenuation or shadowing [49] e.g. communication within cave networks [50].
- Collaborative computing which employs decentralized computing over multi-layered networks, combining cloud and wireless technologies [51].
- Disaster response and emergency rescue, whereby a deployed cellular communication infrastructure might be partially or completely destroyed after a natural disaster, e.g. earthquake or terrorist incident [52].
- Wireless sensor networks consisting of a number of sensor nodes (few tens to thousands) working together to monitor a region to obtain data about the environment, e.g. smart agricultural [53].
- Multi-hop cellular networks (MCN) where communication distances, between mobiles and basetations, in cellular networks, by the employment of intermediate relay(s). [54].
- Incident management through vehicular networks (VANET) where traffic incidents, as observed by one or more vehicles, can be rapidly communicated to other vehicles approaching the incident. A key enabler in the development of autonomous vehicles [55].
- Asset management within 'Smart' factories [56]

This list is by no means exhaustive but serves to demonstrate the diversity in application of ad-hoc networking.

1.1.3 Internet of Things

The term "Internet of Things" (IoT) was first used in 1999 [57] to describe scenarios in which Internet connectivity and computing capability extend to a variety of objects, devices, sensors, and everyday items. IoT is an information-centric network where everyday objects and devices are interconnected through the Internet whatever their location (home, work, city, etc.). Future predictions suggest that the IoT will connect 75 billion objects to the Internet by 2025 [58] with promises of revolutionising our future with new applications in areas such as smart homes, buildings, cities, commerce, agriculture, travel and transportation, health and personal care, construction, and industry [59–63].

The types of wireless networks, typically employed within IoT, include wireless sensor networks (WSNs), ZigBee, Wi-Fi, MANETs [64, 65], for example. These technologies are often inexpensive and have low power consumption, making them suitable for battery powered applications that require long unattended operational life, in particular, Zigbee, LoRa [66], SigFox [67] and NB-IoT [68]. The processing capabilities within IoT networks and sensor nodes similarly rely on inexpensive and low power processor technologies, such as PIC microcontrollers (from Microchip Technologies) and ARM processors [69, 70]. The low power yields performances of the order of 100 million fixed-point instructions per second (MIPS) or less, which is relatively low in comparison to higher power devices that can offer several tera floating-point instructions per second (TFLOPS). The 'Arduino' open-source hardware platform [71] provides a good example of one such inexpensive technology that has enabled the development of IoT networks, e.g. [72] in a weather monitoring context. Similarly, [73] describes a LoRa-based smart agricultural management and monitoring system using Wireless Sensor Networks (WSNs) in a rural environment. This work also shows the use of LoRa's 'chirp' spread spectrum modulation to provide the ability for localisation of sensors and to enhance security.

Relaying, where communication between IoT end devices and a gateway can occur directly or through an intermediary node (a relay), offers a promising solution to extending the coverage of wireless IoT networks whilst maintaining low energy consumption at the sensor nodes and the network as a whole. This multihop approach also serves to deliver high quality-of-service and network resilience to failures within the network. The authors in [74] describe an experimental IoT network employing 2-hop relaying in a rural agricultural context demonstrating significantly improved reliability within the network when employing relaying as opposed to direct connection of sensors to the internet gateway. In [75], and references therein, the authors provide a comprehensive, up to date, survey of relaying strategies within IoT networks; we expand on this in section 1.3.

1.2 Future Gazing

It is clear that wireless communications, in one form or another, have pervaded practically every corner of our lives and continues to influence, and be influenced by, societal and social behaviour as we have developed a high dependence on a 'wireless world' [76] and the information age [77]. The obvious question is what's next?

The growth in capabilities and services, offered by successive cellular networks, shows no signs of abating and researchers are looking towards 6G [78–80] in their endeavours to meet the burgeoning demands of society in areas such as 'Smart Cities' [81], e-commerce [82], e-health [83], enhanced radio localisation [84] and artificial intelligence (AI) [85]. A comprehensive survey of research themes, under the umbrella of 6G, can be found in [86], with examples of some of the key application areas being:

- Smart Grid 2.0 [87] relating to control of power distribution and monitoring;
- Holographic Telepresence [88] relating to the projection of realistic, full-motion, real-time 3D-images;
- Extended reality focused on developing immersive technology fusing physical and virtual worlds to generate human-machine interactions [89];

- Connected and autonomous vehicles looking into the next generation transportation systems such as autonomous driving, cooperative vehicle networks and the Internet-of Vehicles (IoV) [90];
- Industry 5.0 [91] leading the next generation 'industrial revolution';
- Healthcare 5.0 addressing the emergence of digital wellness [92].

In section 1.1.3, we described the primary focus of IoT networks as connecting 'things' without human intervention. Looking ahead, we are starting to see the IoT concept evolving towards the Internet-of-Everything (IoE) [93–95], which considers extending the network of connections between people, things, data and processes that provide general intelligence and improved cognition across the IoT network environment. This is predicted to have a profound effect on society with the authors of [96] creating a vision of how the IoE may alter future business models and the ways in which individuals and organizations create value in the future.

Connected sensors and devices are likely to remain a pervasive reality into the future, as we interact more or less knowingly with smart items every day. While smart-phones represent the main Internet connected devices which people interact with, other intelligent items are increasingly at our disposal. IoE is internet-centric and many of the communications networks, establishing the IoE connections, will be wireless. This has led to the paradigm of Wireless Internet of Everything which is shaping the evolution of the future ubiquitous IoE networks and how the multitude of heterogeneous smart devices are seamlessly connected [97, 98].

In summary, the future offered by wireless networking is clearly rich and diverse in opportunity, but many of the new futuristic and challenging use cases demand further improvements in data throughput, delivery latency, connection density, security, network resilience and Quality-of-Service (QoS), for example. We also see that the boundaries of what we have traditionally referred to as 'cellular', 'Ad-hoc', 'IoT', etc. are becoming increasingly blurred and are subject to greater integration and harmonisation in how they operate and interact. Whatever the future requirements for next generation services, the challenges of operating with

finite or constrained resources, e.g. RF spectrum, will require the application of new wireless concepts and innovations [99].

It is clear that wireless networks are becoming more heterogeneous in their structures, the scale and densities associated with wireless networks are increasing [30] and the degree of coexistence of wireless technologies is also increasing, with the challenges that that introduces [100, 101]. Adding to this, is the increasing focus on reducing carbon footprints [102], lowering the energy consumption within wireless networks and shifting from data oriented networks to energy-efficient oriented networks [103]. One particular area of research, that can exploit network densification, is multihop wireless networking. This topic has been researched, within a number of contexts, over the past few decades, as we discuss in the following section.

1.3 Multihop Wireless Networks

A wireless multihop network can be viewed as a set of nodes able to communicate with each other directly or beyond their transmission range by using nodes as relay points acting as routers [104]. Multihop connectivity, used synonymously with relaying within this thesis, has been a rich topic for researchers since its first introduction in 1971 [105], where the authors took an information theoretic approach to analyse the transmission of information over a communication channel with three terminals; note that the terms node and terminal are used interchangeably within this thesis. In the same decade, [106] demonstrated channel capacity improvement offered by relaying and [107, 108] proposed the use of multihop networking in a personal communications and mobile computing context in the early 1990s; perhaps an early insight into the modern 'smartphone'. Subsequently, multihop communication has been shown to have several advantages in areas such as: interference reduction, spectrum reuse, extension of radio coverage and energy consumption reduction [109–114], to highlight a few. These advantages make multi-hop communication very popular, and several kinds of networks are based on it, most notably within ad-hoc wireless networks as described in section 1.1.2. The utility of multihop networks is clearly wide ranging across both civilian and military sectors [115–121]

and we are starting to see increasing interest within space communications, e.g. [122] in preparation for future Lunar exploration and [123] in a low earth orbit (LEO) satellite network contexts. The concept of multihop relaying was first proposed for the augmentation of cellular networks in [124], but despite subsequent related research, including [125,126], and the Third Generation Partnership Project (3GPP) standardising relaying functionality in Release 10 in early 2011 [127], it has yet to find any real penetration within cellular networks; probably attributed to economic challenges rather than technological [128]. Despite this, many researchers maintain the view that relaying is one of the most promising candidates to accommodate the increasing demands for future data services [129, 130].

In this thesis, we concern ourselves with the viable[1] transfer of information from a source to a destination node, at fixed locations in Euclidean space, typically within the $\mathbb{R}^2$-plane; although our work does not preclude future consideration of higher dimensional Euclidean space or non-Euclidean manifolds, e.g. we may wish to consider multihop connectivity over a network of low-Earth-orbit satellites (LEO) as they orbit the Earth, confined to a 3D-sphere. We define the creation of a multihop network when the information is successively relayed via a number (one or more) of intermediate nodes, referred to as relays. This is depicted in Figure 1.1, showing two viable successive relay paths from source and destination nodes.

Whereas multihop networking is a relatively simple concept, it is subject to a number of challenges that need careful consideration and analysis, not least: network inhomogeneities, increased spatial randomness of networks, routing optimality, information delivery latency and energy consumption, for example. We consider these in greater detail in the following sections and in our subsequent research chapters. We firstly expand on network densification, briefly discussed earlier in this chapter, as an enabler for the creation of multihop relay paths.

The explosive growth in traffic demand, from mobile users in cellular systems, has dominated how successive generations have evolved [131]. The past few decades have seen the traditional macro-cellular networks, as with early generations, being

[1] As defined by meeting some performance metric such as information transfer probability of greater than 0.99 for example.

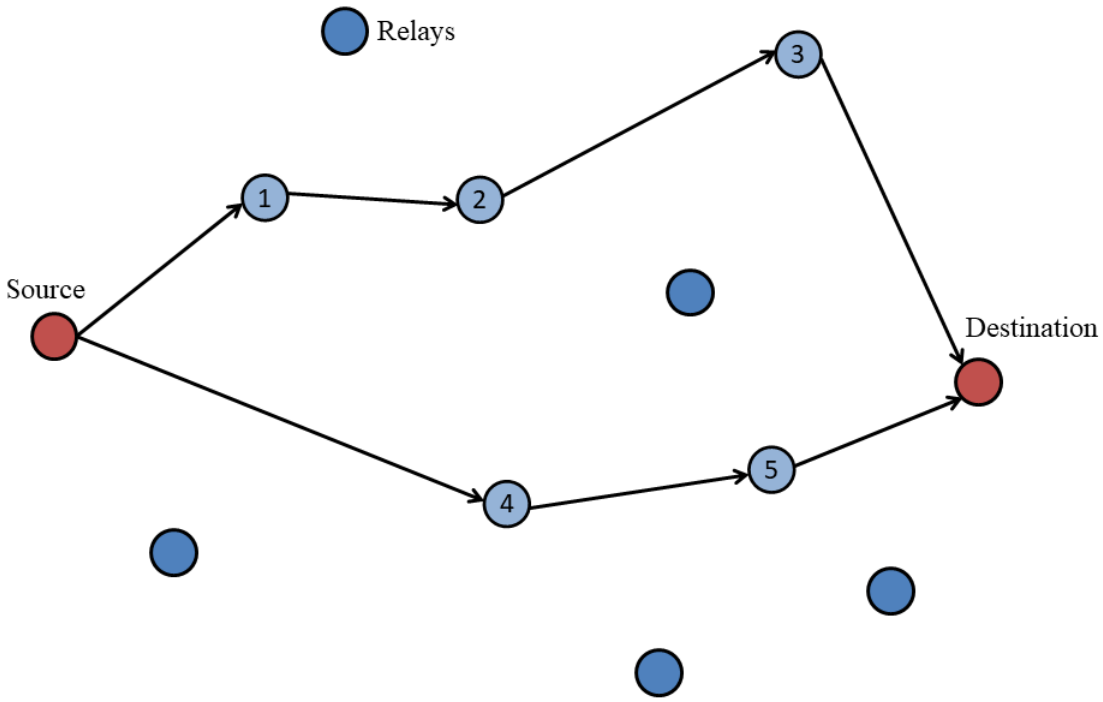


Figure 1.1: Illustration of successive relaying.

augmented with tiered supplemental infrastructures in the forms of micro, pico and femto-cells [27]. The gains and limitations associated with the employment of these denser smaller cell networks are discussed in [132] and references therein. As we move down the tiered structure of the network, from the macro layer, we observe three general trends: the location of cells migrates from being planned to unplanned (increased spatial randomness), energy consumption of the cell decreases and cell densities (number of active nodes per unit area) increase [133] [134]. The 5G cellular network picture is further complicated by the integration of a number of disparate technologies, such as Internet of Things (IoT), Wireless Sensor Networks (WSN) and Wireless Local Area Networks (WLAN), to provide seamless 'always-on' data transfer through the composite 5G network by choosing communication paths that optimise total network performance [29] [135]. From an IoT perpective, the last few years have witnessed an unprecedented growth in services [61, 62], driven by

a number of technological, social, and economic factors [63]. This will undoubtedly fuel further network densification, moving forward.

Researchers consider this network densification [31–33] to be a key enabler in satisfying the increasing capacity demands on wireless communication networks that are constrained by finite spectrum availability [136]. Further, driven by the promise of solving a number of issues: spectral efficiency, energy efficiency and insufficient capacity for example, multihop-cellular-networks (MCN) [124] and device-to-device communications (D2D) [137], [138], look to exploit the benefits offered by multihop connectivity in dense networks. D2D is a mechanism to offload traffic from a network infrastructure by allowing users within range of each other to communicate directly. We consider multihop relaying, in a D2D context, further in chapter 4.

Multi-hop relaying has long been studied as a way to extend coverage in wireless networks, reduce energy consumption, and improve the overall quality of service (QoS). For example, multi-hop network concepts have been applied in IoT networks [121], vehicular networks [117] and numerous publications addressing the challenges associated with Device-to-Device (D2D) communications in future cellular systems (see, e.g., [139] and references therein).

Looking ahead, [140] predicts that multihop networking is likely to play a key role in future wireless networks; optimised towards as few hops as possible in order to minimise end-to-end delivery latency and system complexity. This raises an interesting question: is it better to have fewer longer[2] relay hops or more shorter relay hops?. In [110], Haengii et. al. are clear proponents for long hops as a more competitive strategy, citing routing delay as the main drawback of short hops. [141] provides an overview of the trade space between short and long hops with respect to the metric 'aggregate multi-hop information efficiency (AMIE)', a statistical quantification of the network efficiency in delivering information over a multihop route. If we consider multihop connectivity from a security perspective, we subsequently show in section 2.2.1 that shorter hops can provide a more secure route. In reality the answer depends on the purpose of the multihop communication path.

[2]In terms of Euclidean distance

Expanding on the secrecy theme, multi-hop connectivity has been considered in the context of secrecy [142] which investigates the secrecy connectivity probability in multi-hop ad-hoc networks in the presence of inhomogeneous eavesdropper clusters. Also, Chen et al. studied optimal routing based on the trusted connectivity probability for multi-hop D2D communications with decode-and-forward relaying (see section 1.3.1) in [143]. But, these latter works only focused on the optimal routing based on the snapshot of the networks, which did not consider how to locate the positions of the relays to achieve the optimal performance when we have a large number of relays. We expand on the mutihop routing in dense networks, from a security perspective, in chapter 6.

While researchers conclude that the heterogeneous integration of wireless networks is likely to provide the required levels of connection ubiquity between humans, machines, and devices, it will lead to a number if challenges [144], not least in dealing with inhomogeneous spatial interference characteristics and how we model networks with increasing spatial randomness. Since our research interests lie in developing novel approaches for the determination of optimal multihop routes through large scale networks, we clearly need to be cognisant of the these challenges. The remaining sections of this chapter describe the salient challenges in greater detail.

1.3.1 Relaying Methodologies

Before progressing too far, it is worth discussing the single relay element of the network in more detail.

There are several relaying methodologies that exist that are tailored to meet the needs of the network application [145]. Two of the most common are Amplify-and-Forward (AF) and Decode-and-Forward (DF) relaying. The AF-relaying concept was analysed by Laneman et al. [109], in the context of diversity gain, and is often referred to as non-regenerative relaying, in that the relay does not decode and re-encode the received information prior to relaying it onward. In this scheme, the relay simply amplifies the received signal and re-transmits the amplified signal. This type of relaying has the principle benefits of low complexity and low latency,

the former from only requiring a linear amplifier[3] and the latter from not requiring intermediate demodulation-modulation stages which would otherwise add finite processing delay. The linear amplifier does make the AF scheme attractive in many applications that require relaying of a number of different waveforms, in that the amplification is agnostic of waveform type; with the caveat that the amplifier needs to maintain linearity, avoid amplifier saturation [147] in order to minimise waveform distortion. The main drawback in AF relaying is that the amplifier also amplifies the intrinsic thermal noise in addition to the signal, thus degrading the overall QoS of the network [148].

In DF-relaying, also known as regenerative relaying, the relay node decodes the received information signal sent by a source node, re-encodes it, and then forwards it to the next node in the network or directly to the destination node [149, 150]. This avoids the aforementioned noise amplification problem associated with the AF scheme. However, in contrast to AF, this scheme increases relay complexity in the signal demodulation and re-modulation processes that are required. Further, these processes also add inherent processing delays, potentially making them unsuitable for applications requiring low routing latency.

From the perspective of mathematical tractability, DF lends itself nicely to the performance analysis of multihop wireless networks in that the transmissions, over multiple hops, can be regarded as independent. Since our research interests lie in quantifying the benefits of relaying in an application context and addressing the problems associated with route optimisation in large scale networks, as we shortly discuss, we exploit the mathematical tractability offered by DF relaying as we move forward.

1.4 Summary and Motivation

Thus far, we have highlighted the utility of multihop wireless networking in a number of settings. Compared to networks with single wireless links, multi-hop

[3]Linearity is important to ensure that the relay does not introduce any distortion of the waveform [146]

wireless networks can extend the coverage of a network and therefore improve overall network connectivity. Moreover, transmission over multiple "short" links generally require less transmission power and energy than over "long" links. Also, shorter links can enable higher data rates resulting in higher data throughput and more efficient use of the wireless medium. With network densification, it is possible to have several multihop paths between information sources and destination which also provide enhanced network robustness and resilience to network component failures. In contrast to the benefits offered by multihop networking, there are issues associated with managing network inhomogeneities such as co-channel interference and network boundary effects. Furthermore, determining the optimum multihop route(s) through a large-scale network, in order to maximise or minimise one or more performance metrics can be challenging, particularly with a large number of relays to choose from within the network. This challenge can be further exacerbated by requirements for high speed of route determination, particularly in a very temporally dynamic network with relay nodes entering and exiting the network or simply having high spatial mobility within the network. Adding to the challenge further is the drive for energy efficiency within the network.

In this thesis, we analyze multihop relaying in dense networks, in the endeavour of addressing these aforementioned challenges for existing or next generation networks.

1.5 Thesis Contributions and Organization

This thesis comprises four core research chapters preceded by a literature review and the motivation for our research. The research chapters are followed by key conclusions and a summary of potential future research. The detailed outline of the thesis is as follows:

- **Chapter 2** introduces the necessary background theories and models that have enabled our research to progress and provides the necessary baselines, against which, our research results are compared.

- **Chapter 3** studies the direct (1-hop) and 2-hop connectivity, between two fixed terminal nodes (information source and destination nodes), amongst a network of uniformly randomly distributed relay nodes (e.g. other user nodes), confined to a finite convex geometry, i.e. having a fixed boundary where the straight line between and two points will not intersect the boundary. We develop closed form expressions for average connection probability for special cases of circular and rectangular geometries and consider the case where communication paths are subject to Rayleigh fading. The contents of this initial research are published in *SCC 2017; 11th International ITG Conference on Systems, Communications and Coding* [151]. It should be noted that Chapter 3 and, the following, Chapter 4 can be considered as a single larger chapter as they are contiguous, it is for presentation, within the thesis, that they are separate.

- **Chapter 4** We apply the connection functions, developed in Chapter 3 to a geometrically bounded cellular-type network, where user nodes traditionally access the network via fixed wireless infrastructure. In our model, we allow the connectivity between two arbitrary source and destination nodes (user terminals), within the network, to be established by direct connection, via a relay node (intermediate user terminal) or via the infrastructure (basestation) network; the choice based on link viability in a Rayleigh fading environment. We consider the relay nodes to be uniformly spatially distributed and assume that the infrastructure nodes are non-uniform. We progress in analysing the relationship between relay and infrastructure node densities for a prescribed outage probability between terminal nodes. In employing direct and 2-hop connectivity in this way and with increasing relay node density, we demonstrate that the reliance on infrastructure connectivity can be reduced. This provides a mechanism for energy saving by disabling (switching off) infrastructure nodes. Further, we determine exactly which infrastructure nodes can be disabled based upon knowledge of relay node density and the size of the geometric network boundary.

In this initial work we do not consider co-channel interference by assuming that a suitable medium access control protocol (MAC) [152] is employed. Under these working assumptions, we offer the following contributions:

1. we provide mathematical expressions involving well-understood special functions for the connectivity probability of two terminal nodes in a geometrically bounded network;
2. we exploit this mathematical framework to demonstrate the trade-off in relay and infrastructure node densities for a prescribed level of connectivity;
3. we demonstrate that it is possible to obtain a Pareto frontier in the different node densities by appropriately thinning the active infrastructure set in an inhomogeneous manner.

The main contents of this chapter have been published in *IEEE Transactions on Vehicular Technology* [153].

- **Chapter 5** considers multihop route optimisation in large-scale inhomogeneous networks. For most problem formulations it has been shown that this route optimization problem is complex and often requires the application of heuristic algorithms which, despite their relatively low processing complexity, find sub-optimal solutions. Where optimal solutions can be determined by Lagrangian based constrained optimisation techniques for example, the processing complexity typically scales like $O(N^3)$, N being the number of relays employed. In this chapter, we propose an alternative approach to route optimization by considering the limit of infinite relay node density to develop a continuum model, which yields an optimised equivalent continuous relay path. The model is carefully constructed to maintain a constant connection density even though the node density scales without bound. This leads to a formulation for minimizing the end-to-end outage probability that can be solved using methods from the calculus of variations. With the continuum

model, we show that the processing complexity scales linearly with the number of points that sample the continuous path, which can be lower than the number of relay nodes in a large scale network. We demonstrate the effectiveness of this new approach and its potential by considering a network subjected to point sources of interference.

Although exploratory in nature, this research offers the following contributions:

1. we develop a continuum model that describes the end-to-end outage probability in a multi-hop relay network;
2. we apply the model to find an analytic solution for the outage-optimal device locations when the system is subject to an inhomogeneous scalar field of interference;
3. the efficacy of the continuum model is verified by considering a discrete sampling of the continuum with a finite number of relay nodes.

The main contents of this chapter have been published in *IEEE Transactions on Communications* [154] and *27th European Signal Processing Conference (EUSIPCO)* [155].

- **Chapter 6** considers the problem of covert routing of a large-scale multihop wireless network in the presence of an eavesdropper, capable of joint detection of all transmissions within the network. As before, we consider the limit of infinite relay node density to develop a continuum model, but also consider a constant power density over the continuum. This yields a constrained optimisation problem requiring the combination of Lagrangian optimisation techniques with tools from the field of variational calculus. We develop a low-complexity framework to determine the optimal covert route in maximising connection probability subject to strict covertness criteria imposed by the eavesdropper. We also demonstrate the efficacy of this route optimisation framework with its application to a 'real-world' covert multihop routing problem.

This research offers the following contributions:

1. we develop a continuum model to determine the end-to-end covert connection probability of a multihop wireless communications network;
2. we apply the model to find an analytic solution for the connection-optimal relay locations when the network is subject to an eavesdropper at a known location;
3. the efficacy of the framework is verified by considering the selection of relay nodes from a large-scale discrete network.

The main contents of this chapter are being prepared for submission for possible publication in *IEEE Transactions on Communications*.

- **Chapter 7** discusses the conclusions and potential future research.

Note that most nomenclature and mathematical notations are independently defined and used in each chapter for clarity. Further, most of the analytical results given throughout this thesis are derived manually or with the help of Mathematica$^{\text{TM}}$. Numerical results are generated by Monte Carlo simulations via MATLAB$^{\text{TM}}$.

2
Modelling Fundamentals

2.1 Pairwise Wireless Connectivity Modelling

We firstly introduce the basic connectivity functions relating to the direct wireless link between a transmitting node and a receiving node; we refer to this as 'pairwise connectivity'.

We consider the connectivity between a transmitter node and receiver node located at fixed points $\mathbf{p}_i$ and $\mathbf{p}_j$ respectively, where $\mathbf{p}_i, \mathbf{p}_j \in \mathbb{R}^2$; this is equally applicable to $\mathbb{R}^3$. It should be noted that, throughout this thesis, we use $\mathbf{p}_i$ to represent both the node entity and its location vector interchangeably and use the subscripts $i, j \in \mathbb{Z}^+$ as a convenient mechanism for node indexing.

2.1.1 Pathloss

We consider a node $\mathbf{p}_i$ transmitting an RF signal with power P_t via an antenna with gain G_t, in the direction of the receive node $\mathbf{p}_j$. The effective-isotropic-radiated-power (EIRP) is then simply given by $P_t G_t$. Similarly, the receiver node has an antenna with gain G_r, in the direction of the transmit terminal. Under idealised line-of-sight (LoS) conditions, the received power at the receiver's antenna terminal P_r is given by the Friis transmission equation [156]

$$P_r = P_t G_t G_r \left(\frac{\lambda}{4\pi r_{ij}} \right)^2, \tag{2.1}$$

where λ denotes the wavelength of the RF transmission and $r_{ij} = \|\mathbf{p}_j - \mathbf{p}_i\|$ denotes the Euclidean distance between transmitter and receiver terminals. Note that we consider an idealised LoS condition to mean 'free-space' in the direct path between transmitter and receiver terminals, i.e. no additional obstacles introducing attenuation of the RF signal, and no secondary paths introduced through signal reflections.

In reality, the propagating electromagnetic wave will have some degree of interaction with its environment [157] and a true LoS path is difficult to achieve without highly directive antennas since the RF signal may be subject to reflections from buildings around the transmitter and receiver terminals and the ground. This will, in part, give rise to signal fading in the propagation channel. Furthermore, in more

realistic propagation conditions such as encountered within urban environments, the propagation loss no longer scales with squared distance and it is not uncommon for researchers, e.g [158–160], to modify the Friis equation to include the pathloss exponent parameter η, such that (2.1) becomes

$$P_r = P_t G_t G_r \left(\frac{\lambda}{4\pi}\right)^2 r_{ij}^{-\eta}, \tag{2.2}$$

where $\eta \geq 2$.

2.1.2 Channel Fading

Channel fading occurs in any propagation environment subject to multipath [161] and where there may be movement of elements within the radio communications network and/or within the local environment giving rise to temporal fading. This may include the transmitter or receiver positions, or in the elements that give rise to the reflections, [162] provides an overview of fading mechanisms. For mathematical tractability, we consider slow, flat, Rayleigh fading in this thesis, which is often used to model fading in urban environments where there is typically no direct line-of-sight path (NLoS) between transmitter and receiver and where the environment is rich in scatterers, yielding many independent paths [161]. The term 'slow', in the fading context, refers to the channel coherence time being significantly greater then the time over which the transmission occurs, i.e. the propagation channel is considered to be temporally stationary. The term 'flat' refers to the coherence bandwidth of the propagation channel being significantly greater than the modulation bandwidth of the transmission, i.e there is no frequency selective fading. With a sufficient number of independent multipaths, with uniformly distributed phase between them, the central limit theorem [163] holds and we model the channel fading, between arbitrary points $\mathbf{p}_i$ and $\mathbf{p}_j$, as the complex sum of two zero mean Gaussian random variables with variance σ_F^2, i.e. $h_{ij} \sim \mathcal{CN}(0, \sigma_F^2)$, where the amplitude $|h_{ij}|$ has a Rayleigh distribution. Since we typically concern ourselves with power gain over the propagation channel, we consider $|h_{ij}|^2$ which will have an exponential distribution, i.e. $|h_{ij}|^2 \sim \exp(\sigma_F^2)$, where $\sigma_F^2 = \mathbb{E}[|h_{ij}|^2]$. In what follows, we assume

the expectation of the power fading variable to be 1. Therefore our Rayleigh fading simplifies to $|h_{ij}|^2 \sim \exp(1)$. This fading assumption has been used widely in previous literature, e.g. [159, 164, 165].

It should be noted that alternative fading models can be employed, e.g. Rician or Nakagami-m [161, 166], where a LoS path does exist. However, this will impact mathematical tractability. Since, in this thesis, we primarily concern ourselves with the problem of optimal routing in large scale wireless networks, the consideration of more complex fading models is considered to be out of scope, deferred to a possible future research direction.

2.1.3 Pairwise Connectivity Model

Combining the fading variable to (2.2) yields

$$P_r = P_t G_t G_r |h_{ij}|^2 \left(\frac{\lambda}{4\pi}\right)^2 r_{ij}^{-\eta}. \tag{2.3}$$

We consider a connection is possible between a transmitter $\mathbf{p}_i$ and receiver $\mathbf{p}_j$, when the signal-to-noise ratio at the receiver (SNR_r) exceeds a threshold τ. It is convenient to consider SNR_r as this has a direct bearing on channel capacity, i.e. information rate, as defined by Shannon-Hartley theorem [167]

$$C = B \log_2(1 + \mathrm{SNR}_r), \tag{2.4}$$

where B and C denotes channel bandwidth and channel capacity, respectively. Denoting the receiver's thermal noise power (variance) by N_o, then SNR_r will be given by

$$\mathrm{SNR}_r = \frac{P_t G_t G_r}{N_o} |h_{ij}|^2 \left(\frac{\lambda}{4\pi}\right)^2 r_{ij}^{-\eta}. \tag{2.5}$$

Note, that we assume that the noise contribution due to the receiver's noise figure [168] is included in N_o, where

$$N_o = 10^{(F/10)} k T_o B, \tag{2.6}$$

and k, T_o and F denote Boltzman's constant (2.38×10^{-23} J/K), temperature (typically 230K representing average room temperature) and the noise figure of the receiver in dB, respectively.

The introduction of the fading variable $|h_{ij}|^2$, yields a probabilistic connection model, hereafter we refer to as a 'soft' connection model, where the probability of establishing a pairwise connection, denoted by H_{ij}, is given by [169]

$$\begin{aligned} H_{ij} &= \mathbb{P}[\mathrm{SNR}_r \geq \tau] \\ &= \mathbb{P}\left[\frac{P_t G_t G_r}{N_o}|h_{ij}|^2\left(\frac{\lambda}{4\pi}\right)^2 r_{ij}^{-\eta} \geq \tau\right] \end{aligned} \tag{2.7}$$

Rearranging (2.7) gives

$$H_{ij} = \mathbb{P}\left[|h_{ij}|^2 \geq \frac{\tau N_o}{P_t G_t G_r}\left(\frac{4\pi}{\lambda}\right)^2 r_{ij}^{\eta}\right]. \tag{2.8}$$

Since $|h_{ij}|^2 \sim \exp(1)$, the complementary cumulative distribution function (CCCD) for $|h_{ij}|^2$ is given by $\mathbb{P}[|h_{ij}|^2 \geq x] = \exp(-x)$. Therefore (2.8) becomes

$$H_{ij} = \exp\left(-\frac{\tau N_o}{P_t G_t G_r}\left(\frac{4\pi}{\lambda}\right)^2 r_{ij}^{\eta}\right). \tag{2.9}$$

For convenience, we introduce parameter r_o to represents the maximum distance over which a pairwise connection is possible in the absence of fading (i.e. $|h_{ij}|^2 = 1$). We refer to this distance as the 'hard' connection distance and is given by

$$r_o^{\eta} = \frac{P_t G_t G_r}{\tau N_o}\left(\frac{\lambda}{4\pi}\right)^2 \tag{2.10}$$

As we progress, we find it useful to normalise distances to this hard connection distance such that (2.9) simply becomes

$$H_{ij} = \exp(-s_{ij}^{\eta}), \tag{2.11}$$

where the normalised distance $s_{ij} = r_{ij}/r_o$. We illustrate this soft connection function, for a range of pathloss exponents, in Figure 2.1.

This soft pairwise connection model has been used in many works including [170, 171] where it was applied to modelling connectivity of geometrically bounded wireless networks, as we discuss further in section 2.2.2.

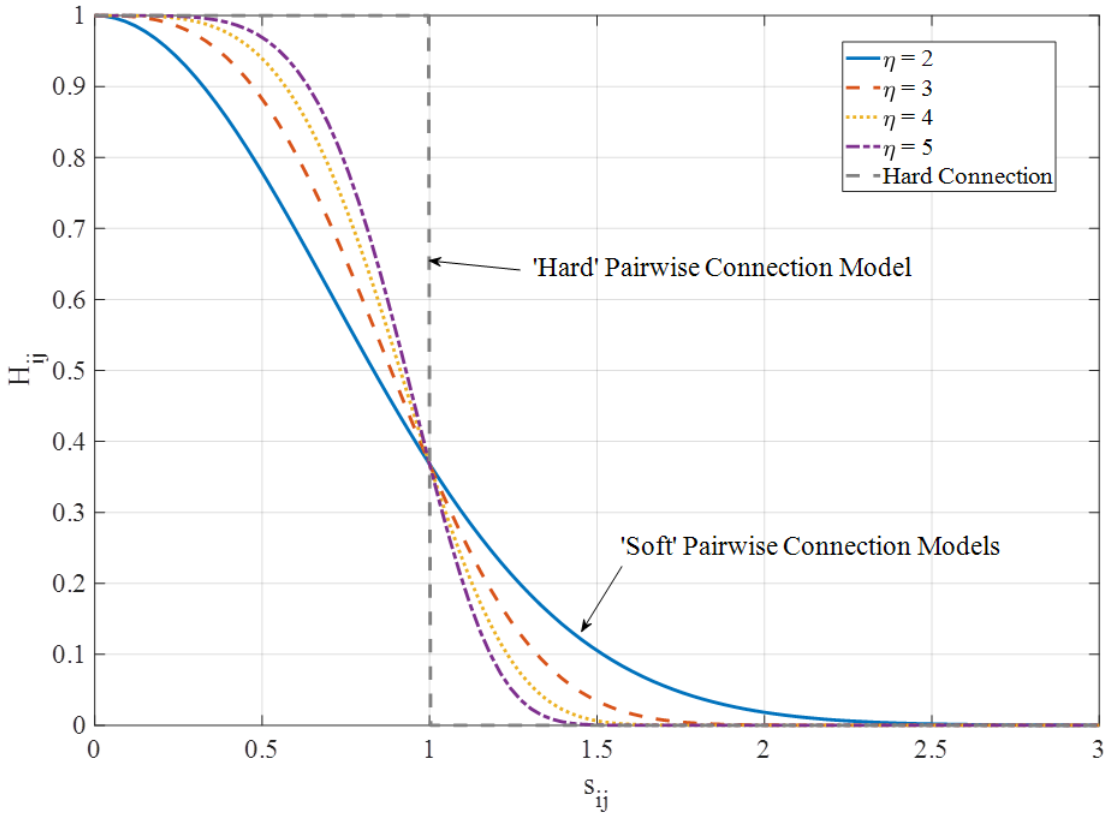


Figure 2.1: 'Hard' and 'Soft' pairwise connection functions for varying pathloss exponents, $\eta \in \{2, 3, 4, 5\}$.

2.1.4 Justification for modelling with square law pathloss and Rayleigh fading

Thoughout much of our research, we specifically employ a square law path loss model and Rayleigh fading, despite realistic propagation environments (e.g. urban) being subject to pathloss exponents $\eta > 2$ and more complex fading characteristics. Our justification is on the grounds of mathematical tractability in that much of the analysis can yield closed form expressions for performance metrics which can be more insightful in terms of the parametric behaviour within the analytical models. For the case $\eta \neq 2$, we find the analysis requires numerical approaches where closed form expressions are either unwieldy or do not exist. This then loses the aforementioned behavioural insight. This does not mean that analysis cannot be undertaken for different, and more complex propagation environments, and we

consider this subject to further work beyond this thesis. However we do provide behavioural insights within our conclusions.

2.2 Network Inhomogeneities

Firstly, let us consider a multihop relay network in a uniform infinite network of relay nodes with finite spatial density and where there is sufficient RF resources to avoid co-channel interference. If a performance metric was purely linked to hop distances, e.g. connection probability which has a strictly decreasing monotonic relationship with Euclidean distance (see section 2.1.3), then it is intuitive that the multihop path of shortest overall distance will yield optimal performance. In reality, however, wireless networks are not infinite and RF resources are finite. 'Real-world' scenarios can often be considered to be geometrically bounded, e.g. a city can be considered to have an approximate circular geometric boundary where nodes outside of the city can be largely ignored.

In analysing the connectivity between nodes, either directly or via multiple hops, in dense wireless networks, the transmit power, interference and spatial distributions of the nodes are critical factors to consider. Following the rationale described in the preceding sections, a transmitters power needs to be high enough to reach its intended destination while generating minimum interference to other receivers in the network sharing the same frequency channel. This yields an optimisation problem where we need to balance connectivity performances across multiple users.

The following sections expand on the network inhomogeneities, pertinent to our research, and introduce analytical tools that provide mathematical tractability in their analysis.

2.2.1 Interference

In Chapter 1, our future gazing 1.2 described a trajectory of increasing densification of wireless devices, greater heterogeneity and network coexistence. Against the backdrop of spectrum exhaustion, often referred to as 'spectrum crunch' [172, 173], co-channel interference poses a significant challenge in meeting the demands of

future wireless networks. Researchers continue to look for novel solutions to meet these demands, e.g [174–176] advocating greater use of mmWave spectrum, use of successive interference cancellation (SIC) techniques and the latter taking a holistic view to interference management in ultra dense wireless networks.

In the design of a wireless communications network, we consider both the impact of interference generated by our network to third party networks, and visa-versa, typically in relation to the degradation in their respective qualities of service. From (2.3) it is clear that interference will follow an exponential decay in power level with respect to distance from the point of transmission. Therefore, the performance of a network will have a spatial dependence upon the relative location of interfering sources and the locations of receivers within the networks, [177] serves to highlight this spatial dependence with the analysis of network connectivity and coverage in an interference limited system.

Multihop networking can provide another mechanism to mitigate co-channel interference, as we demonstrate in the following trivial example, illustrated in Figure 2.2. We consider two methods of communicating between source and destination node: via direct path or via a multihop path comprising N-relay hops. For analytic convenience we locate the relays on a semicircle, centred at point A (the point of bisection of the straight line between source and destination) and having uniform angular spacing. We assume that all pairwise connections are subject to independent Rayleigh fading and pathloss exponent η. We also assume that all relays use the same frequency channel and employ in-band full duplex (IBFD) [178] to avoid self-interference.

Further, we denote the interference power at location A, for the direct communication and N-hop relays paths, by $\mathcal{I}_D$ and $\mathcal{I}_R$ respectively. We now consider the scenario where the end-to-end connection probability of the two communication paths are identical; in the N-hop relay path, we reduce the transmit power to account for the reduced distance between adjacent nodes. Using (2.3) and (2.9), and evaluating expectations, it can be shown that the ratio of expected interference,

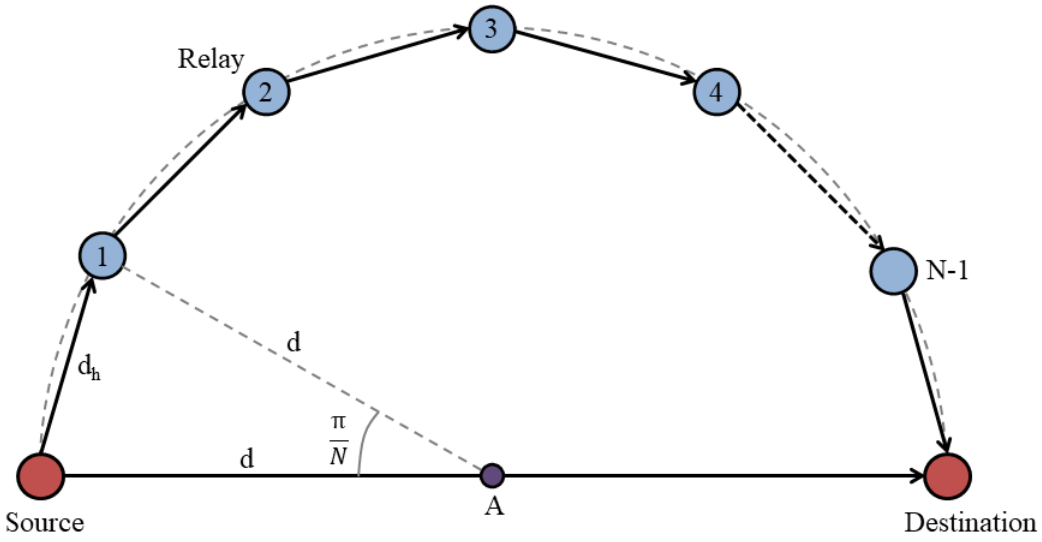


Figure 2.2: Illustration of N-hop relay network.

between the multihop network and the direct path, is given by (see Appendix A.1),

$$\mathcal{R}_{\mathcal{I}} := \frac{\mathbb{E}[\mathcal{I}_R]}{\mathbb{E}[\mathcal{I}_D]} = N^2 \left[\sin\left(\frac{\pi}{2N}\right) \right]^{\eta}, \tag{2.12}$$

where $\mathbb{E}[\cdot]$ denotes the expectation operator. Figure 2.3 illustrates (2.12) on a log-log scale, for convenience, over the set of pathloss exponents $\eta \in \{2, 2.5, 3, 4\}$. For the special case $\eta = 2$, it is straightforward[1] to show that $\mathcal{R}_{\mathcal{I}}$ asymptotically approaches $\pi^2/4$, in the limiting case $N \to \infty$. Clearly in this special case, there is disadvantage to employing multihop networking from a interference perspective. However, with higher pathloss exponents, which typically characterise urban environments for example, significant reduction in interference can be realised with increasing numbers of hops. We consider this further, in a covert communications context, in Chapter 6.

[1]Taking the limiting case, $N \to \infty$, of the Taylor series expansion of (2.12)

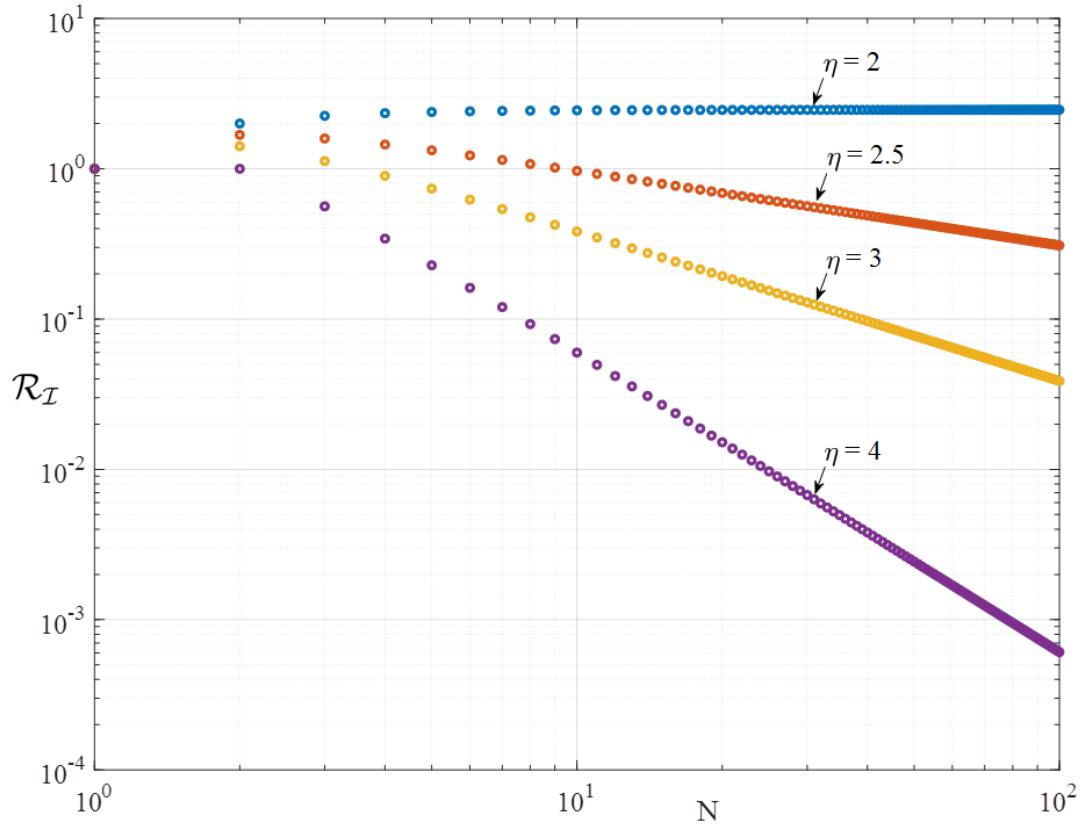


Figure 2.3: Ratio of expectations of interference level with increasing number of multipath hops.

2.2.2 Geometric Boundary Effects

For mathematical tractability, early researchers considered connectivity in multihop networks of infinite extent, i.e. networks that are not constrained by a geometric boundary, typically the $\mathbb{R}^2$-plane. For example, in [179], the authors developed power scaling laws, balancing connectivity and interference, for 'full-connectivity' in the network, i.e. there exists at least one reliable multihop path connecting every two nodes in the network. Similarly, in [180], the authors considered full-connectivity from the perspective of the minimum number of nearest neighbour nodes required to achieve it. In reality, wireless networks can be considered to have finite geometric boundaries, e.g. a city boundary, beyond which the density of wireless devices may be assumed to be zero or negligible in the mathematical analysis of network performance. In a uniform network of infinite extent, one would expect that connectivity performance would exhibit translation invariance over the

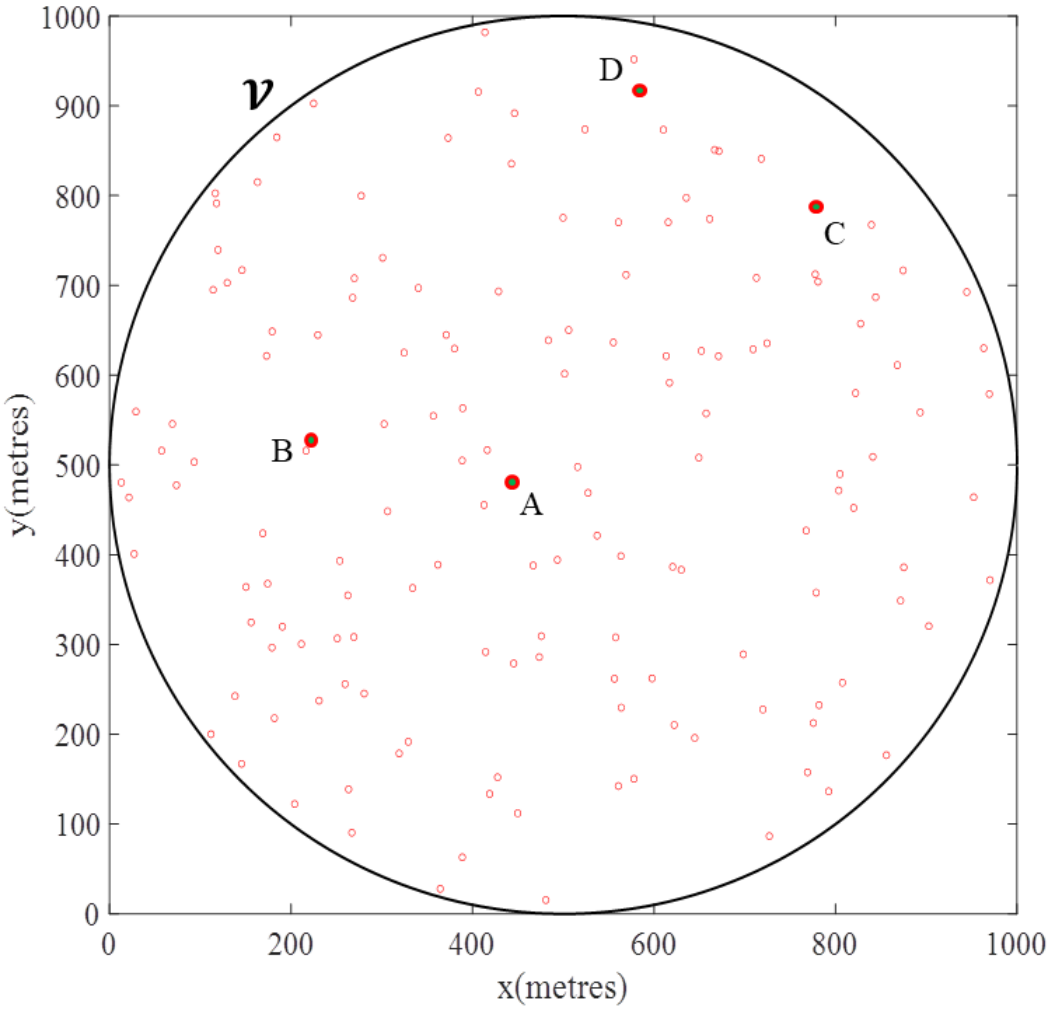


Figure 2.4: Illustration of a uniform random distributed of relay nodes within a circular geometrically boundary.

network; this is not the case, when we impose a geometric boundary. We provide an intuitive explanation for this in the following example. With reference to Figure 2.4, we consider the uniform spatial distribution of relay nodes constrained to a circular geometric domain $\mathcal{V} \in \mathbb{R}^2$. Within this domain, we consider two pairs of nodes that wish to communicate, via an intermediate relay node, forming a simple 2-hop path: $A \to B$ and $C \to D$, located towards the centre of the domain and the domain boundary respectively. It is intuitive that the probability of establishing a multihop path for the communication $A \to B$ is greater than that for $C \to D$ due to the increased local 'mass' of relays close enough to provide a viable 2-hop connection. The notion of 'mass' or 'connectivity mass' was introduced in [170] and, for the

uniform spatial distribution of relay nodes, is defined by the function

$$M_i = \rho \int_{\mathcal{V}} H_{ij} \mathrm{d}\mathbf{p}_j, \tag{2.13}$$

where M_i denotes the connectivity mass at location $\mathbf{p}_i$, H_{ij} is the pairwise connectivity function between nodes $\mathbf{p}_i$ and $\mathbf{p}_j$, e.g. (2.9), and ρ denotes the density of nodes (nodes per unit area) within domain $\mathcal{V}$. It is worth noting that the integral can be considered as the 'connectivity volume'. This notion was used widely in a number of subsequent works, including [181] which considered connectivity of soft random geometric graphs in a unit square and [182] analysing connectivity in more complex scenarios involving non-convex domains with reflections and small openings. Further evidence, demonstrating that boundary effects have a significant impact on the network connectivity properties, can be found in [158] and [183]; the former considering the effect of randomly oriented directive (anisotropic) antennas on network connectivity in infinite and bounded 3D ad-hoc networks and the latter considering the border effects in interference limited ad-hoc networks.

As a preliminary step, we begin our research in Chapter 3, deriving closed form expressions for the average connection probability of 2-hop (single relay) connectivity in uniform networks constrained by circular, square and rectangular geometric boundaries.

2.3 Stochastic Geometry for Network Modelling

As wireless networks have evolved from macro-cell to small-cell network architectures [27], the complexity associated with analysing network performance modelling has become significantly more complex [184, 185]. This is further exacerbated by the exponential increase in users, with each network evolution, and the finite RF spectrum resources that need to be shared across the network. As shown in previous sections, the performance of wireless systems depends strongly on the geometric locations of transmitting, receiving and co-channel interfering nodes. Since the locations of these nodes are subject to considerable uncertainty, we call upon tools from the field of stochastic geometry to predict network performance. Stochastic

geometry allows us to study the average behaviour of wireless networks according to some random point process or processes [160], and references therein. A point process (PP) $\Phi = \{\mathbf{X}_i, i \in \mathbb{N}\}$ is a random collection of points that reside in a measure space. Within this work, we consider bounded spaces within the Euclidean plane $\mathbb{R}^2$, since, in our applications, the points typically represent the locations of wireless nodes in the 'real-world'. It should be noted that point processes can be equally applied to the general Euclidean space $\mathbb{R}^n$ or other non-Euclidean spaces, e.g. the surface of the Earth.

The following subsections introduce the basic theory of point processes, focusing on the binomial point process (BPP) and the Poisson point process (PPP). We also introduce two theorems that allow us to determine the expectation of the sum and product of functions of the point processes.

2.3.1 Binomial Point Process

Within a space $S \subset \mathbb{R}^2$, we consider a point process, denoted by Φ_B, comprising N i.i.d. points uniformly spatially distributed over S. This is illustrated in Figure 2.5, where S is a bounded space, of dimensions 1km x 1km, containing 100 points.

If we let $A \subset S$, the number of points located within A, denoted by $\Phi_B(A)$, follows a binomial probability mass function i.e.

$$\mathbb{P}[\Phi_B(A) = k] = \binom{N}{k} \left(\frac{|A|}{|S|}\right)^k \left(1 - \frac{|A|}{|S|}\right)^{N-k}, \tag{2.14}$$

where $|\cdot|$ denotes the area, or more generally, the Lebesque measure in alternative Euclidean spaces. $\binom{N}{k}$ denotes the 'choose' function, i.e. the binomial coefficient.

A uniform BPP is typically employed to model finite wireless networks, where the exact number of wireless nodes is known. For example, [186] considered a geometrically bounded network and applied a BPP to analyse the effect of co-channel interference to an arbitrarily located reference receiver. This work demonstrated that the performance is location dependent where the aggregate interference seen at the centre of network is different from that at the network boundary. In [187] the authors applied a uniform BPP to analyse a 3-D network

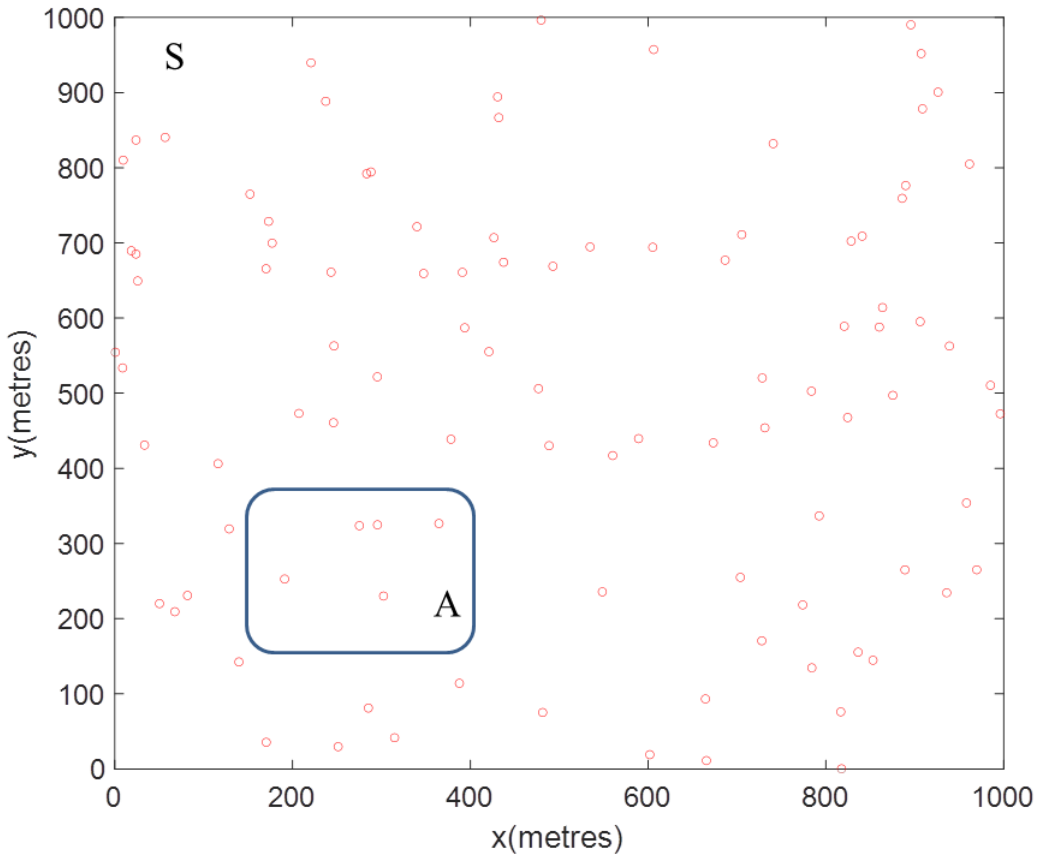


Figure 2.5: Illustration of 100 points generated by uniform BPP.

of unmanned aerial vehicles (UAV), deriving the downlink coverage probability of a reference receiver located at an arbitrary position on the ground assuming Nakagami-m fading for all wireless links. More recently, with the increasing interest in dense Low-Earth-Orbit (LEO) satellite constellations, academics are turning to point processes to provide performance insights. For example, [188] analysed coverage probabilities, achievable data rates and contact distance distributions over an ultra-dense LEO constellation using a BPP.

The principle disadvantages of employing the BPP is the need for prior knowledge of numbers of nodes within a wireless network and the analytical complexities that arise from boundary effects in finite wireless networks. In most cases the number of nodes is often not known and networks are characterised by their node densities. Furthermore, many networks can be considered large enough where boundary effects can be largely ignored or considered negligible within the analysis.

2.3.2 Poisson Point Process

The homogeneous (uniform) Poisson point process (PPP) is characterised by the density of nodes (points). If a homogeneous PPP, denoted by Φ_P, has density λ, then the number of points in any bounded set $A \subset \mathbb{R}^2$ has a Poisson distribution with mean $\lambda|A|$, i.e.

$$\mathbb{P}[\Phi_P(A) = k] = \frac{(\lambda|A|)^k}{k!} \exp(-\lambda|A|). \tag{2.15}$$

Further, the numbers of points in disjoint subsets of S are independent.

Examples of the use of the homogeneous PPP include [189], where the authors applied a homogeneous PPP to determine the pairwise node distance distributions in geometrically bounded wireless network and [190] applying the homogeneous PPP to determine the coverage probability of a bounded wireless networks as a function of the location of an access point (AP).

In many 'real-world' scenarios the node density is not uniform; for example, a shopping centre may have a much higher local density of mobile phones than a park. To account for this inhomogeneity, we consider a location dependent intensity function $\lambda(\mathbf{x})$, where vector $\mathbf{x}$ denotes the location and equation 2.15 becomes

$$\mathbb{P}[\Phi_P(A) = k] = \frac{(\Lambda(A))^k}{k!} \exp(-\Lambda(A)), \tag{2.16}$$

where

$$\Lambda(A) = \int_A \lambda(\mathbf{x}) \mathrm{d}\mathbf{x}. \tag{2.17}$$

2.3.3 Expectation of Sum of Functions over PPP

Often we require the expectation of the summation of functions of the locations of nodes within a wireless network. For example, the aggregation of co-channel interference at a receiver can often dominate the performance of the receiver [190]. Let Φ_P denote a homogeneous PPP, $\mathbf{x} \in \Phi_P$ and let $u(\mathbf{x}) : \mathbb{R}^d \to \mathbb{R}^+$ be a real-valued function of $\mathbf{x}$, then the sum of this function over the PPP is $\sum_{\mathbf{x}\in\Phi_P} u(\mathbf{x})$.

Over a measure space A, the expectation of this sum is given by Campbell's theorem [191], which can be written as

$$\mathbb{E}\Bigg[\sum_{\mathbf{x}\in\Phi_p} u(\mathbf{x})\Bigg] = \lambda \int_A u(\mathbf{x})\mathrm{d}\mathbf{x}. \tag{2.18}$$

For the inhomogeneous case, with location dependent intensity function $\lambda(\mathbf{x})$, we have

$$\mathbb{E}\Bigg[\sum_{\mathbf{x}\in\Phi_p} u(\mathbf{x})\Bigg] = \int_A \lambda(\mathbf{x})u(\mathbf{x})\mathrm{d}\mathbf{x}. \tag{2.19}$$

2.3.4 Expectation of Product of Functions over PPP

For a homogeneous PPP Φ_P, $\mathbf{x} \in \Phi_P$ and let $v(\mathbf{x}) : \mathbb{R}^d \to [0, 1]$ be a real-valued function of $\mathbf{x}$, then the expectation of the product of this function over the PPP is given by the probability generating functional of the PPP

$$\mathbb{E}\Bigg[\prod_{\mathbf{x}\in\Phi_p} v(\mathbf{x})\Bigg] = \exp\Bigg(-\lambda \int_A [1 - v(\mathbf{x})]\mathrm{d}\mathbf{x}\Bigg). \tag{2.20}$$

For the inhomogeneous case, with location dependent intensity function $\lambda(\mathbf{x})$, we have

$$\mathbb{E}\Bigg[\prod_{\mathbf{x}\in\Phi_p} v(\mathbf{x})\Bigg] = \exp\Bigg(-\int_A \lambda(\mathbf{x})[1 - v(\mathbf{x})]\mathrm{d}\mathbf{x}\Bigg). \tag{2.21}$$

2.4 Large Scale Networks and Modelling

Thus far, we have introduced some of the 'real-world' challenges associated with wireless communications, either direct source-to-destination or via a multihop relay network. Since the sources of network inhomogeneities have a spatial dependence, we find ourselves with a challenging optimisation problem in the determination of the most appropriate selection of relays to provide a multihop route through the network.

The majority of previous works that consider multihop connectivity are typically in the context of wireless sensor networks (WSN) or cellular networks, e.g. [192–197] and references therein. In most of these works, the design goal is to optimise some network performance metric, such as connection probability, coverage, data throughput or latency for example, and/or a non-functional metric such as data

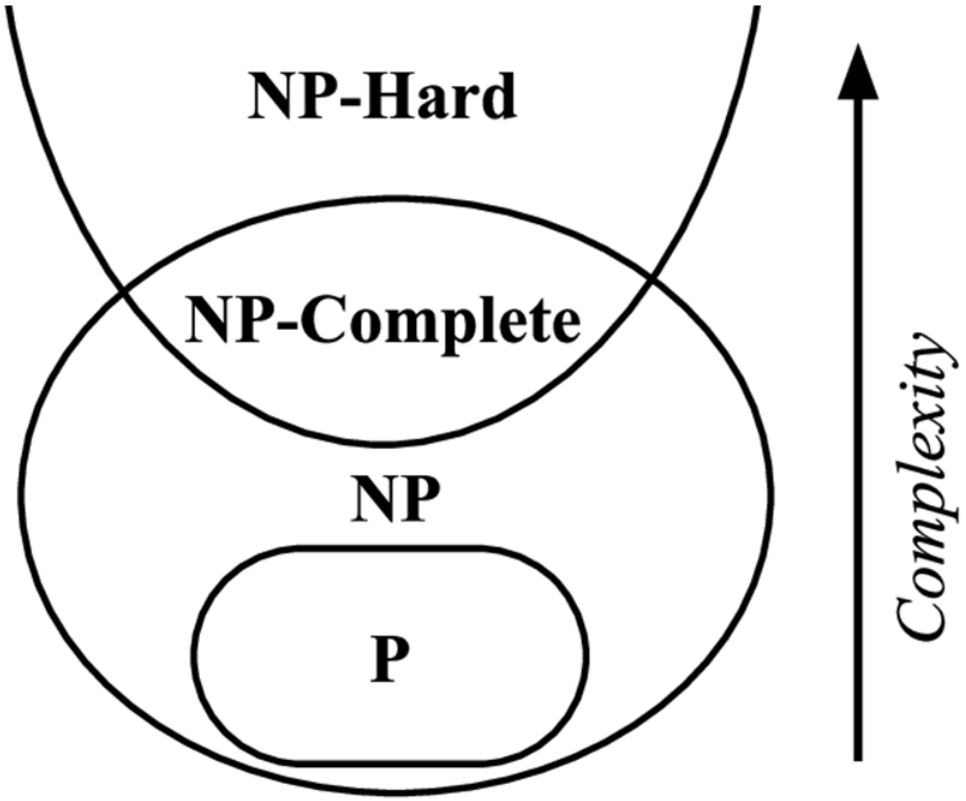


Figure 2.6: Characterisation of Processing Complexity.

integrity. These optimisation challenges are often further compounded by constraints such as total energy consumption or monetary budget, for example. In the multihop context, these problems are often referred to as the relay node placement problem (RNPP), where the objective typically relates to the deterministic placement of the minimum number of relay nodes that meet the design objective(s) as optimally as possible.

Given our research interests lie in developing novel approaches to solving relay node placement problems, we find it convenient to characterise the efficacy of our approach in the form of complexity or relative complexity against a known baseline. As a slight digression; but nonetheless useful in quantifying this complexity, computer science tools from computational complexity theory [198, 199] are often applied to characterise the complexity of a computational problem. Figure 2.6 illustrates the various classes of complexity.

We begin with the concept of polynomial time, which is the time required for a computer to solve a problem, where this time is a simple polynomial function of the size of the input, e.g. the number of relays nodes. If the computation time is strictly dependent upon the size of the input only, it is said to be deterministic polynomial time (denoted by P in the figure). Class NP consists of all those problems whose solution can be found in polynomial time on a non-deterministic Turing machine[2]. Since such a machine does not exist, practically it means that an exponential algorithm can be written for an NP-problem, nothing is asserted whether a polynomial algorithm exists or not. Solving a 'Sudoku' puzzle is an example of an NP problem. A subclass of NP, class NP-complete includes problems such that a polynomial algorithm for one of them could be transformed to polynomial algorithms for solving all other NP problems. Finally, the class NP-hard can be understood as the class of problems that are NP-complete or harder. NP-hard problems have the same trait as NP-complete problems but they do not necessarily belong to class NP, that is class NP-hard includes also problems for which no algorithms at all can be provided.

In many scenarios, the RNPP has been proven to be NP-hard or NP-complete [200–204], even with a relatively low number of relays. In these scenarios, the processing complexity is often unwieldy or impractical; particularly for implementation on the lower power microcontrollers discussed in section 1.1.3. The RNPP has been extensively researched and a common theme is that researchers look towards heuristic or meta-heuristic algorithms to solve it [205–207]. Heuristic algorithms deliver reasonably good solutions, albeit non-optimal, in a reasonable time; [208] provides a general review of heuristic approaches and applications and survey papers [192, 209], with references therein, provides an overview of heuristic strategies and techniques for node placement in wireless sensor networks. Two key observations can be made from prior research relating to the utility of heuristics: the appropriateness and practicality of the heuristic solution is very much dependent upon the problem scenario and that processing efficiency of the routing algorithm is traded against

[2]a general model of a computing machine that has the ability to make correct guesses

the optimality of the final solution. If the sub-optimality is acceptable then the low complexity of the heuristic solution is clearly attractive; with some heuristic processes can approach a linear scaling [210], clearly attractive for systems where computational capability is limited. In [211], the authors provide a comprehensive study of cooperative routing strategies in relay based wireless networks, expanding on the trade-off between computational complexity and routing optimality.

As wireless networks increase in size, the emergence of software defined networking (SDN) [212] may offer attractive solutions to solve challenging management issues in large-scale multi-technological networks [213,214] with [215,216] suggesting the use of SDN in a multihop routing context.

Our research interests focus on finding exact, or as close to exact as possible, methods to obtain optimal solutions that guarantee their optimality with processing complexities that match that achieved with heuristic techniques. In our subsequent research, described in chapters 5 and 6, we consider scenarios where we determine the multihop route, or routes, that yield extrema in some given performance functional. To provide a suitable baseline, for comparison of processing complexity, Lagrangian optimisation is described in Appendix A.2 which shows a processing complexity that scales like $O(N^3)$, assuming a standard algorithm such as Gaussian elimination is employed for matrix inversion [217]. The cubic scaling can be improved by using state-of-the-art algorithms, e.g. Coppersmith−Winograd [218], to approximately $O(N^{2.4})$. Even with these algorithms, however, it is clear that, for large numbers of relays as in our work, the discrete optimisation of relay locations presents a potentially unwieldy processing task.

The following section introduces variational calculus, a field of mathematics that underpin a new and novel approach to solving this multihop route optimality problem.

2.4.1 Variational Calculus

Calculus is concerned with the analysis of rates of change of quantities, i.e. differential calculus or differentiation, and the summation of infinitely many small quantities

to determine some whole, i.e. integral calculus or integration. This is a staple of undergraduate mathematics and is typically applied to the analysis of real-valued functions, although this does extend to the analysis of functions of complex values.

Variational calculus, or calculus of variations [219], is concerned with the analysis of rates of change (variation) of functions or functionals, taking the typical form

$$f \mapsto I[f] = \int_{\Omega} H[x, f(x), \dot{f}(x), \ddot{f}(x), ...]\mathrm{d}x, \tag{2.22}$$

where $\dot{f}(x)$ and $\ddot{f}(x)$ denote the first and second derivative of $f(x)$ with respect to x, and so on. A classic example, and one of the earliest, of the application of variational calculus is the problem posed by Johann Bernoulli 1696 relating to the curve of fastest descent, more commonly referred to as the Brachistochrone problem [220]. In short, the problem posed relates to the determination of the function of curve, lying on the vertical plane between a point A and a lower point B, on which a bead slides frictionlessly under the influence of a uniform gravitational field from point A to B. This is depicted in figure 2.7. Assuming the bead starts with zero initial velocity, then the time for the bead to travel along a curve defined by the function $f := f(x)$ is given by the functional

$$T[f] = \int_{a}^{b} \sqrt{\frac{1 + \dot{f}^2}{-2gf}}\mathrm{d}x. \tag{2.23}$$

Determining the function f that yields the fastest descent, i.e. the stationary path, is given by the Euler Lagrange equation.

2.4.1.1 Euler Lagrange Equation

For the functional of the form

$$I[f] = \int_{\Omega} H[x, f(x), \dot{f}(x)]\mathrm{d}x, \tag{2.24}$$

the stationary function f is determined by solving the Euler Lagrange equation [219]

$$\frac{\partial H}{\partial f} - \frac{\mathrm{d}}{\mathrm{d}x}\left(\frac{\partial H}{\partial \dot{f}}\right) = 0. \tag{2.25}$$

Evaluating (2.25) will generate a differential equation, possibly a non-linear differential equation, that can then be solved to yield the stationary function f. If exact

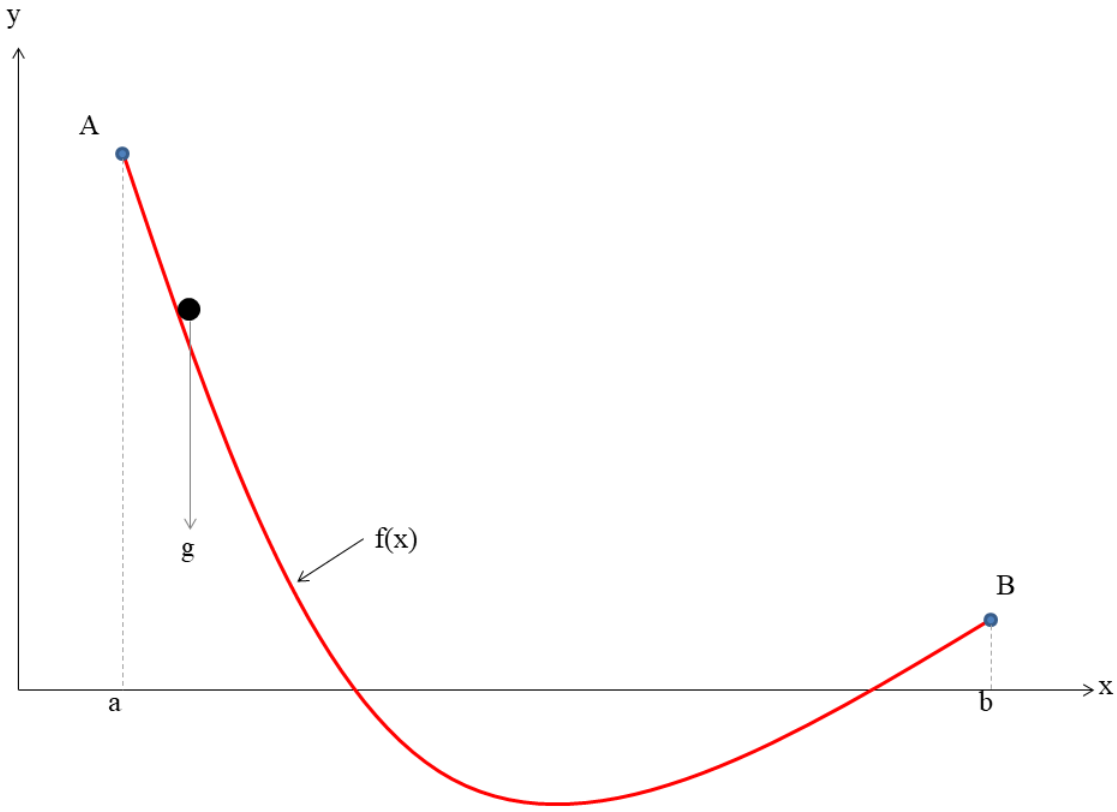


Figure 2.7: Illustration of the Brachistochrone problem.

closed form solutions do not immediately present themselves, numerical techniques can be employed [221], e.g. Euler's method.

2.4.1.2 Beltrami Identity

For the special case where

$$\frac{\partial H}{\partial x} = 0 \tag{2.26}$$

in (2.24) the Euler-Lagrange equation reduces to the Beltrami identity [222]

$$H - \dot{f}\frac{\partial H}{\partial \dot{f}} = C, \tag{2.27}$$

where C is a constant.

2.4.1.3 Legendre-Clebsch Condition

In traditional calculus, we apply the second derivative of a function to determine whether the extremum is a minimum or maximum at the extremum point of the

function. In variational calculus, we apply Legendre–Clebsch condition. This is a second-order condition which a solution of the Euler–Lagrange equation (2.25) must satisfy in order for the function f to be a minima, and is given by

$$\frac{\partial^2 H}{\partial \dot{f}^2} > 0. \tag{2.28}$$

2.5 Summary

In this chapter, we have reviewed a number of important aspects relating to wireless communications, multihop connectivity, spatial inhomogeneities, stochastic geometry and framed the problem of relay node placement in delivering exact solutions to multihop networking problems. Based upon this overview, prior and current research achievements relating to large scale multihop networks, we carry out investigations into the effect of geometric boundaries on 2-hop relay network and progress to model larger scale multihop networks. Our principal research questions can be summarised as follows:

1. How do geometric boundaries affect 2-hop connection probability, between source and destination nodes, via a single relay node selected from a set of uniformly distributed relays with finite density?

2. Can the employment of D2D and 2-hop connectivity, in large scale infrastructure oriented networks, be used as a mechanism to reduce reliance on the fixed network infrastructure?

3. Can we model a large scale multihop network of relay nodes as a 'continuous path' (or continuum) rather than discrete relays?

4. Can we apply variational calculus to the relay node placement problem in delivering exact solutions with low processing complexity i.e. approaching linear complexity scaling as achieved with heuristic algorithms?

5. Can the aforementioned continuum approach be applied to more complex constrained optimisation problem associated with covert multihop communications?

In order to address these five research questions, relevant technical works are presented in the following four chapters in respective order.

3

Two-Hop Relaying in Finite Domains

3.1 Introduction

As we showed in Chapter 2, the connectivity between any two devices, wishing to communicate directly, is governed by their spatial separation, channel fading and a number of other system constants: wavelength, SNR, etc. By allowing the two nodes to communicate via an intermediate node, i.e. forming a 2-hop path, it is possible to increase the communication range and/or connection probability. However, since the intermediate nodes are randomly distributed within the domain, we need to consider their spatial distribution and the distributions of other system variables in order to accurately analyse connectivity performance. Further, in the finite domain, the effects of the domain boundary need to be borne in mind [170] and tools taken from the world of stochastic geometry are often called upon to aid analysis. [223].

In this chapter, we consider the general case of direct (1-hop) and 2-hop connectivity in finite geometrically bounded wireless networks subject to Rayleigh fading and we assume negligible inter-node interference. The consideration of interference is clearly of concern in many applications; however, for this first foray into 2-hop network analysis, we maintain generality by assuming a suitable Medium Access Control (MAC) protocol [152] is employed to ensure interference is prevented.

Previous works that have considered few-hop connectivity in finite domains include [224], which analyses k-hop connectivity using the unit disk model (UDM), and [225], which reports lower and upper bounds for connection probability for 2-hop connectivity in the unit square. The main contribution of this chapter, relative to the state-of-the-art, is the generation of closed form analytic expressions for the direct and 2-hop connection probability between two fixed nodes in circular and rectangular network domains, subject to Rayleigh fading.

The remainder of the chapter is organised as follows. Section 3.2 sets the scene with a system model and details assumptions and constraints. Section 3.3 provides an analysis of the connection probability between two terminal nodes, at fixed locations within finite networks, by considering the special cases of circular and rectangular boundaries. Simple closed form expressions for connection probability are derived. Section 3.4 demonstrates that the asymptotic behaviour of connection

probability, as the domain size increases, tends to the unbounded case in the $\mathbb{R}^2$ plane. We also consider the case of sparse node density and provide simpler closed form approximations and follows with the analysis of connectivity performance at the networks centre and boundary. Section 3.5 takes the results of Section 3.4 and provides further analysis of average connectivity from a fixed location in the network and considers the improvement that 2-hop connectivity yields. Much of the analytical work is validated by Monte-Carlo simulations. Conclusions are detailed in section 3.6.

3.2 Network Definitions and System Model

The network model considered in this chapter is general, but it will become clear that it can be easily applied to a number of scenarios e.g. a D2D cluster where relaying may be employed to maintain low device transmit powers, and thus reduce interference to other cellular devices. However, the model is not limited to any specific case, and thus we abstract our discussion in what follows.

We consider the connectivity between two terminal nodes, node-1 and node-2, at fixed locations, within a finite convex domain $\mathcal{V} \subset \mathbb{R}^2$. Also contained within $\mathcal{V}$, are N identical relay nodes, node-k where $k \in \{3, 4, \ldots, N+2\}$, that are uniformly spatially distributed according to a homogeneous binomial point process (BPP), Φ_B; the node density outside of $\mathcal{V}$ is zero. We denote the location of node-i by the vector $\mathbf{p}_i$ where $i \in I$ and I is the index set $\{1, 2, \ldots, N+2\}$. Hereafter, we use $\mathbf{p}_i$ to represent both node-i and its location interchangeably.

For convenience, we consider a fixed connectivity scale r_0 and, hereafter, normalise all distance variables to this scale. Further, we define r_0 as the hard connection range determined solely by large scale path loss according to the well known modified Friis equation, see section 2.1.3.

$$r_0^{\eta} = \frac{PG_tG_r}{\tau\sigma^2}\left(\frac{\lambda}{4\pi}\right)^2 \tag{3.1}$$

where η is the path loss exponent, τ is the required SNR for signal detection at the receiving node, P is the transmit power, σ^2 represents the thermal noise

variance at the receiving node, G_t and G_r are transmit and receive antenna gains[1] respectively and λ is the wavelength of the RF carrier employed. The receiver performance is assumed to be independent of interference generated by other transmitting nodes in the network.

The direct communication path between any two randomly selected nodes, at locations $\mathbf{p}_i$ and $\mathbf{p}_j$, is considered undirected with reciprocal channel gain and connected with probability $H(r_{ij}) \equiv H_{ij}$ where $r_{ij} = \|\mathbf{p}_i - \mathbf{p}_j\|$. We employ a soft connection model by including a Rayleigh[2] distributed small scale fading component $h_{ij} \sim \mathcal{CN}(0,1)$ which yields a connection probability defined by [169] and described in Chapter 2

$$H_{ij} = e^{-r_{ij}^{\eta}} \tag{3.2}$$

In addition to the direct connection between $\mathbf{p}_1$ and $\mathbf{p}_2$, we allow 2-hop connections to be made via an intermediate node $\mathbf{p}_k \in \Phi_B$, as depicted in Fig. 3.1. For mathematical tractability, we assume that intermediate nodes employ regenerative (decode-and-forward) relaying and the probability of 2-hop connectivity, between $\mathbf{p}_1$ and $\mathbf{p}_2$ via $\mathbf{p}_k$, is given by $H_{1k}H_{2k}$ due to the assumption that the 1-k and 2-k channels are statistically independent[3]. For convenience, we define the average of an observable O (not to be confused with big-O notation in this instance) over all possible spatial configurations of u.i.d. relay nodes by [170]

$$\langle O \rangle = \frac{1}{|\mathcal{V}|^N} \int_{\mathcal{V}^N} O(\mathbf{p}_3, \mathbf{p}_4, \ldots, \mathbf{p}_{N+2}) \mathrm{d}\mathbf{p}_3, \mathrm{d}\mathbf{p}_4, \ldots, \mathrm{d}\mathbf{p}_{N+2} \tag{3.3}$$

3.3 Connectivity Analysis

The probability that fixed nodes $\mathbf{p}_1$ and $\mathbf{p}_2$ can communicate, either directly or via any intermediate node, is given by the complement of the probability that no direct

[1] With constant gain in azimuth i.e. non directional in the $\mathbb{R}^2$ plane

[2] We defer the treatment of more complex fading models to a future research

[3] Although this is not necessarily the case when $\mathbf{p}_i$ and $\mathbf{p}_j$ are located within the coherence distance of each other, it is a standard assumption that has been shown on several occasions to yield accurate results [170].

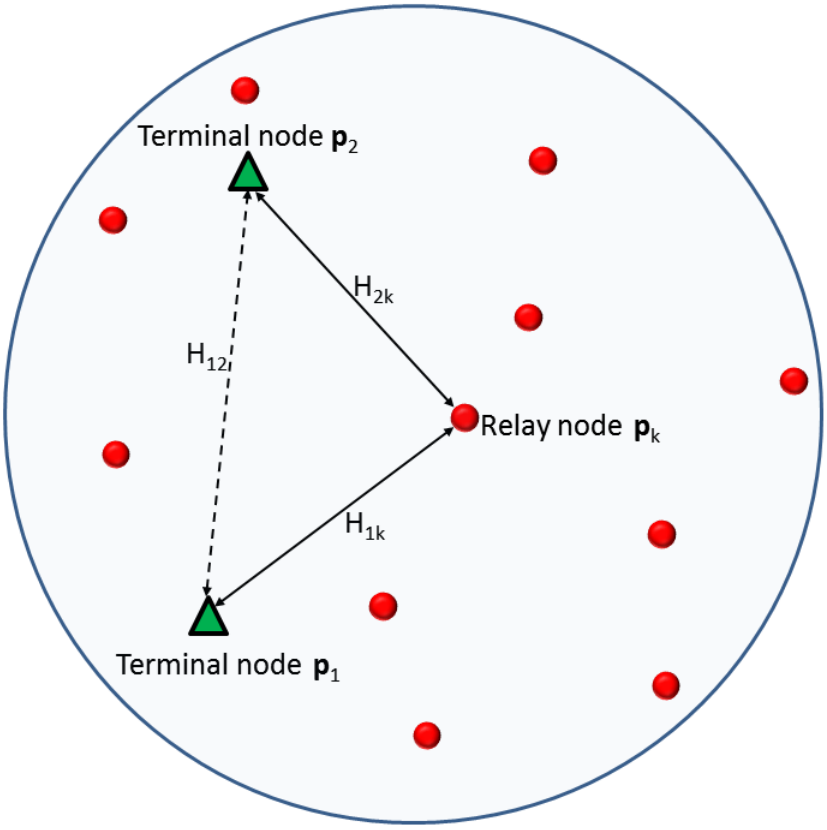


Figure 3.1: Direct and 2-hop connectivity between two terminal nodes, $\mathbf{p}_1$ and $\mathbf{p}_2$, in a finite convex domain $\mathcal{V}$ containing N uniformly distributed intermediate relay nodes $\mathbf{p}_k \in \Phi_B$.

path and no two-hop paths exist and is denoted by $P_{12}^{(1,2)}$, where the superscript denotes 'via 1-hop and/or 2-hop' and is given by

$$P_{12}^{(1,2)} = 1 - (1 - H_{12}) \prod_{\mathbf{p}_k \in \Phi_B} (1 - H_{1k} H_{2k}) \tag{3.4}$$

We now proceed to develop closed form analytic expressions for this connection probability for the bounded network and consider two special cases of finite convex boundary: a circle of radius R and a rectangle of dimension $A \times B$. For comparison we also consider an infinite network in the $\mathbb{R}^2$ plane.

3.3.1 Connectivity in a Finite Domain $\mathcal{V}$

Since the individual pairwise connection probabilities in (3.4) are functions of node locations, we define $\langle P_{12}^{(1,2)} \rangle$ as the connection probability (3.4) averaged over all

locations of intermediate relay nodes over the domain. Since relay node positions are i.i.d. then $\langle P_{12}^{(1,2)} \rangle$ can be simply expressed as

$$\langle P_{12}^{(1,2)} \rangle = 1 - (1 - H_{12})(1 - \langle H_{12}^{(2)} \rangle)^N \tag{3.5}$$

where $\langle H_{12}^{(2)} \rangle$ denotes the average 2-hop connection probability between $\mathbf{p}_1$ and $\mathbf{p}_2$ as defined by

$$\langle H_{12}^{(2)} \rangle = \frac{1}{|\mathcal{V}|} \int_{\mathcal{V}} H_{1k} H_{2k} \mathrm{d}\mathbf{p}_k \tag{3.6}$$

We now solve (3.6) for the two special cases of bounded network.

3.3.1.1 Circular Domain

We employ a polar coordinate system, relative to the centre of the circle of radius R. The Euclidean distance between $\mathbf{p}_i = r_i \angle \phi_i$ and $\mathbf{p}_j = r_j \angle \phi_j$ is given by

$$r_{ij} = \sqrt{r_i^2 + r_j^2 - 2 r_i r_j \cos(\phi_j - \phi_i)} \tag{3.7}$$

and (3.6) becomes

$$\langle H_{12}^{(2)} \rangle = \frac{1}{\pi R^2} \int_0^R \int_0^{2\pi} r_k e^{-(r_{1k}^{\eta} + r_{2k}^{\eta})} \mathrm{d}\phi_k \mathrm{d}r_k \tag{3.8}$$

For mathematical tractability, we consider the case $\eta = 2$ and (3.8) becomes

$$\langle H_{12}^{(2)} \rangle = \frac{2}{\pi R^2} e^{-(r_1^2 + r_2^2)} \int_0^R r_k e^{-2r_k^2} \int_0^{\pi} e^{-2|\overline{\mathbf{p}}_{12}| r_k \cos \phi_k} \mathrm{d}\phi_k \mathrm{d}r_k \tag{3.9}$$

where $\overline{\mathbf{p}}_{12} = (\mathbf{p}_1 + \mathbf{p}_2)/2$ is the mid-point between $\mathbf{p}_1$ and $\mathbf{p}_2$. Evaluation of the inner integral of (3.9) yields

$$\langle H_{12}^{(2)} \rangle = \frac{1}{2R^2} e^{-(r_1^2 + r_2^2)} \int_0^R r_k e^{-2r_k^2} \, \mathrm{I}_0(2|\overline{\mathbf{p}}_{12}| r_k) \mathrm{d}r_k \tag{3.10}$$

where $\mathrm{I}_0(a) = \frac{1}{\pi} \int_0^{\pi} e^{a \cos \theta} \mathrm{d}\theta$ is the zeroth order modified Bessel function of the first kind. It can be shown that evaluating the remaining integral yields the following closed form expression for average 2-hop connection probability in a circular domain

$$\langle H_{12}^{(2)} \rangle = \frac{1}{2R^2} e^{-\frac{1}{2}\|\mathbf{p}_2 - \mathbf{p}_1\|^2} \left[1 - \mathrm{Q}_1 \left(2|\overline{\mathbf{p}}_{12}|, 2R \right) \right] \tag{3.11}$$

where $\mathrm{Q}_1(a,b) = \int_b^\infty x e^{-\frac{(x^2+a^2)}{2}} \mathrm{I}_o(ax)\mathrm{d}x$ is the first order Marcum-Q-function. Substituting (3.11) into (3.5) yields the expected connection probability, between terminal nodes $\mathbf{p}_1$ and $\mathbf{p}_2$, employing direct and 2-hop connectivity.

$\langle H_{12}^{(2)} \rangle$ is clearly governed by the product of two monotonic functions of Euclidean distance, between the terminal nodes, and the position of their mid-point, within the domain $\mathcal{V}$, respectively. Intuitively, the closer the nodes to the domain centre, the higher the probability of connecting to a proximity relay node. Fig. 3.3, with the aid of Fig. 3.2, serves to illustrate the behaviour of (3.11). Note that when nodes lie on the same radial axis (top right panel), the contour of the graph is such that fixing one node and moving another yields improved connectivity up to a maximum before meeting the fixed node, then connectivity reduces. This is further illustrated in Fig. 3.4, where we consider the case $|\mathbf{p}_1| = 0.5$ and the maximum 2-hop connectivity is observed at approximately $|\mathbf{p}_2| = 0.25$. The other (bottom) panels do not exhibit this global maximum since the nodes always move further apart. By equating the first derivative of (3.11) to 0, with respect to r_1, it can be shown that this maximum occurs when the following equality is satisfied for $\Delta\phi < \pi/2$

$$\frac{|\mathbf{p}_2|\cos(\Delta\phi) - |\mathbf{p}_1|}{|\mathbf{p}_2|\cos(\Delta\phi) + |\mathbf{p}_1|} = \frac{\mathrm{Q}_2\left(2|\overline{\mathbf{p}}_{12}|, 2R\right) - \mathrm{Q}_1\left(2|\overline{\mathbf{p}}_{12}|, 2R\right)}{1 - \mathrm{Q}_1\left(2|\overline{\mathbf{p}}_{12}|, 2R\right)} \tag{3.12}$$

where $\mathrm{Q}_2(a,b) = \frac{1}{a}\int_b^\infty x^2 e^{-\frac{(x^2+a^2)}{2}} I_1(ax)\mathrm{d}x$ is the second order Marcum-Q-function, $I_1(a) = \frac{1}{\pi}\int_0^\pi e^{a\cos\theta}\cos\theta \mathrm{d}\theta$ is the first order modified Bessel function of the first kind , and $\Delta\phi = \phi_1 - \phi_2$.

3.3.1.2 Rectangular Domain

We employ the Cartesian coordinate system, $\mathbf{p}_i = (x_i, y_i)$, relative to the centre of the rectangle of dimensions $A \times B$. Again we let $\eta = 2$ and (3.6) becomes

$$\langle H_{12}^{(2)} \rangle = \frac{1}{AB}\int_{-\frac{B}{2}}^{\frac{B}{2}}\int_{-\frac{A}{2}}^{\frac{A}{2}} e^{-(\|\mathbf{p}_k - \mathbf{p}_1\|^2 + \|\mathbf{p}_k - \mathbf{p}_2\|^2)}\mathrm{d}x_k\mathrm{d}y_k \tag{3.13}$$

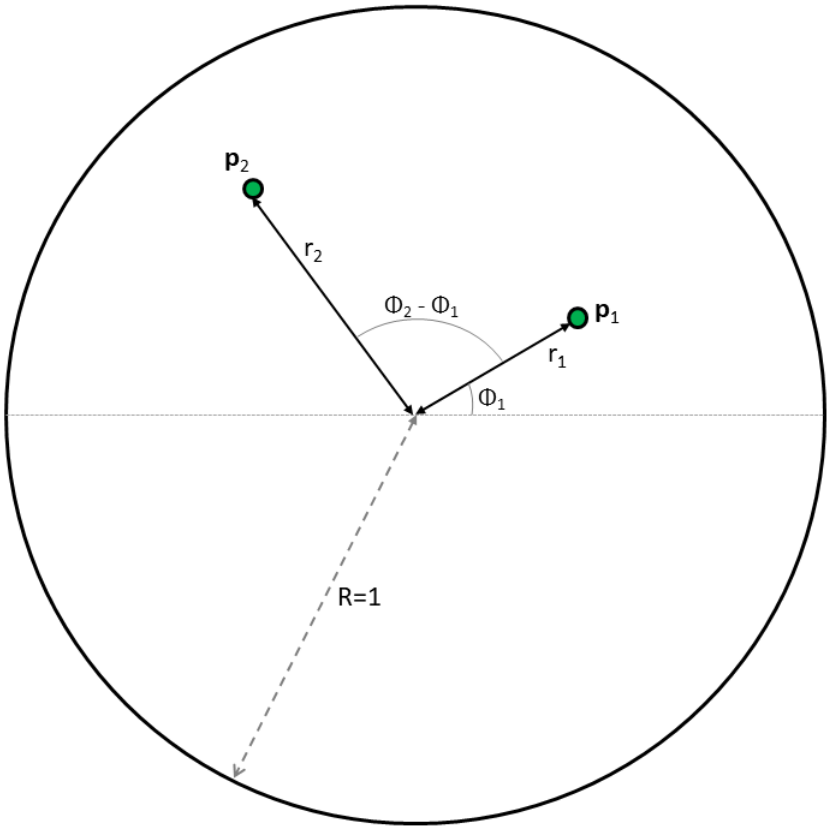


Figure 3.2: Illustration of terminal node locations within circle of unit radius.

Expanding and simplifying the exponent in (3.13) yields

$$\langle H_{12}^{(2)} \rangle = \frac{1}{AB} e^{-(x_1^2+x_2^2+y_1^2+y_2^2)} \int_{-\frac{B}{2}}^{\frac{B}{2}} e^{-2[y_k^2-(y_1+y_2)y_k]} \mathrm{d}y_k \times \int_{-\frac{A}{2}}^{\frac{A}{2}} e^{-2[x_k^2-(x_1+x_2)x_k]} \mathrm{d}x_k \tag{3.14}$$

Evaluating the integrals and simplifying further yields

$$\langle H_{12}^{(2)} \rangle = \frac{\pi}{2AB} e^{-\frac{1}{2}\|\mathbf{p}_2-\mathbf{p}_1\|^2} \mathrm{g}(A, \overline{x}_{12}) \mathrm{g}(B, \overline{y}_{12}) \tag{3.15}$$

where $(\overline{x}_{12}, \overline{y}_{12})$ is the coordinate of the midpoint between $\mathbf{p}_1$ and $\mathbf{p}_2$. The function $\mathrm{g}(\cdot, \cdot)$ is defined by

$$\mathrm{g}(a, b) = \frac{1}{2}\left[\mathrm{erf}\left(\sqrt{2}(a/2 - b)\right) + \mathrm{erf}\left(\sqrt{2}(a/2 + b)\right)\right] \tag{3.16}$$

where $\mathrm{erf}(a) = \frac{2}{\pi} \int_0^a e^{-x^2} \mathrm{d}x$ is the error function. Substituting (3.15) and (3.16) into (3.5) yields the expected connection probability, between terminal nodes $\mathbf{p}_1$ and $\mathbf{p}_2$, employing direct and 2-hop connectivity.

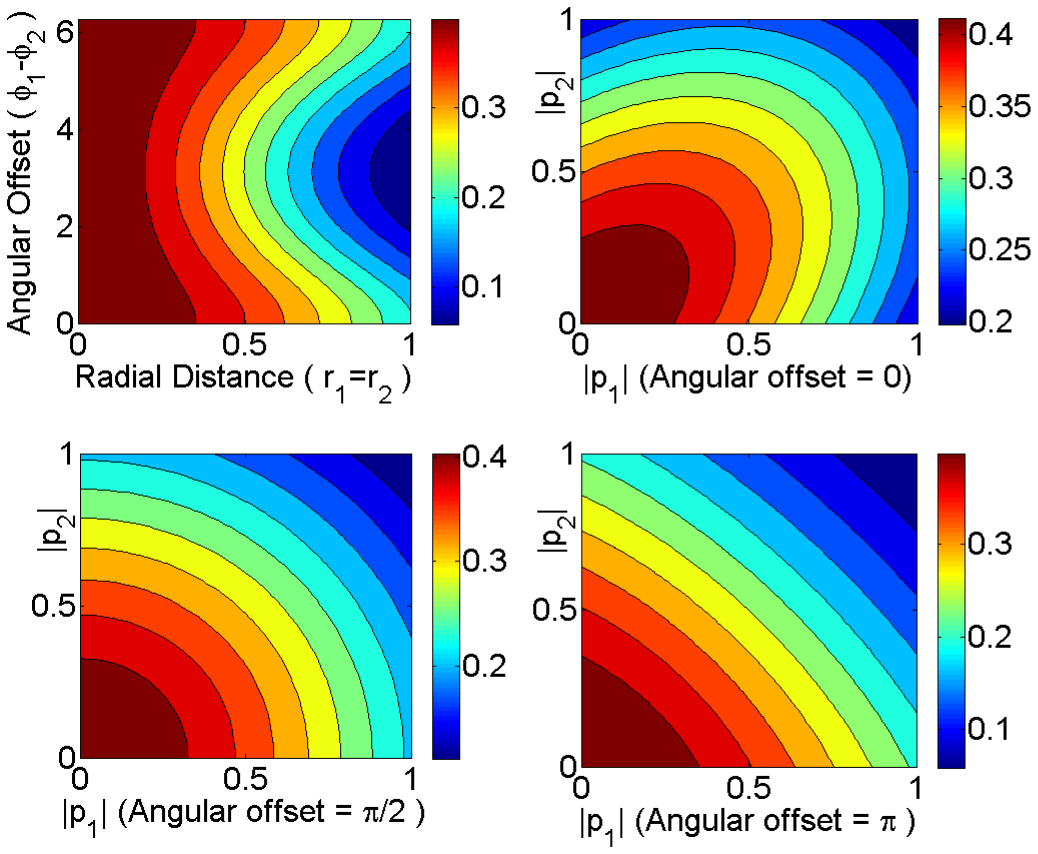


Figure 3.3: $\langle H_{12}^{(2)} \rangle$ as a function of $\mathbf{p}_1$ and $\mathbf{p}_2$ within a circular domain of unit radius. Upper-left panel shows effect of variable angular offset and variable radial offset with $r_i = r_j$ and remaining panels show effect of fixed angular offsets $(0, \pi/2, \pi)$ with variable radial offsets of nodes.

Again, equation (3.15) shows dependence on Euclidean distance between the terminal nodes and the position of their mid-point within the domain and its behaviour is illustrated in Fig. 3.5. Note that when the terminal nodes lie on the same axis (upper right figure) we observe that the maximum in connectivity does not occur when the nodes are colocated; with the exception of when they are both at the centre of the domain. Further analysis of global maximum is omitted for brevity.

3.3.2 Connectivity in the $\mathbb{R}^2$ plane

For comparison, we also consider a network of infinite extent on the $\mathbb{R}^2$ plane, where relay nodes are uniformly distributed according to a spatial Poisson point process (PPP), Φ_U, of intensity ρ. The average connection probability for the

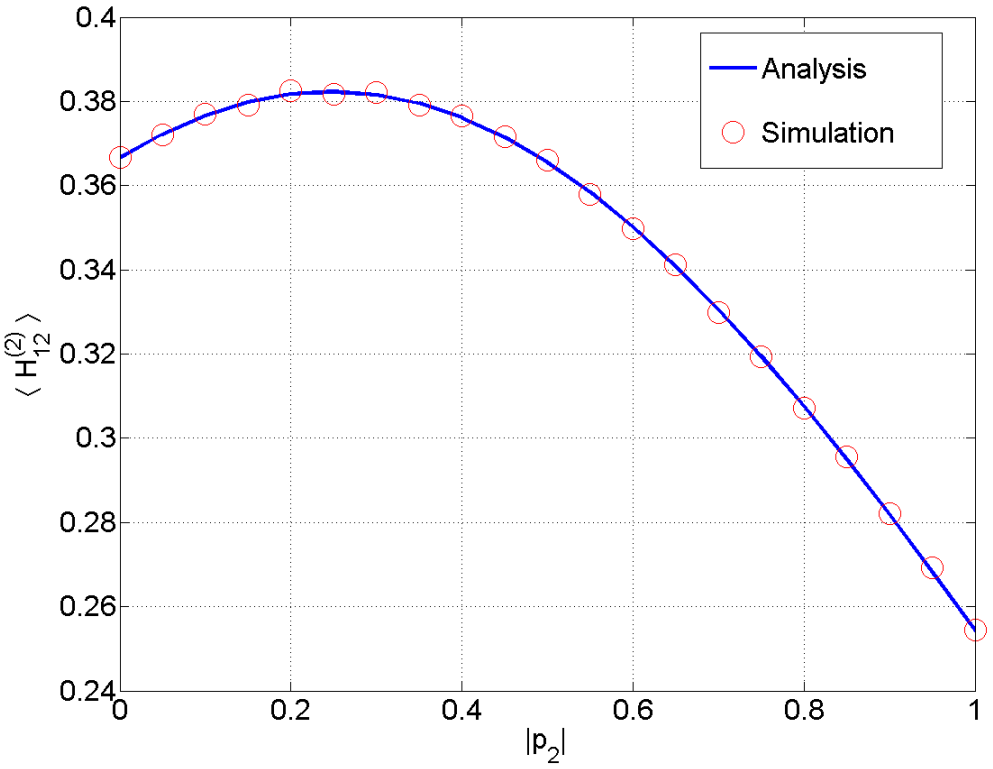


Figure 3.4: $\langle H_{12}^{(2)} \rangle$ as a function of $|\mathbf{p}_2|$ where $|\mathbf{p}_1| = 0.5$ and $\mathbf{p}_1$ and $\mathbf{p}_2$ lie on the same radial axis of a circle of radius $R = 1$. The red circles represent results obtained by Monte-Carlo simulation.

infinite network will be given by

$$\langle P_{12}^{(1,2)} \rangle = 1 - (1 - H_{12}) \mathbb{E}_{\mathbf{p}_k} \left[\prod_{\mathbf{p}_k \in \Phi_U} (1 - H_{1k} H_{2k}) \right] \tag{3.17}$$

Employing the probability generating functional for Φ_U to solve the expectation, gives

$$\langle P_{12}^{(1,2)} \rangle = 1 - (1 - H_{12}) \exp \left(- \rho \int_{\mathbb{R}^2} H_{1k} H_{2k} \mathrm{d}\mathbf{p}_k \right) \tag{3.18}$$

We solve (3.18) by considering the case $\eta = 2$, as before, and employing the Cartesian coordinate system to evaluate the integral. It can be shown that

$$\langle P_{12}^{(1,2)} \rangle = 1 - (1 - H_{12}) \exp \left[- \frac{\pi \rho}{2} e^{-\frac{1}{2} \|\mathbf{p}_2 - \mathbf{p}_1\|^2} \right] \tag{3.19}$$

which, owing to the translation invariance property of Φ_U, is solely a function of the Euclidean distance between the terminal nodes $\mathbf{p}_1$ and $\mathbf{p}_2$ and node intensity, i.e. independent of absolute position within the network.

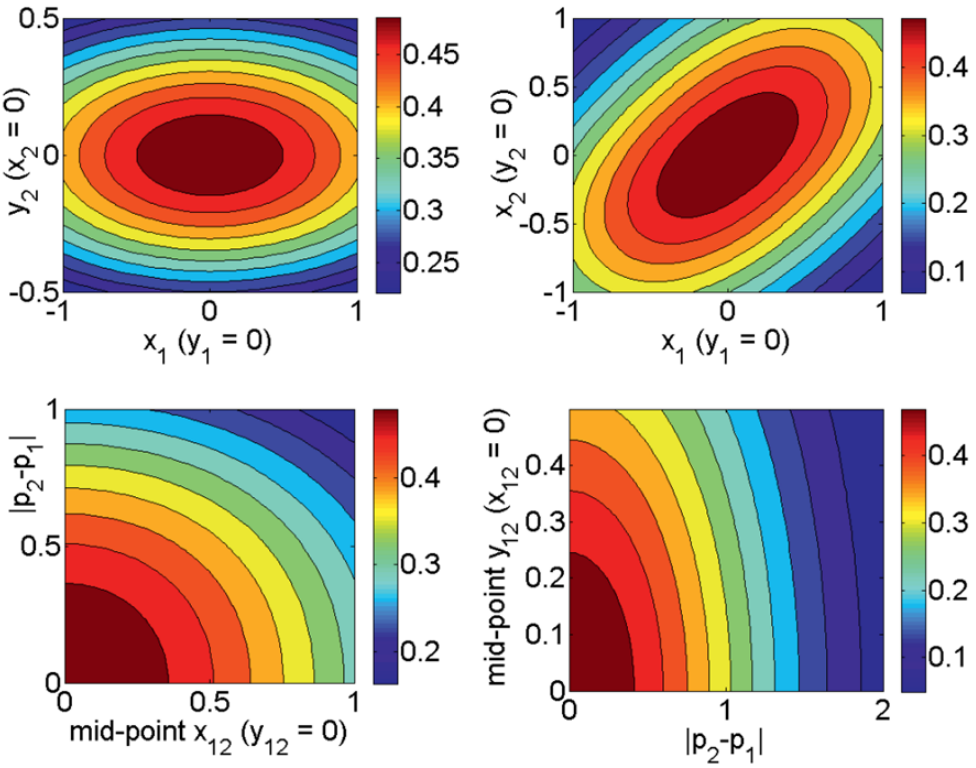


Figure 3.5: $\langle H_{12}^{(2)} \rangle$ as a function of $\mathbf{p}_1$ and $\mathbf{p}_2$ within a rectangular domain of dimension 2×1. Upper-left panel shows excursion of $\mathbf{p}_1$ and $\mathbf{p}_2$ about $y_1 = 0$ and $x_2 = 0$ axes respectively and upper-right panel shows excursion of $\mathbf{p}_1$ and $\mathbf{p}_2$ both located on the central horizontal axes $y_1 = y_2 = 0$. Lower panels shows $\langle H_{12}^{(2)} \rangle$ as a function of position of mid-point $\overline{\mathbf{p}}_{12}$, along central horizontal axis (lower left plot) and along central vertical axis (lower right plot) and separation $|\mathbf{p}_2 - \mathbf{p}_1|$.

3.4 Asymptotic Behaviour of $\langle P_{12}^{(1,2)} \rangle$

We now consider the behaviour of connection probability $P_{12}^{(1,2)}$ as the domain tends to infinite extent, keeping node intensity constant, and also consider the scenario where node intensity is considered sparse. In this way, the number of relay nodes N grows with the size of the domain, but the intensity $\rho = N/|V|$ remains constant. Firstly, the results (3.11) and (3.15) suggests that $\langle H_{12}^{(2)} \rangle$ can be expressed in the general form

$$\langle H_{12}^{(2)} \rangle = \frac{\pi}{2|\mathcal{V}|} e^{-\frac{1}{2}\|\mathbf{p}_2 - \mathbf{p}_1\|^2} f_{\mathcal{V}}(\overline{\mathbf{p}}_{12}, \hat{\mathcal{V}}) \tag{3.20}$$

where $0 \leq f_{\mathcal{V}}(\overline{\mathbf{p}}_{12}, \hat{\mathcal{V}}) \leq 1$ is a domain specific function of the midpoint location, $\overline{\mathbf{p}}_{12}$, of terminal nodes within the domain, and a set of parameter(s), $\hat{\mathcal{V}}$, which

define the domain geometry i.e. $\hat{\mathcal{V}} \in \{R, \{A, B\}\}$ for our special cases of circular and rectangular domains. At this point we can only conjecture that this general form applies to all convex domain geometries. One interesting observation from (3.20) is the property of rotational invariance on the terminal nodes about $\overline{\mathbf{p}}_{12}$ for a fixed spatial separation. For any two nodes located at the extremes of the diameter of a circle, centred at $\overline{\mathbf{p}}_{12}$, then the connection probability is unchanged as the diameter, and the nodes on it, rotates.

3.4.1 $\hat{\mathcal{V}} \to \infty$

In order to consider the domain scaling to infinite extent we rewrite equation (3.5) in the form

$$\langle P_{12}^{(1,2)} \rangle = 1 - (1 - H_{12}) \exp\Big[N \ln(1 - \langle H_{12}^{(2)} \rangle)\Big] \tag{3.21}$$

and taking a series expansion of the $\ln(\cdot)$ terms gives

$$\langle P_{12}^{(1,2)} \rangle = 1 - (1 - H_{12}) \exp\Big[N\Big(- \langle H_{12}^{(2)} \rangle - \frac{\langle H_{12}^{(2)} \rangle^2}{2} - \dots \Big)\Big] \tag{3.22}$$

By substitution of (3.20) into (3.22) and taking the limit $\hat{\mathcal{V}} \to \infty$ it can be trivially shown that

$$\langle P_{12}^{(1,2)} \rangle \sim 1 - (1 - H_{12}) \exp\left[-\frac{\pi\rho}{2} e^{-\frac{1}{2}\|\mathbf{p}_2 - \mathbf{p}_1\|^2}\right] \tag{3.23}$$

which ties up nicely with (3.19).

3.4.2 Sparse Network

Here we consider the condition of network 'sparsity' and show how connection probability can be approximated by simpler expressions. We define a sparse network as meeting the condition $\rho \ll |\mathcal{V}|$ or equivalently $N \ll |\mathcal{V}|^2$. Substituting (3.20) into (3.22) and applying our sparsity condition, the higher order terms of the series expansion become negligible, relative to the first order term, and (3.22) reduces to

$$\langle P_{12}^{(1,2)} \rangle \approx 1 - (1 - H_{12}) \exp\left[- \frac{\pi\rho}{2} e^{-\frac{1}{2}\|\mathbf{p}_2 - \mathbf{p}_1\|^2} f_{\mathcal{V}}(\overline{\mathbf{p}}_{12}, \hat{\mathcal{V}})\right] \tag{3.24}$$

We now consider the behaviour where the midpoint $\overline{\mathbf{p}}_{12}$ approaches the domain centre and boundary and also the asymptotic behaviour as the domain grows in size.

3.4.2.1 Domain centre

In the limit $|\overline{\mathbf{p}}_{12}| \to 0$ we get

$$1 - \mathrm{Q}_1\left(2|\overline{\mathbf{p}}_{12}|, 2R\right)\Big]\Big) \sim 1 - e^{-2R^2} \tag{3.25}$$

and

$$\mathrm{g}(A, \overline{x}_{12})\mathrm{g}(B, \overline{y}_{12}) \sim \mathrm{erf}\left(\frac{A}{\sqrt{2}}\right)\mathrm{erf}\left(\frac{B}{\sqrt{2}}\right) \tag{3.26}$$

By considering the asymptotic expansion for erf, then in the limit, $A, B \to \infty$, (3.26) becomes

$$\mathrm{g}(A, \overline{x}_{12})\mathrm{g}(B, \overline{y}_{12}) \sim \left(1 - \sqrt{\frac{2}{\pi}}\frac{1}{A}e^{\frac{-A^2}{2}}\right)\left(1 - \sqrt{\frac{2}{\pi}}\frac{1}{B}e^{\frac{-B^2}{2}}\right) \tag{3.27}$$

We see that, as the area of the network domains grow large, (3.25) and (3.27) rapidly converge to one and the connection probability tends to the limiting case (3.19).

3.4.2.2 Domain boundary

As $\overline{\mathbf{p}}_{12}$ approaches the domain boundary (one of the horizontal edges in the case of the rectangular boundary)

$$\mathrm{Q}_1\left(2|\overline{\mathbf{p}}_{12}|, 2R\right) \sim \frac{1}{2}\left[1 + e^{-4R^2}\,\mathrm{I}_0(4R^2)\right] \tag{3.28}$$

and, by considering the asymptotic expansion for $\mathrm{I}_0(4R^2)$, in the limit $R \to \infty$, (3.28) reduces to

$$\mathrm{Q}_1\left(2|\overline{\mathbf{p}}_{12}|, 2R\right) \sim \frac{1}{2}\left[1 + \frac{1}{\sqrt{8\pi}}\frac{1}{R}\right] \tag{3.29}$$

For the rectangular domain, as $\overline{\mathbf{p}}_{12} \to (\frac{A}{2}, 0)$, we get

$$\mathrm{g}(A, \overline{x}_{12})\mathrm{g}(B, \overline{y}_{12}) \sim \frac{1}{2}\,\mathrm{erf}\left(\sqrt{2}A\right)\mathrm{erf}\left(\frac{B}{\sqrt{2}}\right) \tag{3.30}$$

which, in the limit, $A, B \to \infty$, becomes

$$\begin{aligned}\mathrm{g}(A, \overline{x}_{12})\mathrm{g}(B, \overline{y}_{12}) \sim \frac{1}{2}&\left(1 - \frac{1}{\sqrt{2\pi}}\frac{1}{A}e^{-2A^2}\right)\\ &\times\left(1 - \sqrt{\frac{2}{\pi}}\frac{1}{B}e^{\frac{-B^2}{2}}\right)\end{aligned} \tag{3.31}$$

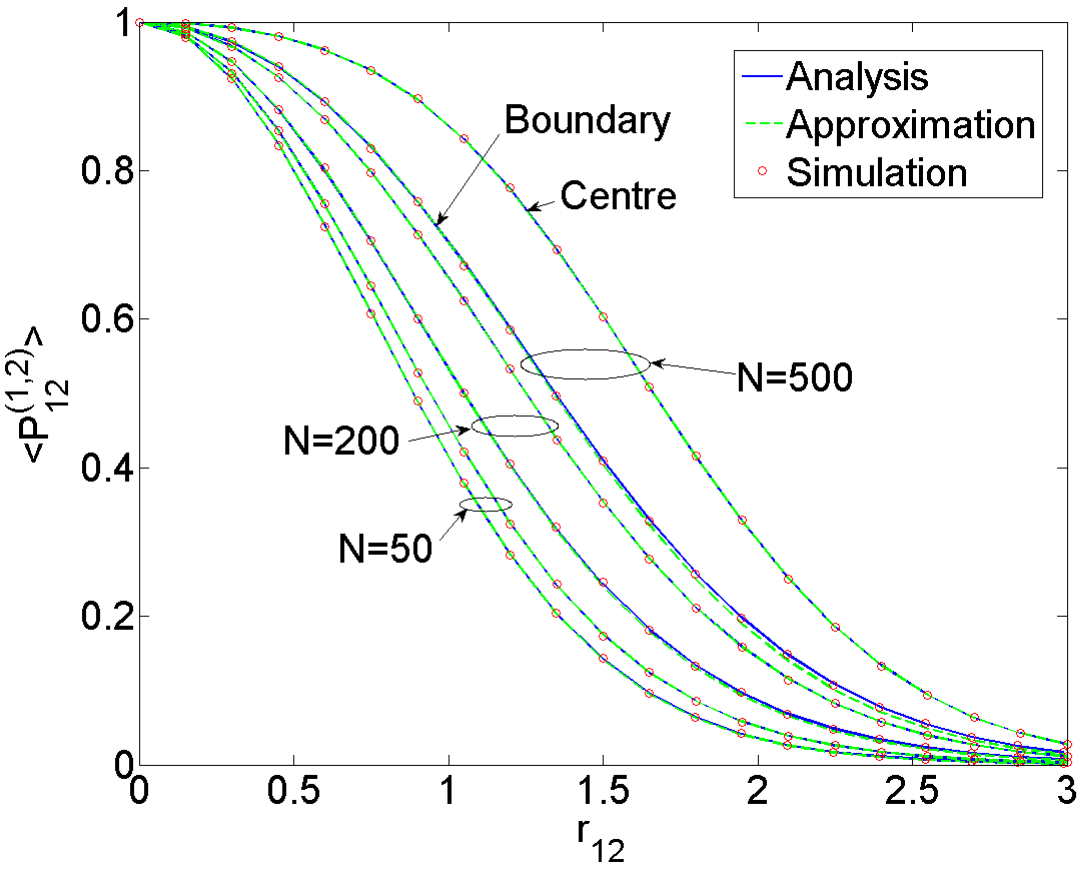


Figure 3.6: Connectivity performance (analysis, approximation and Monte-Carlo simulation) at boundary and centre of circular domain of radius $R = 10$ and total number of nodes $N \in \{50, 200, 500\}$. The boundary and central performances are the left and right curves respectively for each node density.

As the area of the network domains grow large, (3.29) and (3.31) converge to $\frac{1}{2}$ and the connection probability can be approximated by

$$\langle P_{12}^{(1,2)} \rangle \sim 1 - (1 - H_{12}) e^{-\left(\frac{\pi\rho}{4} e^{-\frac{1}{2}\|\mathbf{p}_2 - \mathbf{p}_1\|^2}\right)} \tag{3.32}$$

Provided the sparsity condition $N \ll |\mathcal{V}|^2$ is met, (3.19) and (3.32) provide good approximations for connection probability at the domain centre and boundary respectively. This is illustrated in Fig. 3.6 for a circular domain of radius 10. It should be noted that as the node separation increases, the midpoint necessarily moves away from the boundary of the circle since nodes cannot exist outside of it (the simulation results account for this). Even in this case, the results hold well.

3.5 Averaging over the terminal node $\mathbf{p}_2$

An insightful metric is the average connection probability from a fixed node to any randomly chosen node within the domain. One possible example is a fixed node that acts as the gateway into another fixed network, but is unaware of the position of other nodes to which it needs to communicate. Given we now have closed form expressions for average connection probability, between two fixed nodes, then averaging over all possible positions of one of the terminal nodes[4] is relatively straightforward and given by

$$\langle P_1^{(1,2)} \rangle = \frac{1}{|\mathcal{V}|} \int_{\mathcal{V}} \langle P_{12}^{(1,2)} \rangle \mathrm{d}\mathbf{p}_2 \tag{3.33}$$

Since this does not yield a nice closed form solution for either special case of domain, we evaluate numerically and illustrate in the left plot of Fig. 3.7 for the circular domain. The figure shows loss of connectivity performance towards the boundary, which can be attributed to a reduction in connectivity mass [226] as the node moves towards the boundary. Further, in order to gauge the improvement in employing 2-hop connectivity, we can consider the ratio of $\langle P_1^{(1,2)} \rangle / \langle P_1^{(1)} \rangle$, hereafter called the 'improvement factor', where $\langle P_1^{(1)} \rangle$ is the average connection probability for a direct path only from a fixed terminal node location to any randomly chosen destination node. For the case of the circular domain it can be shown that this is given by

$$\langle P_1^{(1)} \rangle = \frac{1}{R^2} \left[1 - \mathrm{Q}_1 \left(\sqrt{2} r_1, \sqrt{2} R \right) \right] \tag{3.34}$$

where r_1 is the radial offset of the terminal node. Evaluation of the above ratio for the circular domain, of unity radius and varying the number of relay nodes, is shown in the right panel of Fig. 3.7. The figure clearly shows appreciable gain in performance, particularly towards the domain boundary.

[4] Assumed to have uniform spatial distribution within $\mathcal{V}$

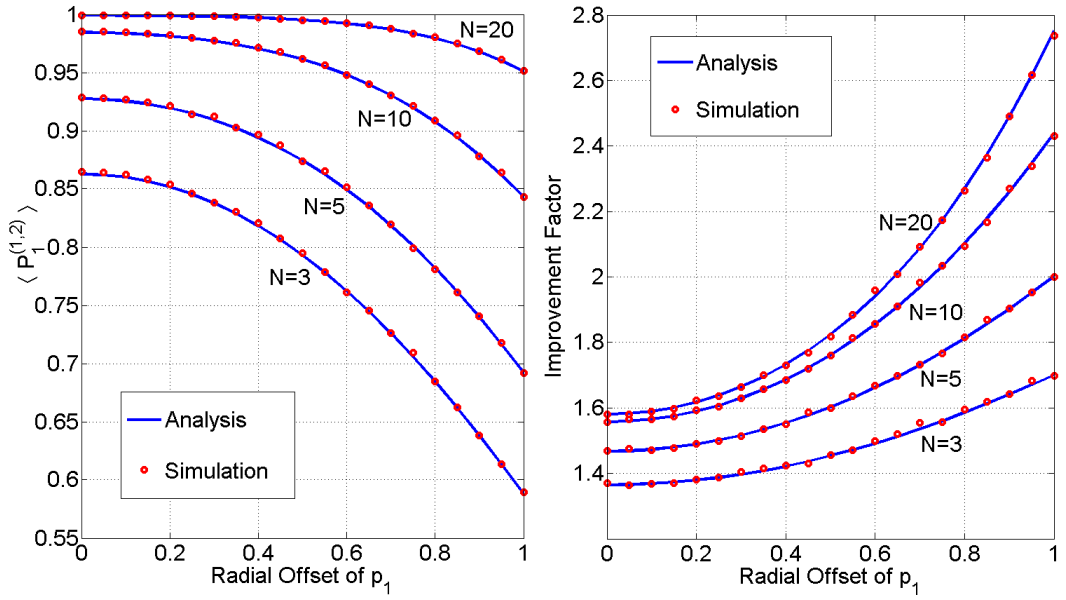


Figure 3.7: Left Panel: Average connection probability, via direct link or 2-hop path, $\langle P_1^{(1,2)} \rangle$, in a circular domain of unity radius and varying the position of a fixed node, $\mathbf{p}_1$, along a fixed radial axis. Right Panel: Improvement in average connection probability. Total relay nodes in network $N \in \{3, 5, 10, 20\}$. Results are supported by Monte-Carlo simulation as shown by red circles.

3.6 Conclusion and Discussions

In this chapter, we have studied the direct and 2-hop connectivity, between two fixed terminal nodes within finite convex geometric boundaries, subject to Rayleigh fading. We derive analytic expressions, in closed form, for average connection probability for circular and rectangular domains which show a dependence on: boundary geometry, spatial separation of nodes and their mid-point location. This yields an interesting property of rotational invariance on the node positions about this mid-point. Boundary effects have been shown to tie up with previous observations [170] and employment of 2-hop connectivity was shown to yield appreciable improvements in connectivity, particularly at the domain boundaries. We also show that, under a condition of low relay node intensity, a simpler approximation can be employed to evaluate this connectivity metric in a finite domain. It is envisaged that these general results can be used in the design and simulation of bounded homogeneous random wireless networks, the analysis of device-to-device (D2D) connectivity

within clusters contained within larger non-homogeneous wireless networks and provides a foundation for chapter 4 of this thesis.

4

Relationship Between Relay and Infrastructure Densities in Geometrically Bounded Relay-Assisted Wireless Networks

4.1 Introduction

The previous chapter concluded that 2-hop connectivity can provide appreciable improvements in connectivity between terminal nodes, particularly at the geometric boundary of finite networks. In this chapter we consider the use of 2-hop connectivity, together with direct (1-hop) connectivity, as a mechanism to reduce the reliance on fixed basestation infrastructure in cellular type networks. This allows infrastructure nodes to be switched off according to the density of relay nodes, e.g. other mobile user equipment (UE), within the network. This has the potential of significant energy saving, a growing concern to network operators in response to global pressure to reduce carbon and maintain profitability.

Given the importance of energy saving, we provide some additional context here. The term 'green network' or 'green cellular network' is often employed to convey an energy efficient network. Related prior research includes [227], which provides a cost-capacity performance analysis of femto-cell and macro-cellular networks, concluding that the optimum network structure depends on capacity demands. [228] provides a quantitative analysis of energy savings in green cellular networks and [229] provides a survey of research issues and challenges associated with managing energy consumption. A consensus is that the capital expenditure (CAPEX), costs associated with commissioning an infrastructure, and operating expenditure (OPEX), ongoing cost associated with running the infrastructure, are dominant in macro-cells but the costs associated with lower tier cells cannot be ignored due to their significantly higher spatial densities compared to macro-cell network. Recent research has concluded that the most efficient way to save energy in cellular networks is to switch base stations on and off dynamically according to the distribution of user equipment in real time. This is often termed 'Idle Mode' capability or 'Basestation Sleeping' and a number of strategies, and their effects on network performance, have been studied, including [230–233].

In what follows, we enable offloading traffic from a network infrastructure by allowing users within range of each other to communicate directly or via a 2-hop route, through other UEs. Spatial densification of UEs is clearly beneficial in this

context. This direct connectivity between proximity UEs has gained rapid traction over the past decade, including [234, 235].

Before progressing further, we chose the following working assumptions:

1. wireless networks are finite (geometrically bounded) because (a) it is realistic (wireless networks are not infinite), (b) connectivity performance analysis is mathematically tractable and (c) it enables us to consider the effects of inhomogeneity on a large scale, which can be useful in practice.

2. Energy saving resulting from switching off infrastructure outweighs the additional energy required by using UEs as relays.

Our approach considers outage probability between terminal nodes as our connectivity metric, which we average over all possible spatial relay/infrastructure node configurations within the network. For tractability, we consider the case of a circularly geometrically bounded wireless network subject to Rayleigh fading and assume negligible inter-node interference. The consideration of interference is clearly of concern in many applications; however we maintain generality by assuming a suitable MAC is employed to ensure interference is prevented, e.g. frequency/time division multiple access (FDMA/TDMA). Under these working assumptions, this chapter provides the following contributions:

1. we provide mathematical expressions involving well-understood special functions for the connectivity probability of two terminal nodes in both homogeneous and inhomogeneous networks;

2. we exploit this mathematical framework to demonstrate the trade-off in relay and infrastructure node densities for a prescribed level of connectivity;

3. we demonstrate that it is possible to obtain a Pareto frontier in the different node densities by appropriately thinning the active infrastructure set in an inhomogeneous manner.

The remainder of the chapter is organised as follows. Section 4.2 details our system model. Section 4.3 derives mathematical expressions involving well-understood special functions for outage probability between fixed terminal nodes, and Section 4.4 provides insights into the relative contributions of relay and infrastructure networks for a prescribed outage probability when averaged over all spatial relay/infrastructure/terminal node configurations. Conclusions are detailed in section 4.5.

4.2 Network Definitions and System Model

As with the previous chapter, we consider the connectivity between two terminal nodes, at fixed locations $\mathbf{p}_1$ and $\mathbf{p}_2$, within a circular domain $\mathcal{V} \subset \mathbb{R}^2$. Also contained within $\mathcal{V}$, are independent identically distributed (i.i.d.) relay nodes and i.i.d. infrastructure nodes, spatially distributed according to independent Poisson point processes (PPP), Φ_{R} and Φ_{I} respectively. Note that the spatial distributions of relay and infrastructure networks are not necessarily identical. We employ PPP in our analysis for mathematical tractability and because we do not assume prior knowledge of the number of nodes in the networks. We characterise our relay and infrastructure networks by their average node densities ρ_{R} and ρ_{I} respectively; with zero node densities in $\mathbb{R}^2 \setminus \mathcal{V}$, i.e., no relay nodes exist outside of the geometric boundary. It is worth noting the distinction between a binomial point process and a PPP in a finite domain $\mathcal{V}$ is that different realisations of the PPP consist of a different number of points having a Poisson distribution [236, sect. 2.4.2]. We assume a homogeneous spatial distribution of relay nodes, whereas the infrastructure nodes can follow an inhomogeneous spatial distribution where the density ρ_{I} is, in general, dependent upon the position within $\mathcal{V}$, as we define later. We denote the location of any arbitrary node-i by the vector $\mathbf{p}_i$ with index $i \in \{1, 2, \ldots, (\Phi_{\mathrm{R}}(\mathcal{V}) + \Phi_{\mathrm{I}}(\mathcal{V}) + 2)\}$, where $\Phi_y(\mathcal{V}) \sim \mathrm{Poisson}(\rho_y|\mathcal{V}|), y \in \{\mathrm{R}, \mathrm{I}\}$. As with previous chapters, we use $\mathbf{p}_i$ to represent both node-i and its location interchangeably.

For mathematical tractability we use the soft pairwise connectivity model defined in section 2.1.3

$$H_{ij} = e^{-r_{ij}^{\eta}}, \tag{4.1}$$

where H_{ij} denotes the connection probability and r_{ij} denotes the Euclidean distance between nodes normalised to the 'hard' connection distance r_0, given in equation (2.10).

We consider three independent mechanisms whereby two terminal nodes $\mathbf{p}_1$ and $\mathbf{p}_2$ can connect: directly, via an intermediate node $\mathbf{p}_k \in \Phi_{\mathrm{R}}$ forming a 2-hop path, or independent connection to two infrastructure nodes $\mathbf{p}_m, \mathbf{p}_n \in \Phi_{\mathrm{I}}$, which is depicted in Fig. 4.1. Although our analysis is limited to the 2-hop relay case, k-hop connectivity could be considered [159]. The connectivity between any two infrastructure nodes is assumed to be guaranteed i.e. there exists some form of low latency fixed network infrastructure with infinite capacity. For mathematical tractability, we assume that relaying nodes employ regenerative (decode-and-forward) relaying which eliminates interdependency on the connectivity of the 2-hops and allows the probability of 2-hop connectivity, between $\mathbf{p}_1$ and $\mathbf{p}_2$ via $\mathbf{p}_k$, to be simply expressed as the product $H_{1k}H_{2k}$. This also assumes that the small scale fading component of the 1-k and 2-k channels are statistically independent[1].

4.3 Connectivity Analysis

We choose outage probability as our connectivity metric between terminal nodes $\mathbf{p}_1$ and $\mathbf{p}_2$, for any spatial relay/infrastructure node configuration, denoted by $\mathcal{O}_{12}$. We assume the three aforementioned connection mechanisms are independent and

[1]Although this is not necessarily the case when $\mathbf{p}_1$ and $\mathbf{p}_2$ are located within the coherence distance r_c of each other since their connectivity behaviour to an arbitrary common relay node will be more highly correlated and therefore independence cannot be assumed. Taking the example of a circular domain $\mathcal{V}$ of radius R and assume $r_c \ll R$, then the measure of space in $\mathcal{V}$ corresponding to the case $\|\mathbf{p}_1 - \mathbf{p}_2\| < r_c$ is small compared to the whole space of node configurations. Therefore, if we average the exponential connectivity functions, between terminal nodes, over all possible node locations, then the portion of the average corresponding to $\|\mathbf{p}_1 - \mathbf{p}_2\| < r_c$, will be negligible. This assumption has been shown on several occasions to yield accurate results [170] [237].

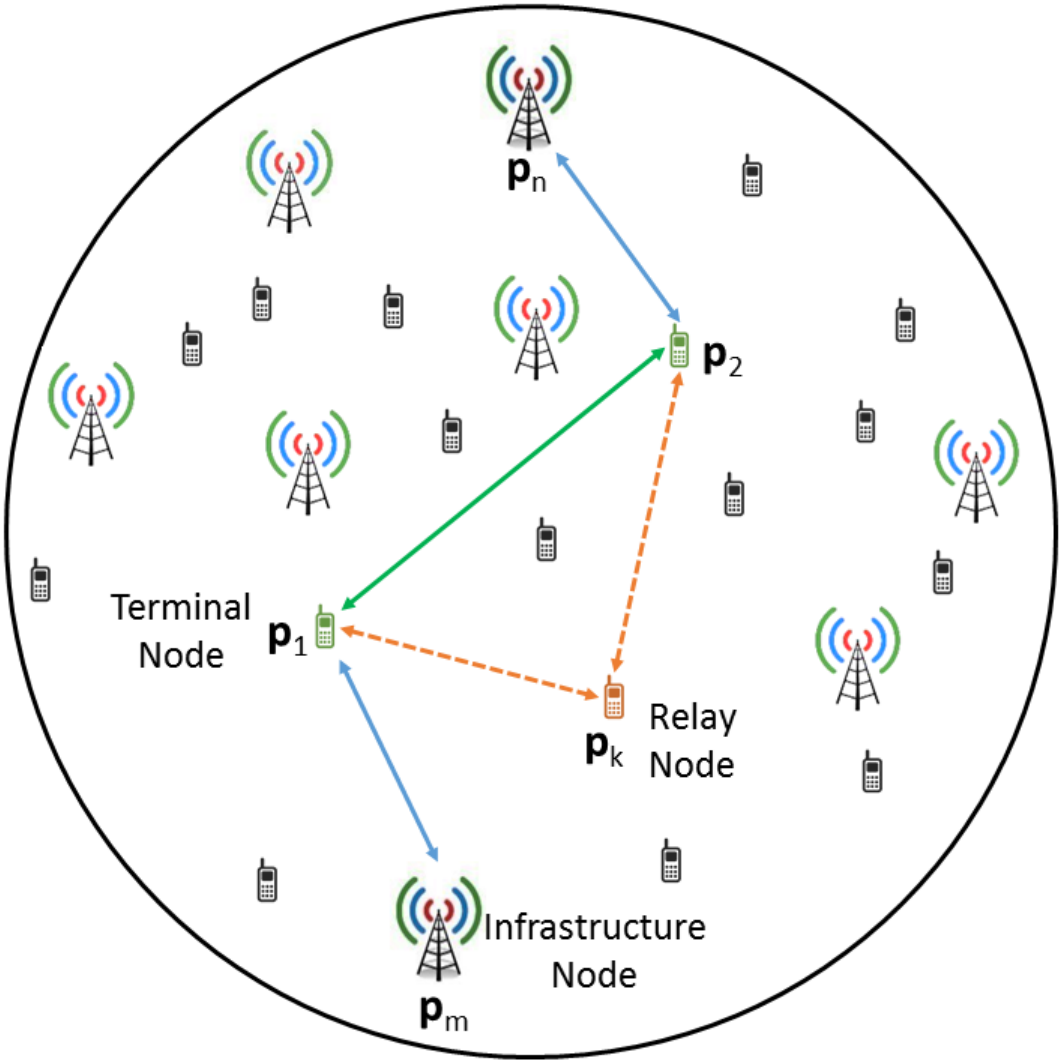


Figure 4.1: Direct and 2-hop connectivity between two terminal nodes, $\mathbf{p}_1$ and $\mathbf{p}_2$, in a finite convex domain $\mathcal{V}$ containing uniformly distributed intermediate relay nodes $\mathbf{p}_k \in \Phi_{\mathrm{R}}$ and non-uniformly distributed infrastructure nodes $\mathbf{p}_m, \mathbf{p}_n \in \Phi_{\mathrm{I}}$.

evaluate $\mathcal{O}_{12}$ as the product of outage probabilities of all possible connection mechanisms[2] such that

$$\mathcal{O}_{12} = (1 - H_{12}) \prod_{\mathbf{p}_k \in \Phi_{\mathrm{R}}} (1 - H_{1k} H_{2k}) \left[1 - \left[1 - \prod_{\mathbf{p}_m \in \Phi_{\mathrm{I}}} (1 - H_{1m}) \right] \left[1 - \prod_{\mathbf{p}_n \in \Phi_{\mathrm{I}}} (1 - H_{2n}) \right] \right]. \tag{4.2}$$

We now proceed to average the outage probability over all spatial relay/infrastructure node configurations within a finite circularly bounded domain $\mathcal{V}$ with radius R. A

[2]We interpret connectivity, between terminal nodes, as a route exists in theory. The mathematical analysis is identical to the case of selection combining [238], although selection combining is impractical at a large scale.

circularly bounded network is considered to be a reasonable approximation to a network constrained to a typical residential area or a clustering of communication nodes within a larger heterogeneous network for example. Alternative geometric boundaries, as discussed in chapter 3, can be treated in a similar manner to that outlined here. We firstly consider the simpler case of a homogeneous infrastructure network, also considering the special case $R \to \infty$, followed by analysis of an inhomogeneous infrastructure network. Closed form expressions are developed wherever possible to provide analytical insights.

4.3.1 Homogeneous Infrastructure

For convenience, we define $\bar{\mathcal{O}}_{12} := \mathbb{E}_{\Phi_\mathrm{R},\Phi_\mathrm{I}}[\mathcal{O}_{12}|\mathbf{p}_1,\mathbf{p}_2]$ as the outage probability (4.2) averaged over all possible locations of relay and infrastructure nodes in $\mathcal{V}$, conditioned on the locations of the terminal nodes $\mathbf{p}_1$ and $\mathbf{p}_2$. Since relay and infrastructure node locations are independent and identically distributed (i.i.d.), this can be expressed as

$$\begin{aligned}\bar{\mathcal{O}}_{12} &= (1-H_{12})\mathbb{E}_{\Phi_\mathrm{R}}\Bigg[\prod_{\mathbf{p}_k\in\Phi_\mathrm{R}}(1-H_{1k}H_{2k})\Bigg] \\ &\times \Bigg\{\mathbb{E}_{\Phi_\mathrm{I}}\Bigg[\prod_{\mathbf{p}_n\in\Phi_\mathrm{I}}(1-H_{1n})\Bigg] \\ &+ \Bigg[\mathbb{E}_{\Phi_\mathrm{I}}\Bigg[\prod_{\mathbf{p}_n\in\Phi_\mathrm{I}}(1-H_{2n})\Bigg] \\ &- \mathbb{E}_{\Phi_\mathrm{I}}\Bigg[\prod_{\mathbf{p}_n\in\Phi_\mathrm{I}}(1-H_{1n})(1-H_{2n})\Bigg]\Bigg\}. \end{aligned} \tag{4.3}$$

Employing the probability generating functional for Φ_R and Φ_I to solve the expectations, gives

$$\begin{aligned}\bar{\mathcal{O}}_{12} = (1-H_{12})\exp\Bigg[-\rho_\mathrm{R}V\bar{H}_{12}^{(2_\mathrm{R})}\Bigg] \\ \times\Bigg\{\exp\Bigg[-\rho_\mathrm{I}V\bar{H}_{1\mathrm{I}}\Bigg]+\exp\Bigg[-\rho_\mathrm{I}V\bar{H}_{2\mathrm{I}}\Bigg] \\ -\exp\Bigg[-\rho_\mathrm{I}V\Bigg(\bar{H}_{1\mathrm{I}}+\bar{H}_{2\mathrm{I}}-\bar{H}_{12}^{(2_\mathrm{I})}\Bigg)\Bigg]\Bigg\},\end{aligned} \tag{4.4}$$

where $V = |\mathcal{V}| = \pi R^2$ and $\bar{H}_{12}^{(2_y)}$, $y \in \{\mathrm{R}, \mathrm{I}\}$, denotes the 2-hop connection probability, between $\mathbf{p}_1$ and $\mathbf{p}_2$ via a relay/infrastructure node, averaged over all possible locations of a relay/infrastructure node in $\mathcal{V}$. $\bar{H}_{i\mathrm{I}}, i \in \{1, 2\}$, is the probability of a terminal node connecting directly to an infrastructure node, averaged over all locations of an infrastructure node in $\mathcal{V}$. Since we consider homogeneous relay and infrastructure networks,

$$\bar{H}_{12}^{(2_y)} = \frac{1}{V} \int_{\mathcal{V}} H_{1k} H_{2k} \mathrm{d}\mathbf{p}_k, \tag{4.5}$$

Note that the r.h.s. of (4.5) exhibits independence in y and the probabilities of terminal nodes connecting via a relay or infrastructure nodes are identical for the homogeneous spatial distribution of the infrastructure. The final term in the curly braces in (4.4) (similarly, (4.3)) is the probability of the union of two events, namely that each of the two terminal nodes does not connect to an infrastructure node. Hence, we can apply the union bound to simplify this expression. Intuitively, as the domain size increases, for a given ρ_I, the probability of the terminal nodes connecting to independent infrastructure nodes will be significantly higher than the probability of terminal nodes connecting to the same infrastructure node. Thus, we expect the union bound to provide a tight upper bound in outage probability. We denote this upper bound by $\bar{\mathcal{O}}_{12}^{\mathrm{UB}}$, where

$$\bar{\mathcal{O}}_{12}^{\mathrm{UB}} := (1 - H_{12}) \exp\left[-\rho_{\mathrm{R}} V \bar{H}_{12}^{(2_{\mathrm{R}})} \right] \left\{ \exp\left[-\rho_{\mathrm{I}} V \bar{H}_{1\mathrm{I}} \right] + \exp\left[-\rho_{\mathrm{I}} V \bar{H}_{2\mathrm{I}} \right] \right\}. \tag{4.6}$$

Hereafter we chose the special case of free-space propagation, $\eta = 2$, to provide mathematical tractability in our analysis. Alternative path loss exponents could be employed but would not necessarily yield behavioural insights due to the limitations of a purely numeric analysis. (4.5) is evaluated in chapter 3, for this special case, yielding

$$\bar{H}_{12}^{(2_y)} = \frac{\pi}{2V} e^{-\frac{r_{12}^2}{2}} \left[1 - \mathrm{Q}_1\left(2\|\overline{\mathbf{p}}_{12}\|, 2R \right) \right], \tag{4.7}$$

where $\mathrm{Q}_1(a, b) = \int_b^\infty x e^{-\frac{(x^2+a^2)}{2}} \mathrm{I}_o(ax) \mathrm{d}x$ is the first order Marcum Q-function, $\mathrm{I}_0(a) = \frac{1}{\pi} \int_0^\pi e^{a \cos\theta} \mathrm{d}\theta$ is the zeroth order modified Bessel function of the first kind

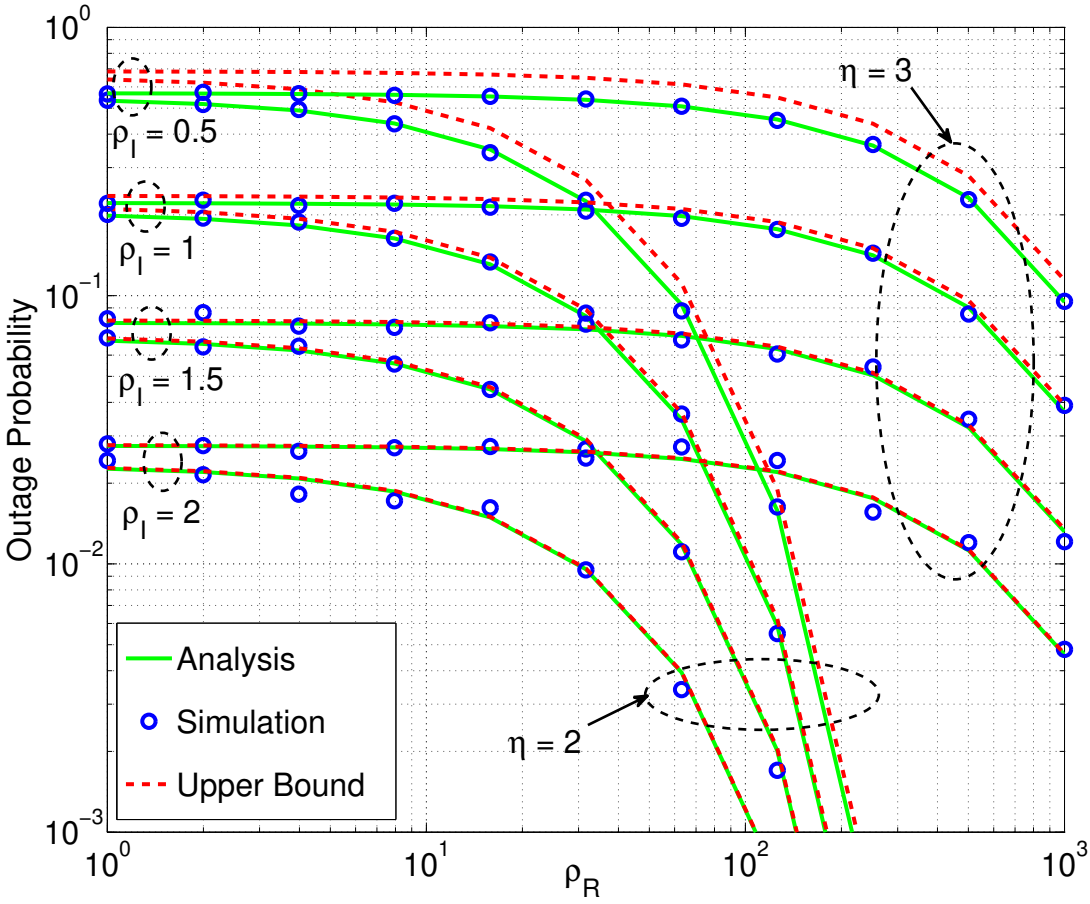


Figure 4.2: Outage probability as a function of ρ_{R}, for $\rho_{\mathrm{I}} \in \{0.5, 1, 1.5, 2\}$ and $\eta \in \{2, 3\}$, averaged over locations of relay and infrastructure nodes in a circular domain $\mathcal{V}$ of radius 2.5, as given by (4.4). Terminal node located at polar coordinates $2\angle 0$ and $2\angle \pi/2$. Blue markers show results from Monte Carlo simulations. Dashed red lines indicate upper bound as given by (4.6).

and $\overline{\mathbf{p}}_{12} = (\mathbf{p}_1 + \mathbf{p}_2)/2$ is the mid-point between $\mathbf{p}_1$ and $\mathbf{p}_2$. Further, since we initially consider a uniform spatial distribution of infrastructure nodes,

$$\bar{H}_{iI} = \frac{1}{V}\int_{\mathcal{V}} H_{im}\mathrm{d}\mathbf{p}_m. \tag{4.8}$$

Using the approach detailed in chapter 3, this evaluates to

$$\bar{H}_{iI} = \frac{\pi}{V}\left[1 - \mathrm{Q}_1\left(\sqrt{2}r_i, \sqrt{2}R\right)\right], \tag{4.9}$$

where $r_i = \|\mathbf{p}_i\|$ is the radial offset of node $\mathbf{p}_i$.

Fig. 4.2 illustrates (4.4), and the upper bound (4.6), for a range of relay and infrastructure densities with fixed terminal nodes, located at polar coordinates

$2\angle 0$ and $2\angle \pi/2$, within a circular domain of radius 2.5. The figure illustrates that our expectation in upper bound tightness is indeed correct. Although we focus our analysis on free space propagation, we demonstrate the tightness of the bound for increased path loss exponent by including the case $\eta = 3$, evaluating (4.5) and (4.8) numerically. Results from Monte Carlo simulations are included to validate the analysis.

Remark (Consideration of Interference)**.** *For the $\eta = 2$ case, Fig. 4.2 clearly shows a much greater rate of reduction in outage probability with increasing density of relays compared to the $\eta = 3$ case. We can attribute this to the reduction of connectivity mass with increasing values of η, or more specifically the connectivity volume (i.e., the integral in 2.13) at arbitrary location $\mathbf{p}_i$, where $H_{ij} = \exp(-\|\mathbf{p}_j - \mathbf{p}_i\|^\eta)$ is our soft pairwise connection probability function. If we had considered co-channel interference in our analysis, similar to that described in [177], then we would find that interference would be more detrimental to pairwise connection probabilities, and therefore connectivity volume, for lower path-loss exponents. This is evidenced in [183], which analyses the spatial variation of the sum of interference, originating from uniformly distributed interferers (modelled as a PPP) within a finite geometric boundary. This work shows that interference decreases with increasing path loss exponent and is also dependent upon the location of the receiving node within the geometric boundary.*

Fig. 4.2 shows an exponential improvement in outage probability with increasing infrastructure density. Since $1-Q_1(x,\cdot)$ is strictly decreasing with respect to x, then (4.7) and (4.9) exhibit a reduction in connection probability as the terminal nodes move closer to the boundary of $\mathcal{V}$; following observations made in [239], [240] where this phenomena is attributed to loss in connectivity mass towards the boundary. We also observe a tight upper bound as the average number of infrastructure nodes increases. If we analyse the asymptotic behaviour of (4.7) and (4.9) with increasing r_{12} and their relative contributions in (4.4), we observe that (4.9) becomes the dominant term due to the exponential term, yielding a tight upper union bound for

larger terminal node separation or when we average connectivity over all possible terminal node positions with increasing domain size. Further, we can approximate performance with the terminal node located towards the domain centre by employing the special cases for the first order Marcum Q-function

$$\mathrm{Q}_1\left(0, x\right) = e^{-x^2/2}, \tag{4.10}$$

and similarly at the boundary

$$\mathrm{Q}_1\left(x, x\right) = \frac{1}{2}\left[1 + e^{-x^2}\,\mathrm{I}_0(x^2)\right] \tag{4.11}$$

which by taking the asymptotic expansion of the modified Bessel function for large argument x becomes

$$\mathrm{Q}_1\left(x, x\right) \sim \frac{1}{2}\left[1 + \frac{1}{\sqrt{2\pi}}\frac{1}{x}\right]. \tag{4.12}$$

The effectiveness of these special cases for approximating performance at the centre and boundary of circular domains is demonstrated in chapter 3. From $\mathrm{Q}_1(x, \infty) = 0$ [241] we can show that, in the limit $R \to \infty$ ($\mathcal{V} \to \mathbb{R}^2$), (4.4) reduces to

$$\bar{\mathcal{O}}_{12} \underset{R\to\infty}{=} (1 - e^{-r_{12}^2}) \exp\left(-\frac{\pi\rho_{\mathrm{R}}}{2} e^{-\frac{r_{12}^2}{2}}\right) \exp(-\pi\rho_{\mathrm{I}}) \left[2 - \exp\left[-\frac{\pi\rho_{\mathrm{I}}}{2}\left(2 - e^{-\frac{r_{12}^2}{2}}\right)\right]\right] \tag{4.13}$$

and similarly

$$\bar{\mathcal{O}}_{12}^{\mathrm{UB}} \underset{R\to\infty}{=} 2(1 - e^{-r_{12}^2}) \exp\left(-\frac{\pi\rho_{\mathrm{R}}}{2} e^{-\frac{r_{12}^2}{2}}\right) \exp(-\pi\rho_{\mathrm{I}}), \tag{4.14}$$

which are solely functions of the Euclidean distance between the terminal nodes and the relay and infrastructure node densities. It is worth noting that the simplicity of (4.14) provides a convenient approximation for outage behaviour in the central bulk region ($r_i < 0.5R, i \in \{1, 2\}$) under the conditions $R > 3$, yielding $0 < \mathrm{Q}_1(\sqrt{2}r_i, \sqrt{2}R) \ll 0.1$ and $\rho_I > 1$, yielding a tighter upper performance bound. Further, for a fixed r_{12} and a prescribed outage probability $\bar{\mathcal{O}}_{12}^{\mathrm{UB}} = \kappa$, we can approximate the infrastructure density required for a given relay infrastructure by simply rearranging (4.14) such that

$$\rho_{\mathrm{I}} \approx -\frac{1}{\pi} \ln\left[\frac{0.5\kappa}{1 - e^{-r_{12}^2}}\right] - 0.5e^{-\frac{r_{12}^2}{2}}\rho_{\mathrm{R}}. \tag{4.15}$$

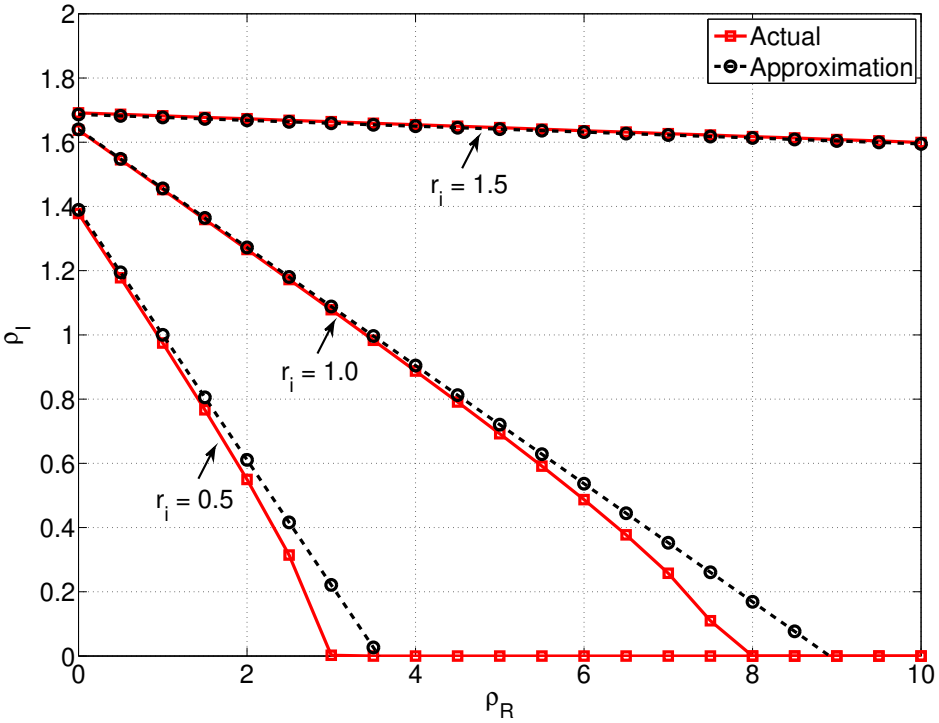


Figure 4.3: Illustration of the accuracy of first order approximation (4.15). The red solid traces show ρ_I as a function of ρ_R as defined by (4.4) (determined through successive approximation) and the black dashed traces show the first order approximation as given by (4.15). We fix $R = 4$ and $\kappa = 0.01$ and consider terminal nodes located within the central bulk region at radial and angular offsets $r_i \in \{0.5, 1.0, 1.5\}$ and $\pi/2$ respectively.

The accuracy of this approximation is illustrated in Fig. 4.3. If we wish to average connectivity performance over terminal node positions within the central bulk region we can employ the probability distribution of r_{12} within a circle [189]. Further analysis in the bulk region of homogeneous networks has not been included for brevity; our main motivation is to understand the relationship between boundary conditions and spatial distribution of the infrastructure network.

4.3.2 Inhomogeneous Infrastructure

Conjecturing that, for a non zero density of relays, an inhomogeneous distribution of infrastructure nodes will mitigate loss in relay assisted 2-hop connectivity between terminal nodes located closer to the boundary, we now consider an inhomogeneous independent thinning [236, section 2.7.3] of our infrastructure network as the density of the relay infrastructure increases. In the thinning process,

we remove infrastructure nodes with probability $1 - g(\mathbf{p}_n)$, independently of all other infrastructure nodes. This process generates an inhomogeneous PPP with intensity function $\rho_{\mathrm{I}} g(\mathbf{p}_n)$, where ρ_{I} is the mean infrastructure density over $\mathcal{V}$. We propose that $g(\mathbf{p}_n)$ has a uniform axial distribution but varies with radial offset $\|\mathbf{p}_n\|$ from the centre of $\mathcal{V}$ according to

$$g(\mathbf{p}_n) = \frac{1}{k}\left[1 + (\alpha - 1)\left(\frac{\|\mathbf{p}_n\|}{R}\right)^{\beta}\right], \tag{4.16}$$

where the normalising constant k is given by

$$\begin{aligned} k &= \int_{\mathcal{V}} \left[1 + (\alpha - 1)\left(\frac{\|\mathbf{p}_n\|}{R}\right)^{\beta}\right] \mathrm{d}\mathbf{p}_n \\ &= \pi R^2 \left[1 + \frac{2(\alpha - 1)}{\beta + 2}\right]. \end{aligned} \tag{4.17}$$

The radial distribution of (4.16) is defined by parameters α and β. The exponent $\beta \in \mathbb{R}^+$ defines the characteristic of the distribution, i.e. $\beta = 1$ for a linear radial distribution and $\beta = 2$ for a quadratic radial distribution. The parameter $\alpha \in \mathbb{R}^+$ is a weighting factor given by the ratio of the intensity measures of infrastructure nodes at the domain's boundary and centre, i.e. $\alpha < 1$ provides a spatial bias towards the centre of the domain, $\alpha > 1$ spatially biases the infrastructure nodes towards the domain boundary and $\alpha = 1$ yields a homogeneous spatial distribution. We illustrate the effect of this spatial bias in Fig. 4.4. Alternative radial distributions could have been considered, e.g. beta distribution, but do not necessarily yield the mathematical tractability offered by (4.16) or the spatial bias simply defined by a single parameter. We now evaluate (4.3), again employing the probability generating functional to solve the expectations. For the thinned infrastructure, we evaluate $\bar{H}_{i\mathrm{I}}$ and $\bar{H}_{12}^{(2_{\mathrm{I}})}$ for the inhomogeneous spatial distribution.

$$\bar{H}_{i\mathrm{I}} = \int_{\mathcal{V}} g(\mathbf{p}_n) H_{in} \mathrm{d}\mathbf{p}_n,$$

which, by employing polar coordinate geometry and firstly integrating over the axial component, as per chapter 3, results in

$$\bar{H}_{i\mathrm{I}} = \frac{2\pi}{k} e^{-r_i^2} \int_0^R r_n e^{-r_n^2} \left[1 + (\alpha - 1)\left(\frac{r_n}{R}\right)^{\beta}\right] \mathrm{I}_0(2 r_i r_n) \mathrm{d}r_n, \tag{4.18}$$

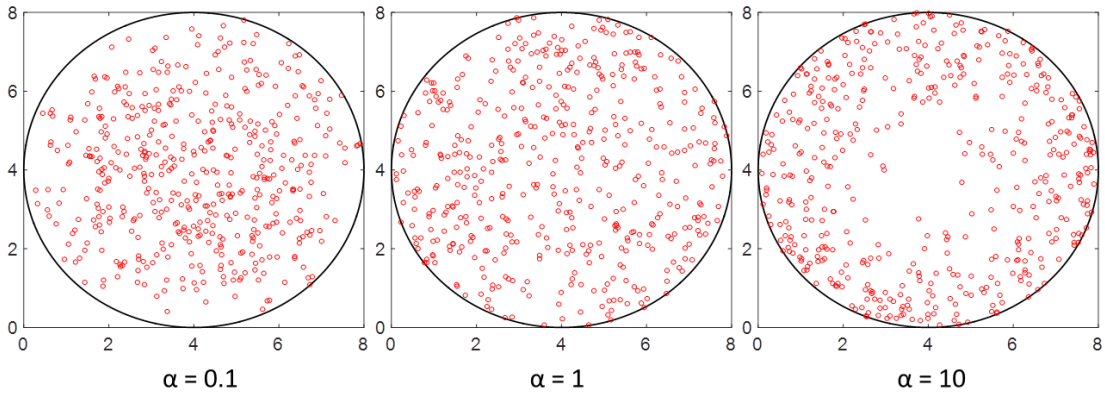


Figure 4.4: Realisations of the spatial distribution of infrastructure nodes, with density $\rho_{\mathrm{I}} = 10$ within a circle of radius $R = 4$, for $\alpha \in \{0.1, 1, 10\}$ and $\beta = 2$.

where $r_i = \|\mathbf{p}_i\|$ is the radial offset of the terminal node and $r_n = \|\mathbf{p}_n\|$. Since (4.18) only produces a closed form expression at even integers for β [242], we chose $\beta = 2$. Since we are interested in observing the effect of this spatial bias this is considered a reasonable assumption. Splitting (4.18) and applying equations (10) and (20) from [242] results in

$$\begin{aligned}\bar{H}_{i\mathrm{I}} = \frac{\pi}{k}\Bigg\{&\left(\frac{(\alpha-1)(r_i^2+1)}{R^2}+1\right)\left[1-\mathrm{Q}_1(\sqrt{2}r_i,\sqrt{2}R)\right]\\&-(\alpha-1)e^{-(r_i^2+R^2)}\left[\frac{r_i}{R}\mathrm{I}_1(2r_iR)+\mathrm{I}_0(2r_iR)\right]\Bigg\},\end{aligned} \tag{4.19}$$

where $\mathrm{I}_1(a) = \frac{1}{\pi}\int_0^{\pi} e^{a\cos\theta}\cos\theta \mathrm{d}\theta$ is the first order modified Bessel function of the first kind. Similarly

$$\bar{H}_{12}^{(2\mathrm{I})} = \int_{\mathcal{V}} g(\mathbf{p}_n) H_{1n} H_{2n} \mathrm{d}\mathbf{p}_n,$$

which, employing a similar approach as before (see Appendix B.1), can be shown to yield

$$\begin{aligned}\bar{H}_{12}^{(2_\mathrm{I})} = &\frac{\pi}{2k} e^{-\frac{1}{2}r_{12}^2} \\ &\times \left\{ \left(\frac{(\alpha-1)(2\|\overline{\mathbf{p}}_{12}\|^2+1)}{2R^2} + 1 \right) \right. \\ &\times \left[1 - \mathrm{Q}_1(2\|\overline{\mathbf{p}}_{12}\|, 2R) \right] \\ &- (\alpha-1) e^{-2(\|\overline{\mathbf{p}}_{12}\|^2+R^2)} \\ &\left. \times \left[\frac{\|\overline{\mathbf{p}}_{12}\|}{R} \mathrm{I}_1(4\|\overline{\mathbf{p}}_{12}\|R) + \mathrm{I}_0(4\|\overline{\mathbf{p}}_{12}\|R) \right] \right\}. \end{aligned} \tag{4.20}$$

It is trivial to show that a substitution of $\alpha = 1$ into (4.19) and (4.20) reduces to (4.9) and (4.7) respectively, i.e. the homogeneous case.

We evaluate (4.4), following substitutions of (4.19) and (4.20), to yield outage probability averaged over all spatial node configurations of our homogeneous relay and inhomogeneous infrastructure networks, between fixed terminal nodes. This is illustrated in Fig. 4.5 for the case where the domain radius is $R = 2.5$, terminal nodes are located at polar coordinates $2\angle 0$ and $2\angle \pi/2$, infrastructure density is fixed at $\rho_\mathrm{I} = 2$, relay density is varied over the range $\rho_\mathrm{R} \in [1, 100]$ and the infrastructure spatial weighting factor is varied over the range $\alpha \in \{0.1, 1, 10\}$. Results from Monte Carlo simulations are included to validate the analysis. The plot clearly shows that infrastructure spatial bias influences outage performance and that a homogeneous spatial bias is non-optimum. The plot also demonstrates the tightness of the upper bound.

Thus far, we have only considered the case for fixed terminals. We now proceed to average (4.4), and the upper bound (4.6), over the locations of uniformly distributed terminal nodes confined within $\mathcal{V}$. We denote these averages by $\bar{\mathcal{O}}$ and $\bar{\mathcal{O}}^{\mathrm{UB}}$ respectively, where

$$\bar{\mathcal{O}} := \mathbb{E}_{\mathbf{p}_1,\mathbf{p}_2}[\bar{\mathcal{O}}_{12}] = \frac{1}{V^2} \int_{\mathcal{V}^2} \bar{\mathcal{O}}_{12} \mathrm{d}\mathbf{p}_1 \mathrm{d}\mathbf{p}_2 \tag{4.21}$$

$$\bar{\mathcal{O}}^{\mathrm{UB}} := \mathbb{E}_{\mathbf{p}_1,\mathbf{p}_2}[\bar{\mathcal{O}}_{12}^{\mathrm{UB}}] = \frac{1}{V^2} \int_{\mathcal{V}^2} \bar{\mathcal{O}}_{12}^{\mathrm{UB}} \mathrm{d}\mathbf{p}_1 \mathrm{d}\mathbf{p}_2 \tag{4.22}$$

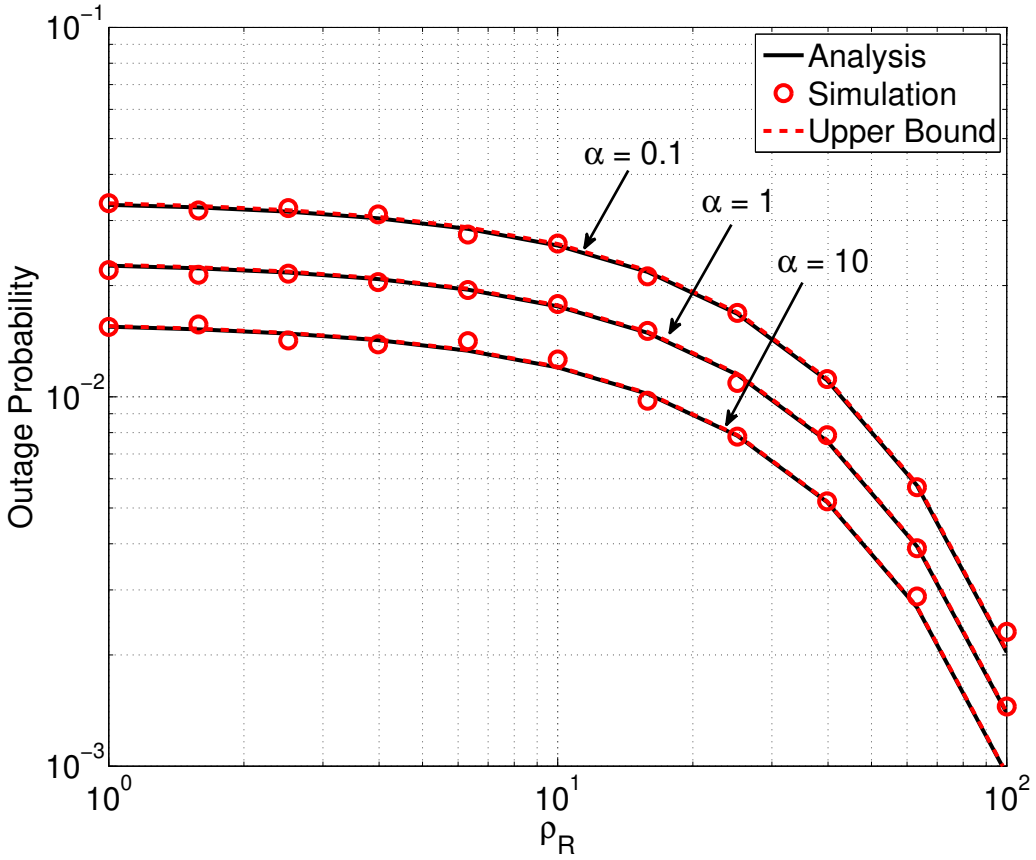


Figure 4.5: Outage probability as a function of ρ_{R}, averaged over locations of relay and infrastructure nodes over a circular domain $\mathcal{V}$ of radius 2.5, as given by (4.4), with appropriate substitutions and $\eta = 2$. Terminal node locations are both fixed at a radial offset of 2 with angular separation of $\pi/2$ and mean infrastructure density is $\rho_{\mathrm{I}} = 2$. Plot illustrates outage probability over a range of infrastructure spatial weighting factors $\alpha \in \{0.1, 1, 10\}$, $\beta = 2$ and includes results from Monte Carlo simulations. Dashed red lines indicate upper bounds derived from the application of the union bound of outage probabilities between terminal nodes and infrastructure nodes.

It should be noted that (4.21) and (4.22) apply to both homogeneous and inhomogeneous cases with appropriate substitutions for $\bar{\mathcal{O}}_{12}$ and $\bar{\mathcal{O}}_{12}^{\mathrm{UB}}$. Since these expression do not produce closed form solutions, we solve numerically by employing the polar coordinate system for $\mathbf{p}_1$ and $\mathbf{p}_2$ and using Riemann integration. We illustrate the relationship with α in Fig. 4.6, for a range of domain sizes. We observe a quasi-convex relationship where the value of α corresponding to the global minimum reduces as the domain size grows, approaching unity in the limit $R \to \infty$. Intuitively, as the domain size grows, the average separation of terminal nodes is

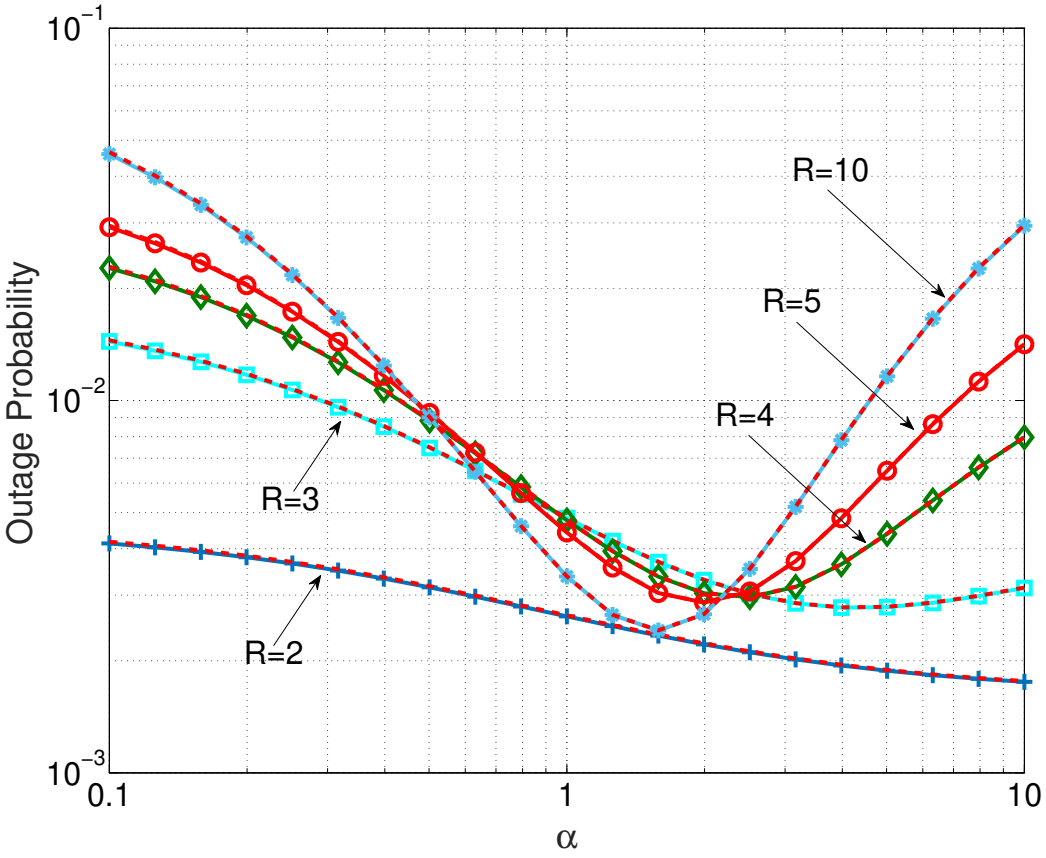


Figure 4.6: Outage probability, averaged over relay, infrastructure and terminal node locations, as a function of weighting factor α for a range of domain radii $R \in \{2, 3, 4, 5, 10\}$. In all cases, mean densities of relay and infrastructure networks are fixed at $\rho_{\mathrm{R}} = 50$ and $\rho_{\mathrm{I}} = 2.5$. Dashed red lines indicate upper bounds derived from the application of the union bound of outage probabilities between terminal nodes and infrastructure nodes averaged over terminal node locations.

such that direct connection, or connection via another relay node, occurs with low probability and connectivity is therefore dominated by the infrastructure. Since terminal nodes are most likely to connect to their proximity infrastructure nodes then a uniform spatial distribution is clearly optimal for larger domain sizes. This can be proven by considering the dominant terms of (4.4) when $r_{12} \gg 1$, and equating their 1st derivatives to zero, which yields the condition that $\alpha = 1$. A very tight upper bound is also observed which simplifies subsequent analysis of quasi-convexity in α, as detailed in Appendix B.2. Although a robust mathematical proof of quasi-convexity is generally not possible in this case, the homogeneity of the

averaging process (over the terminal and relay node positions) intuitively suggests that such a condition is true, and an extensive simulation study has supported this hypothesis. In subsequent analysis we assume quasi-convexity.

4.4 Numerical analysis of relative densities of relay and infrastructure networks

We now consider how our analysis may be applied in a 'real-world' context. By way of example, we may consider cellular[3] or vehicular networks, which typically have fixed infrastructures and where the locations and density of mobile phones, or vehicles, vary as they move, enter and leave the network. Since service providers generally have full or limited control over the network infrastructure, we may wish to determine the minimum infrastructure density and associated spatial distribution that achieves a minimum acceptable quality of service (QoS) from the composite network at a given average density of the relay (mobiles or vehicles) network. The infrastructure can then be controlled dynamically according to the temporal behaviour of the relay network.

In order to provide this behavioural insight, we equate (4.21) to a fixed prescribed outage probability $\kappa \in [0, 1]$. In subsequent analysis we assume that $\kappa = 0.01$ provides an acceptable QoS. Understanding the infrastructure/relay density relationship provides an insight into possible infrastructure activation/deactivation strategies, as relay nodes enter or leave the network. We evaluate (4.21) numerically, following substitutions of (4.4), (4.19) and (4.20), and employ Newton's method of successive approximation to yield ρ_{I}, for a given ρ_{R}. In reality, this approach would be significantly less computationally process intensive than employing a Monte Carlo process. In order to illustrate the effect of infrastructure spatial distribution bias as the domain size increases, we consider a range of biases $\alpha \in \{0.1, 0.5, 1.0, 2.0, 10\}$ and domain sizes $R \in \{1, 1.4, 1.8, 2.5, 4, 5\}$. The results of this analysis are illustrated in Fig. 4.7. Each trace represents a Pareto frontier in the average relay and infrastructure node densities, which vary with spatial distribution of the

[3]Although interference would need to be considered in this case.

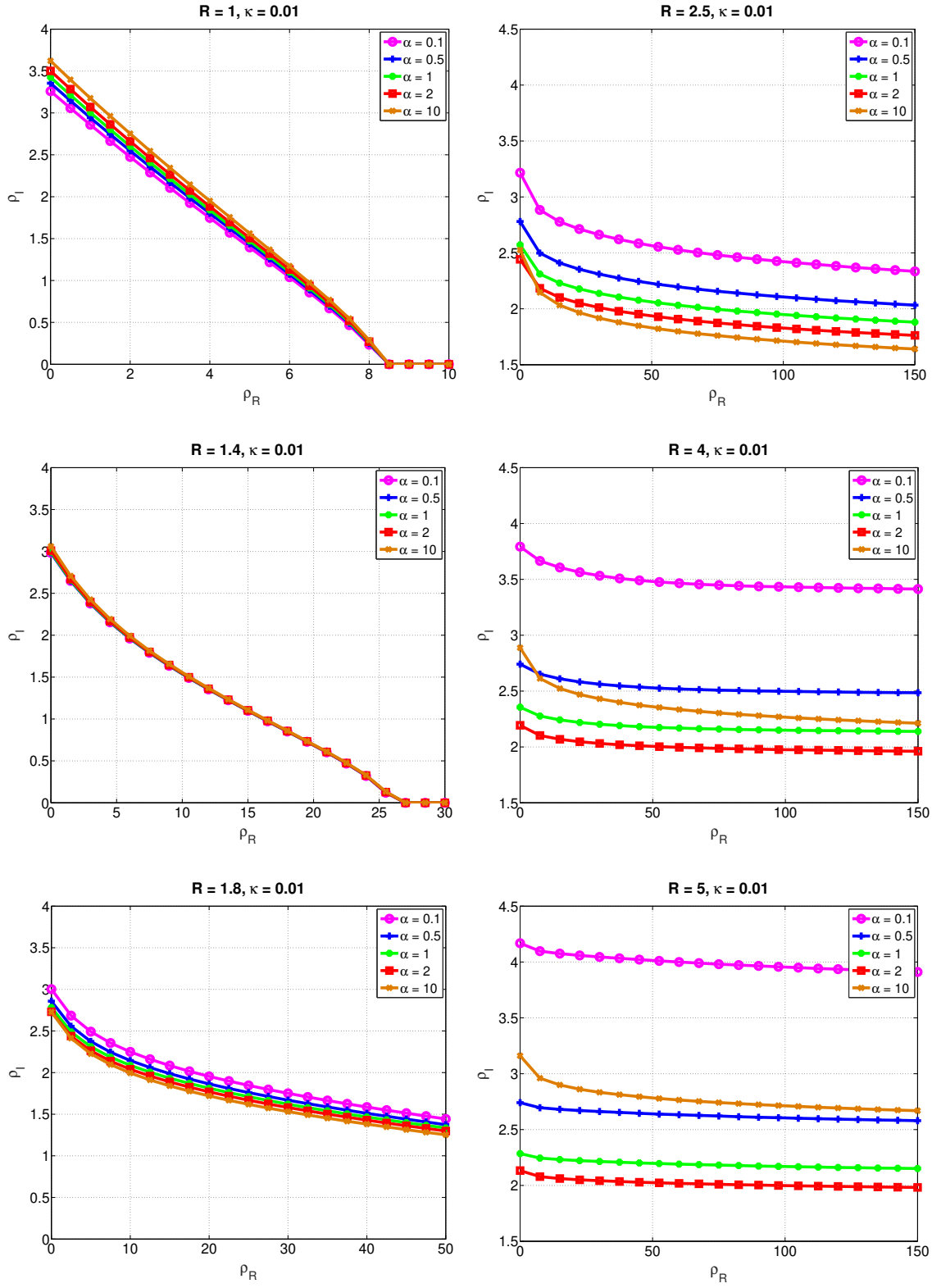


Figure 4.7: Infrastructure density, ρ_{I}, versus relay density, ρ_{R}, achieving an outage probability of $\kappa = 0.01$ averaged over positions of the terminal nodes over circular domain of radii $R \in \{1, 1.4, 1.8, 2.5, 4, 5\}$ and infrastructure spatial distribution weighting $\alpha \in \{0.1, 0.5, 1, 2, 10\}$.

infrastructure network. With knowledge of the average relay density, we can actively reduce or increase the average infrastructure density, by selective deactivation or activation of infrastructure nodes, in order to maintain or exceed our prescribed outage condition; provided the densities lie on or above the Pareto frontier.

Remark (Deactivation Strategy)**.** *Selective deactivation of infrastructure nodes is equivalent to the aforementioned thinning of our point process Φ_I, such that the resultant PPP, representing the infrastructure, has a spatial distribution with weighting factor α. With a 'real-world' network with a finite number of infrastructure nodes at fixed locations, we may employ an infrastructure deactivation strategy that results in a spatial configuration of infrastructure nodes yielding the closest approximation to this optimal spatial distribution, defined by α and β, and the required average density ρ_I.*

We observe, that for lower domain sizes, $R < 2$, appreciable rates of reduction of infrastructure density, with increasing relay density, can be realised to the point whereby the relay density is sufficient to establish the required outage conditions without any infrastructure network. For the cases where $R < 1.4$ and with no relay nodes, a lower density of infrastructure nodes are required when they are spatially biased towards the centre. As the relay density increases, this spatial bias becomes less important. This implies that, as the density of relay nodes increases, infrastructure nodes closer to the boundary should be deactivated in the thinning process. We observe a transition at a radius $R = 1.4$, whereby for increasing radii, lower infrastructure densities are required when spatially biased towards the boundary.

Remark (Transition Radius)**.** *If we assume a fixed infrastructure network density, the expected number of infrastructure nodes will reduce with domain size. For smaller domain sizes (when the domain radius is less than or close to the hard connection range r_0) and with the absence of relay nodes, a randomly located terminal node is likely to have more infrastructure nodes within connection range when they are located towards the centre of the domain. As domain size grows above r_0 and with*

infrastructure nodes centrally biased there will be regions where terminal nodes are located closer to the boundary that will have limited or no access to any infrastructure node, thus requiring an increased spatial bias toward the domain boundary.

As the domain size increases beyond $R = 1.8$, the rate of reduction of infrastructure density, with increasing relay density, is significantly lower and the spatial bias of the infrastructure has a more marked effect on performance, with an optimum spatial bias occurring at approximately $\alpha = 2$ for $R = 5$.

We now focus on the optimum spatial distribution for the infrastructure network, denoted by α_{opt}, that yields a minimum in averaged outage probability as defined by (4.21). Since we conjecture a quasi-convex relationship in (4.21) with respect to α, we solve

$$\frac{\partial \bar{\mathcal{O}}}{\partial \alpha} = \frac{1}{V^2} \int_{\mathcal{V}^2} \frac{\partial \bar{\mathcal{O}}_{12}}{\partial \alpha} \mathrm{d}\mathbf{p}_1 \mathrm{d}\mathbf{p}_2 = 0. \tag{4.23}$$

by employing Newton's method of successive approximation. The derivatives of $\bar{\mathcal{O}}_{12}$, with respect to α are relatively straightforward and not included for brevity. We firstly consider the optimum spatial distribution of a fixed density infrastructure, in the absence of relay nodes, as a function of domain size. This is illustrated in Fig. 4.8 for an infrastructure density $\rho_{\text{I}} = 3$ and zero relay density. We show that for increasing radius, we firstly observe the sharp transition from a centrally biased to boundary biased infrastructure; we remark on this *transition radius* earlier. The spatial bias then reaches a maximum at $R \approx 1.9$, followed by an asymptotic decay towards a uniform spatial distribution. This decay is an intuitive result since, as we approach a network of infinite extent, a uniformly distributed infrastructure is required to provide coverage over the whole domain.

We now proceed to investigate both the minimum infrastructure density, denoted by $\rho_{\text{I}_{\min}}$, and the optimum spatial infrastructure bias, that achieves the prescribed averaged outage probability $\bar{\mathcal{O}} = \kappa$. We evaluate these over a range of relay densities and domain radii using the following process:

1. Fix domain radius R and initially set $\rho_{\text{R}} = 0$ and $\alpha = \alpha_{\text{opt}} = 1$.

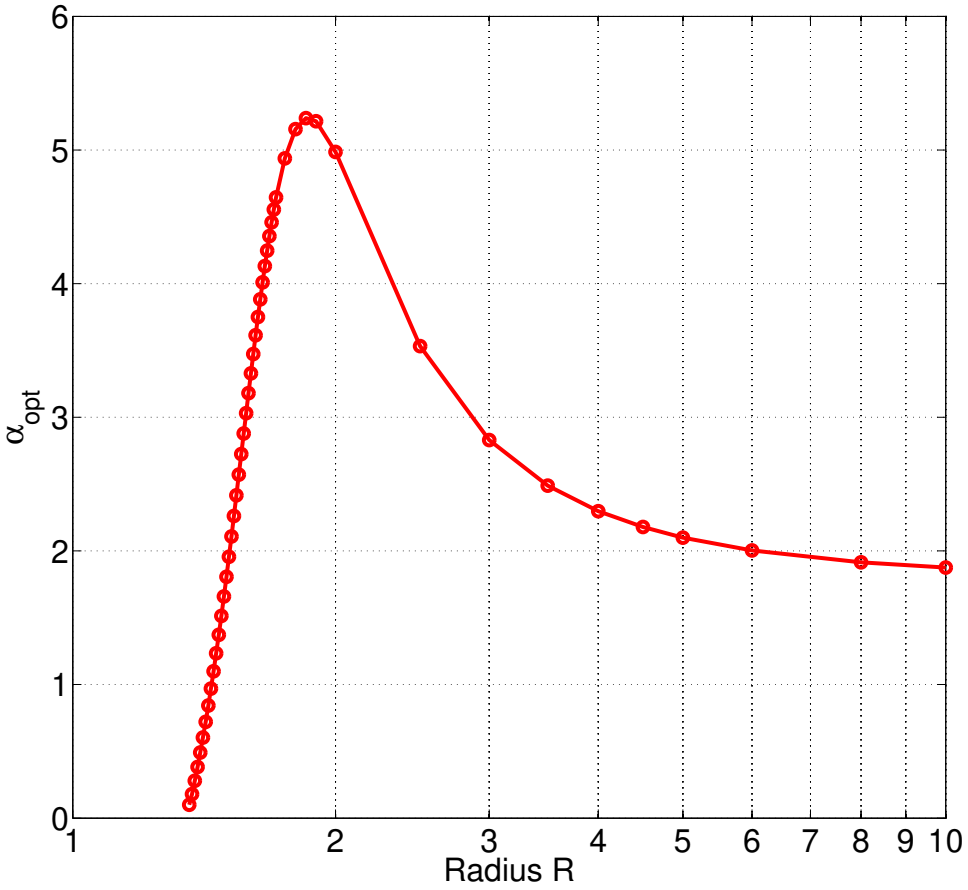


Figure 4.8: For fixed infrastructure density of $\rho_{\mathrm{I}} = 3$ and no relay network, we show the optimum spatial bias α_{opt} (minimising averaged outage probability) as a function of domain radius R.

2. Substitute $(R, \rho_{\mathrm{R}}, \alpha)$ into (4.21) and determine $\rho_{\mathrm{I}_{\mathrm{min}}}$, satisfying $\bar{\mathcal{O}} = \kappa$, by successive approximation.

3. Substitute $(R, \rho_{\mathrm{I}} = \rho_{\mathrm{I}_{\mathrm{min}}})$ into (4.23) and determine α_{opt} by successive approximation.

4. Due to interdependence of α and ρ_{I}, iterate steps 2 and 3 until an acceptably low difference (e.g. 1%) is reached between successive approximations of α and ρ_{I}; we find 2 iterations are satisfactory.

5. Increment ρ_{R} and repeat from step 2 using the previous $\rho_{\mathrm{I}_{\mathrm{min}}}$ and α_{opt} to seed the subsequent successive approximations.

We focus on the larger domains with $R \in \{2.5, 3, 4\}$, since the reduction in infrastructure with spatial bias compared to the uniform distribution case, for lower domain sizes, is negligible. Results are shown in Fig. 4.9 which includes the density relationship for the uniform $\alpha = 1$ case. Firstly, we observe that employing a non-uniform spatial distribution of infrastructure can realise significant reductions in the infrastructure density compared to the uniformly distributed case, as illustrated in Fig. 4.10, where reductions between 8% and 16% are observed. Secondly, if we consider the relationship between optimum α, denoted by α_{opt}, and relay density, we observe that monotonicity of the slopes of the traces change from strictly increasing to decreasing as the domain size increases.

Remark (Optimum Spatial Bias)**.** *The analysis for lower domain sizes, above the aforementioned transition radius but with $R < 3$, shows that, with increasing relay density, infrastructure nodes closest to the domain centre should be deactivated and remaining active infrastructure nodes should be strongly concentrated at the boundary region. This suggests that the relay network dominates connectivity within the bulk and infrastructure nodes at the boundary compensate for loss of relay connectivity mass towards the boundary region. This dominance decreases with increasing domain size and we observe that α_{opt} reduces, an intuitive result since as we approach a network of infinite extent, a uniformly distributed infrastructure is required.*

4.5 Conclusion and Discussions

In this chapter, we have studied the connectivity between two terminal nodes employing direct, 2-hop and infrastructure based connectivity within a circular domain subject to Rayleigh fading. We consolidate the previous mathematical expressions, derived in Chapter 3, with connectivity function between fixed terminal nodes and an inhomogeneously distributed infrastructure network. With the objective of minimising outage probability between two randomly selected independent uniformly distributed (i.u.d.) terminal nodes, we show that employment of direct and relay assisted connectivity can significantly reduce the reliance on

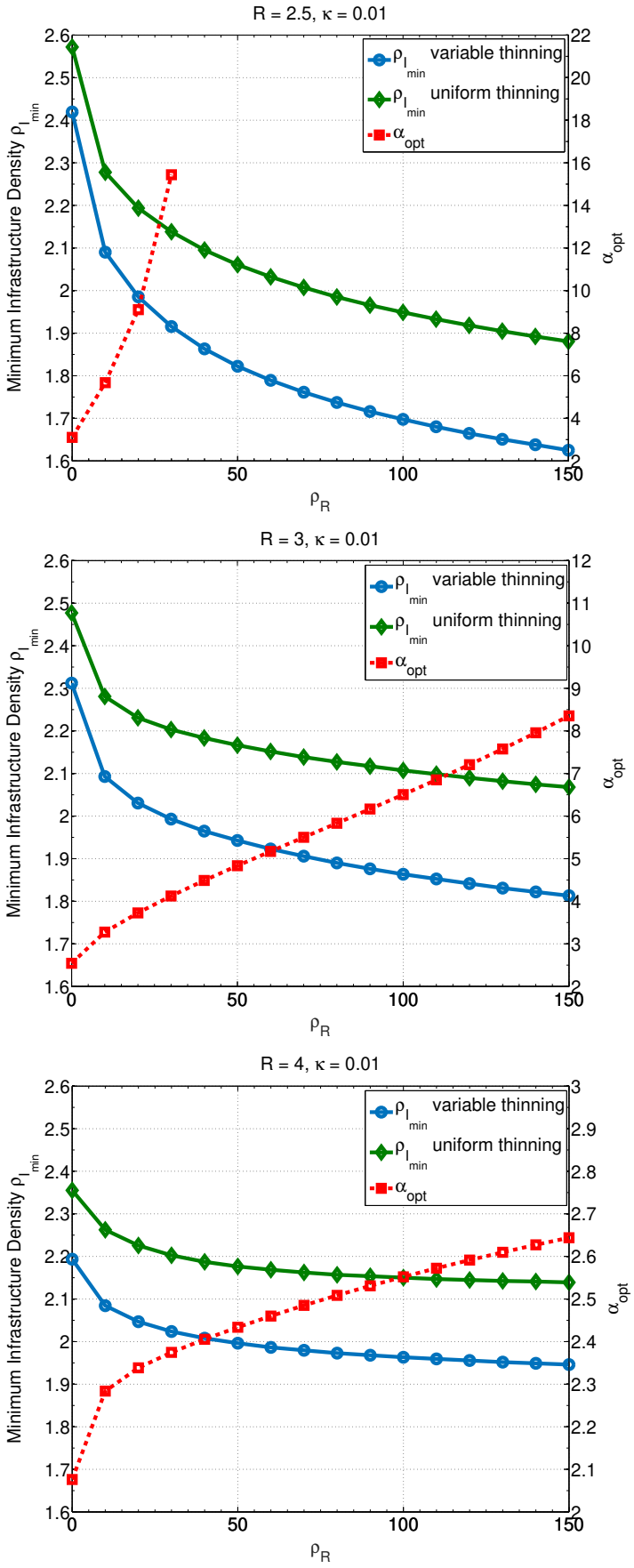


Figure 4.9: Minimum infrastructure density, employing variable (non uniform) and uniform thinning, and optimum infrastructure spatial bias α_{opt} as a function of relay density for radii $R \in \{2.5, 3, 4\}$.

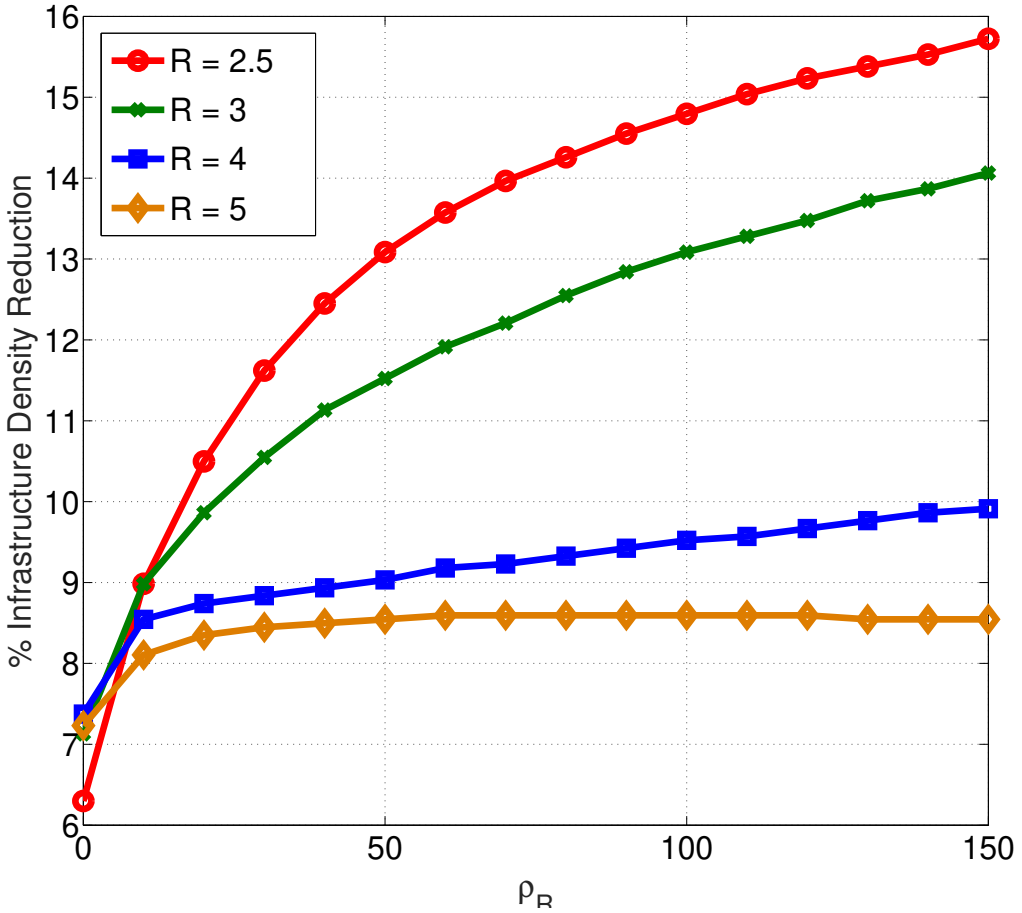


Figure 4.10: Reduction in infrastructure density by employment variable (non uniform) spatial thinning relative to the uniform spatial thinning case.

the infrastructure. Furthermore, the spatial distribution of infrastructure nodes has a marked bearing on connectivity performance in the finite domain regime, opening up the possibility of spatially selective deactivation of infrastructure nodes conditioned on relay density. We provide a mathematical framework that enables the determination of the optimal density and spatial distribution of an infrastructure network, for a given relay density and prescribed outage condition. As the domain sizes increase, we observe diminishing returns in employing direct and relay assisted connectivity due to increased average separation of terminal nodes and therefore an increased reliance on the infrastructure, which could be addressed by allowing 2-hop connectivity between terminal and infrastructure nodes via an intermediate relay node; a possible future extension to this analysis.

5

Continuum Model for Route Optimisation in Large-Scale Inhomogeneous Multi-Hop Wireless Networks

5.1 Introduction

In section 2.4, we introduced the relay node placement problem (RNPP) in large scale multihop wireless networks and described the problem of potentially unwieldy processing complexity in optimising relay node placement. In this chapter, we consider the scenario whereby the placement of N-relays is deterministic and where the computation of network performance is polynomial time solvable to yield optimal solutions (in contrast to aforementioned heuristic approaches), for example by Lagrangian formulation of a constrained optimisation problem. Although robust in determining the optimal solution, they are computationally expensive; requiring matrix manipulation that can scale like $O(N^3)$ [217], although this processing complexity can be reduced by an order of magnitude by using augmented Lagrangian methods that do not require matrix manipulations [243]. Although a number of numerical optimisation tools exist for this purpose, e.g. the MATLAB$^{\text{TM}}$ function fmincon [244], such tools are computational unwieldy and prohibitive when applied in the context of large (e.g. 100s or 1000s of relays [31, 245]), energy-constrained relay networks or where networks are subject to temporal variation necessitating continuous re-routing to maintain performance optimality.

In order to yield optimal solutions through lower complexity computation, we consider an alternate method by considering a relay network of infinite extent to form a continuous equivalent relay path. Our approach is based upon the idea of treating the multi-hop route as a continuum[1]. We argue that this approach has the potential to reduce the complexity in the node placement/route selection process for dense networks. In order to provide a practical context to our work, we consider that the network is subject to spatial inhomogeneity; arising from point sources of co-channel interference[2]. Prior work that has considered continuum modelling include [247] and [248], which treated discrete base station (BS) entities as a continuum of transmitters in order to yield a closed form expression for certain

[1] Continuum mechanics [246] is a field of study whereby accurate behavior models are developed based on the assumption that the substance of an object is assumed to completely fill the space it occupies, even though it actually comprises a large finite number of molecules.

[2] Although other forms of spatial inhomogeneity can be considered.

network performance characteristics, and [249], which discussed the application of variational calculus to a problem of determining the minimal exposure path in wireless sensor networks. However, to the best of our knowledge, no prior work exists relating to the use of continuum modelling for route optimization in large scale multi-hop wireless networks. As such, we believe that the proposed model presents a radically different view of wireless networks, which we hope will stimulate further interest in developing new approaches to treating complex wireless networks in the future, even down to the microscopic level, e.g., nanoscale wireless [250] and molecular communications networks [251].

Although exploratory in nature, this research chapter offers the following contributions:

1. we develop a continuum model that describes the end-to-end outage probability in a multi-hop relay network;

2. we apply the model to find an analytic solution for the outage-optimal device locations when the system is subject to an inhomogeneous scalar field of interference;

3. the efficacy of the continuum model is verified by considering a discrete sampling of the continuum with a finite number of relay nodes.

The remainder of the chapter is organised as follows. In section 5.2, we introduce the discrete optimisation problem. In section 5.3, we introduce the continuum model for end-to-end outage probability calculation. In section 5.4, we elaborate on our continuum model by applying it to study the outage-optimisation problem for a multi-hop wireless network subject to a single interferer. This is followed in section 5.5 where we consider multiple interferers along with the effectiveness of approximating a finite number of spatially distributed interferers by a single equivalent interferer. Section 5.6 provides thoughts on how to sample the continuum to obtain discrete node positions for use in practical, finite systems. Conclusions are drawn in section 5.7.

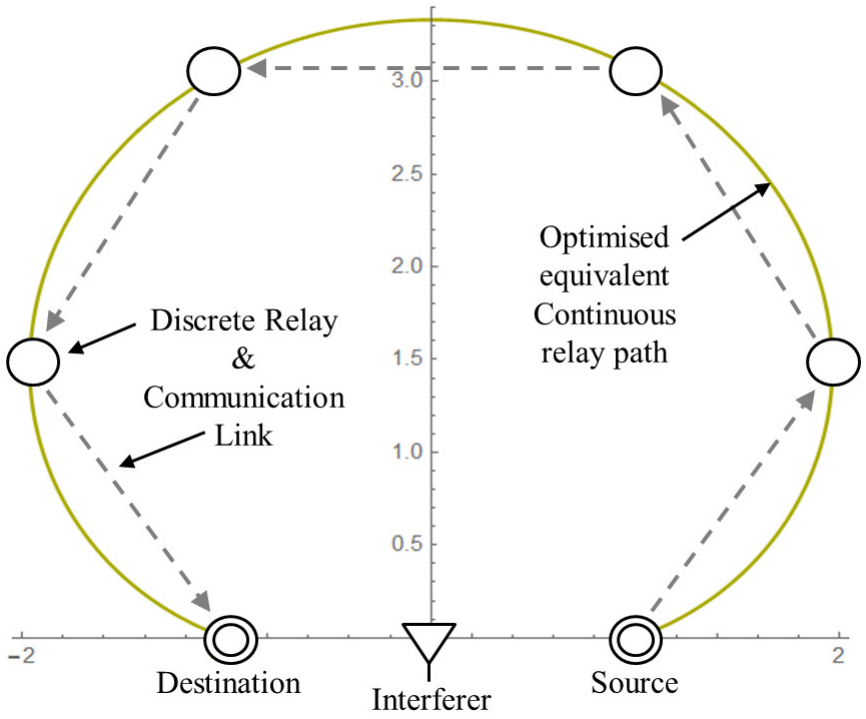


Figure 5.1: Multihop wireless network subject to single interferer.

5.2 Discrete Optimisation of Relay Locations

Consider the goal of transmitting a message from a source node to a destination node via N relay nodes located in Euclidean space[3] $\mathbb{R}^d$, $d \in \{2, 3\}$. We denote the positions of the source and destination nodes by $\mathbf{p}_0$ and $\mathbf{p}_{N+1}$, respectively, and the position of the ith relay node by $\mathbf{p}_i$[4]. For convenience, we collect the positions of the relay nodes in the set $\mathcal{R} = \{\mathbf{p}_1, \mathbf{p}_2, \ldots, \mathbf{p}_N\}$.

Fig. 5.1 illustrates the scenario where a communications network, located in $\mathbb{R}^2$, is subjected to a scalar field of interference originating from a point source. We assume that all node transmissions are co-channel and temporally continuous[5], relays employ perfect self interference cancellation [252], [253] and interference from non-adjacent relay nodes is assumed negligible.

In this example, the average interference level at any node will have a spatial dependence on its location. Given known locations of the source, destination and

[3]The analysis does not preclude the use of alternative topological spaces.
[4]We use $\mathbf{p}_i$ to refer to the ith node, itself, as well as its position in $\mathbb{R}^d$.
[5]The subsequent analysis can also be applied to systems employing time division duplex protocols.

interferer nodes, our goal will be to optimise a performance metric by the appropriate positioning of relay nodes. Here, we chose to minimise the outage probability of the source-destination communication link, as defined by

$$\mathcal{R}^* = \underset{\mathcal{R}}{\operatorname{argmin}}\ \mathrm{f}(\mathcal{R}),\ \text{s.t.}\ \begin{cases} \mathrm{g}(\mathcal{R}) = b \\ \mathrm{h}(\mathcal{R}) \leqslant c \end{cases} \tag{5.1}$$

where $\mathcal{R}^*$ represents the set of optimised relay node locations, $\mathrm{f}(\mathcal{R})$ is the objective function dependent upon the relay, source, destination and interferer locations, $\mathrm{g}(\mathcal{R}) = b$ is an equality constraint function relating to the boundary conditions imposed by fixed positions of the source and destination nodes, $\mathrm{h}(\mathcal{R}) \leqslant c$ represents an arbitrary inequality constraint function and b and c are constants. A more complex scenario may have many more constraints. This problem may be solved with the application of a Lagrangian formulation of the form

$$\mathcal{L}(\mathcal{R}, \lambda_1, \lambda_2) = \mathrm{f}(\mathcal{P}) + \lambda_1(b - \mathrm{g}(\mathcal{R})) + \lambda_2(c - \mathrm{h}(\mathcal{R})), \tag{5.2}$$

where λ_1 and λ_2 are Lagrange multipliers. This is detailed in Appendix A.2. The principal drawback of this approach is the processing complexity that typically scales with $O(N^3)$.

5.3 Continuum Model for End-to-End Outage Probability

Given the aforementioned cubic scaling in processing complexity with the number of relay nodes using a discrete model, we postulate that this processing complexity may be reduced by considering a continuum model whereby we take the limit of infinite relay nodes to derive a continuous relay path. Our goal is to develop a formulation of the end-to-end outage probability for the source-destination link that is a functional of the curve in $\mathbb{R}^d$ along which relay devices are placed, i.e., the points in $\mathcal{R}$ should be contained in (or be very close to) the curve. This curve will effectively signify a path of infinite node density. To maintain a practical viewpoint, however, we will retain a *finite connection density* in the model. It is important to note that without this consideration, the end-to-end outage probability would

converge to zero as $N \to \infty$. To give a better picture of this approach, Fig. 5.1 illustrates a continuous path along with discrete node placements for a system subject to a point source of interference. We will return to this example later.

5.3.1 General Formulation

To make progress, we consider a wireless network in $\mathbb{R}^2$ and a model whereby a connection between two arbitrary points $\mathbf{p}_i$ and $\mathbf{p}_j$ exists with probability $c(\mathbf{p}_i, \mathbf{p}_j)$, which is independent of all other connections. We then form a multi-hop route, between a source $\mathbf{p}_0$ and a destination $\mathbf{p}_{N+1}$, via the sequence of relays at the points in $\mathcal{R}$. The probability that an end-to-end connection exists between the source and destination can be written as

$$P_c = \prod_{n=0}^{N} c(\mathbf{p}_n, \mathbf{p}_{n+1}). \tag{5.3}$$

We define the outage probability as the complement of the connection probability, i.e., $P_o = 1 - P_c$. It will be convenient to define the *logarithmic connection probability* (LCP) as

$$\psi_c \coloneqq \log P_c = \sum_{n=0}^{N} \log c(\mathbf{p}_n, \mathbf{p}_{n+1}). \tag{5.4}$$

We now consider the homogeneous and inhomogeneous cases separately.

5.3.2 Homogeneous System

In the homogeneous case, the connection function between nodes depends only upon the Euclidean distance between them. In this case, we can write

$$\begin{aligned} \psi_c &= \sum_{n=0}^{N} \log c(\|\mathbf{p}_{n+1} - \mathbf{p}_n\|) \\ &= \sum_{n=0}^{N} \frac{\log c(\|\mathbf{p}_{n+1} - \mathbf{p}_n\|)}{\|\mathbf{p}_{n+1} - \mathbf{p}_n\|} \|\mathbf{p}_{n+1} - \mathbf{p}_n\|, \end{aligned} \tag{5.5}$$

where $\|\cdot\|$ is the l^2-norm. We define $\ell_n := \|\mathbf{p}_{n+1} - \mathbf{p}_n\|$. Any line in $\mathbb{R}^2$ can be partitioned into a sequence of points $\mathcal{P} = \{\mathbf{p}_0, \ldots, \mathbf{p}_{N+1}\}$ with $\mathbf{s} = \mathbf{p}_0$ denoting the source and $\mathbf{d} = \mathbf{p}_{N+1}$ denoting the destination such that $\ell_0 + \cdots + \ell_n \leq L$,

the length of the line. Let the mesh of the partition be defined as $\delta_\ell := \max \ell_i$. Suppose as $\delta_\ell \to 0$, we have

$$\frac{\log c(\|\mathbf{p}_{n+1} - \mathbf{p}_n\|)}{\|\mathbf{p}_{n+1} - \mathbf{p}_n\|} \to -q, \quad \forall n \text{ and } q \in \mathbb{R}_+. \tag{5.6}$$

Note that this limit is not dependent upon N since the system is homogeneous. It follows that

$$\bar{\psi} = \lim_{\delta_\ell \to 0} \psi_c = -q \int \mathrm{d}\ell = -qL. \tag{5.7}$$

Thus, we can write the outage probability along the line as

$$P_o = 1 - \mathrm{e}^{-qL}. \tag{5.8}$$

It is clear that the path with the minimum length yields the lowest outage probability. This result is consistent with findings in [254] which discusses a relay selection strategy where the security of a multi-hop network, in the presence of a homogeneous spatial distribution of eavesdroppers, is optimal when relays are chosen that are closest to the midpoint between source and destination nodes i.e. the resultant multi-hop path length is minimised.

5.3.3 Inhomogeneous System

For the case of an inhomogeneous system, we will find it useful to specify point locations in a parametric manner. Define the tagged partition $\mathcal{P}_z^\zeta = \{z_0, z_1, \ldots, z_{N+1}\}$ with $0 = z_0 < z_1 < \cdots < z_{N+1} = 1$ along with a sequence $\zeta_0, \ldots, \zeta_N$, the elements of which satisfy $\zeta_n \in [z_n, z_{n+1}]$. The path of points that the communication will traverse can be written as the sequence $\mathbf{p}(0), \mathbf{p}(z_1), \ldots, \mathbf{p}(z_{N+1})$ where $\mathbf{p}(z) = (x(z), y(z))$. We can no longer say that the connection function is only dependent upon the pairwise distance, so we must write

$$\begin{aligned} \psi_c &= \sum_n \log c(\mathbf{p}(z_n), \mathbf{p}(z_{n+1})) \\ &= \sum_n \frac{\log c(\mathbf{p}(z_n), \mathbf{p}(z_{n+1}))}{z_{n+1} - z_n}(z_{n+1} - z_n). \end{aligned} \tag{5.9}$$

Let the mesh of the partition $\mathcal{P}_z^\zeta$ be denoted by $\delta_z = \max_n(z_{n+1} - z_n)$. Now suppose that as $\delta_z \to 0$, we have

$$\frac{\log c(\mathbf{p}(z_n), \mathbf{p}(z_{n+1}))}{z_{n+1} - z_n} \to -q(\zeta_n) < 0. \tag{5.10}$$

for some function $q : [0, 1] \to \mathbb{R}_+$. It follows that if the function q is Riemann integrable, then

$$\bar{\psi} = \lim_{\delta_z \to 0} \psi_c = -\int_0^1 q(z)\,\mathrm{d}z. \tag{5.11}$$

The outage probability in this case can be written as

$$p_o = 1 - \mathrm{e}^{-\int_0^1 q(z)\,\mathrm{d}z}. \tag{5.12}$$

We note that this result generalizes that presented in (5.8).

5.4 Multi-hop Route Optimisation in the Presence of a Single Interferer

We now proceed to apply our continuum model to optimize the placement of relays, in a multi-hop communications network, when communication takes place in the presence of an inhomogeneous scalar field of interference in $\mathbb{R}^2$ caused by a single interferer at a known location (see Fig. 5.1). Our current analysis focuses on the outage probability of the multi-hop communication link; however, other metrics can be considered.

In order to progress, we must obtain the function $q(z)$. The formulation of q is dependent upon the connection model, which is governed by the channel fading statistics, modulation and coding schemes employed, and various other characteristics of the system including the interferer in this scenario. In what follows, we develop the model further by assuming each pairwise communication link is independent and affected by Rayleigh fading, and the mean path loss follows an inverse power law, with exponent η, with respect to the Euclidean distance between devices. We firstly consider the connectivity between two arbitrary nodes, transmitter $\mathbf{p}_i$ and receiver $\mathbf{p}_j$ separated by distance $d_{ij} = \|\mathbf{p}_i - \mathbf{p}_j\|$. In

this particular example, we can arbitrarily centre the coordinate system on the interference source, located at $(0,0)$. The interferer transmits with power P_I at a distance $d_j = \|\mathbf{p}_j\|$ from the receiving node. We assume that all nodes have antennas with uniform gain G in the $\mathbb{R}^2$-plane.

The signal to noise and interference ratio (SINR) at the receiving node is given by modification of (2.5) taking interference into account. This results in

$$\mathrm{SINR_j} = \frac{PG^2(\frac{\lambda}{4\pi})^2 d_{ij}^{-\eta}|h_{ij}|^2}{\sigma^2 + \mathcal{I}}, \tag{5.13}$$

where P is the transmit power level of $\mathbf{p}_i$, λ is the RF wavelength, $h_{ij} \sim \mathcal{CN}(0,1)$ is the Rayleigh fading coefficient, σ^2 is the thermal noise power and $\mathcal{I}$ is the interference power level at the receiver as given by

$$\mathcal{I} = \zeta d_j^{-\eta}|h_j|^2, \tag{5.14}$$

where $\zeta = P_I G^2(\frac{\lambda}{4\pi})^2$ and $h_j \sim \mathcal{CN}(0,1)$, with P_I denoting the transmit power of the interferer. We will then have a connection probability, conditioned on the interference, defined by

$$\begin{aligned} c|_{\mathcal{I}}(\mathbf{p}_i, \mathbf{p}_j) &= \mathbb{P}[\mathrm{SINR_j} \geqslant \tau] \\ &= \mathbb{P}\left[\frac{PG^2(\frac{\lambda}{4\pi})^2 d_{ij}^{-\eta}|h_{ij}|^2}{\sigma^2} \geqslant \tau\left(1 + \frac{\mathcal{I}}{\sigma^2}\right)\right], \end{aligned} \tag{5.15}$$

where τ is the minimum SINR required to establish a communication link. For convenience, we define a fixed connectivity scale r_0 given by

$$r_0^\eta = \frac{PG^2\left(\frac{\lambda}{4\pi}\right)^2}{\sigma^2\tau}. \tag{5.16}$$

Since $|h_{ij}|^2$ has a standard exponential distribution, (5.15) becomes

$$c|_{\mathcal{I}}(\mathbf{p}_i, \mathbf{p}_j) = \exp\left(-\frac{d_{ij}^\eta}{r_0^\eta}\left(1 + \frac{\mathcal{I}}{\sigma^2}\right)\right). \tag{5.17}$$

We now average over the fading variable $|h_j|^2$ in the interfering path. Since $|h_j|^2$ also has standard exponential distribution, the connection probability is given by

$$\begin{aligned} c(\mathbf{p}_i, \mathbf{p}_j) &= \int_0^\infty \exp\left(-\frac{d_{ij}^\eta}{r_0^\eta}(1 + k d_j^{-\eta}|h_j|^2)\right) \\ &\quad \times \exp(-|h_j|^2)\mathrm{d}|h_j|^2 \\ &= \mathrm{e}^{-\left(\frac{d_{ij}}{r_0}\right)^\eta}\left[\frac{1}{1+\Omega}\right], \end{aligned} \tag{5.18}$$

where $\Omega = kd_{ij}^{\eta} d_j^{-\eta}/r_0^{\eta}$ and $k = \zeta/\sigma^2$. Hereafter, with a slight abuse of terminology, we refer to k as the normalised interference-to-noise ratio (INR)[6].

We proceed with the steps outlined in section 5.3.3 to develop the continuum model further. Having defined our connectivity function, we consider two points close to each other such that

$$\log c(\mathbf{p}(z), \mathbf{p}(z+\delta_z)) = -\Bigg[\frac{1}{r_0^{\eta}}\|\mathbf{p}(z+\delta_z) - \mathbf{p}(z)\|^{\eta} + \log\left(1 + \frac{k}{r_0^{\eta}}\frac{\|\mathbf{p}(z+\delta_z) - \mathbf{p}(z)\|^{\eta}}{\|\mathbf{p}(z+\delta_z)\|^{\eta}}\right)\Bigg] \tag{5.19}$$

Using the Cartesian coordinate system and expanding (5.19) for small δ_z yields

$$\log c(\mathbf{p}(z), \mathbf{p}(z+\delta_z)) = \left[1 + \frac{k}{(x^2+y^2)^{\frac{\eta}{2}}}\right]\frac{(\dot{x}^2+\dot{y}^2)^{\frac{\eta}{2}}}{r_0^{\eta}}\delta_z^{\eta} + O(\delta_z^{\eta+1}). \tag{5.20}$$

For convenience, we omit the argument z in functions x and y such that, e.g., $x := x(z)$ and $\dot{x} := \dot{x}(z)$. The dot notation denotes the first derivative of the function with respect to its argument, e.g. $\dot{x} := \frac{\mathrm{d}x(z)}{\mathrm{d}z}$. We define

$$\mathrm{d}l = \sqrt{(\dot{x}^2+\dot{y}^2)}\delta_z \tag{5.21}$$

to be the path length differential. Then, under the condition that $\mathrm{d}l^{\eta-1}/r_0^{\eta} \to \theta \in \mathbb{R}_+$ as $\delta_z \to 0$, the limit becomes

$$q(z) = \theta\left[1 + \frac{k}{(x^2+y^2)^{\frac{\eta}{2}}}\right]\sqrt{\dot{x}^2+\dot{y}^2}. \tag{5.22}$$

For the special case $\eta = 2$, the ratio $\mathrm{d}l/r_0^2$ is proportional to the connection density, which is defined as the average number of connections per unit of length. Hence, the condition $\mathrm{d}l/r_0^2 \to \theta$ indicates that the connection density must be constant in the limit.

For convenience we introduce the function

$$\mu(x,y) \coloneqq \left[1 + \frac{k}{(x^2+y^2)^{\frac{\eta}{2}}}\right]^{-1}. \tag{5.23}$$

[6]In fact, k is proportional to INR, where the proportionality constant is related to effective antenna aperture.

Specifically, the function $\mu : \mathbb{R}^2 \to \mathbb{R}_+$ signifies the link quality at a given point in the plane. We can now write the outage probability as

$$P_o[x, y] = 1 - \exp\left(-\theta \int_0^1 \frac{\sqrt{\dot{x}^2 + \dot{y}^2}}{\mu(x, y)} \mathrm{d}z\right). \tag{5.24}$$

This formulation provides an expression of the outage probability as a functional[7] of the parametric path variables x and y. We note that the path that minimizes the outage probability is independent of the scaling factor θ.

Remark. *It should be noted that performing the same analysis for an unfaded interferer [155], yields the same result. This is intuitive in that one would conjecture that the interference field, over the continuum, would tend to the unfaded mean power level in the limit of infinite relay nodes.*

5.4.1 Stationary Paths

Our objective now is to determine the functions x and y that yield a global minimum in the functional (5.24). For convenience, we cast the outage probability expression in polar coordinates to obtain

$$P_o[r] = 1 - \exp\left(-\theta \int_{\phi_1}^{\phi_2} \frac{\sqrt{r^2 + \dot{r}^2}}{\mu(r)} \mathrm{d}\phi\right), \tag{5.25}$$

where the link quality function can be expressed as

$$\mu(r) = \left[1 + \frac{k}{r^\eta}\right]^{-1}. \tag{5.26}$$

The radius r is a function of the angle ϕ, and ϕ_1 and ϕ_2 represent the respective angle-ordinates of the source and destination nodes.

We now proceed to apply tools from the calculus of variations [255] to compute the stationary paths in polar coordinates, which are defined by the function $r(\phi)$. Denoting the integrand in (5.24) by $L(r, \dot{r})$ and recognizing that it does not contain any explicit function of ϕ, we invoke the Beltrami identity to determine the stationary paths:

$$L - \dot{r}\frac{\partial L}{\partial \dot{r}} = C_1, \tag{5.27}$$

[7]The notation $P_o[x, y]$ is used to highlight the fact that the outage probability depends on the functions x and y.

where C_1 is a constant. Evaluating (5.27) gives

$$\dot{r} = \frac{1}{C_1}\sqrt{r^{4-2\eta}(k+r^{\eta})^2 - C_1^2 r^2}. \tag{5.28}$$

For the special case $\eta = 2$ and where $C_1 \geqslant 2\sqrt{k}$, there exists a closed form solution to (5.28) as given by the following proposition.

Proposition 1. *The optimum route for the single interferer scenario is given by*

$$r(\phi) = \alpha \ \mathrm{sn}\left(\pm \frac{\gamma(\phi - C_2)}{C_1}, \frac{\alpha}{\gamma} \right), \tag{5.29}$$

where $\mathrm{sn}(u, \kappa)$ *is the Jacobi elliptic function,* $\kappa = \alpha/\gamma$ *is the elliptic modulus,* $\alpha = 0.5C_1 - 0.5\sqrt{C_1^2 - 4k}$, $\gamma = 0.5C_1 + 0.5\sqrt{C_1^2 - 4k}$ *and* C_1 *and* C_2 *are constants. The Jacobi elliptic function is valid over the range* $0 < \kappa^2 < 1$.

Proof. See Appendix C.1. □

Remark. *Although an analytic solution is constrained by the condition* $C_1 \geqslant 2\sqrt{k}$ *in this scenario, numeric solutions to the Euler Lagrange equations can be found generally, as we demonstrate in subsequent sections.*

Given fixed boundary conditions, i.e., the locations of the source and destination nodes, we employ Mathematica to determine the constants C_1 and C_2 for a given value of k. We illustrate the optimum routes for the cases where the terminal nodes are located at Cartesian coordinates $(1, 0)$, $(-1, 0)$ and $(0.5, 0)$, $(0, 1)$, for a range of values of k in Figs. 5.2 and 5.3, respectively. The associated values for the constants C_1 and C_2 are given in Table 5.1.

It can be argued that the paths shown in Figs. 5.2 and 5.3 are all local minima, since one can imagine perturbations of the paths toward the interference source would increase the INR, while perturbations away from the source would lead to a reduction in the connectivity probability (due to the increased path length). More formally, we show that the stationary paths, corresponding to our functional, are minima since they satisfy Legendre's condition. This is detailed in the following proposition.

Proposition 2. *Satisfying Legendre's condition [255] provides formal proof that the stationary paths, which satisfy the Euler Lagrange equation, correspond to minima.*

Proof. See Appendix C.2. □

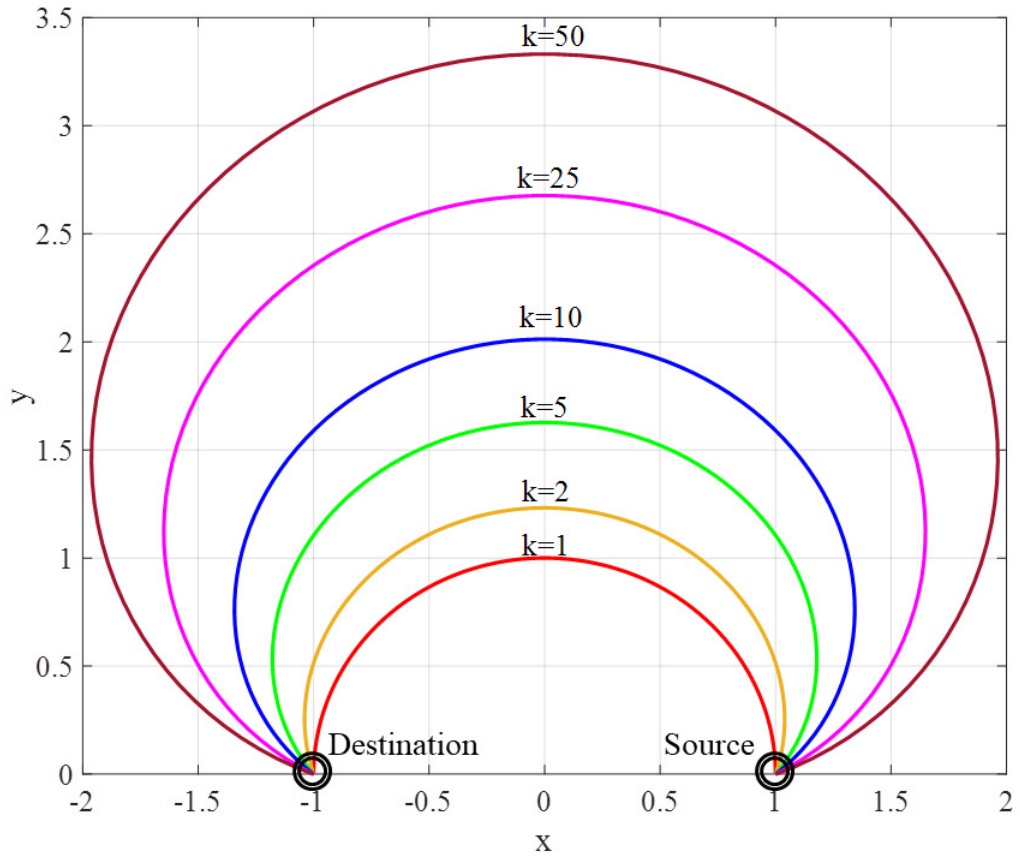


Figure 5.2: Optimal routes with single interferer located at $(0,0)$ for $k \in \{1,3,5,10,25,50\}$, Terminal nodes located at Cartesian coordinates $(1,0)$ and $(-1,0)$.

Table 5.1: Constants C_1 and C_2 associated with Fig. 5.2 (Left most pair) & Fig. 5.3 (Right most pair).

k	C_1	C_2	C_1	C_2
1	2	-18.4508	-	-
3	3.5462	-1.37672	3.99392	-0.700254
5	4.70049	-1.03243	5.90698	-0.618215
10	6.98186	-0.73590	10.5208	-0.548211
25	12.0172	-0.49360	24.0634	-0.500087
50	18.3418	-0.37286	46.4783	-0.482431

5.4.2 Single Directional Interferer

We now introduce a gain function $g := g(\phi)$ into the functional (5.25), which permits a non-uniform spatial distribution of interference. The functional can

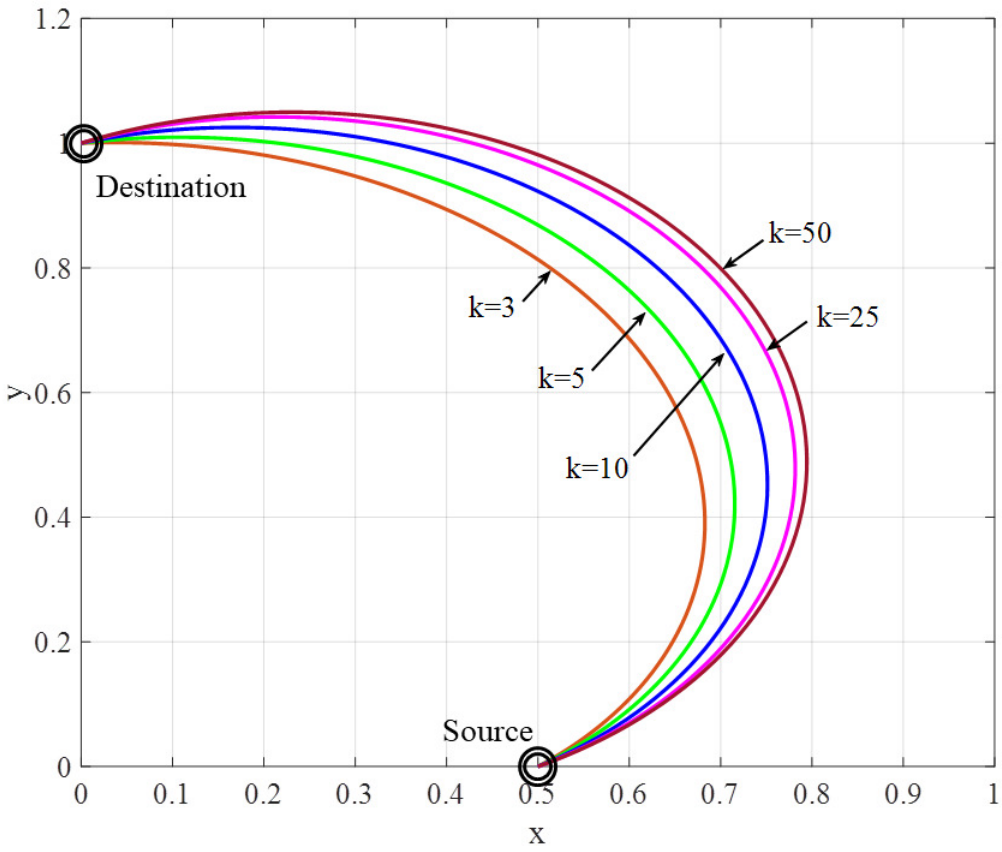


Figure 5.3: Optimal routes with single interferer located at $(0, 0)$ for $k \in \{3, 5, 10, 25, 50\}$ Terminal nodes located at Cartesian coordinates $(0.5, 0)$ and $(0, 1)$.

now be written as

$$P_o[r] = 1 - \exp\left(-\theta \int_{\phi_1}^{\phi_2} \left[1 + \frac{kg}{r^\eta}\right] \sqrt{r^2 + \dot{r}^2} \mathrm{d}\phi\right). \tag{5.30}$$

Since the Beltrami identity is no longer valid, with the inclusion of this explicit function, we invoke the Euler-Lagrange equation

$$\frac{\partial L}{\partial r} = \frac{\mathrm{d}}{\mathrm{d}\phi}\left(\frac{\partial L}{\partial \dot{r}}\right), \tag{5.31}$$

to determine the stationary paths of the functional (5.30), where $L(\phi, r, \dot{r})$ denotes the integrand. For the special case $\eta = 2$, we can show that the Euler-Lagrange equation reduces to

$$F(\phi, r, \dot{r}) := \ddot{r} = r + \frac{2\dot{r}^2}{r} - \frac{(2gr + \dot{g}\dot{r})(1 + \left(\frac{\dot{r}}{r}\right)^2)}{\frac{r^2}{k} + g}, \tag{5.32}$$

where $\dot{g} = \frac{\mathrm{d}g(\phi)}{\mathrm{d}\phi}$. We now suppose the directivity of the interference transmission is given by gain function

$$g(\phi, \phi_o) = 1 + \epsilon \cos(\phi - \phi_o), \qquad \epsilon \in [0, 1]. \tag{5.33}$$

This definition gives a simple cardioid pattern in the azimuth variable ϕ, where ϕ_o denotes the orientation angle of the peak antenna gain. The parameter ϵ defines the magnitude of the peak gain, such that $\epsilon = 1$ provides a peak power gain of two and $\epsilon = 0$ defines an isotropic radiation pattern.

Since, an analytic solution to (5.32) does not immediately present itself, we employ numerical methods to solve the differential equation here. Specifically, Euler's explicit method [217] lends itself to this example. We consider S discrete samples over the continuum between the source and destination nodes, uniformly distributed over the interval $[\phi_1, \phi_2]$, such that the angular sample spacing is $h = (\phi_2 - \phi_1)/(S + 1)$. Let $i \in \{1, 2, \ldots, S + 2\}$ denote the index of these samples, where $(\phi(i), r(i))$ represent the polar coordinates of the ith sample, and $i = 1$ and $i = S + 2$ are the source and destination indices, respectively. By this definition, we have that $\phi(1) = \phi_1$ and $r(1)$ is the radial distance of the source from the origin.

One may estimate $\dot{r}(1)$ and invoke Euler's explicit method to return the calculated polar coordinates of the path described by (5.32). We then successively approximate $\dot{r}(1)$, over the interval $[\dot{r}_l(1), \dot{r}_u(1)]$[8] until the calculated radial ordinate of the destination node $r(S+2)$ is within an acceptable fractional deviation ξ of the actual radial distance r_d. Associated pseudo-code is outlined in Algorithm 2. It is clear from the description of the algorithm that its complexity does not scale with the number of nodes N in the network; instead, it scales linearly in the number of samples S, which may be considerably less than N in large-scale practical scenarios.

As an illustration of this approach, numerically optimized routes for $k \in \{1, 3, 5\}$ and $\epsilon = 1$ are shown in Fig. 5.4 where $S = 1000$. We found that setting $S = 50$ gave

[8]The successive approximation is conditional on the variation of $r(S+2)$ being strictly increasing monotonic over the interval $[\dot{r}_l(1), \dot{r}_u(1)]$. We determine the interval following a coarse search based upon incrementing $\dot{r}(1)$ over a larger estimated range, invoking Euler's explicit method to return the calculated polar coordinates of the path described by (5.32) and determine the value of $\dot{r}(1)$ that yields an acceptable approximation of the path.

Algorithm 1: Successive Route Approximation

initialize S, h, r_d, $r(S+2) \gg r_d$, $\dot{r}_l(1)$, $\dot{r}_u(1)$, ξ;
while $|r(S+2) - r_d|/r_d > \xi$ **do**
  $\dot{r}(1) = (\dot{r}_l(1) + \dot{r}_u(1))/2$;
  `// Euler's Explicit Method`
  for $i = 1 : S+1$ **do**
    $r(i+1) = r(i) + h\dot{r}(i)$;
    $\dot{r}(i+1) = \dot{r}(i) + hF(\phi(i), r(i), \dot{r}(i))$;
    $\phi(i+1) = \phi(i) + h$;
  end
  return $\{r(S+2)\}$;
  if $r(S+2) > r_d$ **then**
    $\dot{r}_u(1) = \dot{r}(1)$;
  else
    $\dot{r}_l(1) = \dot{r}(1)$;
  end
end
return $\{\phi\}, \{r\}$.

satisfactory results. With the direction of the peak gain set to $\phi_o = \pi/4$, we clearly observe longer routes between the source and destination nodes in the half-plane interference is directed. We further observe the optimal routes are repelled from the origin in the direction of peak radiation.

Fig. 5.4 also depicts one path for each value of INR in the lower half-plane. These are also stationary paths that satisfy (5.32). Interestingly, we see the stationary paths veering toward the interference source in the lower half-plane as a result of the lower level of interference; corresponding to a null in the cardioid antenna pattern. Since the gain function g is independent of $\dot{r}$, the formal test for minima, given in Proposition 2, equally applies to this scenario and provides proof that the stationary paths in the upper and lower half planes of Fig. 5.4 are minima of the functional (5.30). These results provide an intuitive illustration of the continuum model in a nontrivial setting with inhomogeneous interference effects.

Fig. 5.5 provides a visualisation of how the algorithm converges to the final continuum path for the previously described directional interferer scenario, where $k = 5$, $\dot{r}_l(1) = 1.4$, $\dot{r}_u(1) = 1.7$ and $\xi = 0.01$. The inner figure also shows the rate of convergence of the algorithm, plotting standard deviation of the radial ordinates

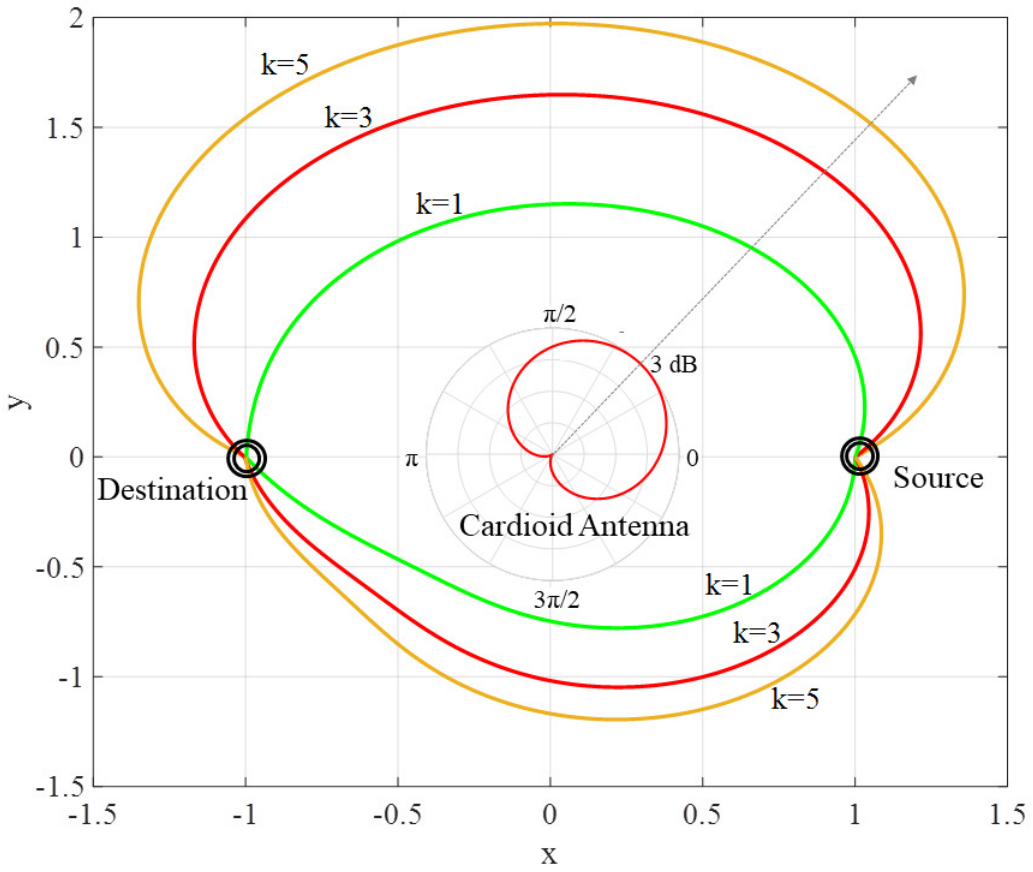


Figure 5.4: Optimised routes in the presence of a directional interferer. The directivity is a cardioid pattern with 3 dB peak gain at $\pi/4$; $k \in \{1, 3, 5\}$.

from the final continuum path as a function of iteration number of consecutive route approximations. The figure shows that, despite the low complexity of the algorithm, the successive approximations converge to the final continuum path in a relatively low number of iterations.

5.5 Multiple Interferers

We now consider application of the continuum model where the multi-hop communications network is subject to interference from multiple independent point sources located in $\mathbb{R}^2$. We consider all interferers are independently subject to Rayleigh fading. The locations of the interferers are given by the polar coordinates $\mathbf{p}_m = (r_m, \phi_m)$, where $m \in M$ and M denotes the index set of interferers. We

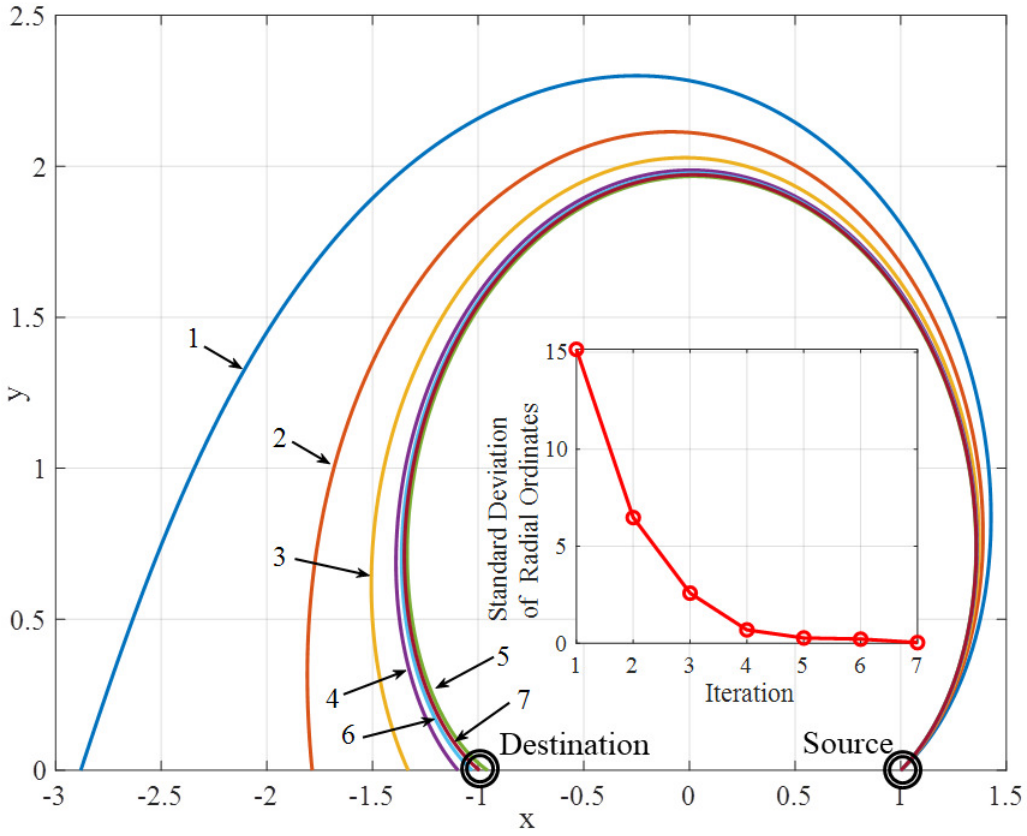


Figure 5.5: Illustration of successive route approximations (labelled by iteration number) and standard deviation of radial offset from optimal route for each iteration (inner figure).

denote the Euclidean distance between a point at (r, ϕ) and (r_m, ϕ_m) by d_m where

$$d_m^2 = r^2 + r_m^2 - 2rr_m \cos(\phi - \phi_m). \tag{5.34}$$

If we extend the analysis detailed in section 5.4 to multiple independently faded interferers then (5.18) becomes

$$c(\mathbf{p}_i, \mathbf{p}_j) = \mathrm{e}^{-\left(\frac{d_{ij}}{r_0}\right)^{\eta}} \prod_{m \in M} \left[\frac{1}{1+\Omega_m}\right], \tag{5.35}$$

where $\Omega_m = k d_{ij}^{\eta} d_m^{-\eta} / r_0^{\eta}$. It is then relatively straighforward to show that the functional for outage probability becomes

$$P_o[r] = 1 - \exp\left(-\theta \int_{\phi_1}^{\phi_2} \left[1 + k \sum_{m \in M} \frac{1}{d_m^{\eta}}\right] \sqrt{r^2 + \dot{r}^2} \mathrm{d}\phi\right). \tag{5.36}$$

Remark. *It can be shown that, repeating the analysis for unfaded interferers also yields (5.36). The sum of interference power, from Rayleigh faded interferers, will have a hypoexponential distribution. Conjecturing (as for the single interferer case), that in the limit of infinite relay extent, the interference field tends to the mean of the distribution, then this will be equivalent to the sum of unfaded interferers which is consistent with the analysis.*

Letting L denote the integrand in (5.36), considering the case $\eta = 2$ and evaluating the Euler-Lagrange equation produces

$$F(\phi, r, \dot{r}) := \ddot{r} = r + \frac{2\dot{r}^2}{r} - \frac{2k(r^2 + \dot{r}^2)[\Sigma_2(r^2 + \dot{r}^2) - \Sigma_3\dot{r}]}{(1 + k\Sigma_1)r^2}, \tag{5.37}$$

where

$$\Sigma_1 = \sum_{m \in M} \frac{1}{d_m^2}, \tag{5.38}$$

$$\Sigma_2 = \sum_{m \in M} \frac{r - r_m \cos(\phi - \phi_m)}{d_m^4}, \tag{5.39}$$

$$\Sigma_3 = \sum_{m \in M} \frac{r\dot{r} - r_m[\dot{r}\cos(\phi - \phi_m) - r\sin(\phi - \phi_m)]}{d_m^4}. \tag{5.40}$$

Again, since an analytic solution to (5.37) does not immediately present itself, we employ Euler's method to solve for r, as outlined previously (see section 5.4.2).

5.5.1 Two Interferers

We start with a simple scenario with two interferers, with $k = 3$, located at polar coordinates $(0, 0)$ and $(1, \pi/2)$. Fig. 5.6 shows three local minimum paths: paths 1 and 3 are similar to previous observations, but with symmetry about the straight line containing the non-directive interferers, and path 2 passing between the two interferers. This third minima is an expected result in that arbitrary paths directly passing through either of the interferers will yield total outage due to the singularities in (5.36) at $r = d_m,\ m \in M$, and a path existing between the two interferers will intuitively yield a lower outage probability. It should be noted that, although the

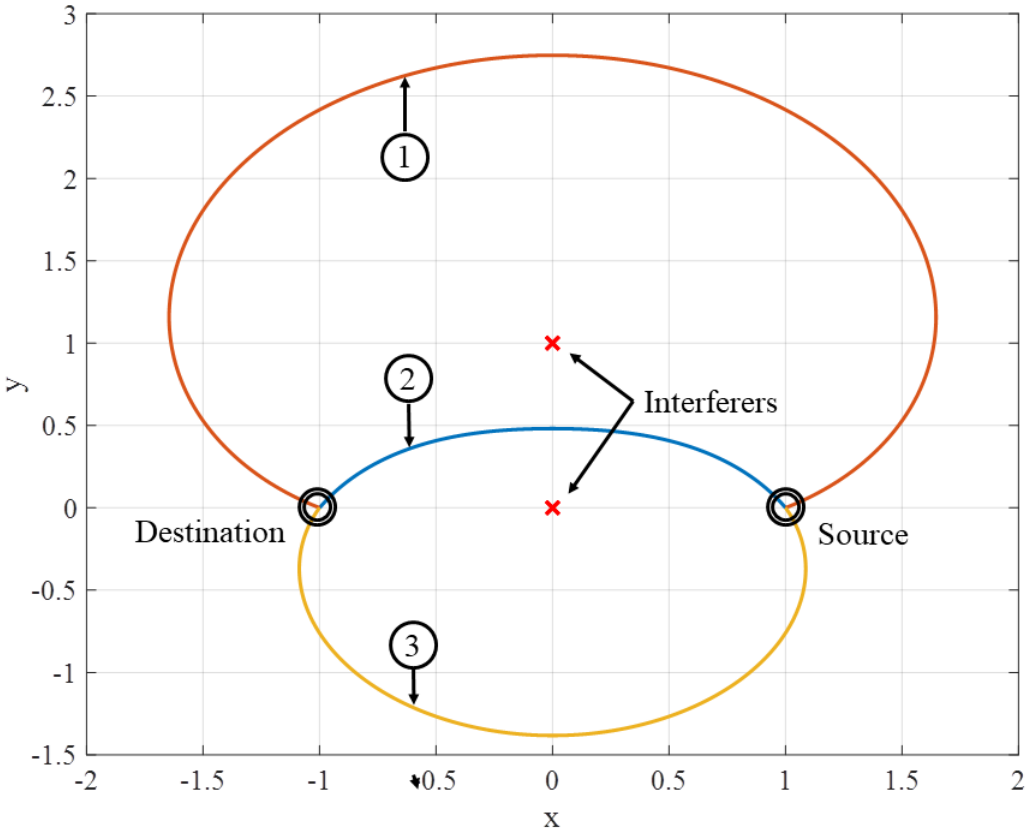


Figure 5.6: Optimal routes for 2 interferer scenario. Interferers located at positions $(0, 0)$ and $(1, \pi/2)$, indicated by crosses, and $k = 3$. The stationary paths from uppermost to lowermost are labelled 1, 2, and 3 respectively.

path 2 is significantly shorter than the paths 1 and 3, it will not necessarily yield the lowest outage probability due to the closer proximity to the interferers. For a given value of θ we can determine the outage probability by substituting r and $\dot{r}$, corresponding to each stationary path, into (5.36).

To provide further evidence to support the stationarity of the three paths by an intuitive visualization, we consider a range of arbitrary routes generated by linear interpolation[9] of radial ordinates of adjacent paths 1, 2, and 3 for fixed angle-ordinates, and calculate the corresponding outage probability of the interpolated paths. Paths above path 1 and below path 3 are simply generated by scaling paths with the function $[1 + \Delta r/r_p]\cos(\phi)$. r_p is the radial ordinate of path-$p \in \{1, 3\}$ at respective angle-ordinates $\{\pi/2, -\pi/2\}$ and Δr is the required deviation of the

[9]Linear interpolation provides a straightforward method, and alternative interpolation approaches would be equally applicable.

radial ordinate at respective angle-ordinates $\{\pi/2, -\pi/2\}$. The effect of this route perturbation on outage probability is illustrated in Fig. 5.7, clearly showing that paths 1, 2, and 3 correspond to minimum stationary paths and total outage occurs when paths pass through an interferer.

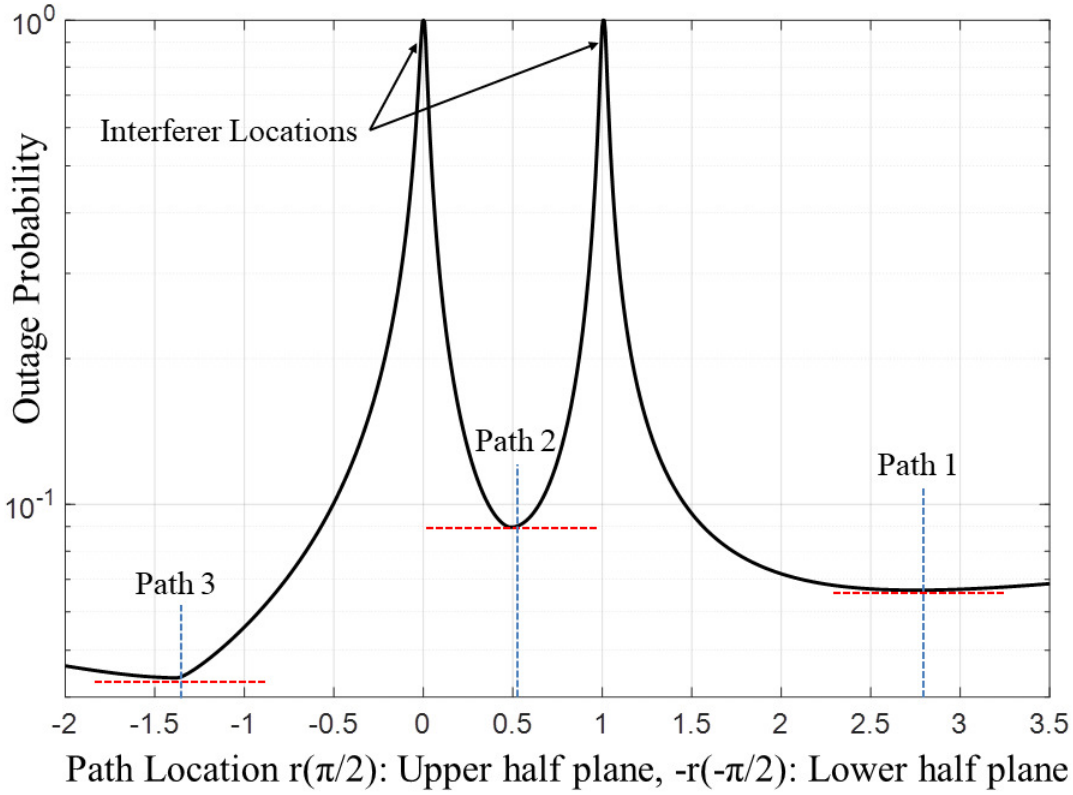


Figure 5.7: Verification of path stationarity by route perturbation.

5.5.2 Three Interferers

We repeat the previous analysis with three interferers located at polar coordinates $(0, 0)$, $(0.5, \pi/3)$ and $(0.5, \pi/6)$ with $k \in \{1, 2, 3\}$. Using Euler's method to solve (5.37), as before, we illustrate the resultant stationary paths in Fig. 5.8. The upper and lowermost paths follow similar observations with the single directive interferer scenario; an intuitive result in that the three interferers with spatial bias is analogous to a single interferer located at the origin having increased directivity at angle $\pi/4$ in this example. We might pursue this analogy to develop

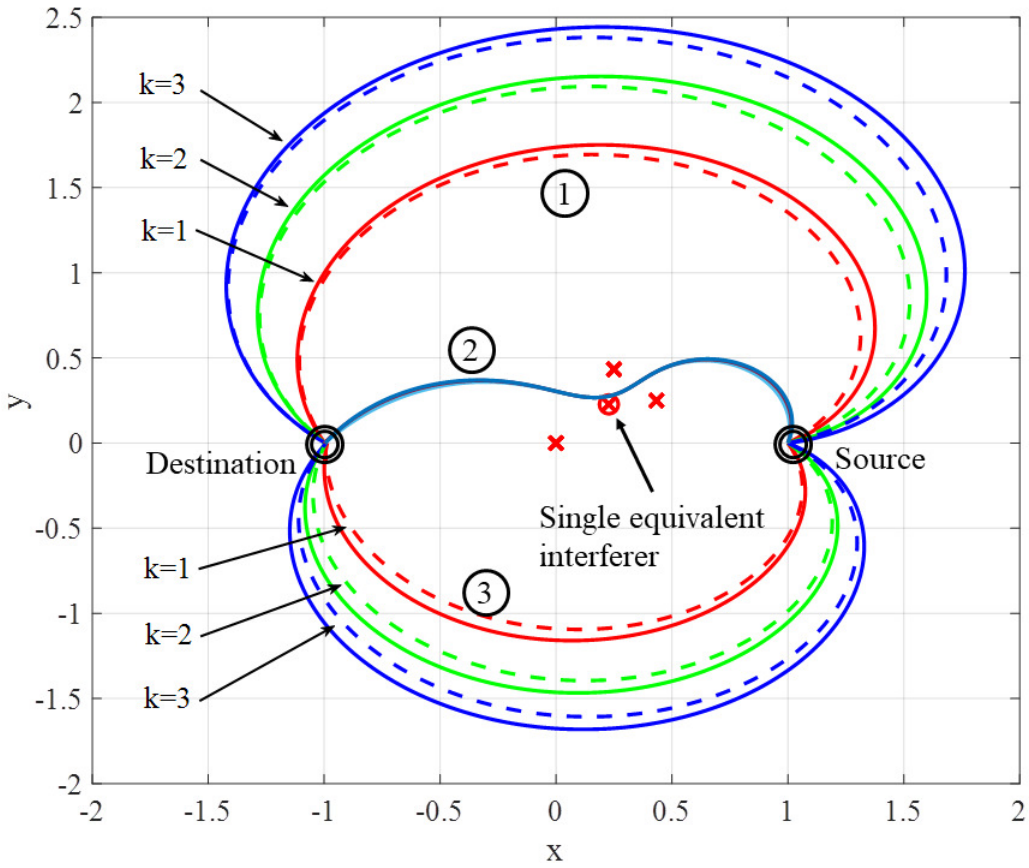


Figure 5.8: Stationary paths (solid lines) for 3 interferer scenario for $k \in \{1, 2, 3\}$. Interferers are located at positions $(0, 0)$, $(0.5, \pi/6)$, $(0.5, \pi/3)$ (red crosses). The dashed lines represent approximations for the stationary paths for a single equivalent interferer located at position $(0.322, \pi/4)$.

a single directive interferer approximation. However, there is little advantage to this approach, since it would not necessarily yield a reduction in processing complexity in determining stationary paths.

Instead, we consider an alternative approximation for a group of interferers. Specifically, one could consider a single non-directive interferer located at an equivalent "centre of interference", given by $\frac{1}{|M|}\sum_{m\in M}\mathbf{p}_m$, with an increased INR given by $k' = |M|k$. In this example, the single equivalent interferer is located at $(0.322, \pi/4)$. Using this approximation, we apply (5.29) to determine stationary paths; avoiding the need for the more cumbersome application of numeric methods in solving (5.37). The resulting approximate stationary paths are shown as dashed lines in Fig. 5.8. In this example, the approximations appear to closely match

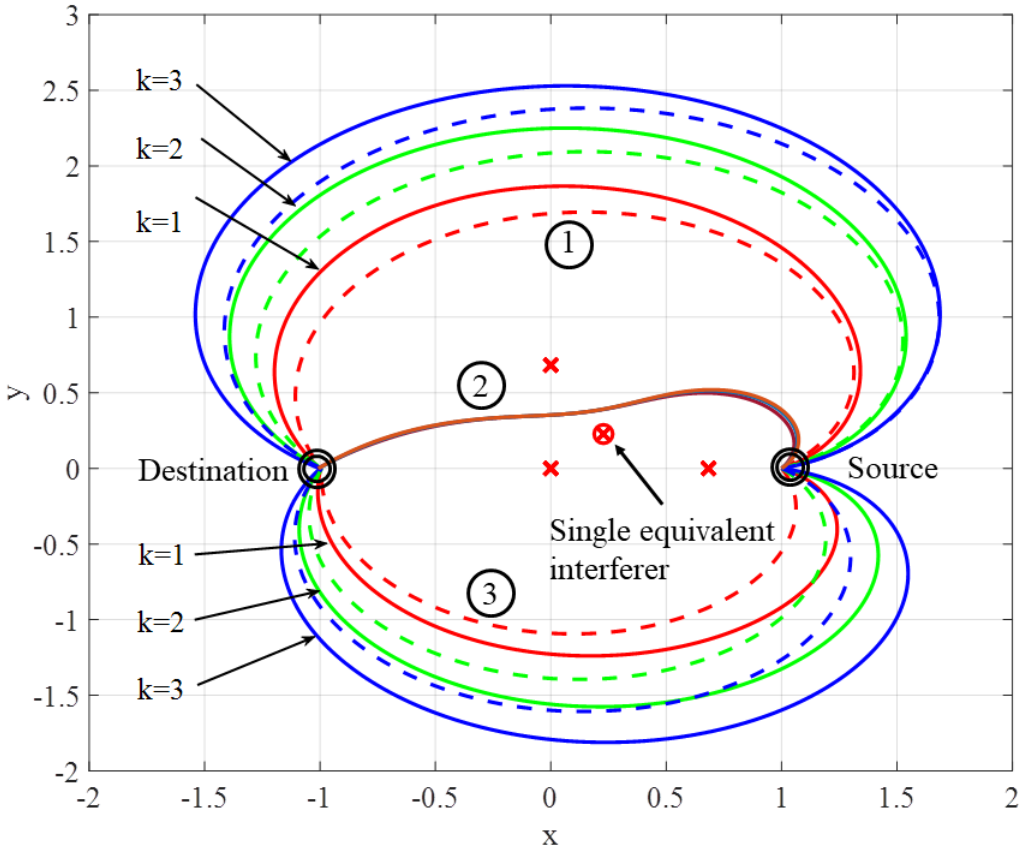


Figure 5.9: Stationary paths (solid lines) for 3 interferer scenario for $k \in \{1, 2, 3\}$. Interferers are located at positions $(0, 0)$, $(0.683, 0)$, $(0.683, \pi/2)$ (red crosses). The dashed lines represent approximations for the stationary paths for a single equivalent interferer located at position $(0.322, \pi/4)$.

the actual stationary paths.

We repeat this analysis for three interferers with increased Euclidean distance between them but with the same equivalent single interferer location as before. The results are shown in Fig. 5.9, which clearly shows the approximate paths deviate to a larger degree from the actual stationary paths. From this observation, we conjecture that the accuracy of the approximation will degrade with increased variance in Euclidean distances of the multiple interferers from the equivalent "centre of interference". We defer further analysis of this approximation of complex spatial distributions of interferers to future work.

Returning to the three interferers, we observe path 2 meandering between interferers; as observed in the previous two interferer scenario. Further, this path is

largely independent of INR close to the interferers, which can be attributed to the effect on the path being analogous to two opposing "forces" equally repelling the path. It is possible to identify other local minima, e.g., meandering from the source towards the lower two interferers and upwards between them and then passing between the left most two interferers towards the destination. However, this path will pass through both lower and upper half planes and $r(\phi)$ becomes non-injective, requiring a change in coordinate system, i.e., parametric Cartesian. Again, we defer treatment of more complex scenarios to future work.

5.6 Sampling the Continuum for Practical Deployments

Having determined a methodology for the creation of an equivalent continuous multi-hop route, we now distribute a finite number of relay nodes onto the stationary path, according to four placement strategies. Here, we list these in increasing order of processing complexity.

- Equi-angle: nodes distributed with constant angular offset
- Equi-spacing: nodes distributed with constant distance along the continuum
- Equi-Euclidean: nodes distributed with constant Euclidean distance
- Optimum-angle: optimal angle ordinates of nodes are determined using the `fmincon` function in MATLAB$^{\text{TM}}$.

We consider the single non-directive interferer scenario discussed in section 5.4 and assume that an outage probability of 0.05 is a realistic target in a practical deployment. We firstly determine the value of θ by rearranging (5.25) such that

$$\theta = -\frac{\log(1 - P_o[r])}{I}, \tag{5.41}$$

where I denotes the integral. We then calculate the length scale

$$r_o = \sqrt{\frac{L}{\theta}}, \tag{5.42}$$

where $L = \int_{\phi_1}^{\phi_2} \sqrt{r^2 + \dot{r}^2}\, \mathrm{d}\phi$ is the length of the continuum. The discrete multi-hop outage probability, employing N relays, is then calculated from

$$P_o = 1 - \prod_{n=0}^{N} \exp\left(-\frac{N+1}{r_0^2} . \frac{\|\mathbf{p}(n+1) - \mathbf{p}(n)\|^2}{\mu(\|\mathbf{p}(n+1)\|)} \right), \tag{5.43}$$

where the link quality function $\mu(\cdot)$ is given by (5.26) with $\eta = 2$. We vary N over the interval $[5, 30]$ and calculate the corresponding outage probabilities for each placement strategy for $k = 5$. Results are shown in Fig. 5.10.

With increasing numbers of nodes, the equi-Euclidean relay spacing converges to the equi-spacing case, which represents uniform relay spacing over the continuum and which satisfies the constant connectivity density condition that underpins our continuum model. In this case, we observe a rapid convergence to the $P_o = 0.05$ asymptote. Since the equi-angle and optimum angle scenarios violate the constant connection density condition, they do not exactly converge to the $P_o = 0.05$ asymptote. Notwithstanding this, the simplest form of relay placement yields an acceptably low deviation from the required outage probability. This is further highlighted in Fig. 5.11, where we vary the effective SNR from the level that yields an outage probability of 0.05 for the continuum.

The nonuniform angular distribution, according to the optimum-angle placement strategy on the continuum, is illustrated in Fig. 5.12 for the placement of 10 relay nodes (as indicated by circle markers); we observe that the Euclidean distance between adjacent nodes reduces where the receiving node is closer to the interferer. This yields a lower outage probability due to the interference being nonuniform over the continuum, and reducing the Euclidean distance between adjacent relay nodes subject to higher interference will intuitively yield lower outage probability overall. Fig. 5.12 also shows node placement for 10 and 50 relay nodes where we allow freedom to optimize both radial and angle ordinates using the `fmincon` function in MATLAB$^{\mathrm{TM}}$. In this discrete optimization case, we provide an equivalence between the continuum model and the discrete optimization by using the length scale defined by

$$r_o = \sqrt{\frac{\sum_{n=0}^{N} \|\mathbf{p}(n+1) - \mathbf{p}(n)\|}{\theta}}, \tag{5.44}$$

where θ is given by (5.41). This length scale is then substituted into the objective function for outage probability given in (5.43). In the limit of an infinite number of relays, where we can consider the path of relay nodes forming a continuum, then (5.44) converges to (5.42), i.e., as the sum of Euclidean distances for each hop approaches the length of the continuum. We observe that for the placement of 50 nodes, according to this discrete optimization, their locations are close to the continuum, which provides further evidence supporting the utility of the continuum model to optimize relay placement in large multi-hop networks.

In contrast however, the placement of 10 nodes shows a reasonable divergence from the continuum. This observation can be attributed to (5.44) and its relation to total available transmit power (5.16), which is equally distributed across the source and relay nodes, i.e., transmit power per relay node is proportional to the sum of Euclidean distances. If the 10 nodes were located on the continuum then the sum of Euclidean distances would be less than the length of the continuum and the nodes would therefore have lower available power, which would result in lower SINR and therefore higher outage probability for the multi-hop network when compared to the continuum. It is intuitive that the optimum placement of relay nodes would be further away from the continuum, which would yield increased transmit power and lower interference, and would mitigate the increase in node separation. This is supported by observations in Fig. 5.10, where for lower numbers of relays ($N < 20$) the outage probability for the discrete optimization case (depicted by the dashed line) is higher than when relays are located on the continuum according to the optimum-angle placement strategy. As the number of nodes increases, we see a convergence between the two placement strategies.

In this example, the least complex strategy for relay node placement on the continuum does not yield the optimal outage probability for a multi-hop relay network. However, we can conclude that the sub-optimality of the continuum approach and relay node placement strategies is not significant.

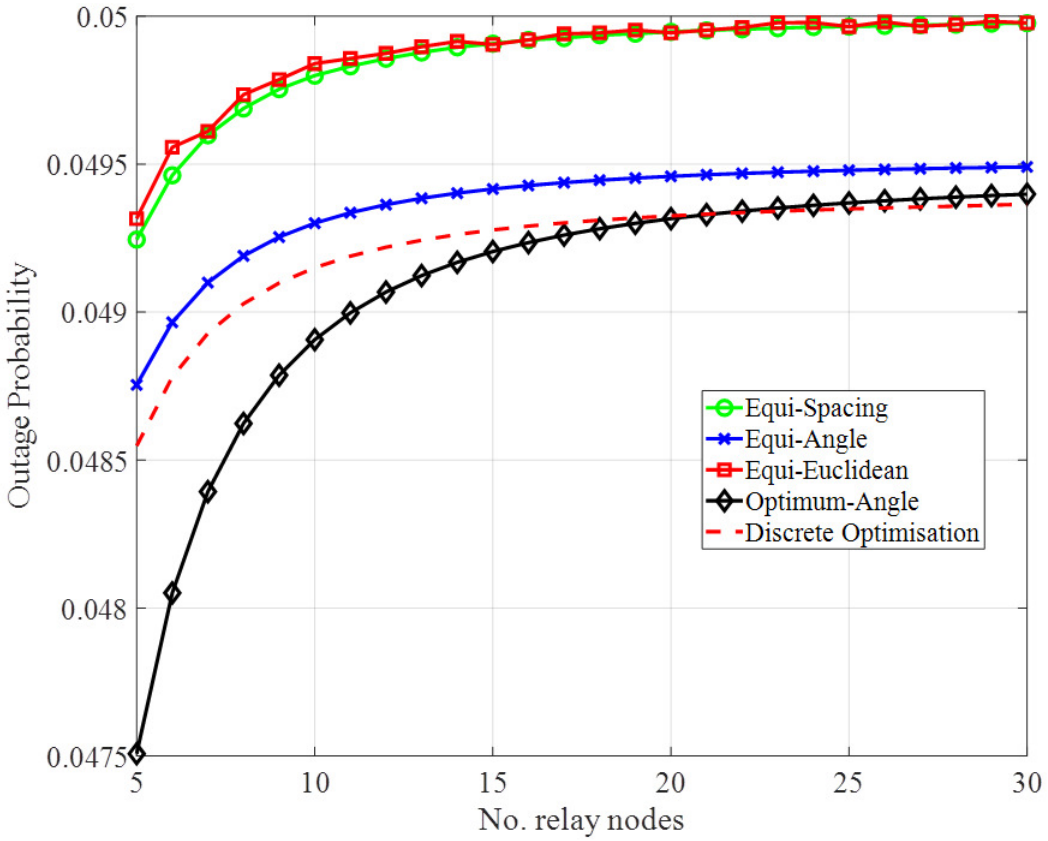


Figure 5.10: Outage probability versus the number of relay nodes placed on the continuum according to equi-spacing, equi-angle, equi-Euclidean and optimum angle placement strategies for $k = 5$. The dashed line represents the outage probability for a relay placement according to the discrete optimization of both radial and angular ordinates of relay nodes where $k = 5$.

5.7 Conclusion and Discussions

In this chapter, we have demonstrated the effectiveness of the continuum model for end-to-end outage probability calculation, when applied to multi-hop route optimisation in a wireless network subject to an inhomogeneous scalar field of interference. Taking a canonical example of interference originating from a single point in $\mathbb{R}^2$, we have shown that the scale of processing complexity reduces from $O(N^3)$ for a discrete Lagrangian method of constrained optimization (where N is the number of relays) to $O(S)$ in the continuum model, with S denoting the number of samples used to approximate the continuous path. Although analytic forms representing the optimal path do not exist in general, it is possible to

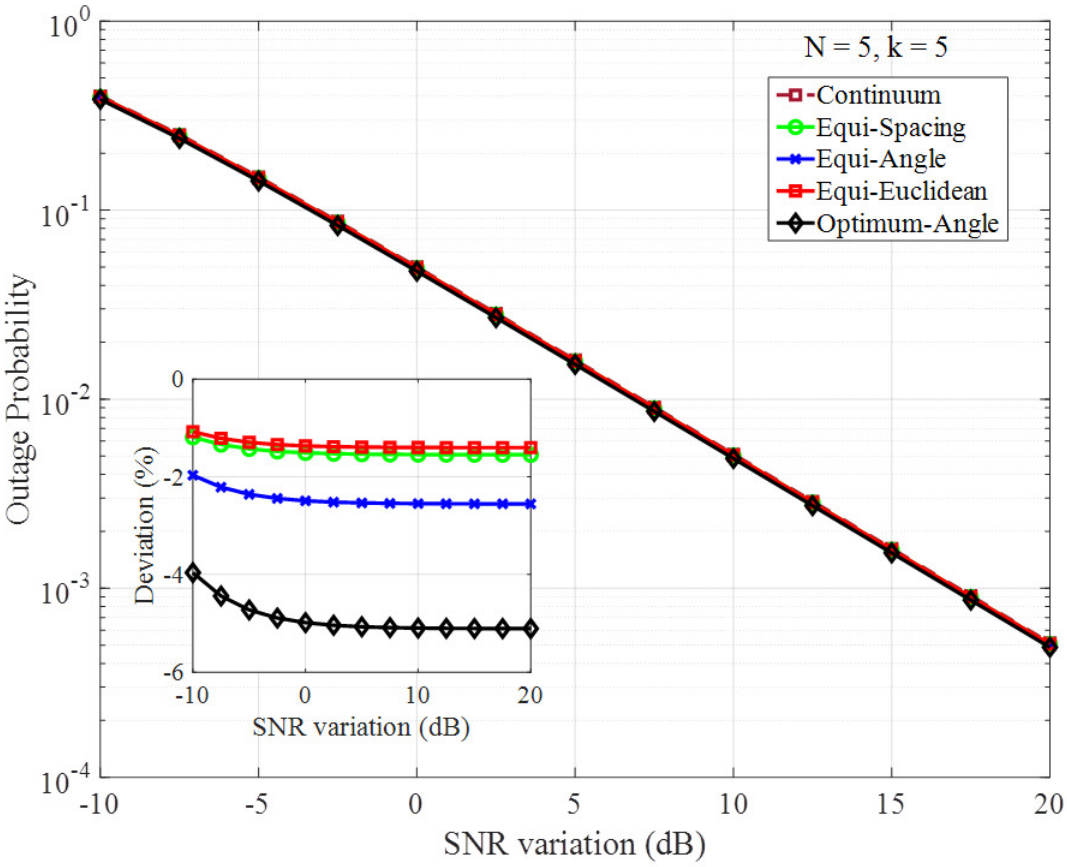


Figure 5.11: Outage probability and % deviation in outage probability from the continuous path versus SNR for five relay nodes placed on the continuous path according to equi-spacing, equi-angle, equi-Euclidean, and optimum angle placement strategies for $k = 5$.

employ basic numerical techniques to approximate it. From this approximation, it is straightforward to sample the continuum with a finite number of points (relays), thus yielding an acceptably low deviation in outage probability relative to the optimum.

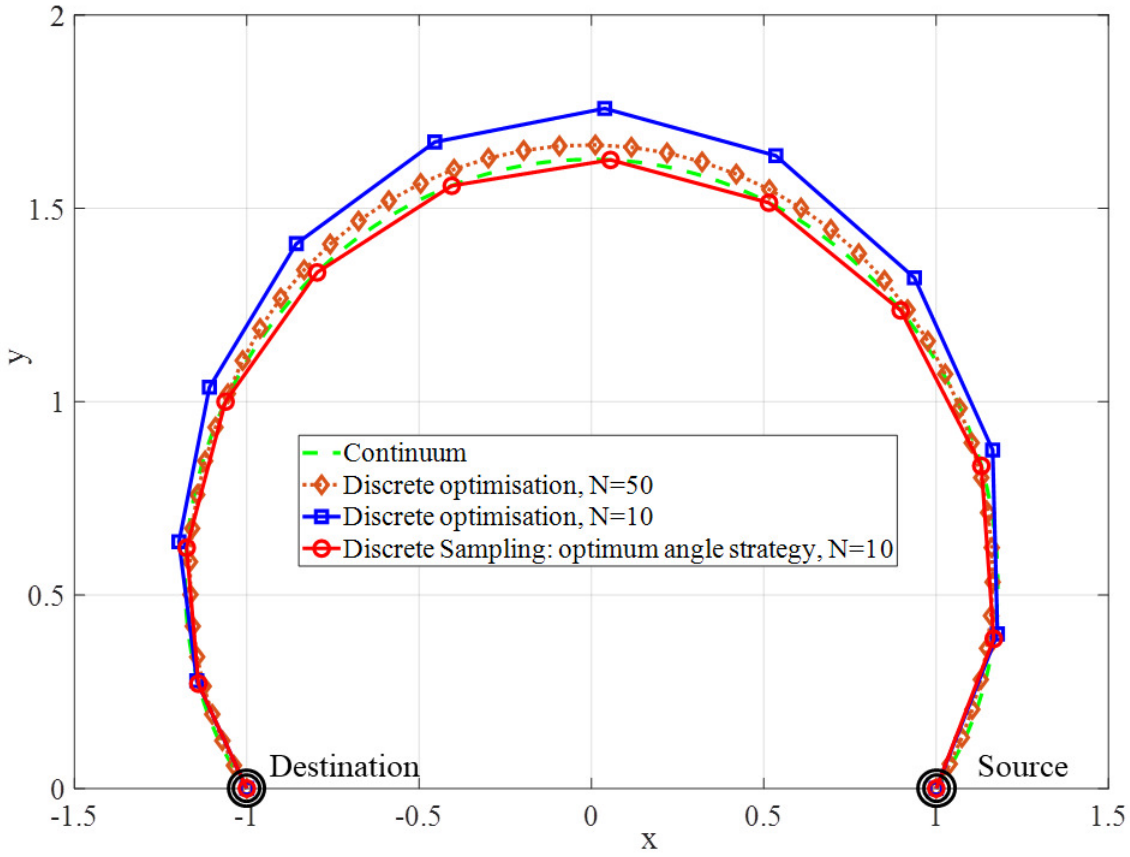


Figure 5.12: An example of the placement of 10 relay nodes according to the optimum-angle placement strategy (circle marker representing relay node location) and optimizing both radial and angle ordinates of 10 and 50 relay nodes (relay node locations represented by square and diamond markers respectively).

6

Framework for Covert Multihop Route Planning

6.1 Introduction

Covert communication systems can be sub-categorised into covert information transmission and covert wireless communication [256]. The former relates to information security, typically achieved using cryptographic techniques at the transport layer [257], and covert wireless communication relates to the application of security mechanisms at the physical layer [258]. Low probability of detection (LPD) is one such technique, with the primary goal of hiding the very existence of a wireless transmission to an adversary. An obvious example is within a military campaign, where soldiers wish to communicate with each other and avoid detection and geolocation by their adversaries. In general, a covert communication system will maximise security and covertness by the application of several mechanisms, at multiple layers within the communication system. This work focuses specifically on LPD communication which has drawn significant research interest since 2013 [259] and remains a vibrant area of study, particularly over the past few years (see [260], and references therein).

LPD is typically achieved by transmitting low EIRP (effective isotropic radiated power), low power spectral density (e.g. Spread Spectrum [261]), signalling optimised for covertness [262], antenna directivity or a hybrid of the above. A commonly employed spread spectrum technique is direct sequence spread spectrum (DSSS) [263]; also the underpinning technology behind 3G (CDMA) networks [264]. The low-power nature of LPD communication, however, significantly restricts the end-to-end communication distance that can be achieved. Multihop communication [265] addresses this limitation by employing intermediate relay nodes between the information source and destination nodes of the network. This effectively redistributes power (EIRP) over multiple transmitting nodes in the multihop network, therefore reducing the transmitted power of any single node. If we consider an environment with spatially homogeneous propagation characteristics, then there will be a strictly decreasing monotonic relationship between the required transmit power of a node, for a given connectivity criteria, and the total number of nodes in the network. If the eavesdropper is only capable of detection of any single

transmission then, in the limit of infinite relay extent, it follows that the network will be undetectable, since the transmit power will tend to zero. If however, we assume the eavesdropper has a more sophisticated capability, whereby it can exploit the joint detection of all transmissions, then this will no longer be the case.

Much of the previous works, associated with covert communication, have adopted an information theoretic approach; see for example [259], which developed a fundamental bound on LPD communication over AWGN channels. [266] applied this information theoretic approach to a one-way wireless relay network with [267] and [268] formulating a covertness QoS metrics for larger scale multihop covert wireless networks. Key conclusions drawn from these works are that the optimal number of relays in a covert multihop wireless network increases with the distance between source and destination nodes and that decode-and-forward (DF) relaying strategy was favourable over amplify-and-forward (AF), in terms of throughput for a given covertness metric.

In [269], the authors introduce the concept of "cumulative security leakeage", whereby a single eavesdropper is capable of the joint coherent detection of all transmissions within a multihop wireless network. This work develops a novel relay selection algorithm that minimises the effective SNR, for joint detection, at the eavesdropper. Other works, relating to optimal node placement, include [270], which discussed optimal routing to maximise the secure connection probability (SCP) in the presence of multiple eavesdroppers of unknown location, and [271], which considers the SCP of a multihop network in the presence of inhomogeneous eaversdropper clusters. Common to both these works is the route being determined by testing all possible routes, in a discrete network, and choosing the one that maximises the SCP. From an algorithmic perspective, this potentially becomes an unwieldy processing problem for larger networks.

In our work, we start with the assertion that the density of uniformly spatially distributed relay nodes is sufficiently large to be able to approximate a multihop path by a continuum, see chapter 5 and/or [272]. As in [269], we assume a worst-case scenario whereby the multihop network is subject to an eavesdropper that employs a

joint detection strategy to detect the presence of a covert communications network. Our challenge then relates to the connection-optimal route planning of a multihop network for a minimal acceptable level of network covertness. In avoiding more traditional heuristic or discrete Lagrangian based optimisation strategies, which can yield unwieldy processing requirements, we develop a framework that employs tools from the field of variational calculus to determine the optimal multihop route plan for network connectivity whilst remaining covert. Further, within our framework, we consider the effect of antenna directivity [273] and large-scale shadowing [274] on route planning.

Although exploratory in nature, this research offers the following contributions:

1. we develop a continuum model to determine the end-to-end covert connection probability of a multihop wireless communications network;

2. we apply the model to find an analytic solution for the connection-optimal relay locations when the network is subject to an eavesdropper at a known location;

3. the efficacy of the framework is verified by considering the selection of relay nodes from a large-scale discrete network.

The remainder of the chapter is organised as follows. In section 6.2, we introduce the system model for our multihop network. In section 6.3 we develop the framework for the route optimisation problem subject to an SNR limit at the eavesdropper. The efficacy of the framework is demonstrated in section 6.4 and section 6.5 demonstrates the framework applied to an ad-hoc network problem. Conclusions are drawn in section 6.6.

6.2 Network Model

For consistency, we adopt the same network model and mathematical notations, as defined in Chapter 5 and summarised here for convenience, with the exception that the interferer is now substituted by a single eavesdropper, as depicted in

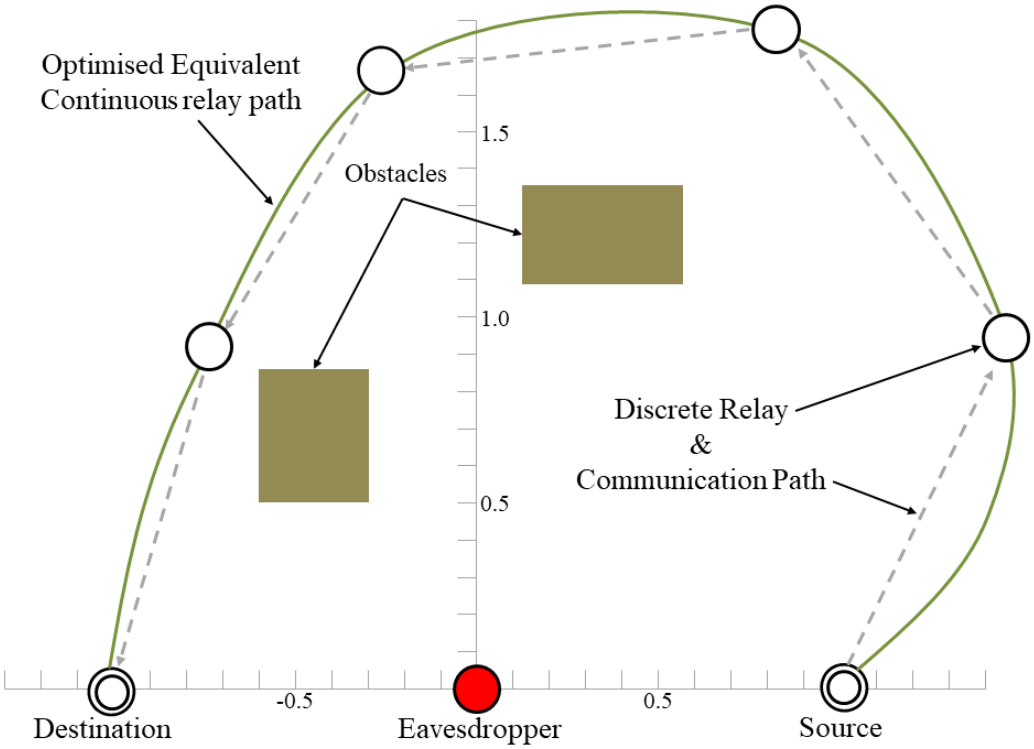


Figure 6.1: Multihop wireless network subject to single eavesdropper

Fig. 6.1. In contrast to the previous chapter, we now have the goal of covertly transmitting a message between source and destination nodes, located at $\mathbf{p}_0$ and $\mathbf{p}_{N+1}$ respectively, via N relays, in Euclidean space $\mathbb{R}^2$. The position of the ith relay node is denoted by $\mathbf{p}_i$ and we collect the relays in the set $\mathcal{R} = \{\mathbf{p}_1, \mathbf{p}_2, \ldots, \mathbf{p}_N\}$. By covertness, we specifically mean the avoidance of detection of the transmissions by the eavesdropper. The source and relay nodes transmit with power level P but now employ directional antennas at their transmitters. We assume that the relay network is cooperative and the communication path between any two neighbouring nodes is optimised by directing the transmitter's antenna boresight towards the receiving node. We assume that the receiving node antenna is isotropic.

In terms of the eavesdropper, we assume that it has no prior knowledge of the topology of the relay network and, as such, employs an isotropic antenna. However, we also assume that the eavesdropper receives and retains information transmitted from the source and relay nodes and performs a joint (coherent) maximum likelihood detection (ML) in order to recover the message sent over the communications network.

How realisable this is, in practice, is subject to further work and we assume that an adversary has no time constraint in processing the retained transmitted information.

Remark. *In reality, in the absence of any apriori knowledge regarding the covert transmission, an eavesdropper is likely to follow a systematic process of hypothesis testing [275], i.e., testing assumptions made about the waveform until some prescribed level of detection can be made. Given the potentially large number of parameters associated with a covert waveform, the total search space is likely to require an unwieldy amount of processing resource at the receiver's location to yield a low detection latency, i.e., very high processing speed and/or significant parallelism [276]. To mitigate this, we assume that the eavesdropper has the ability to quantise a given RF spectrum bandwidth, within which the covert transmission is suspected to occupy, locally store it and pass it on to some form of offline processing platform, e.g., cloud processing [277].*

In order to provide a 'real-world' perspective, we also include obstacles (e.g. buildings) that introduce shadowing (attenuation) of the transmitted signal between nodes in the relay network and the eavesdropper. We model these nodes as rectangles of known size, location, orientation and attenuation[1]. We consider the set $\mathcal{B}$ contains all spatial information pertaining to the obstacles.

6.2.1 End-to-End Connection Probability

We now proceed to develop our optimisation framework by a combination of the continuum based approach, introduced in Chapter 5, and Lagrange multipliers.

We consider the end-to-end connection probability as our objective function, $P_c = f(\mathcal{R})$, that we wish to optimise. We continue with the assumption that pairwise connectivity between adjacent nodes is independently affected by Rayleigh fading and subject to mean path loss that follows an inverse power law, with exponent η_c, with respect to the Euclidean distance between nodes.

[1]For tractability, we assume that the obstacles have a uniform structure and log-attenuation as a function of unit distance is constant.

If we consider the connection between nodes $\mathbf{p}_i$ and $\mathbf{p}_j$, the signal to noise ratio at the receiver of $\mathbf{p}_j$ is given by

$$\mathrm{SINR_j} = \frac{P g_p (\frac{\lambda}{4\pi})^2 d_{ij}^{-\eta_c} |h_{ij}|^2}{\sigma^2}, \tag{6.1}$$

where $d_{ij} = \|\mathbf{p}_j - \mathbf{p}_i\|$ and $|h_{ij}| \sim \mathcal{CN}(0,1)$ and g_p denotes the boresight gain of the transmit antenna directed towards the receiving node. Clearly, this differs from (5.13) with the omission of the interferer term $\mathcal{I}$ and the change in antenna gain. It should be noted that the receiving nodes can similarly use a directive antenna, which simply adds a constant scaling factor in the SNR and has no impact on the power level received at the eavesdropper, we therefore assume unit gain in the receive path of the destination and relay nodes. We consider the exact antenna model in the following section.

Following the steps outlined in the previous chapter, it follows that the soft pairwise connection function between $\mathbf{p}_i$ and $\mathbf{p}_j$, will be given by

$$c(\mathbf{p}_i, \mathbf{p}_j) = \exp\left[-\left(\frac{d_{ij}}{r_0}\right)^{\eta_c} \right], \tag{6.2}$$

with the hard connection range r_o given by

$$r_0^{\eta_c} = \frac{P g_p \left(\frac{\lambda}{4\pi}\right)^2}{\sigma^2 \tau_c}, \tag{6.3}$$

where τ_c denotes the threshold of SNR, below which the pairwise connection is not considered viable. This connection function is now solely a function of the distance between nodes and independent of the eavedropper, in contrast to the interferer scenario previously analysed. Following the steps detailed in section 5.3.2 in considering the limit of infinite relay extent, we arrive at

$$P_c = \mathrm{e}^{-qL}, \tag{6.4}$$

under the condition

$$\frac{\mathrm{d}l^{\eta_c - 1}}{r_0^{\eta_c}} \to q \in \mathbb{R}_+, \tag{6.5}$$

where q is a constant, $\mathrm{d}l$ denotes the path length differential and L denotes the length of the continuous relay path, i.e. the continuum. Since we are concerned with the power level received by the eavesdropper, we find it more convenient to rearrange the limit condition (6.5) in terms of power level P as follows

$$\left(\frac{\tau_c}{\beta g_p}\right)\frac{\mathrm{d}l^{\eta_c-1}}{P} \to q \in \mathbb{R}_+, \tag{6.6}$$

where

$$\beta = \left(\frac{\lambda}{4\pi\sigma}\right)^2. \tag{6.7}$$

Given the parameters within the brackets of (6.6) are constants, then for the special case $\eta_c = 2$, it follows that

$$\frac{\mathrm{d}l}{P} \to \frac{1}{\rho}, \quad \rho \in \mathbb{R}_+, \tag{6.8}$$

where ρ denotes a constant power density (power per unit length of the continuum relay path).

Remark. *We can consider a 'real-world' scenario, as depicted in Fig. 6.7, where a dense network of relays are uniformly distributed in $\mathbb{R}^2$ and transmit a fixed power P. We can then take any arbitrary low curvature line and form a discrete multihop relay network using relays associated with voronoi cells, through which the line traverses. It is intuitive the number of relays, and therefore total power of all relays, will be approximately linearly proportional to the length of the path. We consider this further in section 6.5.*

For convenience, we treat the continuum in polar form by using the radial position function $r \coloneqq r(\phi)$ and arbitrarily centre the coordinate system on the location of the eavesdropper, located at (0, 0). Recognising that the path length differential is given by

$$\mathrm{d}l = \sqrt{(r^2 + \dot{r}^2)}\mathrm{d}\phi, \tag{6.9}$$

it then follows that (6.4) becomes

$$P_c = \exp\left[-\left(\frac{\tau_c}{\beta\rho g_p}\right)\int_{\phi_S}^{\phi_D}\sqrt{(r^2 + \dot{r}^2)}\mathrm{d}\phi\right], \tag{6.10}$$

where ϕ_S and ϕ_D denote the angle ordinates of the source and destination nodes respectively and $\dot{r} \coloneqq \dot{r}(\phi)$ denotes the first derivative of r with respect to ϕ.

Clearly the shortest relay path will yield the maximum connection probability from source to destination. However, the power level received by the eavesdropper will increase with reducing proximity of the relay path to it. Therefore the eavesdropper places a constraint on the path function r.

6.2.2 Antenna Model

To achieve a more realistic network model, the isotropic antenna model commonly assumed in scientific literature is substituted here by that of directional antenna with variable peak directivity. For mathematical tractability, we ignore side-lobes and back-lobes [278] and assume that antenna directivity is rotationally invariant about its normal (boresight) axis. Specifically, we use the following smooth function to model the antenna

$$g(\theta) = k[1 + \cos(\theta)]^{g_p - 1}. \tag{6.11}$$

The parameter g_p denotes the peak boresight gain of the antenna and k denotes the normalising factor as given by

$$k = \frac{2}{\int_0^{\pi} [1 + \cos(\theta)]^{g_p - 1} \sin(\theta) \mathrm{d}\theta}. \tag{6.12}$$

It can be shown that this antenna model provides a good approximation for directive antennas such as parabolic reflector and phased array antennas [278], particularly with increasing directivity, as illustrated in Figure 6.2.

Directing the peak antenna gain to follow the continuum path, will serve to enhance the performance of the multihop network and also reduce the total power received by the eavesdropper. For our antenna model, directivities are illustrated in Fig. 6.3 for a range of boresight gains. Despite the divergence of 'off-boresight' gain between our model and a practical antenna at lower peak gains, particularly at sidelobe boundaries, we are interested in the effect of non-uniformity in directivity on the continuum in the following analysis and a 'smoother' function provides greater tractability in the analysis.

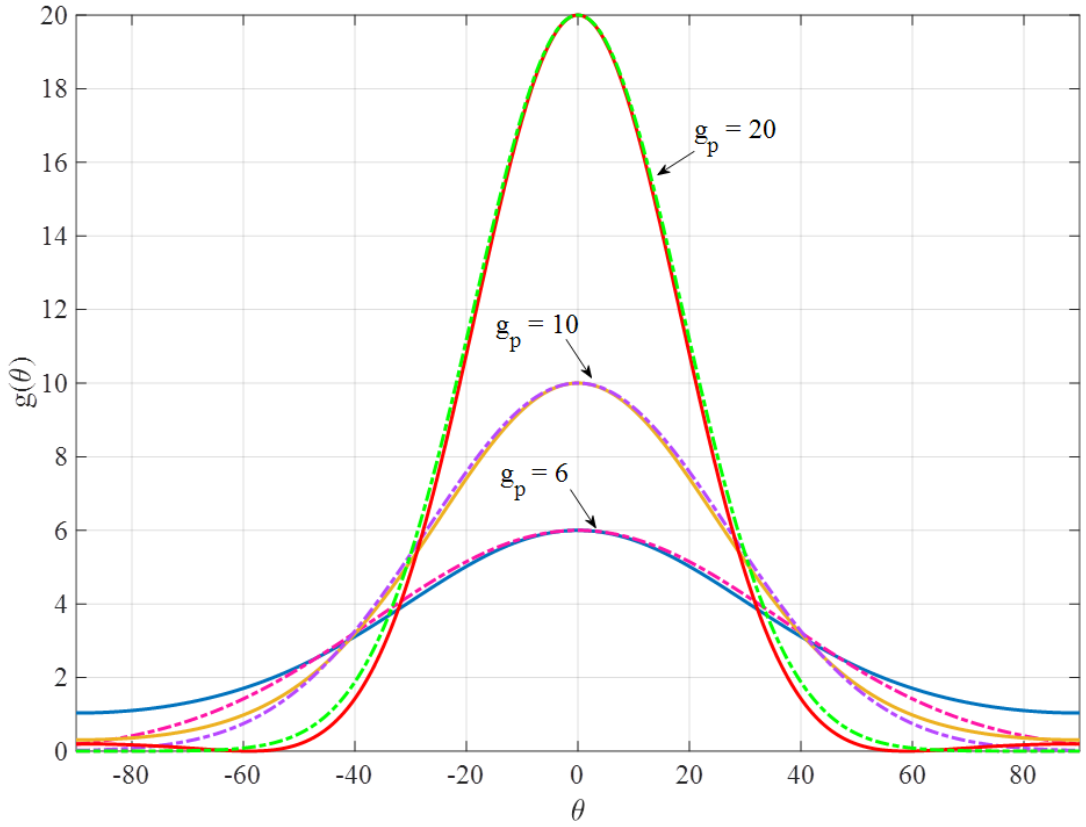


Figure 6.2: Comparison of parabolic dish antenna and the approximation for $g(\theta)$ at peak $g_p \in \{6, 10, 20\}$. The solid line represents the gain of a parabolic antenna and the dashed line represents our antenna model.

6.2.3 Coherent and Joint Detection

We assume that the eavesdropper is capable of receiving and retaining all information transmitted from the $N+1$ transmitting nodes, in our discrete multihop network, and applies joint (coherent) maximum likelihood (ML) detection.

Assuming that the eavesdropper's receiver has equivalent thermal noise variance to that of the network nodes[2], then the effective SNR is the sum of SNR contributions from all transmitting nodes in the network [269].

In our model, the cumulative SNR will have dependence on P, spatial dependence on $\{\mathcal{R}, \mathcal{B}\}$ and also the spatial characteristics of the antennas used in the relay network. As with the multihop communications network, the links from each transmitting node and the eavesdropper are independently affected by Rayleigh

[2]Otherwise a simple constant scalar needs to be applied in the analysis to account for any difference in the noise variance.

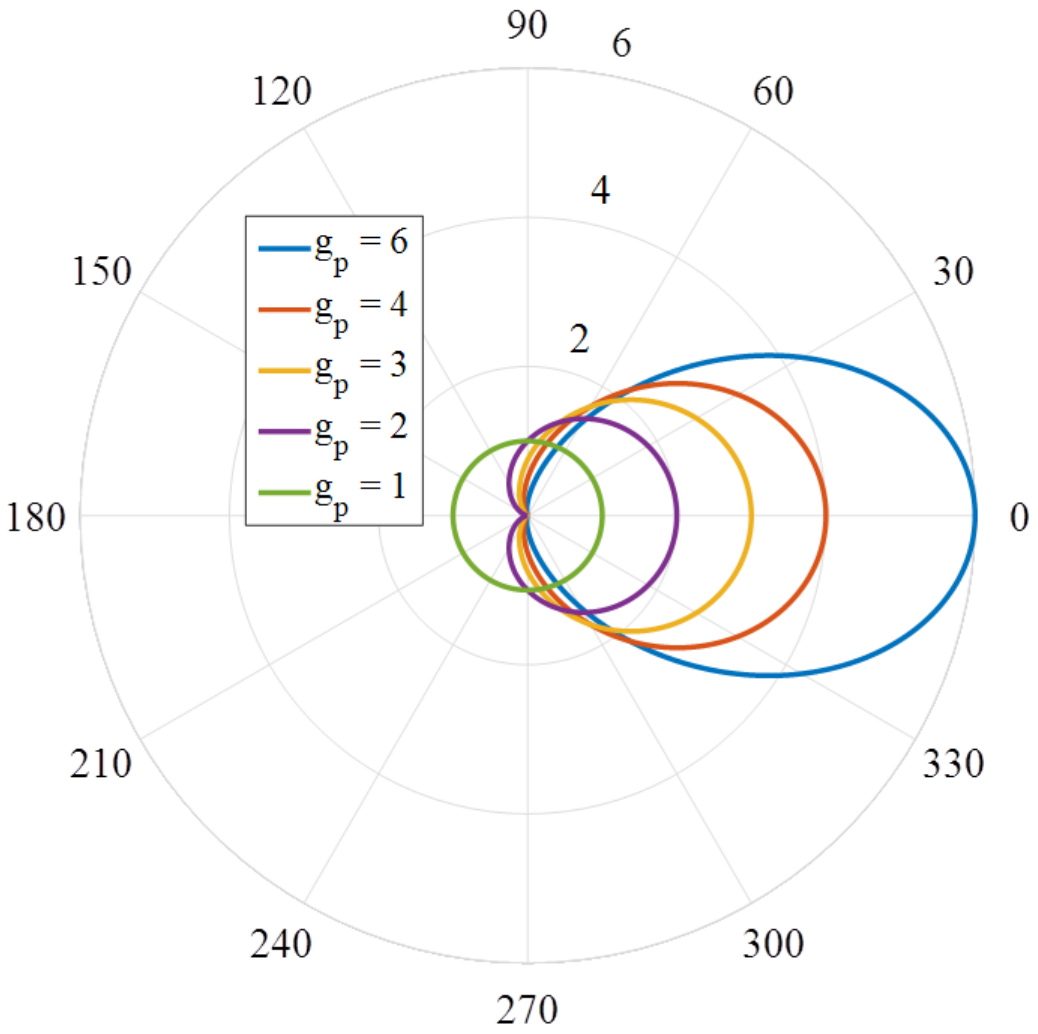


Figure 6.3: Polar Plot of $g(\theta)$, $g_p \in \{1, 2, 3, 4, 6\}$.

fading and subject to mean path loss that follows an inverse power law, with exponent η_e. Note that η_c and η_e are not necessarily equivalent due to the relative distances involved between adjacent relay nodes, in the multihop network, and between relay nodes and the eavesdropper. It would be expected that as the connection distances between relay nodes is reduced then the path loss is more likely to approach a square law, whereas generally larger distances to the eavesdropper may be subjected to higher path loss exponents, particularly in urban environments.

The SNR contribution at the eavesdropper, from the ith transmitting node in the network, is given by

$$\mathrm{SNR}_{ie} = P g_{ie} b_{ie} \beta |h_{ie}|^2 d_{ie}^{-\eta_e}. \tag{6.13}$$

The parameter g_{ie} denotes the gain of the antenna in the direction of the eavesdropper relative to the ith transmitting node; $h_{ie} \sim \mathcal{CN}(0,1)$ is the Rayleigh fading coefficient; b_{ie} denotes the shadowing loss due to obstacles between the ith transmitting node and the eavesdropper. The expectation of the sum of SNR contributions, at the eavesdropper, is given by

$$\begin{aligned} \mathrm{SNR}_e &= \mathbb{E}\left[\sum_{i=0}^{N} P g_{ie} b_{ie} \beta |h_{ie}|^2 d_{ie}^{-\eta_e}\right] \\ &\overset{(a)}{=} \sum_{i=0}^{N} \left(\frac{P}{\ell_i}\right) g_{ie} b_{ie} \beta d_{ie}^{-\eta_e} \ell_i, \end{aligned} \tag{6.14}$$

where $\ell_i = d_{ij},\ j = i+1$, i.e. the distance between adjacent nodes in the relay network. In step (a), the summation of exponential random variables with non-equal rates, is hypoexponentially distributed which has a mean equivalent to the sum of rates of the composite exponential random variables and we follow the approach previously employed in (5.4).

As before, we use the polar coordinate system relative to the location of the eavesdropper, define $\delta_\ell := \max \ell_i$ and take the limit $\delta_\ell \to 0$, i.e. infinite relay extent. By substituting (6.8) and (6.9), it can be shown that (6.14) becomes

$$\mathrm{SNR}_e = \beta \rho \int_{\phi_S}^{\phi_D} g_e I \frac{\sqrt{r^2 + \dot{r}^2}}{r^{\eta_e}} \mathrm{d}\phi, \tag{6.15}$$

where $I := I(\phi)$ denotes the shadowing loss function with respect to ϕ and $g_e := g_e(\phi)$ denotes the gain of the antenna in the direction of the eavesdropper at the point on the continuum at angle ϕ.

With the aid of Fig. 6.4, we consider a node on the continuum at $r(\phi)$, transmitting to a close adjacent node with angular separation $\delta\phi$. In the limit $\delta\phi \to 0$, the angle to the eavesdropper, relative to the antenna boresight, is θ_e, where.

$$\theta_e = \pi/2 + \arcsin\left(\frac{\dot{r}}{\sqrt{r^2 + \dot{r}^2}}\right). \tag{6.16}$$

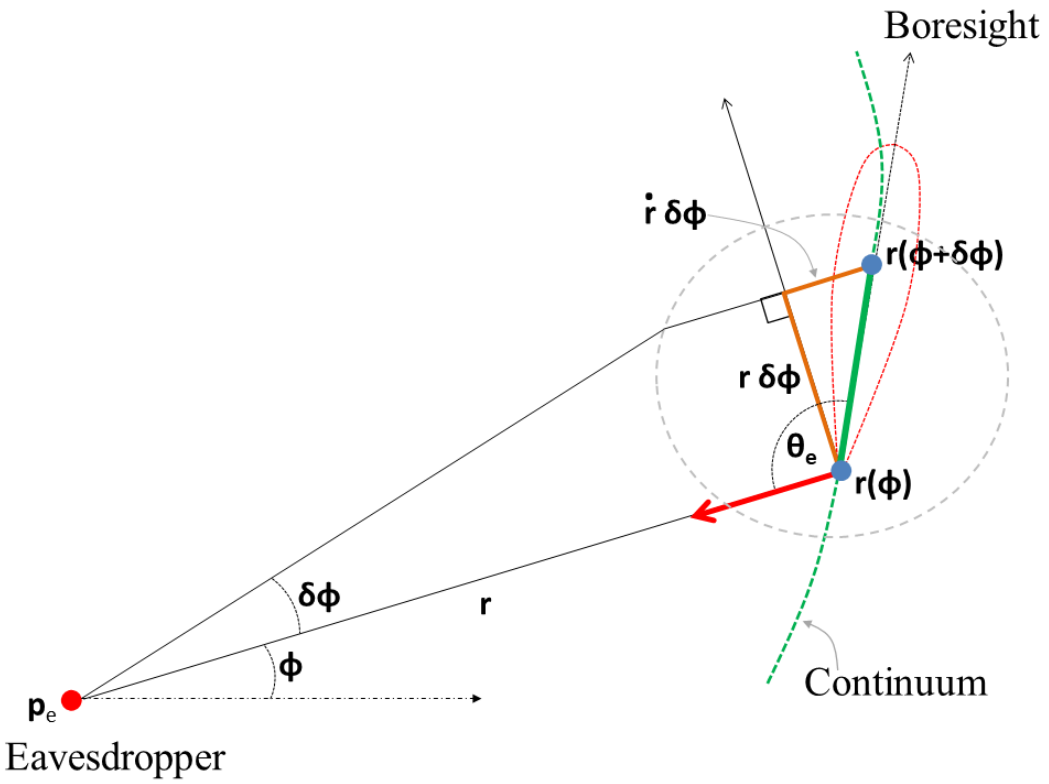


Figure 6.4: Illustration of the connectivity between two infinitesimally close neighbouring nodes on the continuum.

Substituting $\theta = \theta_e$ into (6.11) gives

$$g_e = k\left[1 - \frac{\dot{r}}{\sqrt{r^2 + \dot{r}^2}}\right]^{g_p - 1}. \tag{6.17}$$

Then (6.15) becomes

$$\mathrm{SNR}_e = k\beta\rho \int_{\phi_S}^{\phi_D} I\left[1 - \frac{\dot{r}}{\sqrt{r^2 + \dot{r}^2}}\right]^{g_p - 1} \frac{\sqrt{r^2 + \dot{r}^2}}{r^{\eta_e}} \mathrm{d}\phi \tag{6.18}$$

6.3 Multi-hop Route Optimisation in the Presence of a Single Eavesdropper

Thus far, we have developed two functionals (6.10) and (6.18) representing our objective and constraint functions respectively. Our objective is now to determine the stationary continuum path, defined by r, given a constraint on maximum SNR_e. Since the exp function in (6.10) is strictly monotonic, we can simply

redefine our objective function as

$$F(r,\dot{r}) = \int_{\phi_S}^{\phi_D} \sqrt{r^2+\dot{r}^2}\mathrm{d}\phi. \tag{6.19}$$

Minimisation of $F(r,\dot{r})$, i.e. the length of the continuum line, will maximise the end-to-end connection probability of the network. We seek to minimise $F(r,\dot{r})$ subject to the expected SNR at the eavesdropper not exceeding a threshold τ_e.

To make progress, we can define the following Lagrangian

$$\begin{aligned}\mathcal{L}(r,\Gamma) &= \int_{\phi_S}^{\phi_D} \sqrt{\dot{r}^2+r^2}\mathrm{d}\phi \\ &- \Gamma\left[\tau_e - k\beta\rho\int_{\phi_S}^{\phi_D} I\left[1-\frac{\dot{r}}{\sqrt{\dot{r}^2+r^2}}\right]^{g_p-1}\frac{\sqrt{\dot{r}^2+r^2}}{r^{\eta_e}}\mathrm{d}\phi\right],\end{aligned} \tag{6.20}$$

where Γ is a Lagrange multiplier. This simplifies to

$$\mathcal{L}(r,\Gamma) = \int_{\phi_S}^{\phi_D}\left(1+\frac{\Gamma k\beta\rho I}{r^{\eta_e}}\left[1-\frac{\dot{r}}{\sqrt{\dot{r}^2+r^2}}\right]^{g_p-1}\right)\sqrt{\dot{r}^2+r^2}\mathrm{d}\phi - \Gamma\tau_e \tag{6.21}$$

In order to determine the stationary path $r(\phi)$, satisfying the new functional $\mathcal{L}(r,\Gamma)$, we must meet the conditions

$$\frac{\partial\mathcal{L}}{\partial r} = 0 \tag{6.22}$$

$$\frac{\partial\mathcal{L}}{\partial\Gamma} = 0. \tag{6.23}$$

To solve (6.22), we apply tools from the calculus of variations [255]; more specifically, we invoke the Euler-Lagrange equation

$$\frac{\partial H}{\partial r} - \frac{\mathrm{d}}{\mathrm{d}\phi}\left(\frac{\partial H}{\partial\dot{r}}\right) = 0, \tag{6.24}$$

where

$$H = \left(1+\frac{\Gamma k\beta\rho I}{r^{\eta_e}}\left[1-\frac{\dot{r}}{\sqrt{\dot{r}^2+r^2}}\right]^{g_p-1}\right)\sqrt{\dot{r}^2+r^2}. \tag{6.25}$$

The partial derivative (6.23) reduces to $\mathrm{SNR_e} = \tau_e$ and the solution to (6.24) is given by the second order differential equation

$$F(\phi,r,\dot{r},\Gamma) := \ddot{r} = \frac{F_N(\phi,r,\dot{r},\Gamma)}{F_D(\phi,r,\dot{r},\Gamma)}, \tag{6.26}$$

$$F_N(\phi, r, \dot{r}, \Gamma) = r^{\eta_e+5} - 2(l-2\dot{r})\dot{r}r^{\eta_e+3} - 4(l-\dot{r})\dot{r}^3 r^{\eta_e+1} + \Gamma k\beta\rho s\Big\{\dot{I}(l-\dot{r})\dot{r}^4 - I(\eta_e-1)r^5 + I\dot{r}^3 r[(g_p^2 - 3g_p + 4 - \eta_e)\dot{r} + (g_p-2)(g_p+1-\eta_e)l] + I\dot{r}r^3[(g_p^2 - 3g_p + 5 - 2\eta_e)\dot{r} - (g_p-2)(\eta_e-1)l] + r^4\dot{I}[(g_p-1)l - \dot{r}] - \dot{r}^2 r^2 \dot{I}(2\dot{r} - g_p l)\Big\} \quad (6.27)$$

$$F_D(\phi, r, \dot{r}, \Gamma) = r^{\eta_e+4} - 2\dot{r}(l-\dot{r})r^{\eta_e+2} + \Gamma k\beta\rho s\Big\{r^4(g_p^2 - 3g_p + 3)I + r^2\dot{r}I[(g_p^2 - 3g_p + 3)\dot{r} + (g_p^2 - 2g_p)l]\Big\}. \quad (6.28)$$

where $F_N(\cdot)$ and $F_D(\cdot)$ are given by (6.27) and (6.28) respectively, which are shown at the top of the page. In these two equations, we have used

$$l = \sqrt{\dot{r}^2 + r^2}, \;\; s = \left(1 - \frac{\dot{r}}{l}\right)^{g_p}$$

and $\dot{I}$ denotes the first derivative of I with respect to ϕ.

Since an analytic solution to (6.26) is not obvious, we employ numerical methods to solve the differential equation here. Specifically, Euler's explicit method [217] lends itself to this example. For a specific Lagrange multiplier Γ, we consider S discrete samples over the continuum between the source and destination nodes, uniformly distributed over the interval $[\phi_S, \phi_D]$, such that the angular sample spacing is $h = (\phi_D - \phi_S)/(S+1)$. Let $n \in \{1, 2, \ldots, S+2\}$ denote the index of these samples, where $(\phi(n), r(n))$ represent the polar coordinates of the nth sample, and $n = 1$ and $n = S+2$ are the source and destination indices, respectively. By this definition, we have that $\phi(1) = \phi_S$ and $r(1)$ is the radial distance of the source from the origin.

One may estimate $\dot{r}(1)$ and invoke Euler's explicit method to return the calculated polar coordinates of the path described by (6.26). We then successively approximate $\dot{r}(1)$ over the interval[3] $[\dot{r}_l(1), \dot{r}_u(1)]$ until the calculated radial ordinate of the destination node $r(S+2)$ is within an acceptable fractional deviation ξ of the actual radial distance r_d. We then calculate the approximate signal-to-noise

[3]The successive approximation is conditional on the variation of $r(S+2)$ being strictly increasing monotonic over the interval $[\dot{r}_l(1), \dot{r}_u(1)]$. We determine the interval following a coarse search based upon incrementing $\dot{r}(1)$ over a larger estimated range, invoking Euler's explicit method to return the calculated polar coordinates of the path described by (6.26) and determine the value of $\dot{r}(1)$ that yields an acceptable approximation of the path.

ratio at the eavesdropper, denoted by SNR_e^*, from the Riemann sum

$$\mathrm{SNR}_e^* = k\beta\rho h \sum_{n=1}^{S+1} I(n)\left[1 - \frac{\dot{r}(n)}{\sqrt{\dot{r}(n)^2 + r(n)^2}}\right]^{g_p - 1} \frac{\sqrt{\dot{r}(n)^2 + r(n)^2}}{r(n)^{\eta_e}}. \tag{6.29}$$

We successively approximate the value of Γ, over the interval $[\Gamma_l, \Gamma_u]$,[4] until $\mathrm{SNR_e}$ is within an acceptable fractional deviation ξ of τ_e. Associated pseudo-code for this method is outlined in Algorithm 2, where the inner successive approximation loop returns the stationary path defined by r, for a fixed value of Γ, and the outer loop successively iterates Γ until the constraint on SNR_e^* is satisfied.

Remark. *It should be noted that there will be a maximum power density, denoted by ρ_{max}, beyond which, the condition on the maximum* SNR_e *cannot be satisfied. For the general antenna case, ρ_{max} can be determined by rearranging (6.15), letting* $\mathrm{SNR}_e = \tau_e$ *and determine the stationary path r, that minimises the integral, and back substitute. For the special case where we employ an isotropic antenna, it is intuitive that the route that minimises* SNR_e*, for arbitrary power density ρ, will be straight lines from the source and destination nodes extending directly away from the respective directions of the eavesdropper to ∞. In this case, ρ_{max} is given by*

$$\begin{aligned} \rho_{max} &= \frac{\tau_e}{\beta\Big[\int_{\|\mathbf{p}_S\|}^{\infty} \frac{1}{\ell^{\eta_e}} \mathrm{d}\ell + \int_{\|\mathbf{p}_D\|}^{\infty} \frac{1}{\ell^{\eta_e}} \mathrm{d}\ell\Big]} \\ &= \frac{\tau_e(\eta_e - 1)}{\beta\Big[\|\mathbf{p}_S\|^{1-\eta_e} + \|\mathbf{p}_D\|^{1-\eta_e}\Big]}, \end{aligned} \tag{6.30}$$

where $\mathbf{p}_S$ and $\mathbf{p}_D$ denote the locations of the source and destination nodes respectively.

6.4 Numerical Results

We demonstrate the efficacy of our optimisation framework in the following worked examples.

6.4.1 Single Eavesdropper with No Shadowing

We now apply our framework within a 'real-world' context, by considering the scenario where source and destination nodes are separated by 2km and an eavesdropper

[4]The successive approximation is conditional on the variation of $\mathrm{SNR_e^*}$ being strictly increasing monotonic over the interval $[\Gamma_l, \Gamma_u]$.

Algorithm 2: Successive Route Approximation

initialize Γ_l, Γ_u, $\mathrm{SNR}_{\mathrm{e}}^{*} \gg \tau_e$, ξ;
while $|\mathrm{SNR}_{\mathrm{e}} - \tau_e|/\tau_e > \xi$ **do**
  `// Outer Loop: Lagrange Multiplier`
  $\Gamma = (\Gamma_l + \Gamma_u)/2$;
  initialize S, h, r_d, $r(S+2) \gg r_d$, $\dot{r}_l(1)$, $\dot{r}_u(1)$; **while** $|r(S+2) - r_d|/r_d > \xi$ **do**
    `// Inner Loop: Euler's Explicit Method`
    $\dot{r}(1) = [\dot{r}_l(1) + \dot{r}_u(1)]/2$;
    for $n = 1 : S+1$ **do**
      $r(n+1) = r(n) + h\dot{r}(n)$;
      $\dot{r}(n+1) = \dot{r}(n) + hF(\phi(n), r(n), \dot{r}(n), \Gamma)$;
      $\phi(n+1) = \phi(n) + h$;
    end
    return $\{r(S+2)\}$;
    if $r(S+2) > r_d$ **then**
      $\dot{r}_u(1) = \dot{r}(1)$;
    else
      $\dot{r}_l(1) = \dot{r}(1)$;
    end
  end
  return $\{\phi\}, \{r\}$;
  calculate $\mathrm{SNR}_{\mathrm{e}}^{*}$;
  if $\mathrm{SNR}_{\mathrm{e}}^{*} > \tau_e$ **then**
    $\Gamma_u = \Gamma$;
  else
    $\Gamma_l = \Gamma$;
  end
end

Table 6.1: Parameters associated with Fig. 6.5.

Parameter	Meaning	Value	Unit
S	Samples	1000	–
σ^2	Noise Variance	4.14e-15	W
τ_c	Connection SNR threshold	10	–
τ_e	Eavesdropper SNR threshold	1	–
η_e	Eavesdropper pathloss exponent	3	–
ρ	Power density	5e-6	W/m
λ	RF Wavelength	0.3	m

is located at the mid point in the direct path between them. The communication parameters used in this example are detailed in Table 6.1. To ensure sufficient

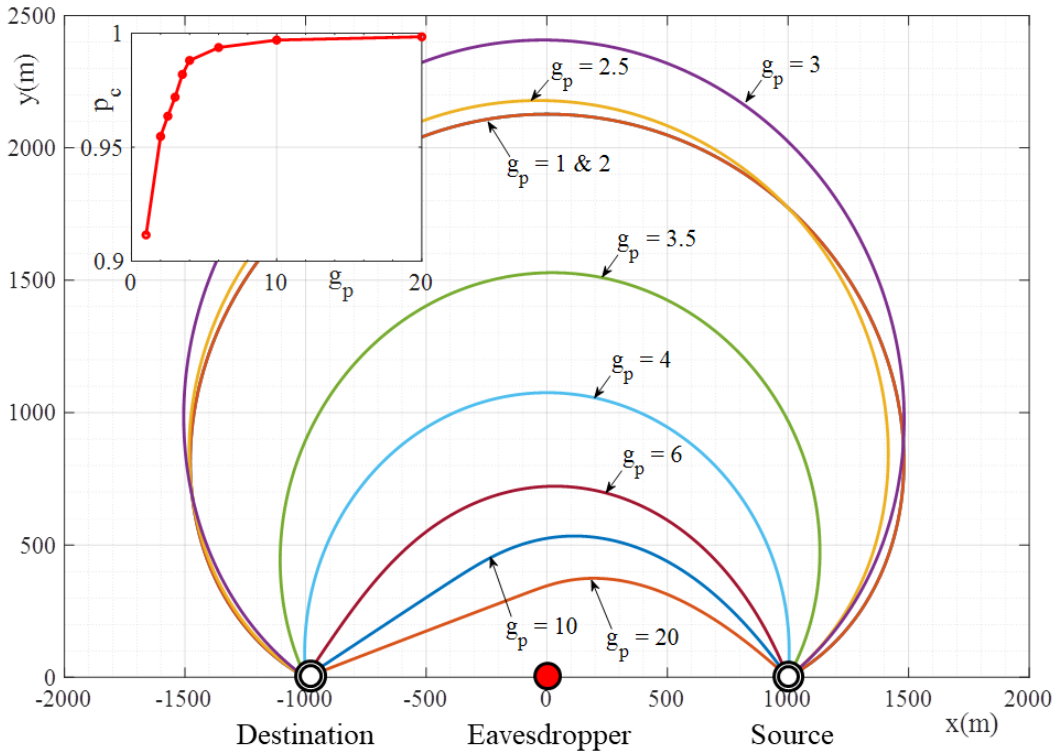


Figure 6.5: Stationary routes for varying antenna peak gains, $g_p \in \{1, 2, 2.5, 3, 3.5, 4, 6, 10, 20\}$.

margin such that the eavesdropper cannot intercept the transmitted information, we constrain the maximum eavesdropper SNR, τ_e, to a factor of 10 below that required for a pairwise connection within the multihop network. In our example, we assume that the noise figure of the eavesdropper's receiver is negligible and $\sigma^2 = \kappa TB$, where κ denotes Boltzman's constant, B denotes the thermal noise (channel) bandwidth and T denotes the temperature. In this example we let B=1e6Hz and T=300K. We apply the aforementioned numerical approach to generate the stationary paths for varying antenna peak gains. In this example, we do not consider the effect of the forcing function I within the differential equation (6.26), i.e we have assumed unit and zero vectors of length $S + 2$ for I and $\dot{I}$ respectively. Results are shown in Fig. 6.5, from which we draw the following key observations:

1. For the isotropic antenna case, $g_p = 1$, the continuum is symmetric about the vertical line intersecting the eavesdropper node. This is attributed to the geometric symmetry, i.e. destination and source nodes are equidistant from

the eavesdropper, and at any arbitrary point on the route, the associated SNR contribution at the eavesdropper is independent of antenna orientation and solely dependent upon the Euclidean distance to the eavesdropper;

2. The continuum for the case $g_p = 2$ is identical to the isotropic antenna case. This is attributed to a combination of the aforementioned geometric symmetry and the fact that the mean gain of the antenna over any arbitrary interval, centred on $\theta = \pi/2$ is constant $g(\pi/2) = 1$;

3. With the exception of the special cases $g_p \in \{1, 2\}$, the continuum has varying degrees of asymmetry due to the fact that the mean gain of the antenna over any arbitrary interval, centred on $\theta = \pi/2$, is no longer constant.

4. The length of the continuum is approximately maximum, in this scenario, at $g_p = 3$. The reason for this is not immediately obvious but thought to be a result of the specific antenna model chosen. This is deferred to possible future work.

5. The length of the continuum decreases, with increasing antenna gain above 3, attributed the the increased spatial rejection provide by the increased antenna directivity.

6. With reference to the inset figure, the connection probability of the network increases with antenna gain and reducing length of the continuum, as given by (6.10).

6.4.2 Single Eavesdropper with Shadowing

We now introduce two arbitrarily located obstacles (e.g. a single large building or amalgamation of smaller buildings) that provide signal attenuation (shadowing) to the paths between transmitters in the multi-hop network and the eavesdropper. For convenience, we model the obstacles as rectangles with uniform log-attenuation per unit distance through the obstacle. This shadowing loss function is then given by

$$I = 10^{-\frac{\mu d_I(\phi)}{10}}, \tag{6.31}$$

where μ denotes the attenuation constant in dB/m and $d_I(\phi)$ denotes the inner distance between sides of the obstacle at angle ϕ about the location of the eavesdropper. For consistency, we employ the communication parameters detailed in Table 6.1 and let $\mu = 0.2$.

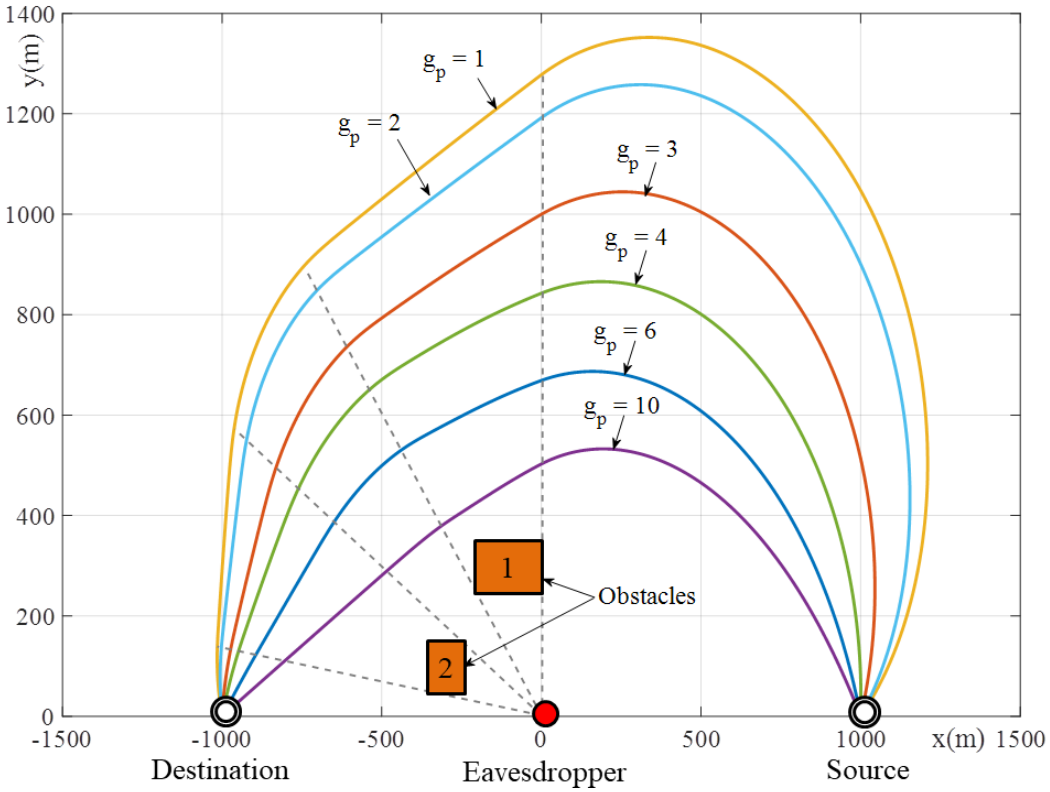


Figure 6.6: Stationary routes, subject to building shadowing, for varying antenna peak gains, $g_p \in \{1, 2, 3, 4, 6, 10\}$. Obstacle-1 is centred at Cartesian coordinates (-100, 300) with length 200m and width 100m and obstacle-2 is centred at Cartesian coordinates (-300, 100) with length 100m and width 100m.

We reapply our framework and generate the results shown in Fig. 6.6, from which we draw the following additional key observations:

1. In constrast to the previous case, the continuum routes are clearly asymmetric, attributed to the non-symmetric placement of the shadowing obstacles;

2. The continuum routes associated with antenna gains of 1 and 2 are no longer identical, again attributed to the aforementioned non-symmetric placement of the shadowing obstacles;

3. There is no longer a peak in the length of the continuum at a specific antenna gain, attributed to increased signal attenuation provided by the obstacles over the interval when the angle between the directions of the antenna boresight and the eavesdropper is reducing.

6.5 Application to Ad-Hoc Network Scenario

In order to demonstrate the efficacy of the framework in a 'real-world' context, we consider the application of this route planning framework to a covert ad-hoc network. We consider a random network of relay nodes which are uniformly spatially distributed in $\mathbb{R}^2$ with density ς. We model this network by a homogeneous PPP, as depicted in Fig. 6.7. For illustration purposes, we also show the Voronoi cell boundaries associated with each relay node. For a given scenario, we generate a

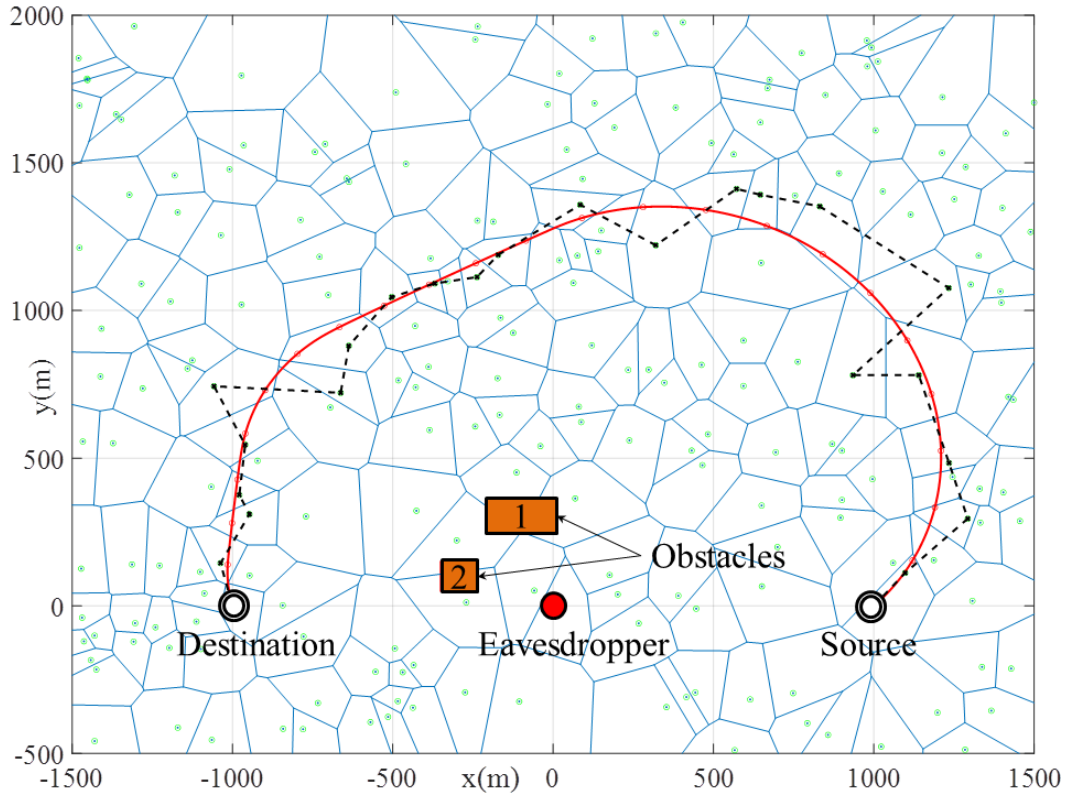


Figure 6.7: Application of the route planning framework to a 'real-world' covert IoT ad-hoc network.

continuum between source and destination nodes using our route planning framework;

in what follows, we employ the communication parameters detailed in Table 6.1, let $\mu = 0.2$ and use the $g_p = 1$ case as illustrated in Fig. 6.6.

Proposition 3. *Consider a Voronoi tesselation generated for points in a homogeneous PPP located in* $\mathbb{R}^2$ *with density* ς*. An arbitrary low-curvature line of length* L *will traverse a mean of* $\sqrt{\varsigma}L$ *Voronoi cells. In this context, it is convenient to define low curvature as the condition that the radius of curvature at any point on the line exceeds the expectation of nearest neighbour distance of points in the PPP,* $0.5/\sqrt{\varsigma}$ *[279].*

Based on proposition 3, we generate $N = \lfloor \sqrt{\varsigma}L \rceil - 2$ discrete samples of the continuum between the source and destination nodes, where $\lfloor \cdot \rceil$ denotes rounding to the nearest integer. The angle-ordinates of these N samples are uniformly distributed over the interval $[\phi_S, \phi_D]$, such that their angular spacing is $(\phi_D - \phi_S)/(N+1)$. From section 5.6 of the previous chapter, it was found that sampling a low curvature continuum, in this way, gave close to optimal results with low processing complexity.

We then proceed to identify the closest relay nodes (with respect to Euclidean distance), within the ad-hoc network, to the N samples of the continuum. For convenience, if samples share a common relay, we assume two co-located relays with a pairwise connection probability of 1. For each of the N relays, and the source node, we calculate their fixed transmit power level P from

$$P = \frac{\rho L}{N+1}. \tag{6.32}$$

Further, we consider two scenarios:

1. the closest relays can be selected, irrespective of their location within the ad-hoc network, or

2. only the closest relays with greater radial offset from the eavesdropper relative to the radial offset of the respective sample can be selected.

For any instantiation of the ad-hoc network, we calculate the effective SNR at the eavesdropper as given by

$$\mathrm{SNR}_e = \beta P \sum_{i=0}^{N} g_{ie} b_{ie} |h_{ie}|^2 d_{ie}^{-\eta_e}, \tag{6.33}$$

and the discrete multihop connection probability P_c from

$$P_c = \prod_{i=0}^{N} c(\mathbf{p}_i, \mathbf{p}_j), \; j = i + 1, \tag{6.34}$$

where $c(\mathbf{p}_i, \mathbf{p}_j)$ is given by (6.2). We then apply a Monte Carlo simulation to determine the expectations of SNR_e and P_c over a range of network (PPP) configurations and densities. Results are shown in Fig. 6.8 and 6.9 respectively.

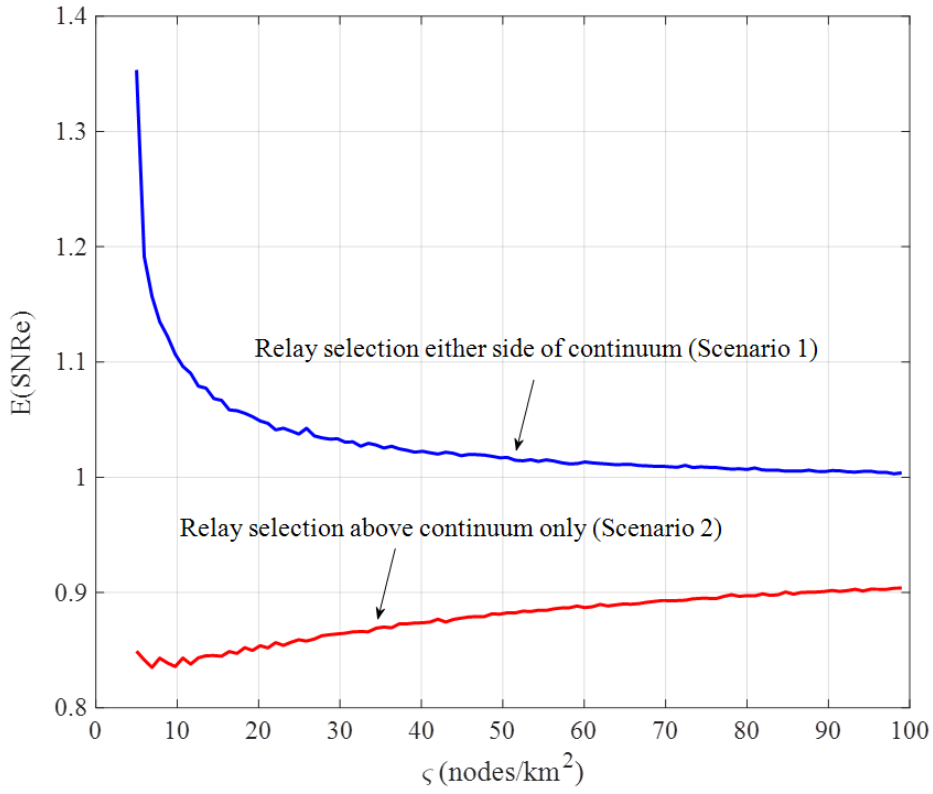


Figure 6.8: Expectation of SNR_e as a function of relay node density in a homogenous PPP.

For scenario 1, we observe a rapid convergence of SNR_e to our target specification $\tau_e = 1$. Similarly we see a rapid convergence to the connection probability given by our continuum model. Note that the ripple in the plots is attributed to the rounding function in generating the number of samples, N.

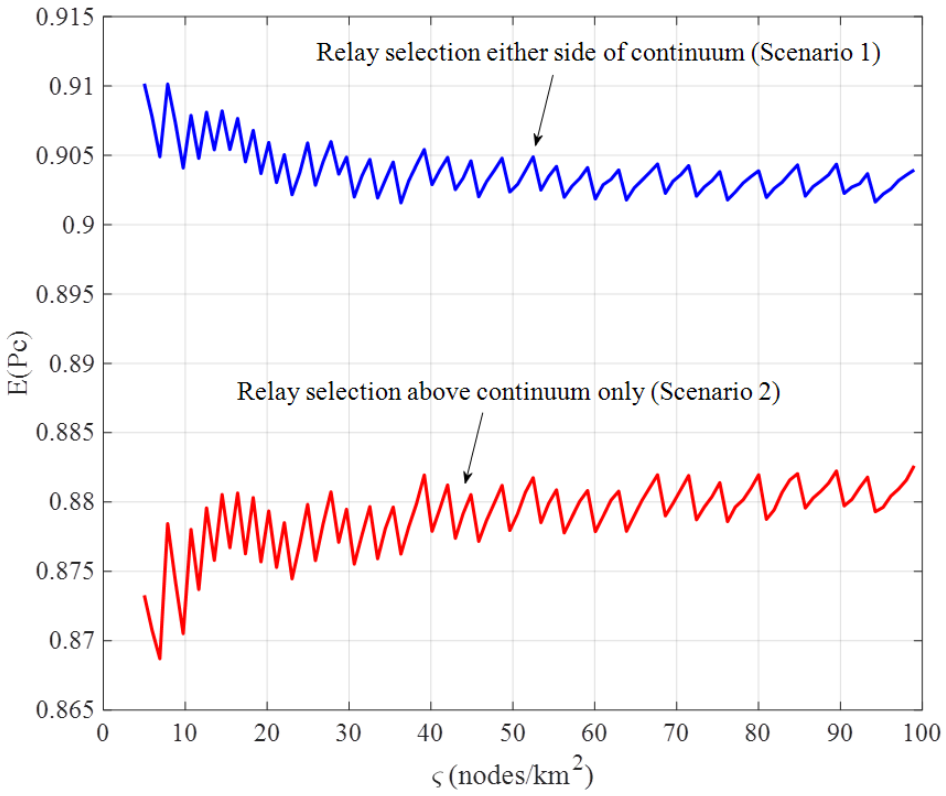


Figure 6.9: Expectation of P_c as a function of relay node density in a homogenous PPP.

For scenario 2, we clearly see that SNR_e never exceeds $\tau_e = 1$, but this is achieved at the expense of a lower multihop connection probability, which is attributed to the longer combined connection path lengths.

6.6 Conclusion and Discussions

In this chapter, we have studied the problem of covert routing of a large-scale multihop wireless network in the presence of an eavesdropper at a known location, capable of joint detection of all transmissions within the network. In addressing the covertness constraint we have shown that application of the continuum modelling framework, developed in Chapter 5, and Lagrangian optimisation can solve the problem of optimal covert routing with low processing complexity.

Although analytic forms representing the optimal relay path do not exist in general, we demonstrated that basic numerical techniques can still be applied to approximate it, even when our framework requires the solution of unwieldy

non-linear differential equations.

We demonstrate the efficacy of our framework with its application to a 'real-world' covert multihop routing problem with its application to a network modelled as a PPP by selecting proximity nodes to the optimal continuum route.

7
Conclusions

7.1 Thesis Summary

In Chapter 1 of this thesis, we provided a brief description of how the more salient wireless technologies have evolved from the birth of wireless communications to date. We also attempt to predict a future trajectory in how wireless technologies are likely to further evolve in meeting the future demands of society. From this initial research, we observed the following trends:

- many wireless networks have evolved from having sparse homogeneous macro-cellular type architectures to higher density heterogeneous network architectures;
- over generational increments of wireless networks, the network performance demands increased exponentially;
- many wireless networks are subject to an increasing spatial densification of users and basestations;
- with increasing concerns over information privacy and security, significant attention is being placed upon network security, vulnerability and resilience;
- with increased global pressure to reduce carbon footprints, wireless networks are subject to increasing scrutiny with respect to their energy consumption;
- with finite, and costly, spectrum resources available there is increasing focus on spectral efficiency and spectrum usage;
- increasing network densification has led to co-channel interference as the limiting source of noise within the network.

We then introduced the concept of multihop connectivity as a mechanism to address future performance demands of wireless networks, mitigate issues associated with energy and RF resource constraints and exploit the increasing densification of wireless devices in networks. We highlighted the benefits and challenges associated with multihop networks and provided examples of their current utility in a number

of settings. Although researchers have demonstrated several benefits offered by multihop networking, there are many issues associated with combating network inhomogeneities and in the determination of optimal node placement/selection in large scale networks. Addressing these issues, in large scale multihop networks subject to inhomogeneities, provided the motivation for our research and this thesis.

In Chapter 2 we described a number of modelling fundamentals, underpinning subsequent research chapters, and concluded with 5 key research questions providing a segue into our principle research chapters. For convenience. The following subsections demonstrate how we have addressed these questions within our research.

7.1.1 Research Question 1

How do geometric boundaries affect 2-hop connection probability, between source and destination nodes, via a single relay node selected from a set of uniformly distributed relays with finite density?

In Chapter 3 we studied the direct (1-hop) and 2-hop connectivity, between two fixed terminal nodes (information source and destination nodes), amongst a network of uniformly randomly distributed relay nodes (e.g. other user nodes), confined to a finite convex geometry, subject to inverse square pathloss-distance relationship and Rayleigh fading. We justified the choice of pathloss and fading model on the grounds of mathematical tractability and behavioural insight of our chosen network performance metrics. In terms of convex geometric boundaries, we specifically considered the special cases of circular and rectangular boundaries, deriving respective closed form analytic expressions for average connection probabilities.

The analytic expression showed a clear dependence on boundary geometry, spatial separation of nodes and their mid-point location leading us to conjecture that the average 2-hop connection probability within a network domain $\mathcal{V}$, with convex geometric boundary, could be generalised in the form

$$\langle H_{12}^{(2)} \rangle = \frac{\pi}{2|\mathcal{V}|} e^{-\frac{1}{2}\|\mathbf{p}_2 - \mathbf{p}_1\|^2} f_{\mathcal{V}}(\overline{\mathbf{p}}_{12}, \hat{\mathcal{V}}) \tag{7.1}$$

where $\mathbf{p}_1$ and $\mathbf{p}_2$ represent the locations of source and destination nodes and $0 \leq f_{\mathcal{V}}(\overline{\mathbf{p}}_{12}, \hat{\mathcal{V}}) \leq 1$ is a domain specific function of the midpoint location, $\overline{\mathbf{p}}_{12}$, of terminal nodes within the domain, and a set of parameter(s), $\hat{\mathcal{V}}$, which define the domain geometry i.e. $\hat{\mathcal{V}} \in \{R, \{A, B\}\}$ for our special cases of circular and rectangular domains. Validation of this conjecture would require the analysis of a suitably representative set of alternate convex geometric boundaries or generation of a mathematical model of the boundary. This is perhaps a consideration for further work in this area.

The boundary effects, defined by function $f_{\mathcal{V}}$ show a clear reduction in 2-hop connection probability as the mid point between terminal nodes located closer to the boundary. This result is consistent with previous observations [170] and attributed to connectivity mass of relays. An interesting observation from our research is the rotational invariance of the connection probability with respect to the location of the source and destination nodes relative to their mid point location.

In considering the ratio of connection probability for combined direct (1-hop) or 2-hop, between two arbitrarily located terminal nodes, and connection probability for direct connectivity only, we showed appreciable gain in performance (we refer to as 'improvement factor'), particularly with the two terminal nodes located towards the domain boundary.

This initial research was subsequently published in *SCC 2017; 11th International ITG Conference on Systems, Communications and Coding* [151].

7.1.2 Research Question 2

Can the employment of D2D and 2-hop connectivity, in large scale infrastructure oriented networks, be used as a mechanism to reduce reliance on the fixed network infrastructure?

In Chapter 4, we continued with the theme of connectivity between two fixed terminal nodes within a geometrically bounded network, focusing specifically on a circular boundary which we considered to be a good approximation for a city

bound wireless network. In addition to device-to-device (D2D) communications, as introduced in Chapter 3, we considered connectivity to a fixed infrastructure comprising inhomogeneously distributed infrastructure nodes. We consolidated the previously developed closed form mathematical expressions, derived in Chapter 3, with connectivity function between fixed terminal nodes and an inhomogeneously distributed infrastructure network.

With the objective of minimising outage probability between two randomly selected (i.u.d.) terminal nodes, we show that employment of direct and relay assisted connectivity significantly reduces the reliance on the fixed infrastructure. Furthermore, we showed that the spatial distribution of the infrastructure nodes has a marked bearing on connectivity performance in the finite domain regime. This opened the possibility of spatially selective deactivation of infrastructure nodes conditioned on relay density within the network. In our work, we provided a mathematical framework enabling the determination of the optimal density and spatial distribution of an infrastructure network, for a given relay density and prescribed outage condition. As the domain sizes increase, we observed diminishing returns in employing direct and relay assisted connectivity due to increased average separation of terminal nodes and therefore an increased reliance on the infrastructure, which could be addressed by allowing 2-hop connectivity between terminal and infrastructure nodes via an intermediate relay node; a possible future extension to this analysis.

This research chapter was subsequently published in *IEEE Transactions on Vehicular Technology* [153].

7.1.3 Research Question 3

Can we model a large scale multihop network of relay nodes as a 'continuous path' (or continuum) rather than discrete relays?

In Chapter 5 we considered the problem of optimal multihop relay placement between two fixed terminal nodes within a large scale network context, where the

number of relay nodes in the discrete multihop path was significantly greater than 1. In order to frame the problem further, we considered end-to-end outage probability as our objective function and subjected our network to a scalar field of interferers and non-uniform antenna directivity, providing realistic spatial inhomogeneities into the network.

We briefly showed that multihop route optimization, of this type of large-scale inhomogeneous network can be determined by Lagrangian based constrained optimization techniques or would otherwise be NP-hard in processing complexity and potentially require the application of heuristic algorithms yielding sub-optimal solutions. Taking the Lagrangian type of approach, the processing complexity would typically scale like $O(N^3)$, N being the number of relays employed in the multihop path.

In our research, we looked to address this high processing complexity by developing a mathematical formulation whereby we considered the limit of infinite relay node density to develop a continuum model which yielded an optimized equivalent continuous relay path. The model was carefully constructed to maintain a constant connection density even though the node density scaled without bound. The resultant analysis yielded a functional for the end-to-end outage probability of the general form

$$P_o[r] = 1 - \exp\left(-\theta \int_{\phi_1}^{\phi_2} L(\phi, r, \dot{r}) \mathrm{d}\phi\right), \tag{7.2}$$

where $r := r(\phi)$ describes the equivalent continuous relay path (continuum) in polar coordinate form, $\dot{r}$ represents the first derivative of r with respect to ϕ, ϕ_1 and ϕ_2 are the phase ordinates of the source and destination nodes and θ is a scalar constant. We note that the polar coordinate system was used for convenience and the subsequent analysis equally applied to Cartesian and parametric forms describing the continuum. From this, the challenge presented was in the determination of the stationary path or paths r yielding an outage probability minimum. Further, could this be achieved with low processing complexity, or at least lower than the aforementioned $O(N^3)$ scaling. This provided a segue into the next research question.

7.1.4 Research Question 4

Can we apply variational calculus to the relay node placement problem in delivering exact solutions with low processing complexity i.e. approaching linear complexity scaling as achieved with heuristic algorithms?

Progressing our research further in Chapter 5, we showed that the functional described by (7.2) could be solved using tools from the field of variational calculus. Specifically, the use of the Euler-Lagrange equation and, for the special case $\partial L/\partial \phi = 0$, the Beltrami identity was used.

For our chosen scenario of multihop connectivity within an inhomogeneous scalar field of interference and application of variational calculus, the resultant differential equations, defining the stationary paths, were typically non-linear second order yielding no obvious closed form solution, other than the case of a single point source of interference.

Despite the unwieldy nature of these differential equations, we found it possible to employ basic numerical techniques to approximate them, specifically Euler's method was shown to yield satisfactory results. Further, we demonstrated that numerically solving the differential equations could be achieved with a processing complexity that scaled linearly with the number of samples S used to approximate the stationary paths, i.e. $O(S)$. This, in contrast to Lagrangian techniques, marked a significant reduction in processing complexity and approaching that typically associated with sub-optimal heuristic techniques.

We found that our technique could be adopted to identify multiple stationary paths in more complex scenarios, e.g. multiple point sources of interference. Further, we demonstrated that closely grouped interferers could be approximated by a single 'equivalent' interferer which reduced the solution for the continuum to a Jacobi Elliptic function.

We concluded Chapter 5 with the analysis of a number of sampling strategies, where we sampled the continuum with a fixed number of relay nodes. We found that in our scenarios, the least complex sampling strategy yielded an end-to-end

outage probability acceptably close to the optimum as achieved using Lagrangian optimisation technique for relay node placement.

Generally, optimal relay node placement could be achieved with high efficacy with our continuum model approach and provided the added benefit of greater insight into network behaviour which would otherwise be considered difficult with discretely located relays resulting from Lagrangian optimisation.

This research chapter was subsequently published in *IEEE Transactions on Communications* [154] and *27th European Signal Processing Conference (EUSIPCO* [155].

7.1.5 Research Question 5

Can the aforementioned continuum approach be applied to more complex constrained optimisation problem associated with covert multihop communications?

In Chapter 6 we re-framed the problem described in Chapter 5 by considering the connection-optimal route planning of a large-scale multihop wireless network in the presence of an eavesdropper. We considered the network to be covert under the condition that the eavesdropper would not observe the presence of the network through joint detection of the network transmissions, referred to as low probability of detection (LPD). In our model we introduced spatial inhomogeneities with the application of directive antennas in the multihop network and shadowing in the location of the network and the eavesdropper.

We developed a continuum model, similar to Chapter 5, by consider the limit of relay extent and considering a constant power density over the continuum (equivalent to a constant connection density for square-law propagation). In contrast to Chapter 5, we formulated a constrained optimisation problem requiring the application of both variational calculus and Lagrangian optimisation techniques to find connection-optimal multihop routes. Further, in our new formulation, the connection-optimal route determination required the application of two nested

successive approximation loops: the inner loop to determine the stationary path using numeric methods (Euler's explicit method), for a given Lagrange multiplier and the outer loop to determine the value of the Lagrange multiplier meeting the constraint condition at the eavesdropper. Although more numerically intensive than our previous example, the processing time still scaled linearly with the number of samples used to approximate the continuum.

To demonstrate the efficacy of our model we considered a 'real-world' example investigating the effect of antenna directivity and shadowing on optimal route planning. The results validated our intuition that higher antenna directivity generally improved link covertness as did shadowing.

We concluded Chapter 6 with the application of our model to a large scale network of randomly located discrete relays modelled as a homogeneous Poisson point Process (PPP). Specifically we determined our connection-optimal route, followed by selection of proximity relay nodes from the PPP. This exercise showed that our continuum approach could be used for relay node selection in large scale relay networks where low processing complexity is required i.e. power frugal scenarios such as IoT networks for example.

This research chapter is being prepared for possible publication in *IEEE Transactions on Communications*.

7.2 Future Work

In Chapters 3 and 4 we employed a square law path loss model and Rayleigh fading for the purpose of mathematical tractability (see section 2.1.4). Subsequent research could consider alternative path loss and fading models, to better reflect a given scenario, but are highly unlikely to result in exact closed form equations in the analysis, requiring potentially unwieldy numeric analysis and lose the aforementioned behavioural insights. It may be possible to mitigate this by generating inexact closed form solutions in order to approximate connection functions in networks subject to geometric bounds.

Similarly, we restricted our early work to 2-hop relaying, again for mathematical tractability and to provide behavioural insights of the networks. It is possible to consider multihop connectivity (i.e. m-hop) in any subsequent work. Again, this would be significantly more process intensive requiring the use of (7.3) to determine the connection probability of at least one common m-hop path between nodes i and j [280]

$$H_{ij}^{(m)} = 1 - \prod_{k \neq i,j} \left[1 - H_{ik}^{m-1} H_{kj}^{(1)} \prod_{n=1}^{m-2} \left(1 - H_{ik}^{(n)} \right) \right] \tag{7.3}$$

Further, Chapter 4 did not consider multihop connectivity from terminal nodes to infrastructure nodes. Intuitively, the use of relaying here should further reduce the reliance on the infrastructure in the scenario described and may be a subject of subsequent analysis.

Also in Chapter 4 we employed the function (4.16) to represent the spatial distribution of infrastructure nodes with parameter α defining spatial bias towards the centre or boundary of the network domain. It would be an interesting exercise to identify the optimum distribution function for infrastructure node placement for a given geometric network topology; perhaps using tools from variational calculus as employed in Chapters 5 and 6. We conjecture that this will provide a more optimal deactivation strategy in larger scale relay assisted infrastructure-centric networks.

In both Chapters 5 and 6, our work considered continuum paths with relatively low curvatures which, again for analytic convenience and tractability, allowed the use of the polar coordinate system in our analysis. More complex scenarios, e.g. complex spatial distributions of interfering or eavesdropping nodes, could result in optimal paths with significantly higher degrees of curvature. This would necessitate the use of parametric equations to represent paths in the $\mathbb{R}^2$-plane, as introduced in section 5.3.3. Furthermore, the rapidly evolving world of high density low earth orbit (LEO) satellites and UAVs could potentially benefit from our modelling framework in determining optimal satellite/UAV relay selection in the $\mathbb{R}^3$ space for given objective functions.

Further, our work has shown that low complexity sampling strategies appear to yield acceptable levels of performance for the low-curvature continuum paths that we have modelled. A future area of interest would be optimal sampling strategies, particularly for more complex routing scenarios; possibly applying heuristic techniques to the sampling problem.

Again, for aforementioned reasons, we focused on square-law propagation in our continuum model. It is possible to account for alternate path loss exponents by ensuring that (6.5) is satisfied in the limit of infinite relay extent, which maintains a constant connection density but a non-linear power density.

Appendices

A

A.1 Interference Reduction in Multihop Networks

With reference to Figure 2.2, we assume the source transmission power is P_D, for the direct source-destination connection case, and the source and relay transmitters power P_R for the multihop case. For the direct case, the connection probability, H_D, will be given by (2.9),

$$H_D = \exp\left(- \frac{\tau N_o}{P_D G_t G_r} \left(\frac{4\pi}{\lambda}\right)^2 (2d)^\eta \right). \tag{A.1}$$

For the multihop case, with the i.i.d. Rayleigh fading assumption, the source-destination connection probability will be given by

$$\begin{aligned} H_R &= \left[\exp\left(- \frac{\tau N_o}{P_R G_t G_r} \left(\frac{4\pi}{\lambda}\right)^2 \left[2d \sin\left(\frac{\pi}{2N}\right) \right]^\eta \right) \right]^N \\ &= \exp\left(- \frac{N\tau N_o}{P_R G_t G_r} \left(\frac{4\pi}{\lambda}\right)^2 \left[2d \sin\left(\frac{\pi}{2N}\right) \right]^\eta \right). \end{aligned} \tag{A.2}$$

Equating (A.1) and (A.2), for equivalent connection probabilities for the two cases, yields

$$\frac{P_R}{P_D} = N \left[\sin\left(\frac{\pi}{2N}\right) \right]^\eta. \tag{A.3}$$

The interference power level, for the direct and multihop cases at point A, will be given by

$$\mathcal{I}_D = P_D G_t G_r |h_{ij}|^2 \left(\frac{4\pi}{\lambda}\right)^2 d^{-\eta} \tag{A.4}$$

and

$$\mathcal{I}_R = P_R G_t G_r |h_i|^2 \left(\frac{4\pi}{\lambda}\right)^2 d^{-\eta} \sum_{i=1}^{N} |h_i|^2 \tag{A.5}$$

respectively, where $|H_{ij}|^2 \sim \exp(1)$ and $|h_i|^2 \sim \exp(1)$ denote the exponentially distributed power fading random variable in the direct path between the source and point A and between relays and point A in the multihop case, respectively. Taking expectations, yields

$$\begin{aligned} \frac{\mathbb{E}[\mathcal{I}_R]}{\mathbb{E}[\mathcal{I}_D]} &= N \frac{P_R}{P_D} \\ &= N^2 \left[\sin\left(\frac{\pi}{2N}\right) \right]^{\eta}. \end{aligned} \tag{A.6}$$

A.2 Lagrangian Optimisation

In mathematical optimization, the method of Lagrange multipliers is a strategy for finding the local maxima and minima of a function subject to equation constraints (i.e., subject to the condition that one or more equations have to be satisfied exactly by the chosen values of the variables) [281]. This method was named after the mathematician Joseph-Louis Lagrange (1736 - 1813).

In the context of this thesis, we consider an arbitrary objective function $\mathrm{f}(\mathcal{R})$, where $\mathcal{R}$ denotes a set of relay locations in two-dimensional Euclidean space. Our objective is to determine the optimal location of relays that minimise, or maximise as required, the objective function. This optimisation problem may be expressed as

$$\mathcal{R}^* = \underset{\mathcal{R}}{\operatorname{argmin}}\ \mathrm{f}(\mathcal{R}),\ \text{s.t.}\ \begin{cases} \mathrm{g}(\mathcal{R}) = b \\ \mathrm{h}(\mathcal{R}) \leqslant c \end{cases} \tag{A.7}$$

where $\mathcal{R}^*$ represents the set of optimized relay locations, $\mathrm{f}(\mathcal{R})$ is the objective function dependent upon the relay, source and destination locations, $\mathrm{g}(\mathcal{R}) = b$ is an arbitrary equality constraint function relating to the boundary conditions imposed by fixed positions of the source and destination nodes, $\mathrm{h}(\mathcal{R}) \leqslant c$ represents an arbitrary inequality constraint function and b and c are constants. A more complex scenario may have many more constraints. A Lagrangian formulation is then defined by

$$\mathcal{L}(\mathcal{R}, \lambda_1, \lambda_2) = \mathrm{f}(\mathcal{P}) + \lambda_1(b - \mathrm{g}(\mathcal{R})) + \lambda_2(c - \mathrm{h}(\mathcal{R})), \tag{A.8}$$

where λ_1 and λ_2 are Lagrange multipliers. Stationary points are then determined by solving

$$\nabla\mathcal{L}(\mathcal{R}, \lambda_1, \lambda_2) = 0, \tag{A.9}$$

where ∇ is the gradient (vector differential) operator. Solving (A.9) requires the solution of $Nd + 2$ simultaneous equations, which is typically done numerically using successive approximation techniques such as Newton's method [282], which yields the estimate update

$$\mathrm{x}_{k+1} = \mathrm{x}_k - [\mathrm{H}\mathcal{L}(\mathrm{x}_k)]^{-1}\nabla\mathcal{L}(\mathrm{x}_k),\ k \geqslant 0, \tag{A.10}$$

where $\mathrm{H}\mathcal{L}(\mathrm{x_k})$ is the Hessian matrix (second-order partial derivatives of the Lagrangian with respect to the elements of x_k) and $\mathrm{x}_k = \{\mathcal{R}_k, \lambda_{1_k}, \lambda_{2_k}\}$.

From an initial approximation for the variables, x_0, we iterate (A.10) until an acceptable level of convergence is achieved. Since, at every iteration, the inverse of the Hessian matrix needs to be evaluated we have a processing complexity that scales like $O(N^3)$, assuming a standard algorithm such as Gaussian elimination is employed for matrix inversion [217].

The Lagrangian approach can deliver an optimal solution in deterministic polynomial time but the final solution is dependent upon the initial choice of elements in set x_0, the estimated initial conditions. Given many scenarios may exhibit multiple extrema, the selection of x_0 can be problematic which, itself, may require some form of 'coarse' search algorithm.

B

B.1 Evaluation of $\bar{H}_{12}^{(2_{\mathrm{I}})}$

$$\begin{aligned}\bar{H}_{12}^{(2_{\mathrm{I}})} &= \int_{\mathcal{V}} g(\mathbf{p}_n) H_{1n} H_{2n} \mathrm{d}\mathbf{p}_n \\ &= \int_0^R \int_0^{2\pi} r_n g(\mathbf{p}_n) e^{-(\|r_{1n}\|^\eta + \|r_{2n}\|^\eta)} \mathrm{d}\phi_n \mathrm{d}r_n, \end{aligned} \tag{B.1}$$

where $g(\mathbf{p}_n)$ is given by (4.16). For mathematical tractability, we assume a path loss exponent $\eta = 2$ and a quadratic spatial distribution function for $\mathbf{p}_n$ i.e. $\beta = 2$. Employing polar coordinate geometry, relative to the centre of the circle where $\mathbf{p}_i = r_i \angle \phi_i$, then

$$r_{in} = \sqrt{r_i^2 + r_n^2 - 2 r_i r_n \cos(\phi_n - \phi_i)}. \tag{B.2}$$

Substituting (B.2) into (B.1) and simplifying gives

$$\begin{aligned}\bar{H}_{12}^{(2_{\mathrm{I}})} &= e^{-(r_1^2 + r_2^2)} \int_0^R r_n g(\mathbf{p}_n) e^{-2r_n^2} \\ &\quad \times \left[\int_0^{2\pi} e^{-2r_n [r_1 \cos(\phi_n - \phi_1) + r_2 \cos(\phi_n - \phi_2)]} \mathrm{d}\phi_n \right] \mathrm{d}r_n. \end{aligned} \tag{B.3}$$

We now use the trigonometric identity

$$r_1 \cos(\phi_n - \phi_1) + r_2 \cos(\phi_n - \phi_2) = \Psi \cos(\phi_n - \varphi), \tag{B.4}$$

where

$$\varphi = \tan^{-1} \left[\frac{r_1 \sin(\phi_1) + r_2 \sin(\phi_2)}{r_1 \cos(\phi_1) + r_2 \cos(\phi_2)} \right] \tag{B.5}$$

and

$$\begin{aligned}\Psi &= \sqrt{[r_1\cos(\phi_1)+r_2\cos(\phi_2)]^2+[r_1\sin(\phi_1)+r_2\sin(\phi_2)]^2}\\ &= \sqrt{r_1^2+r_2^2+2r_1r_2\cos(\phi_2-\phi_1)}\\ &= \|\mathbf{p}_1+\mathbf{p}_2\|\\ &= 2\|\overline{\mathbf{p}}_{12}\|. \end{aligned} \tag{B.6}$$

We use $\overline{\mathbf{p}}_{12}=(\mathbf{p}_1+\mathbf{p}_2)/2$ to represent the mid-point between $\mathbf{p}_1$ and $\mathbf{p}_2$. The inner integral within (B.3), denoted by $F(r_n)$, can now be written as

$$F(r_n)=\int_0^{2\pi} e^{-r_n\|\overline{\mathbf{p}}_{12}\|\cos(\phi_n-\varphi)}\mathrm{d}\phi_n. \tag{B.7}$$

Since we integrate over 2π, the angular offset φ can be ignored and (B.7) becomes

$$\begin{aligned}F(r_n) &= 2\int_0^{\pi} e^{-4r_n\|\overline{\mathbf{p}}_{12}\|\cos(\phi_n)}\mathrm{d}\phi_n\\ &= 2\pi\,\mathrm{I}_0(4r_n\|\overline{\mathbf{p}}_{12}\|),\end{aligned} \tag{B.8}$$

where $\mathrm{I}_0(a)=\frac{1}{\pi}\int_0^{\pi}e^{a\cos\theta}\mathrm{d}\theta$ is the zeroth order modified Bessel function of the first kind. Substituting (B.8) into (B.3) now gives

$$\bar{H}_{12}^{(2_I)}=2\pi e^{-(r_1^2+r_2^2)}\int_0^R r_n g(\mathbf{p}_n)e^{-2r_n^2}\,\mathrm{I}_0(4r_n\|\overline{\mathbf{p}}_{12}\|)\mathrm{d}r_n. \tag{B.9}$$

Expanding $g(\mathbf{p}_n)$ and letting $r_n=\|\mathbf{p}_n\|$ gives

$$\begin{aligned}\bar{H}_{12}^{(2_I)} = \frac{2\pi}{k}e^{-(r_1^2+r_2^2)}\Bigg[&\int_0^R r_n e^{-2r_n^2}\,\mathrm{I}_0(4r_n\|\overline{\mathbf{p}}_{12}\|)\mathrm{d}r_n\\ &+\left(\frac{\alpha-1}{R^2}\right)\int_0^R r_n^3 e^{-2r_n^2}\,\mathrm{I}_0(4r_n\|\overline{\mathbf{p}}_{12}\|)\mathrm{d}r_n\Bigg].\end{aligned} \tag{B.10}$$

Applying [242, eqs. (10) & (20)] to solve the integrals results in

$$\begin{aligned}\bar{H}_{12}^{(2_I)} = \frac{2\pi}{k}e^{-(r_1^2+r_2^2)}\Bigg\{&\frac{1}{4}e^{2\|\overline{\mathbf{p}}_{12}\|^2}[1-\mathrm{Q}(2\|\overline{\mathbf{p}}_{12}\|,2R)]\\ &+\left(\frac{\alpha-1}{8R^2}\right)(2\|\overline{\mathbf{p}}_{12}\|+1)e^{2\|\overline{\mathbf{p}}_{12}\|^2}\\ &\times[1-\mathrm{Q}(2\|\overline{\mathbf{p}}_{12}\|,2R)]\\ &-\left(\frac{\alpha-1}{4}\right)e^{-2R^2}\\ &\times\left[\frac{\|\overline{\mathbf{p}}_{12}\|}{R}\,\mathrm{I}_1(4\|\overline{\mathbf{p}}_{12}\|R)+\mathrm{I}_0(4\|\overline{\mathbf{p}}_{12}\|R)\right]\Bigg\},\end{aligned} \tag{B.11}$$

where $\mathrm{Q}_1(a,b) = \int_b^\infty x e^{-\frac{(x^2+a^2)}{2}} \mathrm{I}_o(ax)\mathrm{d}x$ is the first order Marcum-Q-function and where $\mathrm{I}_1(a) = \frac{1}{\pi}\int_0^\pi e^{a\cos\theta}\cos\theta \mathrm{d}\theta$ is the first order modified Bessel function of the first kind. Factoring out $\frac{1}{4}e^{2\|\overline{\mathbf{p}}_{12}\|^2}$, recognising that $e^{2\|\overline{\mathbf{p}}_{12}\|^2-(r_1^2+r_2^2)} = e^{\frac{1}{2}r_{12}^2}$ and simplifying, yields the final expression

$$\begin{aligned}\bar{H}_{12}^{(2_\mathrm{I})} &= \frac{\pi}{2k}e^{-\frac{1}{2}r_{12}^2} \\ &\times \Bigg\{\left(\frac{(\alpha-1)(2\|\overline{\mathbf{p}}_{12}\|^2+1)}{2R^2}+1\right) \\ &\times \Big[1-\mathrm{Q}_1(2\|\overline{\mathbf{p}}_{12}\|,2R)\Big] \\ &- (\alpha-1)e^{-2(\|\overline{\mathbf{p}}_{12}\|^2+R^2)} \\ &\times \left[\frac{\|\overline{\mathbf{p}}_{12}\|}{R}\mathrm{I}_1(4\|\overline{\mathbf{p}}_{12}\|R)+\mathrm{I}_0(4\|\overline{\mathbf{p}}_{12}\|R)\right]\Bigg\}. \end{aligned} \tag{B.12}$$

B.2 Quasi-Convexity in $\mathcal{O}$

We investigate the quasi-convexity in the upper bound, as defined by (4.22), which expanded gives

$$\begin{aligned}\bar{\mathcal{O}}^{\mathrm{UB}} &= \frac{1}{V^2}\int_{\mathcal{V}^2}(1-H_{12})\exp\Big[-\rho_\mathrm{R}V\bar{H}_{12}^{(2_\mathrm{R})}\Big] \\ &\times \Big\{\exp\Big[-\rho_\mathrm{I}V\bar{H}_{1\mathrm{I}}\Big]+\exp\Big[-\rho_\mathrm{I}V\bar{H}_{2\mathrm{I}}\Big]\Big\}\mathrm{d}\mathbf{p}_1\mathrm{d}\mathbf{p}_2. \end{aligned} \tag{B.13}$$

Since the probabilities of the $\mathbf{p}_1$ and $\mathbf{p}_2$ connecting to an infrastructure node will be identical when averaged over all possible terminal node locations in $\mathcal{V}$, (B.13) can be reduced to

$$\begin{aligned}\bar{\mathcal{O}}^{\mathrm{UB}} &= \frac{1}{V^2}\int_{\mathcal{V}^2}2s(\mathbf{p}_1,\mathbf{p}_2)\exp\Big[-\rho_\mathrm{I}V\bar{H}_{1\mathrm{I}}\Big]\mathrm{d}\mathbf{p}_1\mathrm{d}\mathbf{p}_2 \\ &= \frac{2}{V}\int_{\mathcal{V}}s(\mathbf{p}_1)\exp\Big[-\rho_\mathrm{I}V\bar{H}_{1\mathrm{I}}\Big]\mathrm{d}\mathbf{p}_1 \end{aligned} \tag{B.14}$$

where $s(\mathbf{p}_1,\mathbf{p}_2) = (1-H_{12})\exp\Big[-\rho_\mathrm{R}V\bar{H}_{12}^{(2_\mathrm{R})}\Big]$ and $s(\mathbf{p}_1) = \frac{1}{V}\int_{\mathcal{V}}s(\mathbf{p}_1,\mathbf{p}_2)\mathrm{d}\mathbf{p}_2$, which is a non negative scaling factor independent of the infrastructure. We reduce (4.19) to the form

$$\bar{H}_{1\mathrm{I}} = \frac{A_1\alpha+B_1}{\alpha+1}, \quad \alpha>0 \tag{B.15}$$

where

$$\begin{aligned} A_1 &= \frac{2}{R^2}\Bigg\{\left(\frac{r_1^2+1}{R^2}\right)\Big[1-\mathrm{Q}_1(\sqrt{2}r_1,\sqrt{2}R)\Big] \\ &- e^{-(r_1^2+R^2)}\left[\frac{r_1}{R}\,\mathrm{I}_1(2r_1R)+\mathrm{I}_0(2r_1R)\right]\Bigg\}, \qquad \text{(B.16)} \\ B_1 &= \frac{2}{R^2}\Bigg\{\left(1-\frac{r_1^2+1}{R^2}\right)\Big[1-\mathrm{Q}_1(\sqrt{2}r_1,\sqrt{2}R)\Big] \\ &+ e^{-(r_1^2+R^2)}\left[\frac{r_1}{R}\,\mathrm{I}_1(2r_1R)+\mathrm{I}_0(2r_1R)\right]\Bigg\} \qquad \text{(B.17)} \end{aligned}$$

and $r_1 = \|\mathbf{p}_1\|$. We now define the exponential term within (B.14) as

$$f_{ab}(\alpha,\mathbf{p}_1) = \exp\left[-\frac{a\alpha+b}{\alpha+1}\right], \qquad \text{(B.18)}$$

where $a = \rho_{\mathrm{I}}VA_1$ and $b = \rho_{\mathrm{I}}VB_1$. We now show that, by inspection of sub-level sets and super-level sets, that $f_{ab}(\alpha,\mathbf{p}_1)$ is quasi-linear in $\mathrm{dom}\, f_{ab} = \{\alpha|\alpha > 0\}$. We let S_ε denote a sub-level set, such that

$$\begin{aligned} S_\varepsilon &= \{\alpha \mid \alpha > 0; \quad f_{ab} \leqslant \varepsilon\} \\ &= \{\alpha \mid \alpha > 0; \quad a\alpha + b \geqslant -(\alpha+1)\ln\varepsilon\} \\ &= \left\{\alpha \mid \alpha > 0; \quad \begin{cases} \alpha \geqslant -\frac{b+\ln\varepsilon}{a+\ln\varepsilon}, a+\ln\varepsilon > 0 \\ \alpha \leqslant -\frac{b+\ln\varepsilon}{a+\ln\varepsilon}, a+\ln\varepsilon < 0 \end{cases}\right\} \end{aligned} \qquad \text{(B.19)}$$

Since the intersection of an open convex set and a closed convex set is convex, quasi-convexity follows. The proof of quasi-concavity follows in an analogous manner using super-level sets. Hence, we deduce the function is quasi-linear as stated. We can make further progress by considering monotonicity of the function f_{ab}. Inspection of (B.19) shows that f_{ab}^{-1} is well defined on $(0,\infty)$. Hence, f_{ab} is injective with strict monotonicity for all a, b subject to $a \neq b$. Hence, $\bar{\mathcal{O}}^{\mathrm{UB}}$ is the limit of a positive weighted sum of strictly monotonic functions where the quasi-linear function $f_{ab}(\alpha,\mathbf{p}_1)$ is decreasing monotonic for $b/a < 1$ and increasing monotonic for $b/a > 1$. Denoting the 1st and 2nd derivatives of function f_{ab} as f'_{ab} and f''_{ab} respectively, where

$$\begin{aligned} f'_{ab} &= -\frac{a-b}{(\alpha+1)^2}f_{ab} \qquad \text{(B.20)} \\ f''_{ab} &= \left[2\frac{a-b}{(\alpha+1)^3}+\frac{(a-b)^2}{(\alpha+1)^4}\right]f_{ab}, \qquad \text{(B.21)} \end{aligned}$$

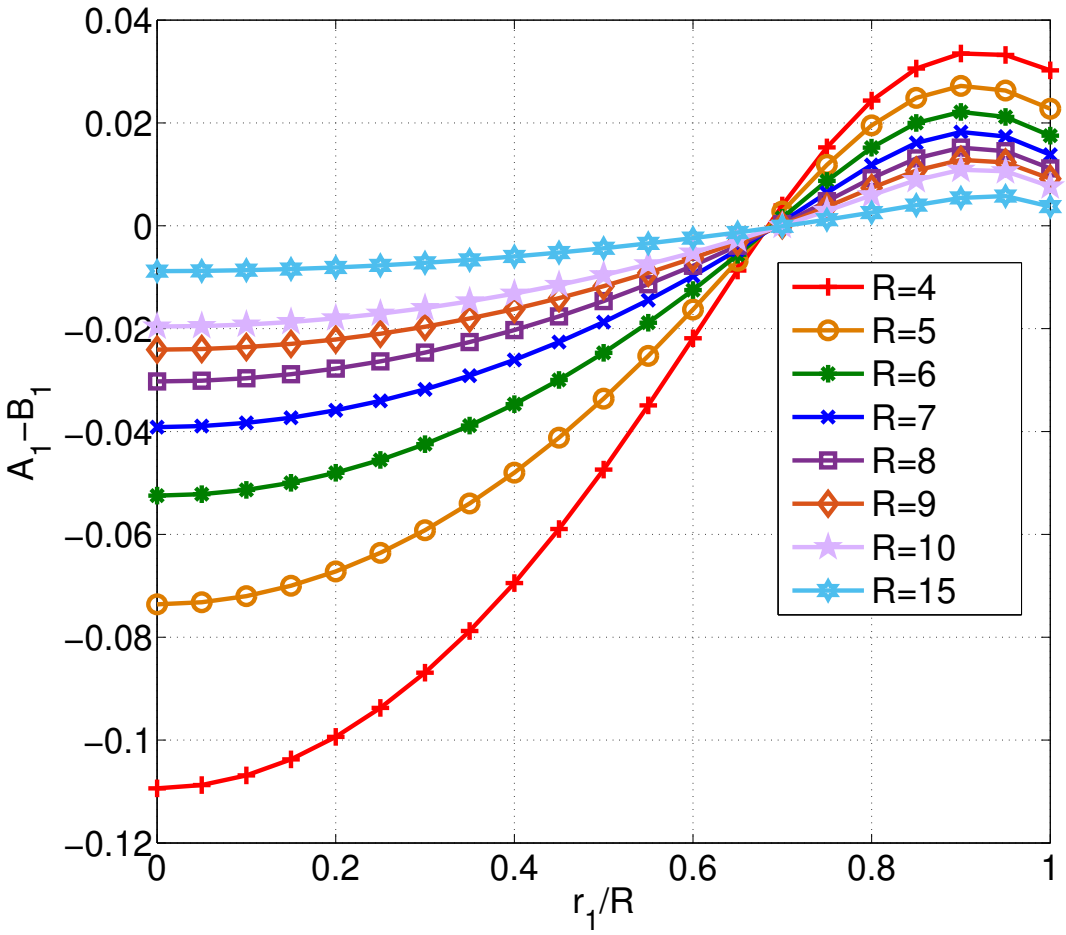


Figure B.1: Illustration of function $A_1 - B_1$ with respect to r_1/R for a range of domain radii $R \in \{6, 7, 8, 9, 10\}$. Showing a single zero crossing.

we can show that when $b/a < 1$, the decreasing monotonic is convex whereas, when $b/a > 1$ the increasing monotonic is concave, under the condition $-2 < (a - b) < 0$ and quasi-linear (convex to concave with increasing α) otherwise, with inflection point at $\alpha = -0.5(a - b) - 1$. We illustrate the function $A_1 - B_1$ with respect to r_1/R, for a range of domain radii, in Fig. B.1, clearly showing a single zero crossing point for each radius. Denoting the radial offset at which the zero crossing occurs by r_t, we observe that r_t can be approximated by the radius where the area of a circle of radius r_t is approaching 50% of the total domain area V; it is relatively straightforward to show that with increasing R, $r_t \to 1/\sqrt{2}$ and $A_1 - B_1 \to 0, \forall r_1$. In summary, $\bar{\mathcal{O}}^{\text{UB}}$ will be sum of a strictly decreasing convex monotone and a

strictly increasing quasi-linear function, in α, which does not prove a uni-modal composite function. Nevertheless, the analysis presented here coupled with extensive numerical simulation suggests that quasi-convexity holds.

C

C.1 Proof of Proposition 1

Substituting $\eta = 2$ into (5.28) and simplifying results in

$$\dot{r} = \frac{1}{C_1}\sqrt{(k + r^2)^2 - C_1^2 r^2}. \tag{C.1}$$

Separating variables and integrating yields

$$\phi = C_1 \int \frac{1}{\sqrt{(k + r^2)^2 - C_1 r^2}} \mathrm{d}r. \tag{C.2}$$

Defining the denominator in the integrand by function $s(r)$ we have

$$s(r) = (k + r^2 + C_1 r)(k + r^2 - C_1 r), \tag{C.3}$$

and we can define the roots of $s(r)$ by

$$r = \pm\frac{C_1}{2} \pm \frac{1}{2}\sqrt{C_1^2 - 4k}. \tag{C.4}$$

If we denote these roots by $\alpha, \beta, \gamma, \delta$ then

$$\phi = C_1 \int \frac{1}{\sqrt{r - \alpha}\sqrt{r - \beta}\sqrt{r - \gamma}\sqrt{r - \delta}} \mathrm{d}r. \tag{C.5}$$

Since $\alpha = -\beta$ and $\gamma = -\delta$ we can write

$$\begin{aligned} \phi &= C_1 \int \frac{1}{\sqrt{(\alpha^2 - r^2)(\gamma^2 - r^2)}} \mathrm{d}r \\ &= C_1 \frac{1}{\alpha\gamma} \int \frac{1}{\sqrt{(1 - \left(\frac{r}{\alpha}\right)^2)(1 - \left(\frac{r}{\gamma}\right)^2)}} \mathrm{d}r. \end{aligned} \tag{C.6}$$

Let $t = \frac{r}{\alpha}$; then $\mathrm{d}r = \alpha \mathrm{d}t$, and we have

$$\phi = C_1 \frac{1}{\gamma} \int \frac{1}{\sqrt{(1-t^2)(1-\kappa^2 t^2)}} \mathrm{d}t, \tag{C.7}$$

where $\kappa = \frac{\alpha}{\gamma}$ is the elliptic modulus. Given the integral in (C.7) is the elliptic integral of the first kind, we have

$$\phi(r) = \pm \frac{C_1}{\gamma} \mathrm{F}\left(\sin^{-1} \frac{r}{\alpha}, \frac{\alpha}{\gamma} \right) + C_2, \tag{C.8}$$

where $u = \mathrm{F}(\psi, \kappa)$ is the elliptic integral of the first kind in Legendre normal form and C_2 is a constant. Now, given that $\psi = \mathrm{F}^{-1}(u, \kappa) = \mathrm{am}(u, \kappa)$ is the Jacobi amplitude, we can write

$$r(\phi) = \alpha \sin \left[\mathrm{am} \left(\pm \frac{\gamma(\phi - C_2)}{C_1}, \frac{\alpha}{\gamma} \right) \right], \tag{C.9}$$

which can be written in the form

$$r(\phi) = \alpha \ \mathrm{sn} \left(\pm \frac{\gamma(\phi - C_2)}{C_1}, \frac{\alpha}{\gamma} \right), \tag{C.10}$$

where $\mathrm{sn}(u, \kappa)$ is the Jacobi elliptic function.

C.2 Proof of Proposition 2

Given a functional

$$P_o[r] = 1 - \exp\left(-\theta \int_{\phi_1}^{\phi_2} \frac{\sqrt{r^2 + \dot{r}^2}}{\mu(r)} \mathrm{d}\phi \right), \tag{C.11}$$

we consider the second variation to determine whether the stationary paths, that satisfy the Euler-Lagrange equation, correspond to minima. Specifically, we invoke Legendre's condition[1],

$$J(r) = \frac{\partial^2 L}{\partial \dot{r}^2} > 0, \tag{C.12}$$

as sufficient proof of minima; L denoting the integrand of (C.11). Evaluating $J(r)$, gives

$$J(r) = \frac{1}{\mu} \left[\frac{1}{\sqrt{r^2 + \dot{r}^2}} - \frac{\dot{r}^2}{(r^2 + \dot{r}^2)^{\frac{3}{2}}} \right]. \tag{C.13}$$

[1]Non Euclidean geometries would also need to satisfy the conjugate point condition. However, conjugate points do not exist in Euclidean space [255].

Since $\mu(r) \in \mathbb{R}_+$, the condition (C.12) is satisfied when the right hand bracketed expression of (C.13) is positive, which reduces to the condition $r > 0$. Therefore, since $r \in \mathbb{R}_+$, the stationary paths correspond to strict minima of the functional.

References

[1] J. Kraus, "Heinrich Hertz-Theorist and Experimenter," *IEEE Transactions on Microwave Theory and Techniques*, vol. 36, no. 5, pp. 824–829, 1988.

[2] M.-G. Di Benedetto, "UWB Communication Systems: a comprehensive overview," 2006.

[3] A. Daniel, G. Tilahun, and A. Teshager, "Effect of Ionosphere on Radio Wave Propagation," *Int. J. Res*, vol. 3, no. 9, 2016.

[4] C. E. Shannon, "A Mathematical Theory of Communication," *The Bell System Technical Journal*, vol. 27, no. 3, pp. 379–423, 1948.

[5] M. Skolnik, "Fifty years of radar," *Proceedings of the IEEE*, vol. 73, no. 2, pp. 182–197, 1985.

[6] A. Abramson, *The history of television, 1942 to 2000*. McFarland, 2003.

[7] P. Angeletti, R. De Gaudenzi, and M. Lisi, "From "Bent pipes" to" software defined payloads": evolution and trends of satellite communications systems," in *26th International Communications Satellite Systems Conference (ICSSC)*, 2008.

[8] B. Hofmann-Wellenhof, H. Lichtenegger, and J. Collins, *Global positioning system: theory and practice*. Springer Science & Business Media, 2012.

[9] T. Farley, "Mobile telephone history," *Privateline. com, http://www. private-line. com/wp-content/uploads/2016/01/TelenorPage_022-034. pdf*, 2005.

[10] R. Hammond, *Digital Business*. Hodder & Stoughton Trade, 1996.

[11] B. M. Leiner, V. G. Cerf, D. D. Clark, R. E. Kahn, L. Kleinrock, D. C. Lynch, J. Postel, L. G. Roberts, and S. Wolff, "A Brief History of the Internet," *ACM SIGCOMM computer communication review*, vol. 39, no. 5, pp. 22–31, 2009.

[12] T. Snyder and G. Byrd, "The Internet of Everything," *Computer*, vol. 50, pp. 8–9, jun 2017.

[13] L. U. Khan, I. Yaqoob, M. Imran, Z. Han, and C. S. Hong, "6G Wireless Systems: A Vision, Architectural Elements, and Future Directions," *IEEE Access*, vol. 8, pp. 147029–147044, 2020.

[14] GSMA, "Mobile Economy 2023," *https://www.gsma.com/mobileeconomy/wp-content/uploads/2023/03/270223-The-Mobile-Economy-2023.pdf.*

[15] F. S. T. Van Diggelen, *A-GPS: Assisted GPS, GNSS, and SBAS.* Artech house, 2009.

[16] J. Kim, G. Casati, N. Cassiau, A. Pietrabissa, A. Giuseppi, D. Yan, E. Calvanese Strinati, M. Thary, D. He, K. Guan, *et al.*, "Design of cellular, satellite, and integrated systems for 5G and beyond," *ETRI Journal*, vol. 42, no. 5, pp. 669–685, 2020.

[17] Q. K. Ud Din Arshad, A. U. Kashif, and I. M. Quershi, "A Review on the Evolution of Cellular Technologies," in *2019 16th International Bhurban Conference on Applied Sciences and Technology (IBCAST)*, pp. 989–993, 2019.

[18] V. Pereira and T. Sousa, "Evolution of Mobile Communications: from 1G to 4G," *Department of Informatics Engineering of the University of Coimbra, Portugal*, vol. 4, pp. 20–0, 2004.

[19] J. Katz and Y. Lindell, *Introduction to modern cryptography.* CRC press, 2020.

[20] J. R. Churi, T. S. Surendran, S. A. Tigdi, and S. Yewale, "Evolution of networks (2G-5G)," in *International Conference on Advances in Communication and Computing Technologies (ICACACT)*, vol. 51, pp. 8–13, Citeseer, 2012.

[21] C. De Alwis, A. Kalla, Q.-V. Pham, P. Kumar, K. Dev, W.-J. Hwang, and M. Liyanage, "Survey on 6G frontiers: Trends, applications, requirements, technologies and future research," *IEEE Open Journal of the Communications Society*, vol. 2, pp. 836–886, 2021.

[22] A. Gurtov, M. Liyanage, and M. Ylianttila, *Software defined mobile networks (SDMN): beyond LTE network architecture*. John Wiley & Sons, 2015.

[23] S. Li, L. D. Xu, and S. Zhao, "The Internet of Things: a survey," *Information systems frontiers*, vol. 17, pp. 243–259, 2015.

[24] H. Lasi, P. Fettke, H.-G. Kemper, T. Feld, and M. Hoffmann, "Industry 4.0," *Business & information systems engineering*, vol. 6, pp. 239–242, 2014.

[25] F. Shrouf, J. Ordieres, and G. Miragliotta, "Smart factories in Industry 4.0: A review of the concept and of energy management approached in production based on the Internet of Things paradigm," in *2014 IEEE international conference on industrial engineering and engineering management*, pp. 697–701, IEEE, 2014.

[26] S. Grabowska, "Smart Factories in the Age of Industry 4.0," *Management Systems in Production Engineering*, vol. 28, no. 2, pp. 90–96, 2020.

[27] A. F. M. Shahen Shah, "A Survey From 1G to 5G Including the Advent of 6G: Architectures, Multiple Access Techniques, and Emerging Technologies," in *2022 IEEE 12th Annual Computing and Communication Workshop and Conference (CCWC)*, pp. 1117–1123, 2022.

[28] A. Gupta and R. K. Jha, "A Survey of 5G Network: Architecture and Emerging Technologies," *IEEE Access*, vol. 3, pp. 1206–1232, 2015.

[29] J. G. Andrews, S. Buzzi, W. Choi, S. V. Hanly, A. Lozano, A. C. K. Soong, and J. C. Zhang, "What will 5G be?," *IEEE Journal on Selected Areas in Communications*, vol. 32, pp. 1065–1082, June 2014.

[30] H. Cho, S. Mukherjee, D. Kim, T. Noh, and J. Lee, "Facing to wireless network densification in 6G: Challenges and opportunities," *ICT Express*, 2022.

[31] N. Bhushan, J. Li, D. Malladi, R. Gilmore, D. Brenner, A. Damnjanovic, R. T. Sukhavasi, C. Patel, and S. Geirhofer, "Network densification: the dominant theme for wireless evolution into 5G," *IEEE Communications Magazine*, vol. 52, no. 2, pp. 82–89, 2014.

[32] J. G. Andrews, X. Zhang, G. D. Durgin, and A. K. Gupta, "Are we approaching the fundamental limits of wireless network densification?," *IEEE Communications Magazine*, vol. 54, no. 10, pp. 184–190, 2016.

[33] J. Liu, M. Sheng, L. Liu, and J. Li, "Network densification in 5G: From the short-range communications perspective," *IEEE Communications Magazine*, vol. 55, no. 12, pp. 96–102, 2017.

[34] M. A. Ferrag, L. Maglaras, A. Argyriou, D. Kosmanos, and H. Janicke, "Security for 4G and 5G cellular networks: A survey of existing authentication and privacy-preserving schemes," *Journal of Network and Computer Applications*, vol. 101, pp. 55–82, 2018.

[35] D. Fang, Y. Qian, and R. Q. Hu, "Security for 5G mobile wireless networks," *IEEE access*, vol. 6, pp. 4850–4874, 2017.

[36] S. Vij and A. Jain, "5G: Evolution of a secure mobile technology," in *2016 3rd International Conference on Computing for Sustainable Global Development (INDIACom)*, pp. 2192–2196, 2016.

[37] M. H. Alsharif, R. Nordin, and M. Ismail, "Survey of green radio communications networks: Techniques and recent advances," *Journal of computer networks and communications*, vol. 2013, 2013.

[38] G. Miao and G. Song, *Energy and spectrum efficient wireless network design*. Cambridge University Press, 2014.

[39] Y. Adediran, H. Lasisi, and O. Okedere, "Interference management techniques in cellular networks: A review," *Cogent Engineering*, vol. 4, no. 1, p. 1294133, 2017.

[40] Z. J. Haas, J. Deng, B. Liang, P. Papadimitratos, and S. Sajama, "Wireless ad-hoc networks," *Wiley Encyclopedia of Telecommunications*, 2003.

[41] S. Corson and J. Macker, "RFC2501: Mobile ad hoc networking (MANET): Routing protocol performance issues and evaluation considerations," 1999.

[42] M. Aoki and H. Fujii, "Inter-Vehicle Vommunication: Technical issues on vehicle control application," *IEEE Communications Magazine*, vol. 34, no. 10, pp. 90–93, 1996.

[43] S. Al-Sultan, M. M. Al-Doori, A. H. Al-Bayatti, and H. Zedan, "A comprehensive survey on vehicular ad hoc network," *Journal of network and computer applications*, vol. 37, pp. 380–392, 2014.

[44] I. F. Akyildiz, W. Su, Y. Sankarasubramaniam, and E. Cayirci, "Wireless Sensor Networks: a survey," *Computer networks*, vol. 38, no. 4, pp. 393–422, 2002.

[45] J. Yick, B. Mukherjee, and D. Ghosal, "Wireless sensor network survey," *Computer Networks*, vol. 52, no. 12, pp. 2292–2330, 2008.

[46] I. F. Akyildiz, X. Wang, and W. Wang, "Wireless Mesh Networks: a survey," *Computer networks*, vol. 47, no. 4, pp. 445–487, 2005.

[47] K. K.C, "Wireless mesh network: A survey," in *2016 International Conference on Wireless Communications, Signal Processing and Networking (WiSPNET)*, pp. 1966–1970, 2016.

[48] T. Plesse, C. Adjih, P. Minet, A. Laouiti, A. Plakoo, M. Badel, P. Muhlethaler, P. Jacquet, and J. Lecomte, "OLSR performance measurement in a military mobile ad-hoc network," *Ad Hoc Networks*, vol. 3, no. 5, pp. 575–588, 2005.

[49] P. M. Shankar, *Fading and shadowing in wireless systems*. Springer, 2017.

[50] A. G. Yavuz, Z. C. Taysi, and E. Celik, "In-Cave Wireless Communication System," in *2009 Third International Conference on Next Generation Mobile Applications, Services and Technologies*, pp. 161–164, 2009.

[51] R.-I. Ciobanu, C. Negru, F. Pop, C. Dobre, C. X. Mavromoustakis, and G. Mastorakis, "Drop computing: Ad-hoc dynamic collaborative computing," *Future Generation Computer Systems*, vol. 92, pp. 889–899, 2019.

[52] D. Reina, M. Askalani, S. Toral, F. Barrero, E. Asimakopoulou, and N. Bessis, "A survey on multihop ad-hoc networks for disaster response scenarios," *International Journal of Distributed Sensor Networks*, vol. 11, no. 10, p. 647037, 2015.

[53] K. E. Khujamatov and T. Toshtemirov, "Wireless sensor networks based Agriculture 4.0: challenges and apportions," in *2020 international conference on information science and communications technologies (ICISCT)*, pp. 1–5, IEEE, 2020.

[54] P. H. Chong, F. Adachi, S. Hamalainen, and V. Leung, "Technologies in Multihop Cellular Networks [Guest Editorial]," *IEEE Communications magazine*, vol. 45, no. 9, pp. 64–65, 2007.

[55] Y. Wiseman, "Autonomous vehicles," in *Research Anthology on Cross-Disciplinary Designs and Applications of Automation*, pp. 878–889, IGI Global, 2022.

[56] D. Lucke, C. Constantinescu, and E. Westkämper, "Smart factory-a step towards the next generation of manufacturing," in *Manufacturing Systems and Technologies for the New Frontier: The 41 st CIRP Conference on Manufacturing Systems May 26–28, 2008, Tokyo, Japan*, pp. 115–118, Springer, 2008.

[57] K. Rose, S. Eldridge, and L. Chapin, "The internet of things: An overview," *The internet society (ISOC)*, vol. 80, pp. 1–50, 2015.

[58] Statista, "IoT: Number of Connected Devices Worldwide 2012-2025," 2012.

[59] A. Djama, B. Djamaa, and M. R. Senouci, "Information-Centric Networking solutions for the Internet of Things: A systematic mapping review," *Computer Communications*, vol. 159, pp. 37–59, 2020.

[60] H. D. Kotha and V. M. Gupta, "IoT application: a survey," *Int. J. Eng. Technol*, vol. 7, no. 2.7, pp. 891–896, 2018.

[61] A. Al-Fuqaha, M. Guizani, M. Mohammadi, M. Aledhari, and M. Ayyash, "Internet of Things: A Survey on Enabling Technologies, Protocols, and Applications," *IEEE Communications Surveys Tutorials*, vol. 17, pp. 2347–2376, Fourthquarter 2015.

[62] D. Lund, C. MacGillivray, V. Turner, and M. Morales, "Worldwide and regional internet of things (IoT) 2014-2020 forecast: A virtuous circle of proven value and demand," *International Data Corporation (IDC), Tech. Rep*, vol. 1, 2014.

[63] J. M. C. Brito, "Trends in wireless communications towards 5G networks; the influence of e-health and IoT applications," in *Computer and Energy Science (SpliTech), International Multidisciplinary Conference on*, pp. 1–7, IEEE, 2016.

[64] W. Alnumay, U. Ghosh, and P. Chatterjee, "A Trust-Based predictive model for mobile ad hoc network in internet of things," *Sensors*, vol. 19, no. 6, p. 1467, 2019.

[65] D. G. Reina, S. L. Toral, F. Barrero, N. Bessis, and E. Asimakopoulou, "The role of ad-hoc networks in the internet of things: A case scenario for smart environments," *Internet of things and inter-cooperative computational technologies for collective intelligence*, pp. 89–113, 2013.

[66] S. Sen, J. Koo, and S. Bagchi, "TRIFECTA: Security, Energy Efficiency, and Communication Capacity Comparison for Wireless IoT Devices," *IEEE Internet Computing*, vol. 22, no. 1, pp. 74–81, 2018.

[67] A. Lavric, A. I. Petrariu, and V. Popa, "SigFox Communication Protocol: The New Era of IoT?," in *2019 International Conference on Sensing and Instrumentation in IoT Era (ISSI)*, pp. 1–4, 2019.

[68] M. Kanj, V. Savaux, and M. Le Guen, "A Tutorial on NB-IoT Physical Layer Design," *IEEE Communications Surveys Tutorials*, vol. 22, no. 4, pp. 2408–2446, 2020.

[69] A. Jain and A. Kumar, "Smart agriculture monitoring system using IoT," *International Journal for Research in Applied Science & Engineering Technology*, 2020.

[70] N. Suma, S. R. Samson, S. Saranya, G. Shanmugapriya, and R. Subhashri, "IoT based smart agriculture monitoring system," *International Journal on Recent and Innovation Trends in computing and communication*, vol. 5, no. 2, pp. 177–181, 2017.

[71] Y. A. Badamasi, "The working principle of an Arduino," in *2014 11th International Conference on Electronics, Computer and Computation (ICECCO)*, pp. 1–4, 2014.

[72] J. Mabrouki, M. Azrour, D. Dhiba, Y. Farhaoui, and S. E. Hajjaji, "IoT-based data logger for weather monitoring using arduino-based wireless sensor networks with remote graphical application and alerts," *Big Data Mining and Analytics*, vol. 4, no. 1, pp. 25–32, 2021.

[73] S. Suji Prasad, M. Thangatamilan, M. Suresh, H. Panchal, C. A. Rajan, C. Sagana, B. Gunapriya, A. Sharma, T. Panchal, and K. K. Sadasivuni, "An efficient LoRa-based smart agriculture management and monitoring system

using wireless sensor networks," *International Journal of Ambient Energy*, vol. 43, no. 1, pp. 5447–5450, 2022.

[74] M. DIOP and C. PHAM, "Increased flexibility in long-range IoT deployments with transparent and light-weight 2-hop LoRa approach," in *2019 Wireless Days (WD)*, pp. 1–6, 2019.

[75] U. Uyoata, J. Mwangama, and R. Adeogun, "Relaying in the Internet of Things (IoT): A Survey," *IEEE Access*, vol. 9, pp. 132675–132704, 2021.

[76] S. C. Yang, "Toward a Wireless World," *IEEE Technology and Society Magazine*, vol. 26, no. 2, pp. 32–42, 2007.

[77] M. Castells, "An Introduction to the Information Age," *City*, vol. 2, no. 7, pp. 6–16, 1997.

[78] C. D. Alwis, A. Kalla, Q.-V. Pham, P. Kumar, K. Dev, W.-J. Hwang, and M. Liyanage, "Survey on 6G Frontiers: Trends, Applications, Requirements, Technologies and Future Research," *IEEE Open Journal of the Communications Society*, vol. 2, pp. 836–886, 2021.

[79] Q. Bi, "Ten Trends in the Cellular Industry and an Outlook on 6G," *IEEE Communications Magazine*, vol. 57, no. 12, pp. 31–36, 2019.

[80] S. Dang, O. Amin, B. Shihada, and M.-S. Alouini, "What Should 6G be?," *Nature Electronics*, vol. 3, no. 1, pp. 20–29, 2020.

[81] A. Kirimtat, O. Krejcar, A. Kertesz, and M. F. Tasgetiren, "Future trends and current state of smart city concepts: A survey," *IEEE access*, vol. 8, pp. 86448–86467, 2020.

[82] D. Chaffey, D. Edmundson-Bird, and T. Hemphill, *Digital Business and e-Commerce Management*. Pearson UK, 2019.

[83] R. Gumzej, *E-Health*, pp. 45–51. Cham: Springer International Publishing, 2021.

[84] A. Elzanaty, A. Guerra, F. Guidi, D. Dardari, and M.-S. Alouini, "Towards 6G Holographic Localization: Enabling Technologies and Perspectives," *IEEE Internet of Things Magazine*, pp. 1–7, 2023.

[85] T. B. Ahammed, R. Patgiri, and S. Nayak, "A Vision on the Artificial Intelligence for 6G Communication," *ICT Express*, vol. 9, no. 2, pp. 197–210, 2023.

[86] W. Jiang, B. Han, M. A. Habibi, and H. D. Schotten, "The Road Towards 6G: A Comprehensive Survey," *IEEE Open Journal of the Communications Society*, vol. 2, pp. 334–366, 2021.

[87] J. Cao and M. Yang, "Energy Internet – Towards Smart Grid 2.0," in *2013 Fourth International Conference on Networking and Distributed Computing*, pp. 105–110, 2013.

[88] X. Xu, Y. Pan, P. P. M. Y. Lwin, and X. Liang, "3D holographic display and its data transmission requirement," in *2011 international conference on information photonics and optical communications*, pp. 1–4, IEEE, 2011.

[89] Y. Siriwardhana, P. Porambage, M. Liyanage, and M. Ylianttila, "A Survey on Mobile Augmented Reality With 5G Mobile Edge Computing: Architectures, Applications, and Technical Aspects," *IEEE Communications Surveys Tutorials*, vol. 23, no. 2, pp. 1160–1192, 2021.

[90] F. Yang, S. Wang, J. Li, Z. Liu, and Q. Sun, "An overview of internet of vehicles," *China communications*, vol. 11, no. 10, pp. 1–15, 2014.

[91] P. K. R. Maddikunta, Q.-V. Pham, P. B, N. Deepa, K. Dev, T. R. Gadekallu, R. Ruby, and M. Liyanage, "Industry 5.0: A survey on enabling technologies and potential applications," *Journal of Industrial Information Integration*, vol. 26, p. 100257, 2022.

[92] B. Mohanta, P. Das, and S. Patnaik, "Healthcare 5.0: A paradigm shift in digital healthcare system using artificial intelligence, IOT and 5G communication," in *2019 International conference on applied machine learning (ICAML)*, pp. 191–196, IEEE, 2019.

[93] M. H. Miraz, M. Ali, P. S. Excell, and R. Picking, "A review on Internet of Things (IoT), Internet of Everything (IoE) and Internet of Nano Things (IoNT)," in *2015 Internet Technologies and Applications (ITA)*, pp. 219–224, 2015.

[94] A. Raj and S. Prakash, "Internet of Everything: A survey based on Architecture, Issues and Challenges," in *2018 5th IEEE Uttar Pradesh Section International Conference on Electrical, Electronics and Computer Engineering (UPCON)*, pp. 1–6, 2018.

[95] D. Chauhan and J. K. Jain, "A Journey from IoT to IoE," *International Journal of Innovative Technology and Exploring Engineering (IJITEE)*, vol. 8, no. 11, 2019.

[96] D. J. Langley, J. van Doorn, I. C. Ng, S. Stieglitz, A. Lazovik, and A. Boonstra, "The Internet of Everything: Smart things and their impact on business models," *Journal of Business Research*, vol. 122, pp. 853–863, 2021.

[97] D. Lee, K.-h. Choi, and H. Kim, "Smart Devices Smart Spaces in Wireless Internet of Everything (Wireless-IoE)," *Wireless Personal Communications*, vol. 94, pp. 145–147, 2017.

[98] Z. Qadir, K. N. Le, N. Saeed, and H. S. Munawar, "Towards 6G Internet of Things: Recent advances, use cases, and open challenges," *ICT Express*, 2022.

[99] W. Saad, M. Bennis, and M. Chen, "A Vision of 6G Wireless Systems: Applications, Trends, Technologies, and Open Research Problems," *IEEE Network*, vol. 34, no. 3, pp. 134–142, 2020.

[100] G. Naik, J. Liu, and J.-M. J. Park, "Coexistence of wireless technologies in the 5-GHz bands: A survey of existing solutions and a roadmap for future research," *IEEE Communications Surveys & Tutorials*, vol. 20, no. 3, pp. 1777–1798, 2018.

[101] A. Hasan and B. M. Khan, "Coexistence Management in Wireless Networks-A survey," *IEEE Access*, 2022.

[102] T. Wiedmann and J. Minx, "A definition of 'carbon footprint'," *Ecological economics research trends*, vol. 1, no. 2008, pp. 1–11, 2008.

[103] R. Mahapatra, A. De Domenico, R. Gupta, and E. C. Strinati, "Green framework for future heterogeneous wireless networks," *Computer Networks*, vol. 57, no. 6, pp. 1518–1528, 2013.

[104] H. Badis and A. Rachedi, "Chapter 23 - Modeling tools to evaluate the performance of wireless multi-hop networks," in *Modeling and Simulation of Computer Networks and Systems* (M. S. Obaidat, P. Nicopolitidis, and F. Zarai, eds.), pp. 653–682, Boston: Morgan Kaufmann, 2015.

[105] E. C. Van Der Meulen, "Three-terminal communication channels," *Advances in applied Probability*, vol. 3, no. 1, pp. 120–154, 1971.

[106] T. Cover and A. Gamal, "Capacity Theorems for the Relay Channel," *IEEE Transactions on Information Theory*, vol. 25, no. 5, pp. 572–584, 1979.

[107] C. E. Perkins and P. Bhagwat, "Highly Dynamic Destination-Sequenced Distance-Vector Routing (DSDV) for Mobile Computers," *ACM SIGCOMM computer communication review*, vol. 24, no. 4, pp. 234–244, 1994.

[108] C. Lin and M. Gerla, "Asynchronous Multimedia Multihop Wireless Networks," in *Proceedings of INFOCOM '97*, vol. 1, pp. 118–125 vol.1, 1997.

[109] J. Laneman, D. Tse, and G. Wornell, "Cooperative diversity in wireless networks: Efficient protocols and outage behavior," *IEEE Transactions on Information Theory*, vol. 50, no. 12, pp. 3062–3080, 2004.

[110] M. Haenggi and D. Puccinelli, "Routing in Ad-Hoc Networks: a case for long hops," *IEEE Communications Magazine*, vol. 43, no. 10, pp. 93–101, 2005.

[111] M. Haenggi, "Twelve reasons not to route over many short hops," in *IEEE 60th Vehicular Technology Conference, 2004. VTC2004-Fall. 2004*, vol. 5, pp. 3130–3134 Vol. 5, 2004.

[112] Z. Fei, B. Li, S. Yang, C. Xing, H. Chen, and L. Hanzo, "A Survey of Multi-Objective Optimization in Wireless Sensor Networks: Metrics, Algorithms, and Open Problems," *IEEE Communications Surveys Tutorials*, vol. 19, no. 1, pp. 550–586, 2017.

[113] O. Oyman, J. N. Laneman, and S. Sandhu, "Multihop Relaying for Broadband Wireless Mesh Networks: From Theory to Practice," *IEEE Communications Magazine*, vol. 45, no. 11, pp. 116–122, 2007.

[114] O. Oyman, "Opportunistic Scheduling and Spectrum Reuse in Relay-Based Cellular Networks," *IEEE Transactions on Wireless Communications*, vol. 9, no. 3, pp. 1074–1085, 2010.

[115] J. Liu, H. Nishiyama, N. Kato, T. Kumagai, and A. Takahara, "Modeling ad-hoc mobile networks: The general k-hop relay routing," in *Global Communications Conference (GLOBECOM), 2013 IEEE*, pp. 25–29, Dec 2013.

[116] F. L. Lewis *et al.*, "Wireless sensor networks," *Smart environments: technologies, protocols, and applications*, pp. 11–46, 2004.

[117] W. Zhang, Y. Chen, Y. Yang, X. Wang, Y. Zhang, X. Hong, and G. Mao, "Multi-Hop Connectivity Probability in Infrastructure-Based Vehicular Networks," *IEEE Journal on Selected Areas in Communications*, vol. 30, pp. 740–747, May 2012.

[118] G. Wu, S. Talwar, K. Johnsson, N. Himayat, and K. D. Johnson, "M2M: From mobile to embedded internet," *IEEE Communications Magazine*, vol. 49, pp. 36–43, April 2011.

[119] X. Lin and J. G. Andrews, "Connectivity of Millimeter Wave Networks With Multi-Hop Relaying," *IEEE Wireless Communications Letters*, vol. 4, pp. 209–212, April 2015.

[120] R. Sanchez, J. Evans, and G. Minden, "Networking on the battlefield: challenges in highly dynamic multi-hop wireless networks," in *MILCOM 1999. IEEE Military Communications. Conference Proceedings (Cat. No.99CH36341)*, vol. 2, pp. 751–755 vol.2, 1999.

[121] G. Chen, J. P. Coon, A. Mondal, B. Allen, and J. A. Chambers, "Performance Analysis for Multi-Hop Full-Duplex IoT Networks Subject to Poisson Distributed Interferers," *IEEE Internet of Things Journal*, 2018.

[122] A. Phipps, A. da Silva Curiel, M. Meerman, D. Gibbon, M. Sweeting, and L. Gomes, "Low cost lunar orbiter system design," in *2003 IEEE Aerospace Conference Proceedings (Cat. No.03TH8652)*, vol. 1, pp. 1–237 vol.1, 2003.

[123] I. Leyva-Mayorga, B. Soret, M. Röper, D. Wübben, B. Matthiesen, A. Dekorsy, and P. Popovski, "LEO Small-Satellite Constellations for 5G and Beyond-5G Communications," *IEEE Access*, vol. 8, pp. 184955–184964, 2020.

[124] Y.-D. Lin and Y.-C. Hsu, "Multihop Cellular: A New Architecture for Wireless Communications," in *Proceedings IEEE INFOCOM 2000. Conference on Computer Communications. Nineteenth Annual Joint Conference of the IEEE Computer and Communications Societies (Cat. No. 00CH37064)*, vol. 3, pp. 1273–1282, IEEE, 2000.

[125] L. Le and E. Hossain, "Multihop Cellular Networks: Potential Gains, Research Challenges, and a Resource Allocation Framework," *IEEE Communications Magazine*, vol. 45, no. 9, pp. 66–73, 2007.

[126] K. Zheng, B. Fan, Z. Ma, G. Liu, X. Shen, and W. Wang, "Multihop cellular networks toward LTE-advanced," *IEEE Vehicular Technology Magazine*, vol. 4, no. 3, pp. 40–47, 2009.

[127] S. Jung and J. Kim, "A new way of extending network coverage: Relay-assisted D2D communications in 3GPP," *ICT Express*, vol. 2, no. 3, pp. 117–121, 2016. Special Issue on ICT Convergence in the Internet of Things (IoT).

[128] X. J. Li, B.-C. Seet, and P. H. J. Chong, "Multihop Cellular Networks: Technology and Economics," *Computer Networks*, vol. 52, no. 9, pp. 1825–1837, 2008.

[129] M. Dohler and Y. Li, *Cooperative communications: hardware, channel and PHY*. John Wiley & Sons, 2010.

[130] P. Murphy and A. Sabharwal, "Design, implementation, and characterization of a cooperative communications system," *IEEE Transactions on Vehicular Technology*, vol. 60, no. 6, pp. 2534–2544, 2011.

[131] H. Cho, S. Mukherjee, D. Kim, T. Noh, and J. Lee, "Facing to wireless network densification in 6G: challenges and opportunities," *ICT Express*, vol. 9, no. 3, pp. 517–524, 2023.

[132] D. Lopez-Perez, M. Ding, H. Claussen, and A. H. Jafari, "Towards 1 Gbps/UE in Cellular Systems: Understanding Ultra-Dense Small Cell Deployments," *IEEE Communications Surveys Tutorials*, vol. 17, pp. 2078–2101, Fourthquarter 2015.

[133] X. An and F. Pianese, "Understanding co-channel interference in LTE-based multi-tier cellular networks," in *Proceedings of the 9th ACM symposium on Performance evaluation of wireless ad hoc, sensor, and ubiquitous networks*, pp. 107–112, ACM, 2012.

[134] I. Hwang, B. Song, and S. S. Soliman, "A holistic view on hyper-dense heterogeneous and small cell networks," *IEEE Communications Magazine*, vol. 51, pp. 20–27, June 2013.

[135] M. Ahsen, S. A. Hassan, and D. N. K. Jayakody, "Propagation Modeling in Large-Scale Cooperative Multi-Hop Ad-Hoc Networks," *IEEE Access*, vol. 4, pp. 8925–8937, 2016.

[136] CISCO, "Cisco visual networking index: Global mobile data traffic forecast update, 2016—2021 White Paper," *Technical Report, Cisco, Tech. Rep.*, 2017.

[137] L. Wei, R. Hu, Y. Qian, and G. Wu, "Enable device-to-device communications underlaying cellular networks: challenges and research aspects," *IEEE Communications Magazine*, vol. 52, pp. 90–96, June 2014.

[138] A. Asadi, Q. Wang, and V. Mancuso, "A Survey on Device-to-Device Communication in Cellular Networks," *IEEE Communications Surveys Tutorials*, vol. 16, pp. 1801–1819, Fourthquarter 2014.

[139] F. Jameel, Z. Hamid, F. Jabeen, S. Zeadally, and M. A. Javed, "A Survey of Device-to-Device Communications: Research Issues and Challenges," *IEEE Communications Surveys Tutorials*, vol. 20, pp. 2133–2168, thirdquarter 2018.

[140] Networld, "White Paper for Research Beyond 5G," *Proceedings of the First International Conference on Communications and Networking in China (CHINACOM 2006)*, 2006.

[141] P. H. J. Nardelli, P. Cardieri, and M. Latva-aho, "Efficiency of Wireless Networks under Different Hopping Strategies," *IEEE Transactions on Wireless Communications*, vol. 11, no. 1, pp. 15–20, 2012.

[142] G. Chen, J. P. Coon, and S. E. Tajbakhsh, "Secure Routing for Multihop Ad Hoc Networks With Inhomogeneous Eavesdropper Clusters," *IEEE Transactions on Vehicular Technology*, vol. 67, no. 11, pp. 10660–10670, Nov. 2018.

[143] G. Chen, J. Tang, and J. P. Coon, "Optimal Routing for Multihop Social-Based D2D Communications in the Internet of Things," *IEEE Internet of Things Journal*, vol. 5, no. 3, pp. 1880–1889, June 2018.

[144] G. Khanna and S. K. Chaturvedi, "A comprehensive survey on multi-hop wireless networks: milestones, changing trends and concomitant challenges," *Wireless Personal Communications*, vol. 101, no. 2, pp. 677–722, 2018.

[145] M. Kamal, M. Ibrahim, S. Mir, and M. N. Aman, "Comparison of multihop relaying protocols in cognitive radio networks," in *2016 Sixth International Conference on Innovative Computing Technology (INTECH)*, pp. 611–616, 2016.

[146] Y. Rolain, W. Van Moer, R. Pintelon, and J. Schoukens, "Experimental characterization of the nonlinear behavior of RF amplifiers," *IEEE Transactions on Microwave Theory and Techniques*, vol. 54, no. 8, pp. 3209–3218, 2006.

[147] D. E. Simmons and J. P. Coon, "Two-Way OFDM-Based Nonlinear Amplify-and-Forward Relay Systems," *IEEE Transactions on Vehicular Technology*, vol. 65, no. 5, pp. 3808–3812, 2016.

[148] M. Hasna and M.-S. Alouini, "A performance study of dual-hop transmissions with fixed gain relays," *IEEE Transactions on Wireless Communications*, vol. 3, no. 6, pp. 1963–1968, 2004.

[149] A. H. Mohammed, B. Dai, B. Huang, M. Azhar, G. Xu, P. Qin, and S. Yu, "A survey and tutorial of wireless relay network protocols based on network coding," *Journal of Network and Computer Applications*, vol. 36, no. 2, pp. 593–610, 2013.

[150] A. Chandra, C. Bose, and M. K. Bose, "Wireless Relays for Next Generation Broadband Networks," *IEEE Potentials*, vol. 30, no. 2, pp. 39–43, 2011.

[151] D. A. Hedges, J. P. Coon, and O. Georgiou, "On the Connectivity of Two-Hop Networks in Finite Domains," in *SCC 2017; 11th International ITG Conference on Systems, Communications and Coding*, pp. 1–6, VDE, 2017.

[152] S. Kumar, V. S. Raghavan, and J. Deng, "Medium access control protocols for ad hoc wireless networks: A survey," *Ad Hoc Networks*, vol. 4, no. 3, pp. 326 – 358, 2006.

[153] D. A. Hedges and J. P. Coon, "On the Relationship Between Relay and Infrastructure Densities in Geometrically Bounded Relay-Assisted Wireless Networks," *IEEE Transactions on Vehicular Technology*, vol. 67, pp. 10983–10994, Nov 2018.

[154] D. A. Hedges, J. P. Coon, and G. Chen, "A Continuum Model for Route Optimization in Large-Scale Inhomogeneous Multi-Hop Wireless Networks," *IEEE Transactions on Communications*, vol. 68, no. 2, pp. 1058–1070, 2019.

[155] D. Hedges, J. Coon, and G. Chen, "A Continuum Model for Route Optimization in Large-Scale Inhomogeneous Multi-Hop Wireless Networks," *EUSIPCO 2019, 27th European Signal Processing Conference*, 2019.

[156] H. T. Friis, "A note on a simple transmission formula," *Proceedings of the IRE*, vol. 34, no. 5, pp. 254–256, 1946.

[157] C. J. Coleman, *Analysis and modeling of radio wave propagation.* Cambridge University Press, 2017.

[158] O. Georgiou, C. P. Dettmann, and J. P. Coon, "Connectivity of Confined 3D Networks With Anisotropically Radiating Nodes," *IEEE Transactions on Wireless Communications*, vol. 13, no. 8, pp. 4534–4546, 2014.

[159] O. Georgiou and C. Nguyen, "Multihop Connectivity of Ad-Hoc Networks With Randomly Oriented Directional Antennas," *Wireless Communications Letters, IEEE*, vol. 4, pp. 369–372, Aug 2015.

[160] J. G. Andrews, R. K. Ganti, M. Haenggi, N. Jindal, and S. Weber, "A primer on spatial modeling and analysis in wireless networks," *IEEE Communications Magazine*, vol. 48, no. 11, pp. 156–163, 2010.

[161] J. G. Proakis and M. Salehi, "Digital Communications, 5th Edition," 2008.

[162] S. Popa, N. Draghiciu, and R. Reiz, "Fading types in wireless communications systems," *Journal of Electrical and Electronics Engineering*, vol. 1, no. 1, pp. 233–237, 2008.

[163] H. Fischer, *A history of the central limit theorem: from classical to modern probability theory*. Springer, 2011.

[164] G. Chen, J. P. Coon, and M. Di Renzo, "Secrecy Outage Analysis for Downlink Transmissions in the Presence of Randomly Located Eavesdroppers," *IEEE Transactions on Information Forensics and Security*, vol. 12, no. 5, pp. 1195–1206, 2017.

[165] G. Chen, J. P. Coon, A. Mondal, B. Allen, and J. A. Chambers, "Performance Analysis for Multihop Full-Duplex IoT networks Subject to Poisson Distributed Interferers," *IEEE Internet of Things Journal*, vol. 6, no. 2, pp. 3467–3479, 2019.

[166] M. Tarique and M. T. Hasan, "Impact of Nakagami-m fading model on multi-hop mobile ad hoc network," *International Journal of Computer Applications*, vol. 26, no. 2, pp. 5–12, 2011.

[167] E. Price and D. P. Woodruff, "Applications of the Shannon-Hartley theorem to data streams and sparse recovery," in *2012 IEEE International Symposium on Information Theory Proceedings*, pp. 2446–2450, IEEE, 2012.

[168] H. Friis, "Noise Figures of Radio Receivers," *Proceedings of the IRE*, vol. 32, no. 7, pp. 419–422, 1944.

[169] D. Tse and P. Viswanath, *Fundamentals of Wireless Communication*. Wiley series in telecommunications, Cambridge University Press, 2005.

[170] J. Coon, C. Dettmann, and O. Georgiou, "Full Connectivity: Corners, Edges and Faces," *Journal of Statistical Physics*, vol. 147, no. 4, pp. 758–778, 2012.

[171] O. Georgiou, S. Wang, M. Z. Bocus, C. P. Dettmann, and J. P. Coon, "Location, location, location: Border effects in interference limited ad hoc networks," *ArXiv e-prints*, Apr. 2015.

[172] D. Goldman, "Sorry, America: your wireless airwaves are full," *CNN Money*, vol. 3, 2012.

[173] J. Rodriguez, *The Wireless Spectrum Crunch*, pp. 165–189. 2014.

[174] R. I. Ansari, H. Pervaiz, S. A. Hassan, C. Chrysostomou, M. A. Imran, S. Mumtaz, and R. Tafazolli, "A New Dimension to Spectrum Management in IoT Empowered 5G Networks," *IEEE Network*, vol. 33, no. 4, pp. 186–193, 2019.

[175] X. Zhang and M. Haenggi, "The Performance of Successive Interference Cancellation in Random Wireless Networks," *IEEE Transactions on Information Theory*, vol. 60, no. 10, pp. 6368–6388, 2014.

[176] J. Liu, M. Sheng, L. Liu, and J. Li, "Interference Management in Ultra-Dense Networks: Challenges and Approaches," *IEEE Network*, vol. 31, no. 6, pp. 70–77, 2017.

[177] M. Z. Bocus, O. Georgiou, J. P. Coon, and D. A. Hedges, "Location-based coverage probability for distributed antenna systems in finite-area networks," in *2017 IEEE International Conference on Communications (ICC)*, pp. 1–6, IEEE, 2017.

[178] G. Liu, F. R. Yu, H. Ji, V. C. M. Leung, and X. Li, "In-Band Full-Duplex Relaying: A Survey, Research Issues and Challenges," *IEEE Communications Surveys Tutorials*, vol. 17, no. 2, pp. 500–524, 2015.

[179] P. Gupta, "Critical power for asymptotic connectivity in wireless networks," 1999.

[180] F. Xue, "The number of neighbors needed for connectivity of wireless networks," *Wireless networks*, vol. 10, pp. 169–181, 2004.

[181] M. D. Penrose, "Connectivity of soft random geometric graphs," 2016.

[182] O. Georgiou, M. Z. Bocus, M. R. Rahman, C. P. Dettmann, and J. P. Coon, "Network Connectivity in Non-Convex Domains With Reflections," *IEEE Communications Letters*, vol. 19, no. 3, pp. 427–430, 2015.

[183] O. Georgiou, S. Wang, M. Z. Bocus, C. P. Dettmann, and J. P. Coon, "Location, location, location: Border effects in interference limited ad hoc networks," in *2015 13th International Symposium on Modeling and Optimization in Mobile, Ad Hoc, and Wireless Networks (WiOpt)*, pp. 568–575, 2015.

[184] P. G. Harrison and N. M. Patel, *Performance modelling of communication networks and computer architectures*. Addison-Wesley Longman Publishing Co., Inc., 1992.

[185] S. Wang and C. Ran, "Rethinking cellular network planning and optimization," *IEEE Wireless Communications*, vol. 23, no. 2, pp. 118–125, 2016.

[186] M. Afshang and H. S. Dhillon, "Fundamentals of Modeling Finite Wireless Networks Using Binomial Point Process," *IEEE Transactions on Wireless Communications*, vol. 16, no. 5, pp. 3355–3370, 2017.

[187] V. V. Chetlur and H. S. Dhillon, "Downlink Coverage Analysis for a Finite 3-D Wireless Network of Unmanned Aerial Vehicles," *IEEE Transactions on Communications*, vol. 65, no. 10, pp. 4543–4558, 2017.

[188] R. Wang, M. A. Kishk, and M.-S. Alouini, "Ultra-Dense LEO Satellite-Based Communication Systems: A Novel Modeling Technique," *IEEE Communications Magazine*, vol. 60, no. 4, pp. 25–31, 2022.

[189] D. Moltchanov, "Survey Paper: Distance distributions in random networks," *Ad Hoc Networks*, vol. 10, no. 6, pp. 1146–1166, 2012.

[190] M. Z. Bocus, O. Georgiou, J. P. Coon, and D. A. Hedges, "Location-based coverage probability for distributed antenna systems in finite-area networks," in *2017 IEEE International Conference on Communications (ICC)*, pp. 1–6, 2017.

[191] J. F. C. Kingman, *Poisson processes*, vol. 3. Clarendon Press, 1992.

[192] M. Younis and K. Akkaya, "Strategies and techniques for node placement in wireless sensor networks: A survey," *Ad Hoc Networks*, vol. 6, no. 4, pp. 621 – 655, 2008.

[193] M. Radi, B. Dezfouli, K. A. Bakar, and M. Lee, "Multipath routing in wireless sensor networks: survey and research challenges," *sensors*, vol. 12, no. 1, pp. 650–685, 2012.

[194] M. Minelli, M. Ma, M. Coupechoux, J. Kelif, M. Sigelle, and P. Godlewski, "Optimal Relay Placement in Cellular Networks," *IEEE Transactions on Wireless Communications*, vol. 13, pp. 998–1009, February 2014.

[195] M. Zolotukin, A. Sayenko, and T. Hamalainen, "On Optimal Relay Placement for Improved Performance in Non-coverage Limited Scenarios," in *Proceedings of the 17th ACM International Conference on Modeling, Analysis and Simulation of Wireless and Mobile Systems*, MSWiM '14, (New York, NY, USA), pp. 127–135, ACM, 2014.

[196] S. Y. Lee and T. Kim, "Optimal relay station placement with non-uniform user distribution," *Wireless Personal Communications*, vol. 107, pp. 121–136, Jul 2019.

[197] M. Minelli, M. Maode, M. Coupechoux, J. Kelif, M. Sigelle, and P. Godlewski, "Uplink Energy-Delay Trade-Off under Optimized Relay Placement in Cellular

Networks," *IEEE Transactions on Mobile Computing*, vol. 15, pp. 2376–2387, Sep. 2016.

[198] C. H. Papadimitriou, "Computational complexity," in *Encyclopedia of computer science*, pp. 260–265, 2003.

[199] S. A. Cook, "An Overview of Computational Complexity," *Commun. ACM*, vol. 26, pp. 400–408, June 1983.

[200] A. Efrat, S. Har-Peled, and J. S. Mitchell, "Approximation algorithms for two optimal location problems in sensor networks," in *2nd International Conference on Broadband Networks, 2005.*, pp. 714–723, IEEE, 2005.

[201] X. Cheng, D.-Z. Du, L. Wang, and B. Xu, "Relay sensor placement in wireless sensor networks," *Wireless Networks*, vol. 14, no. 3, pp. 347–355, 2008.

[202] S. Poduri, S. Pattem, B. Krishnamachari, and G. S. Sukhatme, "Sensor network configuration and the curse of dimensionality," in *Proc. Third Workshop on Embedded Networked Sensors (EmNets 2006), Cambridge, MA, USA*, Citeseer, 2006.

[203] A. Mazumder, Chenyang Zhou, A. Das, and A. Sen, "Budget constrained relay node placement problem for maximal "connectedness"," in *MILCOM 2016 - 2016 IEEE Military Communications Conference*, pp. 849–854, Nov 2016.

[204] X. Gao, J. Lu, H. Wang, F. Wu, and G. Chen, "Algorithm Design and Analysis for Wireless Relay Network Deployment Problem," *IEEE Transactions on Mobile Computing*, 2018.

[205] N. Kokash, "An introduction to heuristic algorithms," *Department of Informatics and Telecommunications*, pp. 1–8, 2005.

[206] G. Kumar and V. Ranga, "Meta-heuristics for relay node placement problem in wireless sensor networks," in *2016 Fourth International Conference on Parallel, Distributed and Grid Computing (PDGC)*, pp. 375–380, Dec 2016.

[207] J. M. Lanza-Gutiérrez, N. Caballé, J. A. Gómez-Pulido, B. Crawford, and R. Soto, "Toward a Robust Multi-Objective Metaheuristic for Solving the Relay Node Placement Problem in Wireless Sensor Networks," *Sensors*, vol. 19, no. 3, p. 677, 2019.

[208] A. Gogna and A. Tayal, "Metaheuristics: review and application," *Journal of Experimental & Theoretical Artificial Intelligence*, vol. 25, no. 4, pp. 503–526, 2013.

[209] F. Kuipers, P. Van Mieghem, T. Korkmaz, and M. Krunz, "An overview of constraint-based path selection algorithms for QoS routing," *IEEE Communications Magazine*, vol. 40, pp. 50–55, Dec 2002.

[210] K. M. Alzoubi, Peng-Jun Wan, and O. Frieder, "New distributed algorithm for connected dominating set in wireless ad-hoc networks," in *Proceedings of the 35th Annual Hawaii International Conference on System Sciences*, pp. 3849–3855, Jan 2002.

[211] F. Mansourkiaie and M. H. Ahmed, "Cooperative Routing in Wireless Networks: A comprehensive Survey," *IEEE Communications Surveys Tutorials*, vol. 17, no. 2, pp. 604–626, 2015.

[212] W. Xia, Y. Wen, C. H. Foh, D. Niyato, and H. Xie, "A Survey on Software-Defined Networking," *IEEE Communications Surveys Tutorials*, vol. 17, no. 1, pp. 27–51, 2015.

[213] A. Al Hayajneh, M. Z. A. Bhuiyan, and I. McAndrew, "Improving Internet of Things (IoT) security with software-defined networking (SDN)," *Computers*, vol. 9, no. 1, p. 8, 2020.

[214] K. Sood, K. K. Karmakar, S. Yu, V. Varadharajan, S. R. Pokhrel, and Y. Xiang, "Alleviating Heterogeneity in SDN-IoT Networks to Maintain QoS and Enhance Security," *IEEE Internet of Things Journal*, vol. 7, no. 7, pp. 5964–5975, 2020.

[215] A. Zahmatkesh and T. Kunz, "Software defined multihop wireless networks: Promises and challenges," *Journal of Communications and Networks*, vol. 19, no. 6, pp. 546–554, 2017.

[216] J. Wang, Y. Miao, P. Zhou, M. S. Hossain, and S. M. M. Rahman, "A software defined network routing in wireless multihop network," *Journal of Network and Computer Applications*, vol. 85, pp. 76–83, 2017.

[217] K. E. Atkinson, *An introduction to numerical analysis*. John Wiley & Sons, 2008.

[218] D. Coppersmith and S. Winograd, "Matrix multiplication via arithmetic progressions," *Journal of Symbolic Computation*, vol. 9, no. 3, pp. 251 – 280, 1990. Computational algebraic complexity editorial.

[219] B. Dacorogna, *Introduction to the Calculus of Variations*. World Scientific Publishing Company, 2014.

[220] A. Parnovsky, "Some generalisations of brachistochrone problem," *Acta Physica Polonica-Series A General Physics*, vol. 93, no. 145, pp. 55–64, 1998.

[221] K. Atkinson, *An introduction to numerical analysis*. John wiley & sons, 1991.

[222] E. W. Weisstein, "Euler-Lagrange differential equation," *https://mathworld. wolfram. com/*, 2005.

[223] M. Haenggi, J. G. Andrews, F. Baccelli, O. Dousse, and M. Franceschetti, "Stochastic geometry and random graphs for the analysis and design of wireless networks," *IEEE Journal on Selected Areas in Communications*, vol. 27, pp. 1029–1046, September 2009.

[224] G. Mao, Z. Zhang, and B. D. O. Anderson, "Probability of k-Hop Connection under Random Connection Model," *IEEE Communications Letters*, vol. 14, pp. 1023–1025, November 2010.

[225] J. Karlsson, J. Eriksson, and H. Li, "Two hop connectivity for uniformed randomly distributed points in the unit square," *Proceedings of the First International Conference on Communications and Networking in China (CHINACOM 2006). 25-27 October 2006, Beijing, China.*, 2006.

[226] C. P. Dettmann and O. Georgiou, "Random geometric graphs with general connection functions," *Physical Review E*, vol. 93, no. 3, p. 032313, 2016.

[227] J. Markendahl and Mäkitalo, "A comparative study of deployment options, capacity and cost structure for macrocellular and femtocell networks," in *2010 IEEE 21st International Symposium on Personal, Indoor and Mobile Radio Communications Workshops*, pp. 145–150, Sept 2010.

[228] K. Davaslioglu and E. Ayanoglu, "Quantifying Potential Energy Efficiency Gain in Green Cellular Wireless Networks," *IEEE Communications Surveys Tutorials*, vol. 16, pp. 2065–2091, Fourthquarter 2014.

[229] Z. Hasan, H. Boostanimehr, and V. K. Bhargava, "Green Cellular Networks: A Survey, Some Research Issues and Challenges," *IEEE Communications Surveys Tutorials*, vol. 13, pp. 524–540, Fourth 2011.

[230] N. Yu, Y. Miao, L. Mu, H. Du, H. Huang, and X. Jia, "Minimizing Energy Cost by Dynamic Switching ON/OFF Base Stations in Cellular Networks," *IEEE Transactions on Wireless Communications*, vol. 15, no. 11, pp. 7457–7469, 2016.

[231] A. Bousia, A. Antonopoulos, L. Alonso, and C. Verikoukis, "Green; distance-aware base station sleeping algorithm in LTE-Advanced," in *2012 IEEE International Conference on Communications (ICC)*, pp. 1347–1351, June 2012.

[232] M. Ding, D. Lopez-Perez, G. Mao, and Z. Lin, "Performance impact of idle mode capability on dense small cell networks with LoS and NLoS transmissions," *arXiv preprint arXiv:1609.07710*, 2016.

[233] M. Ding, D. L. Pérez, G. Mao, and Z. Lin, "Study on the Idle Mode Capability with LoS and NLoS Transmissions," *arXiv preprint arXiv:1608.06694*, 2016.

[234] A. Asadi, Q. Wang, and V. Mancuso, "A survey on device-to-device communication in cellular networks," *IEEE Communications Surveys & Tutorials*, vol. 16, no. 4, pp. 1801–1819, 2014.

[235] M. Nitti, G. A. Stelea, V. Popescu, and M. Fadda, "When social networks meet d2d communications: A survey," *Sensors*, vol. 19, no. 2, p. 396, 2019.

[236] M. Haenggi, *Stochastic Geometry for Wireless Networks*. New York, NY, USA: Cambridge University Press, 1st ed., 2012.

[237] O. Georgiou, C. P. Dettmann, and J. P. Coon, "Network connectivity: Stochastic vs. deterministic wireless channels," in *2014 IEEE International Conference on Communications (ICC)*, pp. 77–82, June 2014.

[238] J. Hu and N. C. Beaulieu, "Performance Analysis of Decode-and-Forward Relaying with Selection Combining," *IEEE Communications Letters*, vol. 11, pp. 489–491, June 2007.

[239] J. P. Coon, C. P. Dettmann, and O. Georgiou, "Connectivity of confined dense networks: boundary effects and scaling laws," *arXiv preprint arXiv:1201.4013*, 2012.

[240] J. P. Coon, O. Georgiou, and C. P. Dettmann, "Connectivity scaling laws in wireless networks," *IEEE Wireless Communications Letters*, vol. 4, no. 6, pp. 629–632, 2015.

[241] G. Amparo, S. Javier, and T. N. M., "The Asymptotic and Numerical Inversion of the Marcum Q-Function," *Studies in Applied Mathematics*, vol. 133, no. 2, pp. 257–278.

[242] A. H. Nuttall, "Some Integrals Involving the Q-Function," 1972.

[243] S. Arreckx, A. Lambe, J. R. R. A. Martins, and D. Orban, "A matrix-free augmented lagrangian algorithm with application to large-scale structural design optimization," *Optimization and Engineering*, vol. 17, pp. 359–384, Jun 2016.

[244] "Matlab® Documentation Optimization Toolbox, fmincon." `http://mathworks.com`.

[245] S. K. Sharma and X. Wang, "Towards massive machine type communications in ultra-dense cellular IoT networks: Current issues and machine learning-assisted solutions," *IEEE Communications Surveys & Tutorials*, 2019.

[246] A. A. Shabana, *Computational continuum mechanics*. John Wiley & Sons, 2018.

[247] J. Kelif, M. Coupechoux, and P. Godlewski, "Fluid Model of the Outage Probability in Sectored Wireless Networks," in *2008 IEEE Wireless Communications and Networking Conference*, pp. 2933–2938, March 2008.

[248] J.-M. Kelif, M. Coupechoux, and P. Godlewski, "A Fluid Model for Performance Analysis in Cellular Networks," *EURASIP J. Wirel. Commun. Netw.*, vol. 2010, pp. 1:1–1:11, Jan. 2010.

[249] H. Feng, L. Luo, Y. Wang, M. Ye, and R. Dong, "A novel minimal exposure path problem in wireless sensor networks and its solution algorithm," *International Journal of Distributed Sensor Networks*, vol. 12, no. 8, p. 1550147716664245, 2016.

[250] H. Elayan, R. M. Shubair, J. M. Jornet, and P. Johari, "Terahertz Channel Model and Link Budget Analysis for Intrabody Nanoscale Communication," *IEEE Transactions on NanoBioscience*, vol. 16, pp. 491–503, Sep. 2017.

[251] L. Felicetti, M. Femminella, G. Reali, and P. Liò, "Applications of molecular communications to medicine: A survey," *Nano Communication Networks*, vol. 7, pp. 27 – 45, 2016.

[252] M. Jain, J. I. Choi, T. Kim, D. Bharadia, S. Seth, K. Srinivasan, P. Levis, S. Katti, and P. Sinha, "Practical, real-time, full duplex wireless," in *Proceedings of the 17th annual international conference on Mobile computing and networking*, pp. 301–312, ACM, 2011.

[253] B. Debaillie, D.-J. van den Broek, C. Lavin, B. van Liempd, E. A. Klumperink, C. Palacios, J. Craninckx, B. Nauta, and A. Pärssinen, "Analog/RF solutions enabling compact full-duplex radios," *IEEE Journal on Selected Areas in Communications*, vol. 32, no. 9, pp. 1662–1673, 2014.

[254] C. Cai, Y. Cai, X. Zhou, W. Yang, and W. Yang, "When Does Relay Transmission Give a More Secure Connection in Wireless Ad Hoc Networks?," *IEEE Transactions on Information Forensics and Security*, vol. 9, pp. 624–632, April 2014.

[255] M. Morse, *The calculus of variations in the large*, vol. 18. American Mathematical Soc., 1934.

[256] Z. Liu, J. Liu, Y. Zeng, and J. Ma, "Covert Wireless Communications in IoT Systems: Hiding Information in Interference," *IEEE Wireless Communications*, vol. 25, no. 6, pp. 46–52, 2018.

[257] M. M. Alani, "OSI model," in *Guide to OSI and TCP/IP Models*, pp. 5–17, Springer, 2014.

[258] N. Xie, J. Zhang, and Q. Zhang, "Security Provided by the Physical Layer in Wireless Communications," *IEEE Network*, pp. 1–7, 2022.

[259] B. A. Bash, D. Goeckel, and D. Towsley, "Limits of Reliable Communication with Low Probability of Detection on AWGN Channels," *IEEE Journal on Selected Areas in Communications*, vol. 31, no. 9, pp. 1921–1930, 2013.

[260] S. Yan, X. Zhou, J. Hu, and S. V. Hanly, "Low Probability of Detection Communication: Opportunities and Challenges," *IEEE Wireless Communications*, vol. 26, no. 5, pp. 19–25, 2019.

[261] B. A. Bash, D. Goeckel, D. Towsley, and S. Guha, "Hiding information in noise: fundamental limits of covert wireless communication," *IEEE Communications Magazine*, vol. 53, no. 12, pp. 26–31, 2015.

[262] S. Yan, Y. Cong, S. V. Hanly, and X. Zhou, "Gaussian Signalling for Covert Communications," *IEEE Transactions on Wireless Communications*, vol. 18, no. 7, pp. 3542–3553, 2019.

[263] T. Kang, X. Li, C. Yu, and J. Kim, "A survey of security mechanisms with direct sequence spread spectrum signals," *Journal of Computing Science and Engineering*, vol. 7, no. 3, pp. 187–197, 2013.

[264] W. Lee, "Overview of cellular cdma," *IEEE Transactions on Vehicular Technology*, vol. 40, no. 2, pp. 291–302, 1991.

[265] A. Sheikholeslami, M. Ghaderi, D. Towsley, B. A. Bash, S. Guha, and D. Goeckel, "Multi-Hop Routing in Covert Wireless Networks," *IEEE Transactions on Wireless Communications*, vol. 17, no. 6, pp. 3656–3669, 2018.

[266] J. Hu, S. Yan, X. Zhou, F. Shu, and J. Wang, "Covert Communication in Wireless Relay Networks," in *GLOBECOM 2017 - 2017 IEEE Global Communications Conference*, pp. 1–6, 2017.

[267] X. Yu, S. Yan, J. Hu, P. Haskell-Dowland, Y. Han, and D. W. K. Ng, "On Relaying Strategies in Multi-Hop Covert Wireless Communications," in *ICC 2022 - IEEE International Conference on Communications*, pp. 666–672, 2022.

[268] Y. Su, H. Sun, Z. Zhang, Z. Lian, Z. Xie, and Y. Wang, "Covert Communication With Relay Selection," *IEEE Wireless Communications Letters*, vol. 10, no. 2, pp. 421–425, 2021.

[269] S. Bashar and Z. Ding, "Optimum routing protection against cumulative eavesdropping in multihop wireless networks," in *MILCOM 2009-2009 IEEE Military Communications Conference*, pp. 1–7, IEEE, 2009.

[270] J. Yao, S. Feng, X. Zhou, and Y. Liu, "Secure routing in multihop wireless ad-hoc networks with decode-and-forward relaying," *IEEE Transactions on Communications*, vol. 64, no. 2, pp. 753–764, 2016.

[271] G. Chen, J. P. Coon, and S. E. Tajbakhsh, "Secure routing for multihop ad hoc networks with inhomogeneous eavesdropper clusters," *IEEE Transactions on Vehicular Technology*, vol. 67, no. 11, pp. 10660–10670, 2018.

[272] D. A. Hedges, J. P. Coon, and G. Chen, "A Continuum Model for Route Optimization in Large-Scale Inhomogeneous Multi-Hop Wireless Networks," *IEEE Transactions on Communications*, vol. 68, no. 2, pp. 1058–1070, 2020.

[273] O. Georgiou, S. Wang, M. Z. Bocus, C. P. Dettmann, and J. P. Coon, "Directional antennas improve the link-connectivity of interference limited ad hoc networks," in *2015 IEEE 26th Annual International Symposium on Personal, Indoor, and Mobile Radio Communications (PIMRC)*, pp. 1311–1316, 2015.

[274] M. Tsai, "Path-loss and shadowing (large-scale fading)," *National Taiwan University October*, vol. 20, p. 2011, 2011.

[275] M. Gölz, A. M. Zoubir, and V. Koivunen, "Multiple hypothesis testing framework for spatial signals," *IEEE Transactions on Signal and Information Processing over Networks*, vol. 8, pp. 771–787, 2022.

[276] V. Zakharov, "Parallelism and array processing," *IEEE transactions on computers*, vol. 100, no. 1, pp. 45–78, 1984.

[277] B. Berisha, E. Mëziu, and I. Shabani, "Big data analytics in cloud computing: an overview," *Journal of Cloud Computing*, vol. 11, no. 1, p. 24, 2022.

[278] C. A. Balanis, *Antenna theory: analysis and design*. John wiley & sons, 2015.

[279] M. Haenggi, *Stochastic geometry for wireless networks*. Cambridge University Press, 2012.

[280] O. Georgiou and C. Nguyen, "Multihop connectivity of ad hoc networks with randomly oriented directional antennas," *IEEE Wireless Communications Letters*, vol. 4, no. 4, pp. 369–372, 2015.

[281] H. Li, "Lagrange multipliers and their applications," *Department of Electrical Engineering and Computer Science, University of Tennessee, Knoxville, TN*, vol. 37921, 2008.

[282] B. T. Polyak, "Newton's method and its use in optimization," *European Journal of Operational Research*, vol. 181, no. 3, pp. 1086–1096, 2007.